



EBERHARD KARLS
UNIVERSITÄT
TÜBINGEN



**PETROGENESIS AND GEOCHRONOLOGY OF THE DELIKTAŞ,
SIVRIKAYA AND DEVREKANI GRANITIDS AND BASEMENT,
KASTAMONU BELT-CENTRAL PONTIDES (NW TURKEY):
EVIDENCE FOR LATE PALAEOZOIC-MESOZOIC PLUTONISM,
AND GEODYNAMIC INTERPRETATION**

DISSERTATION

**INSTITUT FÜR GEOWISSENSCHAFTEN
UNIVERSITÄT TÜBINGEN-DEUTSCHLAND**

**ODILIA MBONGUH NZEGGE
CAMEROON**

~~2008~~

**PETROGENESIS AND GEOCHRONOLOGY OF THE DELIKTAŞ,
SIVRIKAYA AND DEVREKANI GRANITIDS AND BASEMENT,
KASTAMONU BELT-CENTRAL PONTIDES (NW TURKEY):
EVIDENCE FOR LATE PALAEOZOIC-MESOZOIC PLUTONISM
AND GEODYNAMIC INTERPRETATION**

DISSERTATION

Zur Erlangung des Doktorgrades
der Naturwissenschaften

der Geowissenschaften Fakultät
der Eberhard-Karls-Universität, Tübingen

Vorgelegt von

ODILIA MBONGUH NZEGGE

aus Babubock-Cameroon

~~2008~~

Tag der mündlichen Prüfung

13/12/ 2007

Dekan:

Prof. Dr. Peter Grathwohl

1. Berichterstatter

Prof. Dr. Muharrem Satir

2. Berichterstatter

Prof. Dr. Durmuş Boztuğ

For my father (Nzegge Francis Akang, † 1984), my mother (Nzegge-Ebong Agnes, † September 2003), sisters (Nzegge Apollonia and Epah Angela, † December 2003), senior brother (Nzegge Charles Onyong, † March 2004) and aunt (Ayuk-Ebong Asumpta, † March 2005). For God almighty!

TABLE OF CONTENTS

Table of content	6
Abstract	8
Kurzfassung	11
Acknowledgements	15
1. INTRODUCTION	16
1.1. Tectonic framework.....	19
1.2. Previous studies.....	20
1.3. Geological setting.....	24
1.4. Aims of this study.....	26
2. ANALYTICAL METHODS	28
2.1. Determination of major and trace elements concentrations.....	28
2.2. Whole-rock Nd-Sr isotopic and Rb-Sr minerals isotopic analyses.....	28
2.3. Oxygen isotopes analytical procedures.....	29
2.4. U-Pb zircon isotope dilution analyses.....	29
2.5. Pb-Pb zircon evaporation method.....	30
2.6. Cathodoluminescence.....	30
- Zircon internal structure.....	30
2.7. Classification of rocks-granite types.....	32
3. SIVRIKAYA AND DELIKTAŞ GRANITES	34
3.1. PETROGRAPHY.....	34
3.2. GEOCHEMISTRY.....	37
3.2.1. Major and trace elements.....	37
3.2.2. Rare earth elements.....	43
3.2.3. Sr-Nd-O isotopic compositions.....	45
3.2.4. Discussion on geochemistry.....	49
3.2.4.1. Petrogenetic considerations.....	49
3.2.4.2. Fractional crystallization.....	50
3.2.4.3. Nature of parental magma and possible sources.....	52
3.2.4.4. Tectonic implications.....	54
3.2.4.5. Conclusion on geochemistry and isotopic systematics.....	56
3.3. GEOCHRONOLOGY.....	59
3.3.1. Zircon internal structure.....	59
3.3.2. U-Pb, Pb-Pb and Rb-Sr data.....	61
3.3.3. Discussion and conclusions on geochronology.....	69

4. DEVREKANI GRANITOID	71
4.1. PETROGRAPHY.....	72
4.2. GEOCHEMISTRY.....	74
4.2.1. Major and trace elements geochemistry.....	74
4.2.2. Rare earth elements.....	79
4.2.3. Sr-Nd-O isotopic compositions.....	82
4.3. GEOCHRONOLOGY.....	84
4.3.1. Zircon internal structure.....	84
4.3.2. U-Pb, Pb-Pb and Rb-Sr data.....	86
4.4. DISCUSSION.....	90
4.4.1. Magma genesis and possible sources	90
4.4.2. Subduction versus mantle wedge components	92
4.4.3. Tectonic implications: evidence of slab break-off.....	93
4.5. CONCLUSIONS.....	94
4.6. General conclusion on granitoids: geodynamic model.....	96
5. EURASIAN-DERIVED BASEMENT COMPLEX	100
5.1. PETROGRAPHY.....	102
5.2. GEOCHEMISTRY.....	108
5.3. GEOCHRONOLOGY.....	113
5.3.1. U-Pb and Pb-Pb Zircon data.....	114
5.3.2. Rb-Sr whole-rock data.....	126
5.4. DISCUSSION.....	127
5.5. CONCLUSIONS.....	128
5.5.1. Regional geological implications	128
5.5.2. Precambrian basement.....	130
6. REFERENCES	132
7. APPENDIX	157
- Deliktas-Sivrikaya granites Rb-Sr mineral ages.....	157
- Tables geochemical analyses of basement.....	158
- Table isotope analyses for basement.....	162
- Table U-Pb zircons isotope dilution analyses	164
8. PUBLICATIONS	165
-First page of published Paper and Manuscripts in review.....	166

Abstract

The Pontides orogenic belt (Ketin, 1966), is the central portion of an extensive belt running from western Bulgaria (Rhodope Mountains) through northern Turkey to the Caucasus. Three tectono-stratigraphically different sectors can be distinguished: the Western Pontides (İstanbul zone), the Central Pontides and the Eastern Pontides (Sakarya zone). The Central Pontides, located between the İzmir-Ankara suture to the south and the Black Sea to the north is the geographical term for the arched central part of the Pontides orogenic belt (Fig. 1.1). The Central Pontides is one of the well preserved areas where the late Early Cretaceous juxtaposition of the Western Pontides (İstanbul Zone) and the Eastern Pontides (Sakarya Zone) (Okay and Tüysüz, 1999; Tüysüz, 1999) can be observed (Şengör and Yılmaz, 1981). Four main units are comprised in the Central Pontides: two major tectonic units, the Devrekani metamorphic unit (Eurasian-derived basement) and the Çangaldağ arc complex separated by two oceanic basins, the Küre and the Domuzdağ-Saraycıkadağ complexes.

The study area is marked by the Çangaldağ arc complex, and numerous granitoids and associated volcanics collectively called the Kastamonu granitoid belt (KGB) (Yılmaz and Boztuğ, 1986), that pierced the imbricated Palaeotethyan continental and oceanic basement assemblage. The Kastamonu belt documents large scale, multi-episodic magmatism, formed in response to subduction of the Palaeotethys and the subsequent late orogenic tectonics. The occurrence of these plutons and ophiolites in the Central Pontides has attracted geologists for several decades, because of their importance in understanding Palaeotethyan evolution, and the Tethysides-Variscides connection. However, data necessary to identify the type and origin of all the intrusions are not available. On the basis of stratigraphic correlation and a few K-Ar data earlier workers assigned Middle Jurassic emplacement time to all the plutons of the KGB. In an attempt to elucidate the petrogenetic and magmatic evolution of this belt, zircons from Deliktaş, Sivrikaya and Devrekani granitoids and their basement have been analyzed by means of Pb-Pb evaporation and U-Pb isotope dilution combined with isotope and geochemical data. Geochemical compositions, isotopic data and geochronological constraints are presented and interpreted for the evolution of the Palaeotethys in the Central Pontides.

The Late Carboniferous Sivrikaya granitoid (SG) comprises biotite-hornblende granodiorite, tonalites and minor two-mica granites. Sivrikaya rocks are slightly metaluminous to peraluminous, and transitional to S-type ($ASI = 0.9$ to > 1.1). The rocks are characterized by variably low initial $^{87}\text{Sr}/^{86}\text{Sr}$ ratios [$\text{Sr}_{(i)} = 0.705 - 0.708$], moderate $\epsilon\text{Nd}_{(t)}$ values (-1 to -3.8) and young Nd-model ages ($T_{\text{DM}} = 0.75 - 1.05$ Ga), suggesting variable degrees of mixing

between mantle and crustal components. Chondrite-normalized (cn) rare earth element (REE) patterns are characterized by fractionation between the light (LREE, $[La/Yb]_{cn} = 9 - 49$) and heavy REEs (HREE, $[Gd/Yb]_{cn} = 0.79 - 2.37$) and no to strong Eu depletion ($Eu/Eu^* = 1.19 - 0.18$). All these characteristics, combined with moderate $\delta^{18}O_{(whole-rock)}$ values (10 - 11.6 ‰) point to dehydration melting of heterogeneous amphibolites-metagreywackes-type sources with variable mantle contribution.

The Early Permian Deliktaş leucogranite (DLG) is host to muscovite-bearing monzogranites. Deliktaş rocks are strongly peraluminous S-type granites ($ASI > 1.1$), as reflected in the mineralogy that includes highly aluminous phases such as muscovite and cordierite. DLG samples exhibit strongly fractionated REE patterns ($[La/Yb]_{cn} = 3.6 - 35$), rather flat HREE ($[Gd/Yb]_{cn} = 0.59 - 0.78$) and small positive to distinct negative Eu- anomalies ($Eu/Eu^* = 1.15 - 0.42$) suggesting melting of metapelitic-type source with residual plagioclase and/or high degree fractional crystallization. Rocks from this intrusion have high $Sr_{(i)}$ ratios (0.7103 - 0.7123) and low $\epsilon Nd_{(t)}$ values (-2.2 to -5.0), indicating an arc underlain by a mature continental crust. Nearly constant $\delta^{18}O_{(whole-rock)}$ values (~11.5 ‰) and old Nd-model ages ($T_{DM} = 1.2 - 2.2$ Ga) of the rocks, in conjunction with the geochemical characteristics further support material contribution from mature continental crust in their genesis.

The Middle Jurassic Devrekani pluton (DG) consists of metaluminous I-type ($ASI = 0.55 - 0.88$) hornblende-biotite diorites and tonalites. The samples have low $Sr_{(i)}$ ratios (0.705 - 0.706) and very low negative $\epsilon Nd_{(t)}$ values (-0.8 to -2.2). These features together with the low $\delta^{18}O_{(whole-rock)}$ values (7 - 9 ‰), very high Mg# values, young model T_{DM} ages (1.04 - 1.6 Ga) and high CaO/Al_2O_3 ratios suggests dehydration melting of mafic lower crustal rocks, and/or derivation from amphibolite-type source with significant upper mantle-derived material input. DG rocks are further characterized by moderately fractionated REE patterns ($[La/Yb]_{cn} = 2 - 11$), flat HREE patterns ($(Gd/Yb)_{cn} = 1.35 - 1.68$) indicating garnet and zircon accumulation. The high Sr/Y ratios (10-37), no to distinct positive Eu-anomalies ($Eu/Eu^* = 0.72 - 0.95$), and Sr-spikes, indicate plagioclase accumulation. These geochemical characteristics indicate magmas derivation from an enriched mantle and/or metasomatized mantle sources with minor crustal contamination. It is suggested that, after the Cimmeridgian continent collided with the south Eurasian margin subsequent slab break-off and flip in subduction polarity, resulted in asthenospheric upwelling and the production of the near primary melts of the Devrekani pluton. The melts en route to higher levels interacted or not with mantle- and crustal-derived magmas. It can be concluded that the Middle Mesozoic magmatism was initiated by the brief

southward subduction of the Küre marginal basin (e.g. Ustaömer and Robertson, 1997) beneath the newly formed Late Carboniferous orogen (e.g. Okay et al. 2006).

The mineralogy and geochemistry of the rocks distinct from those closer to the Black sea coast, and their location in the far south of the Küre ophiolite, the similar WSW-ENE orientation of the Devrekani pluton and the major thrust system that resulted from the gravitational collapse, indicate a juvenile stage of a subduction system (Nzegge et al. in review). Because the intrusion is late syn-tectonic with respect to the shear fabric it is reasonable to assume that its generation in some way is related to the extension-collapse events. According to Dewey (1988) large volumes of mantle partial melts are injected into the lower crust during gravitational collapse of mountain chains by detachment faulting. I speculate that during this collapse event the geotherm crossed the garnet-lherzolite solidus and mafic melts were produced. The melt had little interaction with the felsic upper crust, accumulated plagioclase, and intruded in the shear zones, giving rise to the Devrekani I-type pluton.

Geochronologic analyses yielded ages ranging from 295-270 Ma for DLG, and 303-300 Ma for SG and in the south of the belt DG 190-165 Ma. Zircon xenocryst ages as old as ~2.7 Ga provide evidence for Proterozoic protolith, and highlights the association of the Central Pontides with Laurasia and Gondwana. The 360-340-320 Ma episodes of Pb loss in zircons are indicative of Variscan metamorphism. These new geochemical and age data from the Sivrikaya, Deliktaş and Devrekani granitoids indicate the evolution of the Kastamonu magmatism from tholeiitic to calc-alkaline to tholeiitic compositions with time. Furthermore, the presence of Late Palaeozoic pre- to post-collisional, transitional to peraluminous granites and Middle Mesozoic juvenile arc (post-collisional) rocks challenges previous evolution models for the Kastamonu granitoid belt and the Central Pontides.

The data presented herein underlines the complex thermo-tectonic history of the Central Pontides, and the magmatism associated with a “*long-lasting*” northward and a “*short-lived*” southward subduction of the Palaeotethys respectively during the Palaeozoic and Mesozoic times (*proposed model*), and the subsequent crustal growth processes (collision-accretion of Gondwanan-derived continental fragments with Laurasia).

The Precambrian-Palaeozoic Eurasian-derived basement (Devrekani metamorphic unit) of the Central Pontides is exposed between the Küre and Çangaldağ complexes. Evidence of the

Precambrian basement in the Central Pontides comes from a Büyükçay sample (BÜ-20, ortho-amphigneiss, ~502 Ma), from inherited zircons (U-Pb upper intercept ages) and Nd isotope data. Probably the BÜ-20 zircons crystallized in the Late Cambrian-Early Ordovician magmatic event as part of the wide-spread subduction-related magmatism in the Gondwana-derived terranes (e.g. Linnemann et al. 2000 and the references therein).

Key words: Central Pontides-Turkey; Variscan plutonism; Palaeotethyan convergence system; Palaeozoic oceanic crust; long-lasting Palaeozoic subduction; Late Palaeozoic pre-collisional magmatic arc (Çangaldağ complex); Palaeotethyan collision-accretion; extensional collapse of orogen; Late Palaeozoic rift; Eurasian continental fragment; slab roll-back; Küre back arc (marginal) basin (IAT-MORB-type); short-lived subduction flip; Mesozoic post-collisional magmatic arc; VAG, volcanic-arc granitoids; Kastamonu granitoid belt; Sivrikaya, Deliktaş and Devrekani granitoids; basement complex; whole-rock Sr-Nd-O isotopes; geochemistry; major and trace elements; petrogenesis; U-Pb and Pb-Pb zircon dating; Rb-Sr ages; suggested geodynamic model for magmas genesis.

Kurzfassung

Die Pontiden (Ketin, 1966), sind der zentrale Teil eines ausgedehnten Gebirgsgürtels der sich von West-Bulgarien (Rhodope Berge) über die Nord-Türkei bis in den Kaukasus erstreckt. Sie lassen sich in drei tektono-stratigrafische Abschnitte gliedern: die West-Pontiden (İstanbul Zone), die Zentral-Pontiden und die Ost-Pontiden (Sakarya Zone). Die Zentral-Pontiden, zwischen der İzmir-Ankara-Sutur im Süden und dem Schwarzen Meer im Norden gelegen, sind geographisch gesehen der gebogene, zentrale Teil des Pontidengürtels (Fig. 1.1). Die Zentral-Pontiden sind eines der am besten erhaltenen Gebiete wo die frühkretazische Nebeneinanderstellung der West- und Ost-Pontiden (Okay and Tüysüz, 1999; Tüysüz, 1999) beobachtet werden kann (Şengör and Yılmaz, 1981). Die Zentral-Pontiden umfassen vier Hauptabschnitte: Zwei tektonische Großeinheiten, die metamorphe Eurasische Devrekani- und die Çangaldağ-Einheit, die durch zwei ozeanische Becken, den Küre- und den Domuzdağ-Saraycikadağ-Komplex getrennt sind. Der metamorphe präkambrisch-paläozoische Devrekani Abschnitt ist ein Störungsgebundenes tektonisches Fenster, das zwischen der Küre- und der Çangaldağ-Einheit liegt, und die zusammen das Grundgebirge der zentralen Pontiden bilden.

Im Untersuchungsgebiet liegen der Çangaldağ-Inselbogen-Komplex und zahlreiche Granitoide und mit ihnen verbunden Vulkanite, die als Kastamonu-Granitoid-Gürtel (KGB)

bezeichnet werden. Die Magmen durchdrangen die Vergesellschaftung der paläotethischen Kontinental- und Ozeanboden-Einheiten. Der KGB dokumentiert großmaßstäblichen, vielphasigen Magmatismus, der im Zusammenhang mit der Subduktion der Paläotethys und spätorogener Kollisions-Tektonik der Pontiden gebildet wurde. Für das Verständnis des Tethys-Varisziden-Übergangs hat das Auftreten dieser Granitoide und Ophiolite in den zentralen Pontiden große Bedeutung. Wie auch immer, Daten über Typ und Ursprung der Intrusionskörper sind nicht vorhanden. Auf Grundlage stratigrafischer Korrelationen und wenigen K-Ar-Daten haben frühere Geologen mitteljurassische Alter für die gesamten Kastamonu-Plutone angenommen. Um über Petrogenese und Magmenentwicklung die Bildung des Gebirgsgürtels zu klären, wurden Zirkone von den Deliktaş-, Sivrikaya- and Devrekani-Granitoiden mit der Pb-Pb-Evaporationsmethode und der U-Pb-Isotopenverdünnungsmethode untersucht und mit geochemischen Daten kombiniert.

Die spätkarbonische Sivrikaya Granitoide (SG) besteht aus Biotit-Hornblende-Granodioriten, Tonaliten und wenigen Zweiglimmer-Graniten. Sivrikaya Gesteine sind schwach metaluminöse bis peraluminöse, und in Richtung S-Typ entwickelt ($ASI = 0.9$ to > 1.1). Die Gesteine zeichnen sich durch niedrige initiale Sr-Verhältnisse [$Sr_i = 0.705 - 0.708$], moderate initiale $\epsilon Nd_{(t)}$ -Werte (-1 to -3.8) und junge Nd-Modellalter ($T_{DM} = 0.75 - 1.05$ Ga) aus, die auf unterschiedliche Mischungsverhältnisse zwischen Mantel- und Krustenkomponenten hinweisen. Chondritnormierte (cn) Seltene Erden-Elementmuster zeigen Fraktionierung zwischen leichten ($[La/Yb]_{cn} = 9 - 49$) und schweren Seltenen Erden ($[Gd/Yb]_{cn} = 0.79 - 2.37$), sowie keine zu starke Eu-Abreicherung ($Eu/Eu^* = 1.19-0.18$) an. Diese Charakteristika kombiniert mit moderaten $\delta^{18}O$ -Werte ($10 - 11.6$ ‰) weisen auf Dehydratationsschmelzen von heterogenen Amphibolit-Metagrauwacken-Typen mit variabler Mantelmaterialbeteiligung hin (Nzegge et al. 2006).

Der frühpermische Deliktaş-Leukogranit (DLG) enthält muskovitführende Monzogranite. Deliktaş Gesteine sind stark peraluminöse S-Typ Granite ($ASI > 1.1$), was die Mineralogie mit hochaluminösen Phasen wie Muskovit und Cordierit zeigt. DLG Proben zeigen stark fraktionierte Seltene Erden- ($[La/Yb]_{cn} = 3.6 - 35$), eher flache schwere Seltene Erden-Elementmuster ($[Gd/Yb]_{cn} = 0.59 - 0.78$) und kleine, positive bis deutlich negative Eu-Anomalien ($Eu/Eu^* = 1.15 - 0.42$), die auf Schmelzen von metapeltischen Gesteinen mit Restplagioklas und/oder hochgradige Kristallisationsfraktionierung hinweisen. Gesteine dieser Intrusion haben hohe $Sr_{(t)}$ -Verhältnisse ($0.7103 - 0.7123$) und niedrige $\epsilon Nd_{(t)}$ -Werte (-2.2 bis -5.0), die einen Inselbogen mit unterlagernder, entwickelter kontinentalen Kruste nahelegen. Nahezu konstante $\delta^{18}O$ -Werte (~ 11.5 ‰) und alte Nd-Modelalter ($T_{DM} = 1.2 - 2.2$ Ga) der

Gesteine, in Verbindung mit geochemischen Charakteristika unterstützen weiter die Beteiligung von entwickelter kontinentaler Kruste in ihrer Genese.

Der mitteljurassische Devrekani pluton (DG) besteht hauptsächlich aus metaluminösen I-Typ (ASI = 0.55 - 0.88) Hornblende-Biotit Dioriten und wenigen Tonaliten. Die Proben haben niedrige $Sr_{(t)}$ -Verhältnisse (0.705 - 0.706), sehr niedrige negative $\epsilon Nd_{(t)}$ -Werte (-0.8 bis -2.2). Diese Merkmale zusammen mit den niedrigen $\delta^{18}O$ -Werten (7 - 9 ‰), sehr hohen Mg# Werten, jungen Nd-Modellaltern ($T_{DM} = 1.04 - 1.6$ Ga) und hohen CaO/Al_2O_3 -Verhältnissen legen Dehydrationsschmelzen von mafischen Unterkrusten-Gesteinen und/oder die Abstammung von amphibolithischen Quellen mit einem signifikantem Beitrag von Material aus dem oberen Mantel nahe. DG Gesteine sind weiterhin durch moderat fraktionierte leichte Seltene Erden- ($[La/Yb]_{cn} = 2 - 11$), flache schwere Seltene Erden-Elementmuster ($[Gd/Yb]_{cn} = 1.35 - 1.68$), welche Granat- und Zirkon-Anreicherung anzeigen, charakterisiert. Die hohen Sr/Y-Verhältnisse (10 - 37), keine bis deutlich positive Eu-Anomalien ($Eu/Eu^* = 0.72 - 0.95$), und Sr-spikes, zeigen Plagioklas-Anreicherung an. Diese chemischen Charakteristika zeigen Magmenabstammung von einer angereicherten und/oder metasomatischen Mantelquelle mit geringer krustaler Kontamination an. Es liegt nahe, dass nachdem der kimmeridgische Kontinent mit dem Südrand Eurasiens kollidierte, Platten-Abbruch und Subduktion eintraten, was in einer Asthenospärenaufwölbung und der Produktion von nahezu primären Schmelzen des Devrekani-Plutons führte. Die aufsteigenden Schmelzen interagierten mit vom Mantel und der Kruste abstammenden Magmen. Es kann gefolgert werden, dass der mittelmesozoische Magmatismus durch die kurze südwärts gerichtete Subduktion des Küre-Randbeckens (Ustaömer and Robertson, 1997) unter das neu gebildete spätkarbonische Orogen (Okay et al. 2006) ausgelöst wurde. Die WSW-ENE-Orientierung des Devrekani-Plutons und der Scherzone, die mit dem gravitativen Kollaps verbunden sind, die Mineralogie und Chemie der Gesteine Verschieden von der, die näher an der Schwarzmeerküste liegen, und der DG Lage weit im Süden des Küre-Ophioliths zeigt ein Subduktionssystem in jungem Stadium (Nzegge et al. in review). Da die Intrusion bezogen auf die Schergefüge spät syntektonisch ist, kann angenommen werden, dass ihre Bildung mit dem Dehnungs-Kollaps-Ereignis zusammenhängt. Nach Dewey (1988) spritzen, verursacht durch Trennungsbruch während Gravitations-Kollaps eines Gebirges große Volumina von Mantelpartiellschmelzen in die untere Kruste. Es ist vorgeschlagen, dass während dieser Einstürzung die Geotherme den Granat-Lherzolite-Solidus überschritten hat und mafischen Schmelzen erzeugt wurden. Die Schmelze wurde kaum von der felsischen Oberkruste beeinflusst, reichert Plagioklas an, und drang in die Scherzonen ein, den Devrekani metaluminöse I-Typ Pluton bildend.

Geochronologische Analysen lieferten Alter, die für Deliktaş zwischen 295-270 Ma, für Sivrikaya zwischen 303-300 Ma und für den Devrekani Granitoid im Süden des Gürtels bei 190-165 Ma liegen. Zirkonxenokristall-Alter von ~2,7 Ga liefern den Nachweis für proterozoischen Protolith, und unterstreichen die Verbindung der zentralen Pontiden mit Laurasia und Gondwana. Die 360-340-320 Ma Phasen von Bleiverlust in Zirkonen sind für variskischen Metamorphismus bezeichnend. Diese neuen geochemischen Daten, und Altersdaten der Sivrikaya-, Deliktaş- und Devrekani- Granitoide zeigen die Entwicklung des Kastamonu Magmatismus mit tholeiitischer bis kalk-alkaliner zu tholeiitischer Zusammensetzung in Abhängigkeit der Zeit an. Weiterhin stellt das Vorkommen von spätpaläozoischen prä- bis postkollisionalen Graniten, Übergangsganiten und peraluminösen Graniten, sowie mittelmesozoische junge Inselbögen bisherige Entwicklungsmodelle für den Kastamonu-Granitgürtel und die zentralen Pontiden in Frage.

Die hier präsentierten Daten unterstreichen die komplexe thermo-tektonische Geschichte der Zentralen Pontiden, den damit verbundenen Magmatismus mit einer *“long-lasting”* nordwärtigen und einer *“short-lived”* südwärtigen Subduktionsphase der Paläotethys (beziehungsweise während des Paläozoikums und Mesozoikums??) (*vorgeschlagenes Modell*), und der folgende Krustenwachstumsprozess (Kollision-Akkretion von Gondwana Kontinent Fragmenten mit Laurasia).

Das präkambrisch-paläozoisch von Eurasien stammende Basement (Devrekani Metamorphe Einheit) der Zentralen Pontiden liegt zwischen den Küre und Çangaldağ-Komplexen. Der Nachweis des präkambrischen Basements in den Zentralen Pontiden kommt von einer Büyükçay-Probe (BÜ-20, Ortho-Amphigneis, ~502 Ma), von ererbten Zirkone und Nd Isotopen Daten. Wahrscheinlich kristallierten die BÜ-20 Zirkone in einem spätkambrischen-frühordovizischen magmatischen Ereignis als Teil des weit verbreiteten subduktionsgebundenen Magmatismus Nördliche von Gondwana (e.g. Linnemann et al. 2000).

Acknowledgements

This study would have been impossible without the support of the Almighty God. I am particularly indebted to Him for giving me the strength to be able to earn money side-by-side this Study. Many thanks to Dr R. Brunner of the foreign students' office, University of Tübingen, for the prompt financial support, during three very difficult moments when I had to go urgently to Cameroon to assist in the burial of my mother, two sisters and my senior brother, food tickets, and for supporting me morally during six knee/heel operations. I remember when my senior brother died, he was on holidays in Italy and the secretary (Ms. Völker) had to call him for help. God bless you guys! Thanks also to Pfarrerin Abe.

More than 96 % of laboratory work was accomplished by me. X-ray analyses by G. Bartholomä and oxygen isotopes analyses by Dr. Taubald. They are gratefully acknowledged here. Microphotographs of rock-sections were made at Frisch AG. I wish to thank Prof. Dr. Durmuş Boztuğ for fruitful discussions on the geology of Turkey and for reviewing my manuscripts, Mr. J. Mällich for thin-sections preparation, and Drs. T. Wenzel and H. Schultz for assistance during cathodoluminescence analyses. Dr. H. Taubald is thanked for sponsoring my trace elements analyses. I am very thankful to Dr. N. Terzioğlu of the Turkish Petroleum Organisation, Ankara-Turkey for providing the first trickle of samples, for companionship and assistance during fieldtrip. The logistic support of the Turkish Petroleum Organisation, Ankara-Turkey during field work is heartily appreciated. I was introduced to Rb-Sr and Sm-Nd and to Pb-Pb and U-Pb zircon analyses by E. Reitter and Prof. F. Chen respectively.

It would have been even more difficult without the encouragements and moral support of Ms. Bartholomä, Dr Brunner and Ms. Völker, who were always by my side especially during the very difficult moments of hopelessness. Merci beaucoup! I thank Prof. Satir for proposing this study and for his role. Even those who delayed this work are thanked, however, “...*time and hour runs through the roughest day...*” (Lady Macbeth, Shakespeare), i.e. “*Time waits for nobody*”! For more than three years I had nothing, no computer, no data, no financing, no working partner, I had to wait for everybody. So much time wasted! Once in a while I got 20-33 hours HIWI (rarely more, thanks to Drs. Siebel W/Kaufmann B & Blaha U). I worked for every Cent and even more! However, if I worked for my country; I would have got pay for my work and maintained my work place!

Thank God, for the strength and courage to withstand the loss of my dear ones and the delays. Due thanks to the Kügler family, W. Scheidt and my family!

1. INTRODUCTION

The Pontides (Ketin, 1966) is a prominent segment of the Tethyside superorogenic system, and bear the records of Variscide, Cimmeridgian and Alpidic orogenic events (e.g. Şengör, 1987). This belt is an amalgamated tectonic entity that differs in their metamorphic, magmatic and tectono-stratigraphic character (Robertson and Dixon, 1984; Şengör et al. 1984). Of all the Turkish blocks, the Pontides alone preserve a nearly complete record of the evolution of the Tethysides (Yılmaz et al. 1997). The Pontides belt shows a complex history beginning with the separation of micro-continents from Gondwana in the Early Palaeozoic and culminating in collision of these fragments and island arc segments with Variscan Laurasia (Okay et al. 1996; Robertson and Dixon, 1984; Şengör et al. 1993; Stampfli 2000, Stampfli et al. 2002; Chen et al. 2002b; von Raumer et al. 2003). The continental fragment in the Central Pontides have Proterozoic-Palaeozoic basement (e.g. Devrekani metasedimentary group, e.g. Tüysüz, 1990; Yılmaz, 1980), overlain by the fossiliferous Ordovician-Devonian Samatlar metacarbonate group (Boztuğ, 1992a). During the Palaeozoic-Mesozoic, this basement and the overlying units were soaked with mafic to felsic magmas (e.g. Peccerillo and Taylor, 1976; Ustaömer and Robertson, 1993), grouped together in the Kastamonu granitoid belt (KGB) (e.g. Yılmaz and Boztuğ 1986).

The Central Pontides includes two Pontides Terranes: The Western Pontides (İstanbul Zone, Tüysüz, 1990) and the Eastern Pontides (Sakarya Zone) juxtaposed during the Early Cretaceous opening of the Black Sea basin (e.g. Tüysüz, 1999), structurally mixing Cimmeridgian and Eurasian continental fragments (Şengör et al. 1988), and Palaeotethyan oceanic assemblages (Yılmaz et al. 1997). The İstanbul zone (Western Pontides) is characterized by an Ordovician-Carboniferous sedimentary succession of passive margin type overlain by Triassic to younger rocks (e.g. Görür et al. 1997). In contrast, the Sakarya Zone (Eastern Pontides) is made up of Permo-Triassic subduction-accretion complexes overlain by Triassic and younger sediments (Okay and Tüysüz, 1999; Okay and Göncüoğlu, 2004).

The Eurasian-derived basement of the Central Pontides (Devrekani metamorphic unit), is a fault-bound tectonic window, exposed between the Palaeozoic-Early Jurassic Küre Complex to the north (e.g. Yılmaz et al. 1981; Yılmaz and Tüysüz, 1991; Ustaömer and Robertson, 1994, 1995, 1997) and the Late Palaeozoic-Early Triassic Çangaldağ Complex to the south (e.g. Aydın et al. 1995; Okay et al. 1994, 1996; Ustaömer and Robertson, 1991, 1993, 1994, 1997) (Figs. 1.2). This highly sheared and isoclinally folded basement unit is interpreted as a fragment rifted off the south Eurasian continental margin, to form a continental sliver within the Palaeotethys (e.g. Ustaömer and Robertson, 1990, 1991, 1994, 1997).

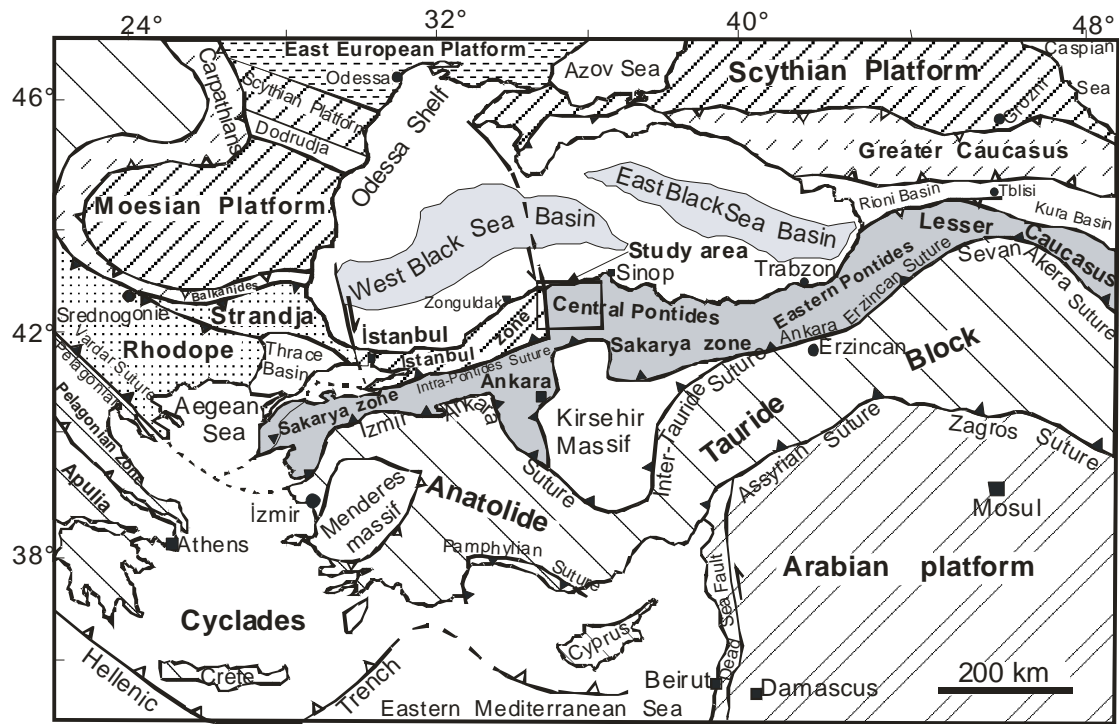


Fig. 1.1- Tectonic map of Aegean and Black Sea region showing the location of main Tethyan sutures and major continental blocks and study area (modified from Okay and Tüysüz, 1999)

Based on metamorphic-grade, source material and assumed age, the basement of the Central Pontides is sub-divided into two groups (Yılmaz and Boztuğ, 1995): (1) The Precambrian Devrekani metasedimentary group (DM), made up of basic to felsic high-grade amphibolite- to granulite-facies (Ustaömer and Robertson, 1991, 1997) metasedimentary rocks (Boztuğ et al. 1984, 1995) of south Eurasian continental origin (Robertson and Dixon, 1984; Boztuğ et al. 1984; Ustaömer and Robertson, 1997). The Devrekani metasedimentary group (DM) comprises gneisses, amphibolites and high-grade metacarbonates at the base (Yılmaz, 1981), (2) transgressively overlain by the Lower-Middle Palaeozoic Samatlar group (epicontinental cover), composed of low-grade metacarbonates.

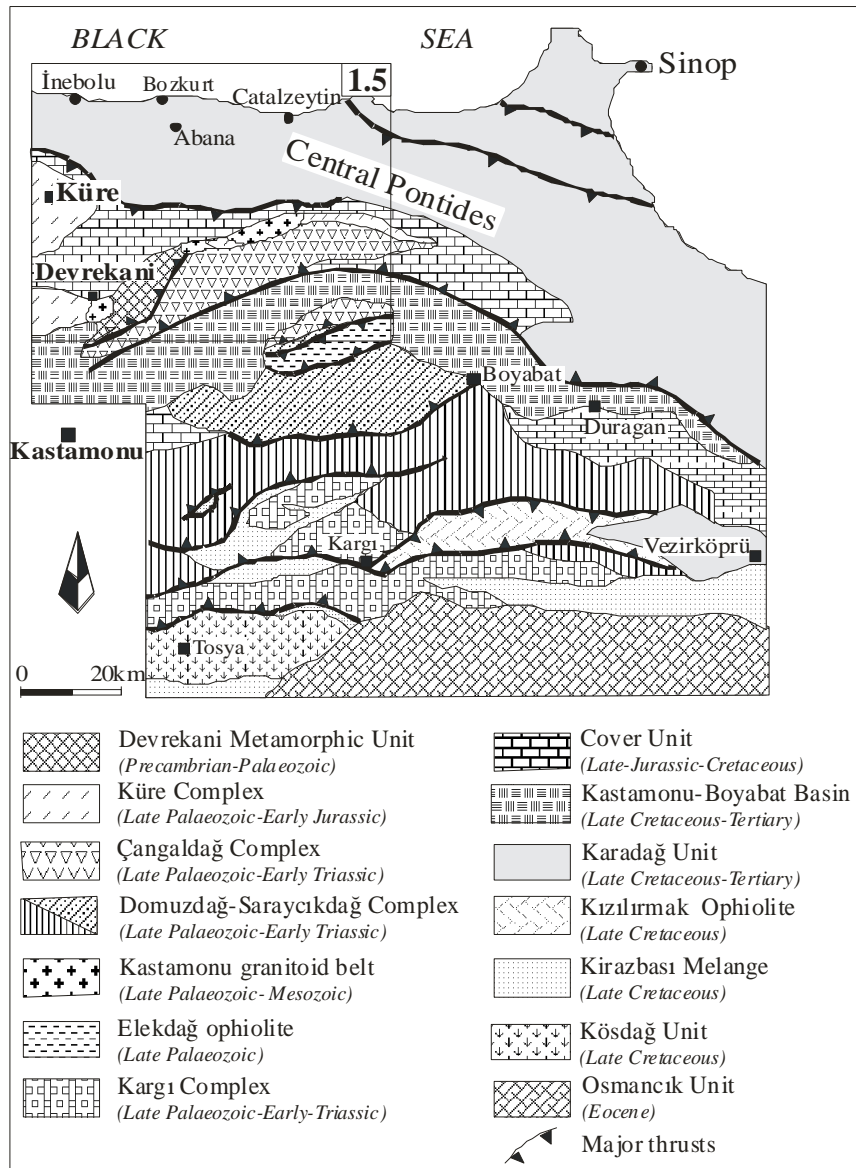


Fig. 1.2- Simplified geological map of the Central Pontides showing the main tectonic units and study area after Ustaömer and Robertson, (1997).

This Eurasian-derived basement is lithologically and stratigraphically similar to the Precambrian continental basement units of the Rhodope-Pontides belt and the Caucasus (Ustaömer and Robertson, 1991, 1997). Based on stratigraphic correlation with the Cambrian-Silurian sequence of the Palaeozoic of Istanbul zone (Okay and Tüysüz, 1999), both Precambrian (Yılmaz, 1980) and Palaeozoic ages (Tüysüz, 1990) have been suggested for the Devrekani metamorphic Unit. This imbricated Precambrian-Palaeozoic (e.g. Yılmaz, 1980; Tüysüz, 1990; data herein) Eurasian-derived continental basement assemblage (e.g Aydın et al. 1995; Ustaömer and Robertson, 1993; 1994; 1997), and the Triassic-Early Jurassic country-rocks (i.e. Akgöl formation) are pierced by the Late Palaeozoic to Middle Mesozoic Kastamonu intrusions (Nzegge et al. 2006, in review). A low-grade contact aureole developed

within the country-rocks (e.g. Yılmaz et al., 1996; 1997), but contact with the basement is mylonitized/sheared. The Devrekani metamorphic unit (DM) crops out between the Deliktaş and Sivrikaya granites, in the Ösek area and Büyükçay river valley, and in the south Musa-Osman river valley, NE of the Devrekani town (Figs. 1.2, 2.1, 3.1).

1.1. Tectonic framework of Turkey

The Pontide orogenic belt (Ketin 1966), of NW Turkey is the central portion of an extensive belt (Tethysides) running from the Balkans (Rhodope-Serbo-Macedonian Massif) through north Turkey to the Caucasus (e.g. Boccaletti et al. 1974; Burchfield 1980; Yılmaz et al. 1997; Stampfli 2000; Stampfli et al. 2001). It shows a complex history beginning with separation of micro-continents from Gondwana in the Early Palaeozoic and cumulating in collision of these fragments and island arc segments with Variscan Eurasia (e.g. Okay et al. 1996; Okay and Tüysüz, 1999; Robertson and Dixon 1984; Şengör et al. 1993; Stampfli, 2000; Stampfli et al. 2002; Chen et al. 2002b; von Raumer et al. 2003) (Fig. 1.1). The northern boundary of the Pontides is hidden under the waters of the black Sea.

The southern boundary is the Erzincan-Ankara suture in the east, which splays into the Intra-Pontides suture and the İzmir-Ankara suture in the west. The Intra-Pontides and the İzmir-Ankara Oceans separated Turkey into three continental blocks through most of the Mesozoic (Okay and Tüysüz, 1999; Okay et al. 1996, 2001, 2006; Şengör and Yılmaz, 1981) (Fig. 1.1). The Intra-Pontide suture separates the İstanbul and Strandja Zones from the Sakarya Zone (Sakarya continent, Şengör and Yılmaz, 1981). The Sakarya Zone had an important Carboniferous (Variscan) and Triassic (Cimmeride) orogenic history. The İstanbul-Strandja Zone was a peri-Gondwana terrane until Earliest Silurian (e.g. Stampfli, 2000), but during the Late Mesozoic was an appendage of Laurasia (e.g. Okay et al. 1996, 2001, 2006; Chen et al. 2002b; Evans et al. 1991; Kalvoda, 2003; Kalvoda et al. 2003). The Strandja Zone is part of the Balkan block and crops out both in Turkey and Bulgaria.

The İstanbul Zone, the Moesian and Scythian Platforms formed the Late Proterozoic-Early Palaeozoic Moesian-Istanbul-Scythian Terrane (Okay et al. 1996, 2006; Okay and Tüysüz, 1999) (Fig. 1.1). The closure of the Intra-Pontide Ocean and the Cretaceous-Palaeocene collision of the İstanbul Zone with the Sakarya continent led to the Present-day plate tectonic assembly in NW Turkey (Okay et al. 1994, 1996, 2006; Yiğitbaş et al. 1999).

1.2. Previous works

Northwestern Turkey comprises several Palaeozoic and Mesozoic continental and oceanic fragments assembled during the Variscan and Cimmeridgian orogenic events (e.g. Okay et al. 1996, 2006; Yiğitbaş et al. 1999). The strong effects of the Alpine orogeny have wiped out some of the characteristic features of the older events, and the lack of detailed geochronologic data base render the presentation of a convincing model for the Palaeo-Tethyan evolution in the NW Turkey very difficult. Most studies (e.g. Aydın et al. 1986; Boztuğ et al. 1984, 1995; Okay et al. 1996, 2002, 2006, 2007; Pickett and Robertson, 1996; Robertson and Dixon, 1984; Şengör, 1984; Şengör et al. 1980, 1984; Stampfli, 2000; Tüysüz, 1990; Ustaömer and Robertson, 1993, 1994, 1997; Yılmaz, 1980; Yılmaz and Şengör, 1985; Yılmaz and Boztuğ, 1986; Yılmaz et al. 1997; Robertson et al. 2004) from the Central Pontides play an important role in models regarding the evolution of the Palaeotethys.

The Palaeotethys was initially believed to have been located to the north of the İstanbul Zone (Okay, 1989; Okay et al. 1994; Şengör et al. 1980, 1984). However, recent evidence demonstrating the continuity of the İstanbul Zone (Western Pontides) and Laurasia until the Late Cretaceous opening of the Black Sea shows that that could not be the case (e.g. Okay et al. 1994). On the other hand, Robertson and Dixon (1984) and Okay (1989) have placed the Palaeotethys between the İstanbul and Sakarya zones (e.g. The Carboniferous-Triassic Intra-Pontides Ocean, Ustaömer and Robertson, 1997) and have left the Sakarya Zone (Eastern Pontides) as part of the Gondwana margin, in continuity with the Anatolide-Tauride block. According to Okay et al. (1994, 1996) the Palaeotethys has been located to the south of the Sakarya Zone, leaving the Palaeozoic basement of the Sakarya Zone in possible continuity with the Moesia-Istanbul-Strandja zones, all presenting a post-Variscan continental area along the southern margin of Laurasia. The northwestward emplacement of the Late Palaeozoic carbonate thrust sheets and the inferred Lower Triassic back-arc-related rifting in the Anatolide-Tauride block indicate a southeastward-dipping subduction (Okay et al. 1996, 2006). The formation of the Karakaya (Alköy) subduction-accretionary complex which reflects the final Palaeotethys ocean closure was caused by the Latest Triassic collision and thrusting of the oceanic arc and the associated accretionary complexes with the Laurasian passive continental margin (e.g. Okay et al. 1996; Tüysüz et al. 1993). These processes ended the Palaeotethyan episode in the Pontides as a whole but later (Dogger) in the Central Pontides (Tüysüz, 1990).

There are still contrasting views on the location, age span, even the number and the name of the Tethyan oceans that existed after the Precambrian (e.g. Şengör and Yılmaz, 1981; Robertson and Dixon, 1984; Şengör et al. 1984; Decourt et al. 1986; Robertson et al. 1996; Ricou, 1994; Stampfli et al. 2001, 2002). However, existing models for the Palaeotethys evolution consider the continental units of the Pontides as remnants of the continental margins bordering the Palaeotethys. The numerous geological data obtained until now from the Central Pontides have been used to interpret two controversial hypothesis by different authors grouped together in two tectonic models:

► **The Şengör (1984) southward subduction model** (Fig. 1.3). The Palaeotethyan ocean was located to the north of the Cimmeridgian continent, part of which form the Pontides basement. During the closure of the Palaeotethys, an “Andean-type” magmatic belt was developed on the Cimmeridgian continent due to the southward subduction of the Palaeotethyan ocean floor. During this period, the Neotethys began to open as back-arc basins behind the Cimmeridgian continent.

The Dogger collision between the the Scythian platform of Laurasia and Cimmeridgian continent (Gondwana fragment) that took place in the north, eliminated most of the Palaeotethys ocean floor, while the Neotethys grew in the south. The Late Cretaceous witnessed the gradual elimination of the Neotethys due to its northward subduction under the Pontides, thus creating a new active continental margin arc. Collision between the Pontides arc and the Tauride-Anatolide Platform resulted in the final closure of the Neotethys.

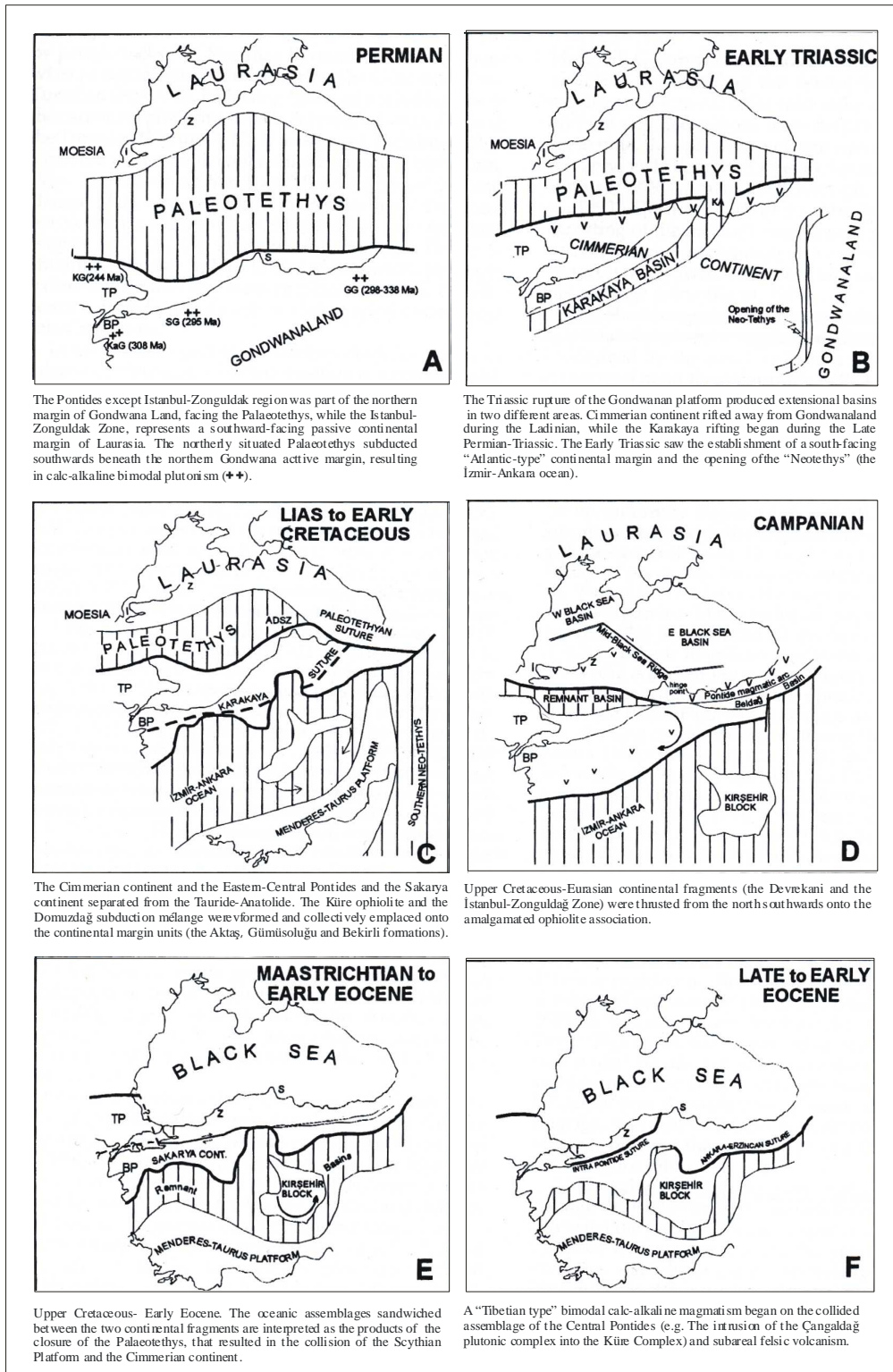


Fig. 1.3-Şengör (1984) southward subduction model (Yılmaz et al., 1997). Palaeotectonic maps depicting the tectonic evolution of the Pontides from the Permian to the Eocene. **, Arc plutonics; **vv**, arc volcanics. Heavy black lines, subduction zones; lines with half arrows, transform faults. Thin lines, Atlantic-type continental margins. ADSZ, Araç-Daday shear zone; BP, Bigam Peninsula; GG, Gümüşhane granite; KaG, Kazdağ granite; KA, Kargı area; KG, Kırklareli granite; S, Sinop; SG, Söğüt granite; TP, Tharce Peninsular; İ, İstanbul; Z, Zonguldak.

➤ The **Robertson and Dixon (1984)** (Fig. 1.4) **northward subduction model** proffers the northward underthrusting of a southerly situated Palaeotethys oceanic basin (represented by the Domuzdağ-Sarayıkdağ complex, Figs. 1.2, 1.4d) beneath the the Pontic basement that formed the southern tip of Eurasian continent, during the Late Palaeozoic-Mid-Jurassic.

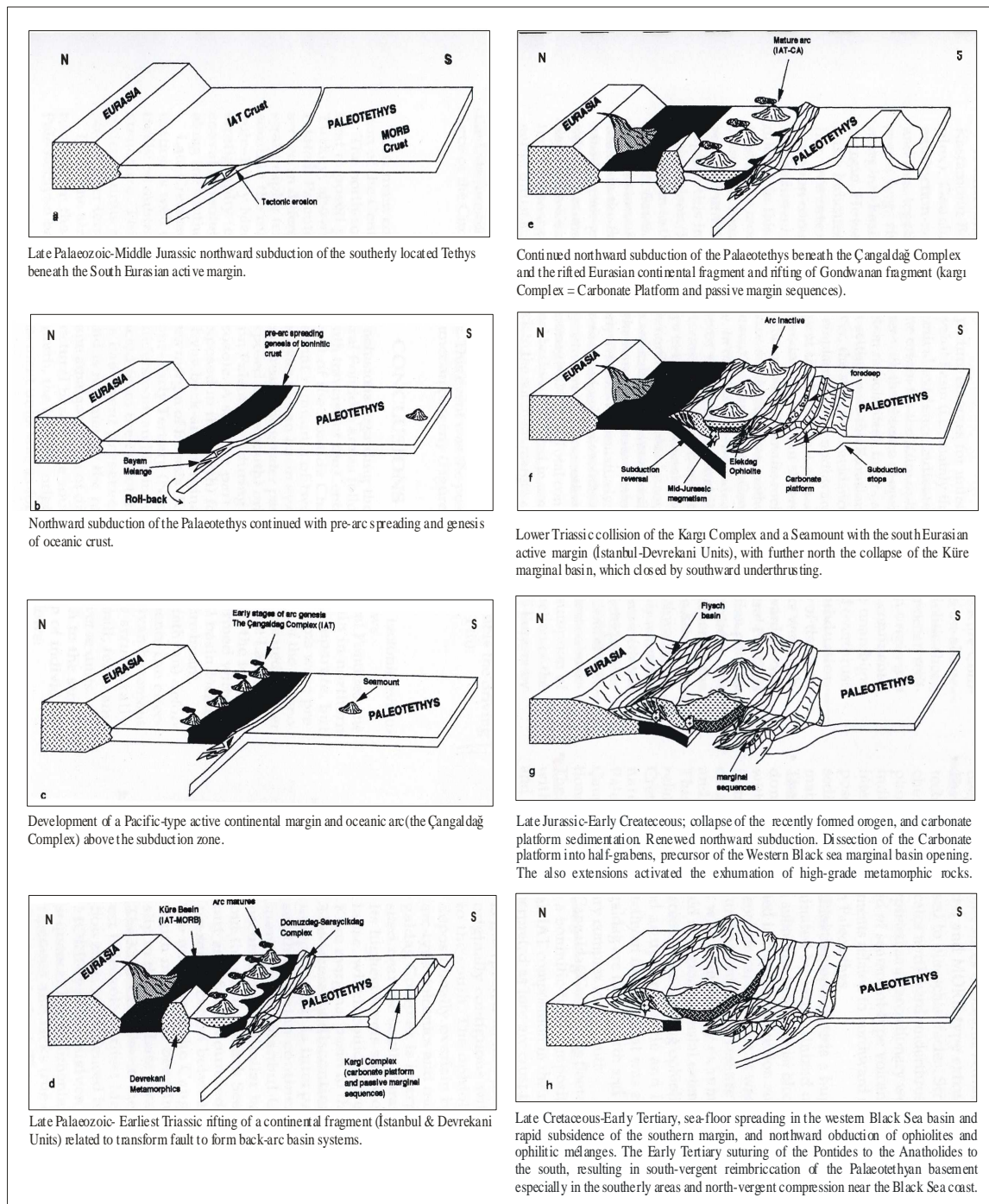


Fig. 1.4-The Robertson and Dixon (1984) northward subduction model (from Ustaömer and Robertson, 1997). Pre-Jurassic tectonic evolution of the northern Tethyan margin in the Central Pontides. MORB=mid-ocean rich basalt.

A “Pacific-type” oceanic arc (the Çangaldağ arc complex) developed above the subduction zone, followed by the rifting of a continental fragment (İstanbul and Devrekani units), related to transform and/or active margin processes, to form marginal basin system (the Küre complex and equivalents) in the Latest Palaeozoic-Earliest Triassic times. A carbonate platform and passive margin sequence (the Kargı Complex, Fig. 1.4d), of Gondwana-origin, drifted northwards, collided with the trench, subsided and was then overridden by the accretionary complex, partially closing the Palaeotethys. This collision triggered the southward underthrusting of the Küre marginal basin, in the Jurassic. The Upper Jurassic closure of the Küre marginal basin led to accretion of the entire tectonic assemblage to the southern margin of Eurasia during the “Cimmeridgian orogeny”. The Late Palaeozoic-Middle Mesozoic granitoids of the Central Pontides could relate to the northward Palaeotethyan subduction (Nzegge et al. 2006, in review) and/or to the southward underthrusting of the Küre basin (e.g. Ustaömer and Robertson, 1997; Nzegge et al. in review). During the Late Jurassic-Early Cretaceous, the recently formed Late Carboniferous orogen subsided, possibly triggered by renewed northward subduction of Tethys.

In this model, the “Palaeotethys” is considered as essentially a Palaeozoic ocean that finally closed during the Early Tertiary time and the “Neotethys” is the collective name for oceanic basins that rifted in the Early Mesozoic.

1.3. Regional geologic setting

The Central Pontides (Fig. 1.1) is the Early Cretaceous juxtaposition of the Western Pontides (İstanbul Zone) and the Eastern Pontides (Sakarya Zone) (Ustaömer and Robertson 1991; Okay and Tüysüz 1999; Tüysüz 1999; Şengör and Yılmaz, 1981). Four major tectonic units are identified in the Central Pontides (Fig. 1.2): (1) the continental basement unit comprised of Precambrian-Palaeozoic Devrekani metamorphic unit in the Devrekani-Kastamonu region (Yılmaz 1980; Tüysüz 1990; data herein); the Dorukyayla gneiss in the Karadere-Araç, Kastamonu region (Boztuğ 1992a, Boztuğ and Yılmaz 1995) and the Dönmeyol metamorphics in the Küre-Kastamonu region (Boztuğ, 1992b). This unit is inferred to have rifted from the south Eurasian active margin, thereby producing the Küre marginal basin (Ustaömer and Robertson, 1997) in the Late Permian (Robertson and Dixon 1984; Aydın et al. 1986, 1995; Ustaömer and Robertson 1993, 1994). (2) A Late Palaeozoic-Mesozoic subduction-accretion Küre complex in the north, related to the southward-directed subduction and closure of Palaeotethyan Küre marginal basin (e.g. IAT-MORB type, Robertson and Dixon, 1984; Ustaömer and Robertson, 1993, 1997). (3) The Çangaldağ complex, interpreted as a Late Palaeozoic-Early Triassic south-facing oceanic-arc-trench complex (e.g. Ustaömer,

1993; Ustaömer and Robertson, 1997). (4) To the south is the Palaeozoic-Mesozoic Domuzdağ-Saraycıkdağ subduction-accretion complex of northward polarity (e.g. Tüysüz and Yiğitbaş, 1994; Ustaömer and Robertson 1997). The latter complex is underlain by the Late Palaeozoic-Early Triassic Kargı complex (e.g. Ustaömer and Robertson 1997). All the above units are overlain by the Late Jurassic-Cretaceous Cover units (Yaraligöz group) (Figs. 1.5, 3.1), comprising basal conglomerates, limestones, sandstone-shale intercalated with marl, representing the new sedimentary cycle that followed the major collision and uplift (e.g. Yılmaz, 1980).

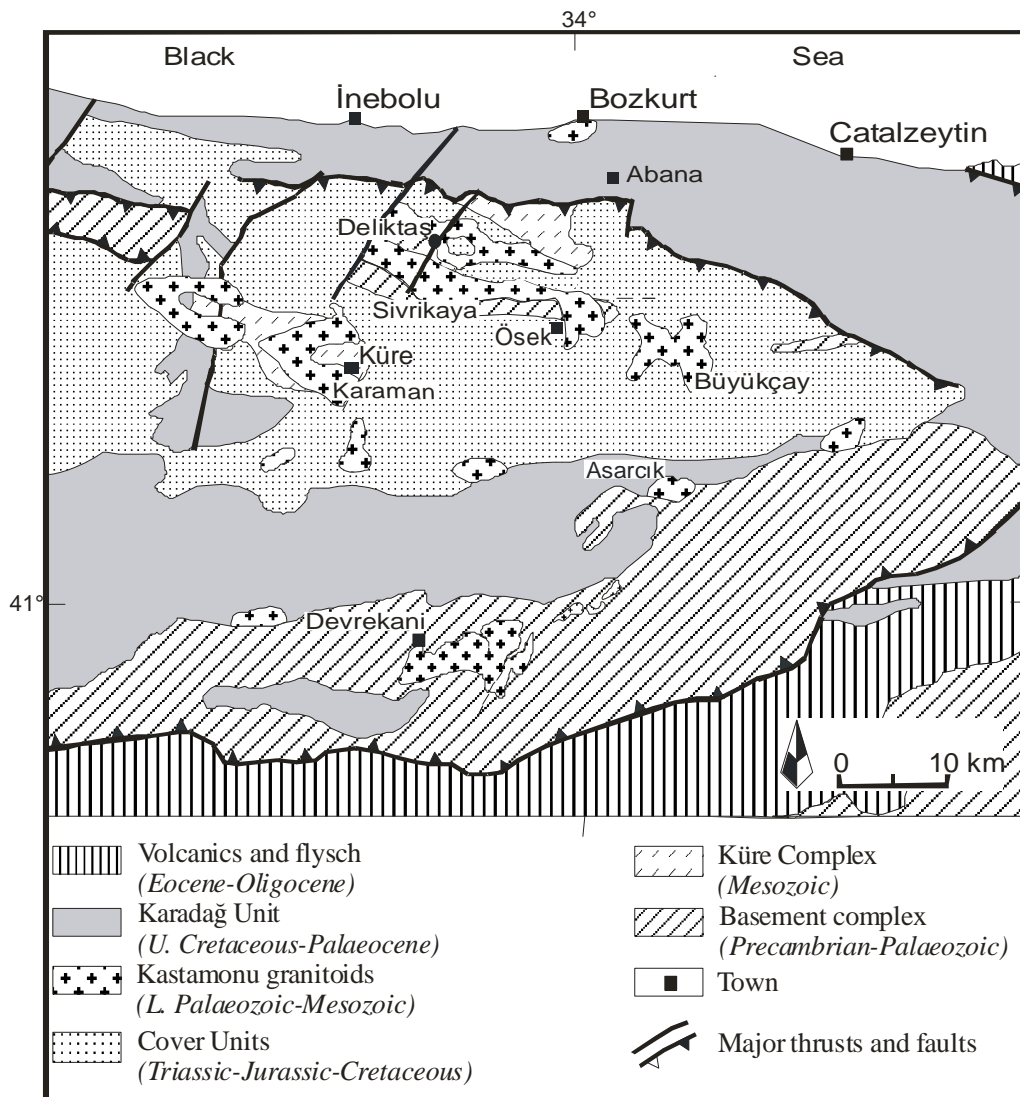


Fig. 1.5- Simplified geological map of the Kastamonu granitoid belt (modified from Aydın et al. 1995; Boztug, 1983).

The first three units are in tectonic contact in the south (Fig. 1.2), and are all intruded by the fifteen plutons of the Kastamonu belt (Boztuğ et al. 1984, 1995; Yılmaz and Boztuğ 1986). The intrusions crop out in an area of about 200 x 50 km² south of İnebolu-Abana towns about 30 km away from the Black Sea coast (Fig. 1.5). In earlier studies Boztuğ et al. (1984, 1995)

and Yılmaz and Boztuğ (1986) attributed all the Kastamonu granitoids to Middle Jurassic arc- and collision-related magmatism, produced during the northward subduction of Palaeotethys oceanic crust beneath south Eurasian margin, that subsequently closed during the Latest Carboniferous-Early Permian/Triassic. However, recent studies (Nzegge et al. in review) attributed the Middle Jurassic Devrekani granitoid to post-collisional magmatism, related to the collision of Gondawa- and Eurasian-derived fragments, following the southward underthrusting and closure of the Küre marginal basin.

Another interpretation is that the granitoids are related to the southward subduction of Palaeotethys beneath the Cimmeridgian continent during the Silurian-Early Carboniferous time (Sengör, 1980). A third possibility refers to them as granitoids related to subduction and closure of the Küre marginal basin in the Middle Jurassic (Robertson and Dixon, 1984; Yılmaz and Boztuğ, 1986; Ustaömer and Robertson, 1997). The genesis of these granitoids remains enigmatic because data necessary to identify the type, origin and emplacement time of all the plutons are not available.

1.4. Aims of this study

There are no reliable age data for the Kastamonu granitoid belt (KGB), due primarily to the lack of published geochronological and geochemical data. Until recent years the Kastamonu granitoids were generally believed to be hybrid products geochemically related through fractional crystallization and emplaced during the Middle Jurassic. Detailed geochemical and geochronological data for the Kastamonu granitoids are very limited and imprecise. The few ages published so far are: K-Ar K-feldspar age of 134 ± 6 Ma obtained from a late pegmatite vein cutting the Deliktaş and Sivrikaya granitoids in the north of the belt (e.g. Boztuğ and Yılmaz, 1991; Yılmaz and Bonhomme, 1991). Boztuğ and Yılmaz (1995) reported K-Ar hornblende and biotite ages of 146 ± 6 to 176 ± 7 Ma and 162 ± 5 Ma respectively, from the Asarcık granitoid in the southeast of KGB. Generally K-Ar biotite and feldspar ages date a cooling process and not intrusion, so that the Middle Jurassic emplacement time assigned to all the plutons of the Kastamonu belt is incorrect.

The main questions are: Are all the Kastamonu granitoids of the same origin but separated only by younger events, did they derive from different geochemically distinct magma chambers and at different times? Is the basement really Eurasian-derived and Variscan? To address these problems zircon U-Pb isotope dilution and Pb-Pb evaporation complemented with isotopic and whole-rock geochemical analyses have been performed, on the three largest

and most accessible granitoids, with contrasting geochemical characteristic (i.e. representative) and their basement.

The ultimate goals are: (1) to present the new major and trace element and isotopic data, and first absolute ages of selected plutons and basement rocks exposed in the Kastamonu area. (2) To discuss the petrogenesis of the plutonic rocks and their tectonic setting. (3) To re-evaluate the relationship between the Precambrian-Palaeozoic Eurasian-derived basement and the Kastamonu granitoids. The data in this thesis will contribute in the understanding of Palaeotethyan subduction processes in the NW Turkey and, the formation, growth and preservation of the Eurasia continental crust in the Central Pontides.

The results reveal Late Palaeozoic to Middle-Mesozoic igneous activities in the Central Pontides, and that the KGB displays many features common to modern collisional belts such as: (1) syn-post-collision-related granitic magmatism associated with the Deliktaş and Sivrikaya granitoids, (2) juvenile magmatism (e.g. Devrekani and Asarcık granitoids), and (3) deformation and regional metamorphism. Besides shedding light on the intrusion time, the data provide the first direct evidence for the existence of Late Variscan magmatic events in the Central Pontides, the involvement of Proterozoic protoliths in magma genesis and pre-Variscan basement relic. Such old ages (Late Palaeozoic) are the first of their kind reported from the KGB, but have been identified in the other parts of the Sakarya Zone. This study therefore, indicates that the magmatism and/or crust-formation processes in the Central Pontides was longer than previously alleged, and thus correlates well with those of the Western and Eastern Pontides.

2. ANALYTICAL METHODS

2.1. Determination of major and trace element concentrations

Rock samples (>5 kg) were splintered using a jaw crusher and splits powdered (grain-size <63 μm) in an Agate mortar. Major and trace elements abundances were determined by X-Ray Fluorescence (XRF) spectrometry (Bruker AXS S4 Pioneer spectrometer) at the University of Tübingen, using standard techniques. Loss on ignition (LOI) was calculated after heating the sample powder to 1000°C for one hour. Major and trace element analyses were performed on fused glass disks made from rock powder/Lithium borate ($\text{Li}_2\text{Br}_2\text{O}_7$, 1.5:7.5) and melted at 1150°C. Total iron concentration is expressed as Fe_2O_3 . Analytical uncertainties range from <1-2 % and 5-16 ppm respectively, for major and trace elements. The trace elements Cs, Th, U, Ta, Hf, Sc and Pb and REE were determined by Inductive Coupled Plasma-Mass Spectrometry (ICP-MS) at the Memorial University of St. John's Newfoundland, Canada using the sodium peroxide (Na_2O_2) sinter technique, which ensures a complete digestion of resistant REE-bearing accessory phases such as zircon and allanite. The detailed analytical procedure, precision and accuracy of the data are outlined in Longerich et al. (1990) and Dostal et al. (1986, 1994).

2.2. Whole-rock Nd-Sr isotopic compositions and Rb-Sr isotopes of minerals

Mineral concentrates were separated from whole-rock samples by standard procedures using jaw crusher, steel rolling mill, Frantz Isodynamic magnetic separator, Wilfley table and heavy liquids. Finally, biotite, muscovite and K-feldspar were hand-picked under the binocular microscope to avoid visible features that might be associated with hydrothermal activity.

For the determination of Nd and Sr isotopic ratios, ~50 mg sample splits of whole-rock and minerals (biotite, K-feldspar and muscovite) were spiked with mixed ^{84}Sr - ^{87}Rb and ^{150}Nd - ^{149}Sm tracer solution, and decomposed in a mixture of conc. HF- HNO_3 in Teflon vials in PTFE bombs at 180°C for 6 days. Digested samples were dried and redissolved in 2.5N HCl. Rb, Sr, Sm, Nd and REE were separated by conventional cation exchange chromatography techniques. Rb, Sm and Nd were run on Re double filaments. Sr was run on W single filament with a Ta-HF activator. A detailed description of the analytical procedures is outlined in Hegner et al. (1995). Isotopic compositions were measured on a Finnigan MAT 262 multi-collector mass spectrometer at the University of Tübingen in data static collection mode. The Sr and Nd isotopic ratios were corrected for mass fractionation by normalizing to $^{86}\text{Sr}/^{88}\text{Sr}=0.1195$ and $^{146}\text{Nd}/^{144}\text{Nd}=0.7219$, respectively. Total procedural blanks were <160 pg for Sr and <80 pg for Nd. Replicate analyses of the NIST-987 Sr standard during the course of this

study yielded a mean value of $^{87}\text{Sr}/^{86}\text{Sr} = 0.71026 \pm 10$ (2σ). Measurement of the Ames Nd standard prepared at Tübingen, within the same period, gave a mean $^{143}\text{Nd}/^{144}\text{Nd}$ ratio of 0.512129 ± 8 (2σ , $n=5$). $^{87}\text{Rb}/^{86}\text{Sr}$ ratios for whole-rock samples were calculated based on the measured $^{87}\text{Sr}/^{86}\text{Sr}$ ratios and the Rb and Sr concentrations determined by XRF. Errors are given in 2 sigma (95 %) confidence level.

2.3. Oxygen isotopes analytical procedures

Minerals were concentrated by hand-picking under the binocular microscope. Quartz was further purified by treating with warm hydrofluoric acid (HF), to eliminate residual feldspars. Oxygen was extracted from ~5mg of silicate minerals and ~10mg of dried whole-rock powder at 550°C using BrF_5 as a reagent following the technique of Clayton and Mayeda (1963). Oxygen yields were between 95 and 100 %. The Oxygen was converted to CO_2 using graphite rod heated by a Pt-coil. CO_2 was analysed for its $^{18}\text{O}/^{16}\text{O}$ ratios with a Finnigan Mat 252 gas source mass spectrometer, at the University of Tübingen. The isotopic ratios are reported in δ -notation relative to Vienna Standard Mean Ocean Water (V-SMOW). All analyses have been duplicated with analytical precision better than ± 0.1 ‰. Replicate analyses of the NBS-28 standard quartz were $\delta^{18}\text{O}_{(\text{V-SMOW})}$ of $+9.7 \pm 0.1$ ‰ (2σ). All data have been normalized to $\text{NBS-28} = +9.7$ ‰.

2.4. U-Pb zircon isotope dilution analyses

For U-Pb analysis, zircons were hand-picked under a binocular microscope to avoid inclusions, turbidity and visible features that might be associated with grains affected by alteration. Single- and multiple-grained fractions were made on the basis of morphology, colour, limpidity and size, and air-abraded (Krogh, 1982). Prior to dissolution, the abraded grains were washed in warm 6N HCl and 7N HNO_3 for about 30 and 10 mins respectively, followed by intermediate and repeated rinsing with ultra-pure water and ultrasonication. After spiking with a mixed $^{205}\text{Pb}/^{235}\text{U}$ tracer solution, zircon fractions were vapour digested by 22N HF in micro-Teflon beakers put in steel-jacketed digestion bombs at 200°C for 6 days, following the procedure of Parrish (1987). After decomposition, HF was replaced by HCl and the bomb was heated at 180°C over night to convert fluorite salts into more soluble chlorite salts. Separation and purification of Pb and U were performed in Teflon mini-columns with a 40 μl anion exchange resin (Bio-Rad, AG1-X8, 100-200 mesh) chromatography (Krogh, 1973) and HBr-HCl- HNO_3 chemistry, following a similar method described in Poller et al. (1997). Pb and U were loaded with silica gel and 1N HNO_3 respectively on Re-filament and measured

in single- and double-filament configuration. Isotopic ratios were measured in a static mode using a Finnigan MAT 262 solid-source multicollector mass spectrometer. The Pb standard NBS 981 was measured for the determination of the thermal fractionation of Pb isotopes and the isotopic ratios were corrected for 0.11% fractionation per atomic mass unit. Total procedural Pb and U blanks were <10 pg. Initial common Pb remaining after correction for tracer and blank was corrected using the Stacey and Kramers (1975) model. U-Pb data were evaluated using the software PbDat (Ludwig, 1994) and were regressed using ISOPLOT program of Ludwig (2000). Errors are given as 2σ standard deviations. The zircon standard 91500/Canada analysed by isotope dilution method during the course of this study yielded nearly concordant U-Pb age of 1065.6 ± 2.2 Ma (e.g. Chen et al., 2002a), consistent with the U-Pb age of 1065.4 ± 0.3 Ma obtained in different laboratories (e.g. Wiedenbeck et al. 1995).

2.5. Pb-Pb zircon evaporation method

The $^{207}\text{Pb}/^{206}\text{Pb}$ zircon evaporation method was performed following the technique developed by Kober (1986, 1987). The measurement of isotopic abundances was performed in dynamic mode with a mass sequence 206-207-208-204-206-207 using an ion counter. Data collection started at 1450°C and the temperature was increased by 20-30°C after each evaporation-deposition cycle. The ages were calculated from $^{207}\text{Pb}/^{206}\text{Pb}$ ratios obtained on a stable ion beam, and only ratios with $^{206}\text{Pb}/^{204}\text{Pb} > 5000$ were considered. Common lead correction was after Cocherie et al. (1992) using a Pb composition with a two-stage evolution (Stacey and Kramers, 1975). Five measurements of Pb standard NBS 981 in ion-counting mode yielded an average fractionation of ~0.1 % per atomic mass unit. This value is considered the best estimate for the fractionation of Pb isotopes, and it was used for the correction of the $^{207}\text{Pb}/^{206}\text{Pb}$ ratio. The errors on the ages are reported as $2\sigma_{\text{mean}}$ of the population of weighted $^{207}\text{Pb}/^{206}\text{Pb}$ ratios. Details on the analytical techniques are given in Chen et al. (2002a, b).

2.6. Cathodoluminescence and internal structure of zircons

Prior to isotopic analysis, representative zircon grains (~63-200 μm) were encased in low luminescence epoxy mount, polished down to expose grains centre. After polishing the mounts were carbon-coated and investigated under cathodoluminescence (CL) and back-scattering imagery using a JEOL JXA-8900RL microprobe at the Institute of Geosciences, University of Tübingen. Operating condition of 15 KV accelerating voltage, 12-15 nA beam current, and a 1 μm beam diameter.

The external morphology and the internal zonation patterns of zircon have been proven to be of petrogenetic and paragenetic significance (e.g. Poldervaart, 1955, 1956; Larsen and Poldervaart, 1957; Hanchar and Miller, 1993; Hoskin and Black, 2000; Hoskin et al. 2000). The internal textures are observed by cathodoluminescence (CL) and back-scattered electron (BSE) imaging (Ono, 1976; Paterson et al. 1989; Vavra, 1990; Benisek and Finger, 1993; Koschek, 1993; Hanchar and Miller, 1993; Hanchar and Rudnick, 1995; Watson and Liang, 1995; Watson, 1996; Cherniak et al. 1997a, b; Rubatto and Gebauer, 2000; Kempe et al. 2000; Corfu et al. 2003; Hoskin and Schaltegger, 2003). These techniques are applicable because of the heterogeneous distribution of elements in most zircons, particularly trace elements. These images allow for visual distinction between oscillatory/magmatic and sector zoning, metamorphic growth zones, preserved igneous cores, new zircon, recrystallized domains and domains showing other types of structural reorganization.

While CL spectra are primarily controlled by trace constituents in zircon, particularly the REE, BSE reveals contrasts in average atomic number of regions of a mineral phase, i.e. the higher the number the brighter the area (e.g. Paterson et al. 1989). CL and BSE images are very similar, except that dark areas in CL are bright in BSE, and vice versa. Some subtleness in zonation is often visible in one but not in the other. For example, CL images of zircons from the Central Pontides usually show more details than BSE images. Both techniques are particularly useful in identifying different growth phases within zircons and to recognize inherited cores and overgrowth patterns (Vavra, 1990, 1994, 1996; Vavra et al. 1996; Hanchar and Miller, 1993; Poller, 1997; Hoskin and Black, 2000; Hoskin et al. 2000). BSE method can give more information on inclusions, which could be further quantitatively identified using the energy dispersion system (EDS). These methods further allow the identification of resorbed areas in zircon grains (e.g. Hanchar and Miller, 1993; Hoskin and Schaltegger, 2003).

The internal structure of zircon could be regarded as primary (formed during crystallization) or secondary (formed after crystallization). Although the internal growth patterns in igneous zircons has been documented in numerous cases (e.g. Pidgeon, 1992; Vavra, 1994; Hoskin et al. 2000 for example), there are relatively few cases of well-described metamorphic zircons (e.g. Hoffmann and Long, 1984; Vavra et al. 1996; Kröner and Willner, 1998; Schaltegger et al. 1999). Vavra et al. (1996) related sector zoning patterns to abrupt changes in zircon growth rate, probably caused by small environmental changes such as temperature or variations in supersaturation of crystallizing particles.

During high-grade metamorphism, some sort of ripening mechanism occurs in which the zircon material contained in small crystals are dissolved and transferred to larger grains,

thereby forming overgrowth (e.g. Hanchar and Millar, 1993; Hanchar and Rudnick, 1995; Vavra et al. 1996), a coarsening mechanism (Poitrasson et al. 2002), by way of solid-state, closed system recrystallization (e.g. Hoskin and Black, 2000; Hoskin et al. 2000) of preexisting zircon along chemical reaction fronts migrating from outer surface towards the interior of the zircon crystals (e.g. Schaltegger et al. 1999), the consequence of recrystallization, the present evidence of partial resetting of the Th/U ratios, U/Pb and Pb/Pb ages (e.g. Pidgeon et al. 1998; Geisler et al. 2002). However, the resistance of zircon confirms that, the total resetting of the U/Pb system in zircon during metamorphism process is a rarity rather than a norm (e.g. Maurel et al. 2002). Recent Pb diffusion experiments on pristine zircon (e.g. Cherniak and Watson, 2000) suggest that mean closure temperatures are in excess of 900°C, higher than that reached during the Variscan metamorphism. In general, resetting appears to depend mainly on the hydrous content of the subducted rocks and on the importance of fluid circulation driving zircon dissolution and recrystallization, or growth of new grain. It is inferred that in the absence of penetrative deformation and fluid circulation at high to moderate pressure, zircon cannot exchange Pb via diffusion, allowing the preservation of pre-metamorphic U/Pb ages (e.g. Maurel et al. 2002). Pb exchange occurs when fluids can freely infiltrate the rocks and partially dissolves zircons, most likely at the time the subducted rocks reached upper crustal levels (e.g. Maurel et al. 2002).

Hence, the combination of CL technique and isotope dilution (ID)-thermal ionization mass spectrometry (TIMS) are very useful tools for geochronology allowing more precise evaluation and better constraints of zircon U-Pb data.

2.7. Classification of rocks-granite types

To stress on their different origin Chappell and White (1974) described the two contrasting granite types in the Lachlan Fold Belt-Australia as: the S- (sedimentary) type, derived from the partial melting of sedimentary source-rocks and I- (igneous) type originating from the melting of igneous rocks. Studies on granitic rocks by O'Neil and Chappell (1977); Chappell and White (1987); White and Chappell (1988); White (1986), have demonstrated that S- and I-type granitoids can be distinguished on the basis of $\delta^{18}\text{O}_{(\text{V-SMOW})}$ values and initial $^{87}\text{Sr}/^{86}\text{Sr}$ ($\text{Sr}_{(i)}$) ratios. For example the S-types are characterized by higher values $\delta^{18}\text{O}$ (10.4 - 12.5 ‰) and initial Sr ratios ($\text{Sr}_{(i)} > 0.708$), while I-types have lower $\delta^{18}\text{O}_{(\text{V-SMOW})}$ values (7.7 - 9.9 ‰) and $\text{Sr}_{(i)}$ ratios (< 0.708). The $\delta^{18}\text{O}_{(\text{V-SMOW})}$ values and initial Sr ratios have then been used as criteria for the classification of I- and S-type granitoids (e.g. Chappell and White, 1974; 1983; Didier et al. 1982; Pitcher, 1982; White and Chappell, 1988).

Table 1.1- Summary classification criteria for I- and S-type granites after Chappell and White (1974, 1983); Didier et al. (1982); White and Chappell (1988)

	I-Type	S-Type
SiO ₂	Variable from mafic to felsic	Narrow range
Hornblende	More abundant than biotite	Muscovite, biotite, no hornblende
Na ₂ O	> 3.2 wt % in felsic and ~2.2 wt % in mafic rocks	<3.2 wt %
ASI	<1.1, metaluminous	>1.1, peraluminous
C.I.P.W. normative corundum	<1%	>1%
Harker trends	More regular linear trends	Irregular trends
⁸⁷ Sr/ ⁸⁶ Sr _(i) ratios	<0.708	>0.708
εNd _(t) values	High and variable	Low and constant
Texture	Often unfoliated, discordant contacts	Foliated, contact aureole
δ ¹⁸ O _(SMOW)	<10 ‰	>10‰

Applying the Chappell and White (1974, 1983); Didier et al. (1982); Pitcher (1982); White and Chappell (1988) criteria and compared to the typical Lachlan Fold Belt granites (Chappell and White, 1992), the Andean granites (Pitcher, 1985) and Hercynian/Variscan granites of Western and Central Europe (e.g. Pagel and Laterrier, 1980; Lameyer et al. 1980, Liew et al. 1989; Barbarin, 1999; Fernandez-Saúrez et al. 2000), the Deliktaş, Sivrikaya and Devrekani granitoids can be classified as S- type, transitional- (e.g. Liew and Hofmann, 1988) to S- type and I-type respectively.

Analyzed Deliktaş samples (DLG) have normative corundum of 2.0 - 5.0 % and ASI > 1.1, Sr_(i) and δ¹⁸O_(V-SMOW) values ranging from 0.7326 - 0.7482 and 11.5 to 12.1 ‰ respectively. Whereas the Sivrikaya granitoid samples (SG) have transitional values of normative corundum (0.9 to 4.7 %), ASI of 0.92 to 1.8, Sr_(i) of 0.704 to 0.708 and δ¹⁸O_(V-SMOW) values of 10.3 to 12.4 ‰. In contrast, the Devrekani rocks (DG) have ASI in the range of 0.76 to 0.94, and Sr_(i) and δ¹⁸O_(V-SMOW) values ranging from 0.705 to 0.706 and 7.2 to 9.5 ‰ respectively. The presence of hornblende xenoliths, the absence of primary muscovite and high HFSEs contents (e.g. Nb and Zr) support I-type sources (low Rb/Zr ratios) for the DG (e.g. Harris et al. 1986).

3. THE SIVRIKAYA (SG) AND DELIKTAŞ (DLG) GRANITES

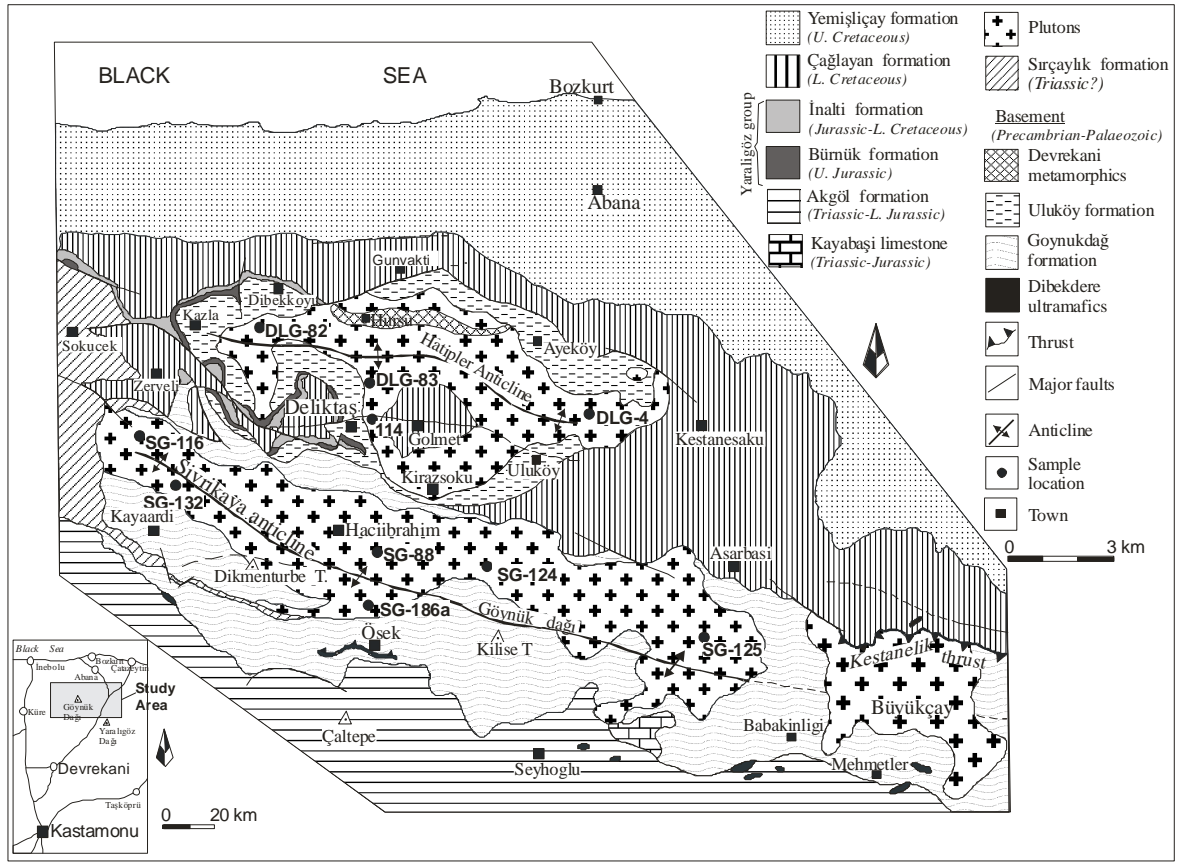


Fig. 3.1- Simplified geological map of Sivrikaya-Deliktaş area (modified after Aydın et al. 1995; Boztuğ and Yılmaz 1983).

3.1. PETROGRAPHY

Sivrikaya samples (SG) were collected at new road cuttings and quarries in the Sivrikaya/Elmalıçay village and SG-186a was collected at the Dikmentürbet village quarry, close to Ösek town (Fig. 3.1). The SG is host to medium- to coarse-grained hornblende-biotite granodiorites, tonalites and two-mica granites. The major mineral assemblage of this granitoid is quartz, K-feldspar (orthoclase-microcline), dark-green hornblende, brown biotite (in mafic members), quartz and euhedral plagioclase (anorthite in the more basic samples). Zircon, calcite, hematite, apatite and allanite are the subordinate phases. In some samples the plagioclase grains are twinned and faintly zoned. Quartz forms aggregates and displays undulatory extinction under polarized light. Locally, biotite and hornblende are partially chloritized and epidotized, and usually contain zircon inclusions (Fig. 3.2).

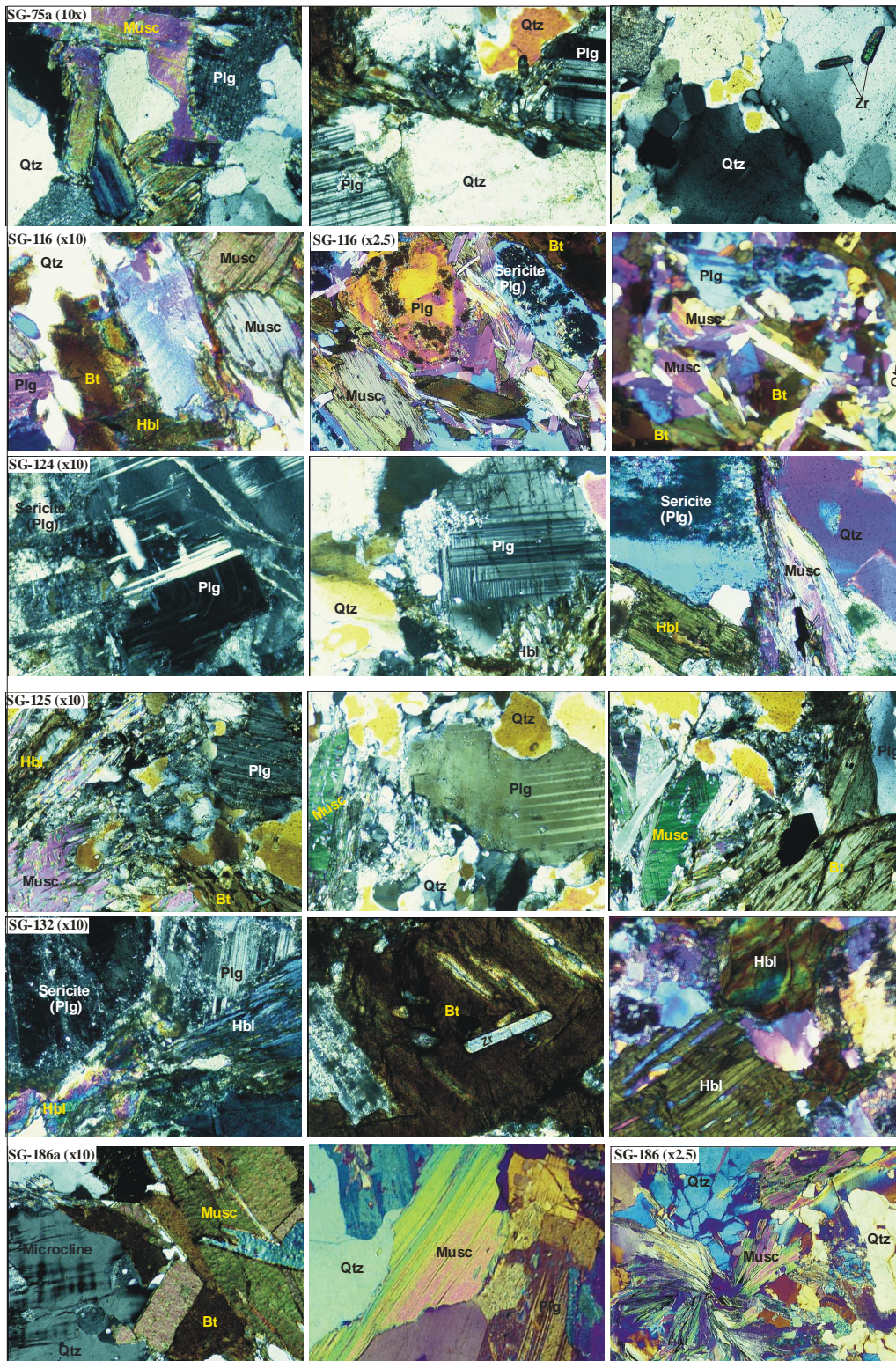


Fig. 3.2- Representative microphotographs showing microstructures of Sivrikaya granite rocks. Abbreviations: *K-F*, k-feldspar; *Bt*, biotite; *Plg*, plagioclase; *Musc*, muscovite; *Hbl*, hornblende; *Qtz*, quartz; *Zr*, zircon.

The presence of hornblende in some SG samples (granodiorites, tonalites) suggests magma-water contents of ≥ 4 wt% (e.g. Naney, 1983). The muscovite in the Sivrikaya leucocratic members is almost completely altered. K-feldspar exhibits a micropertthitic to perthitic texture

wrapped around the plagioclase. Some Sivrikaya samples are relatively poor in silica and alkalis, and rarely orthopyroxene occurs in the more mafic samples.

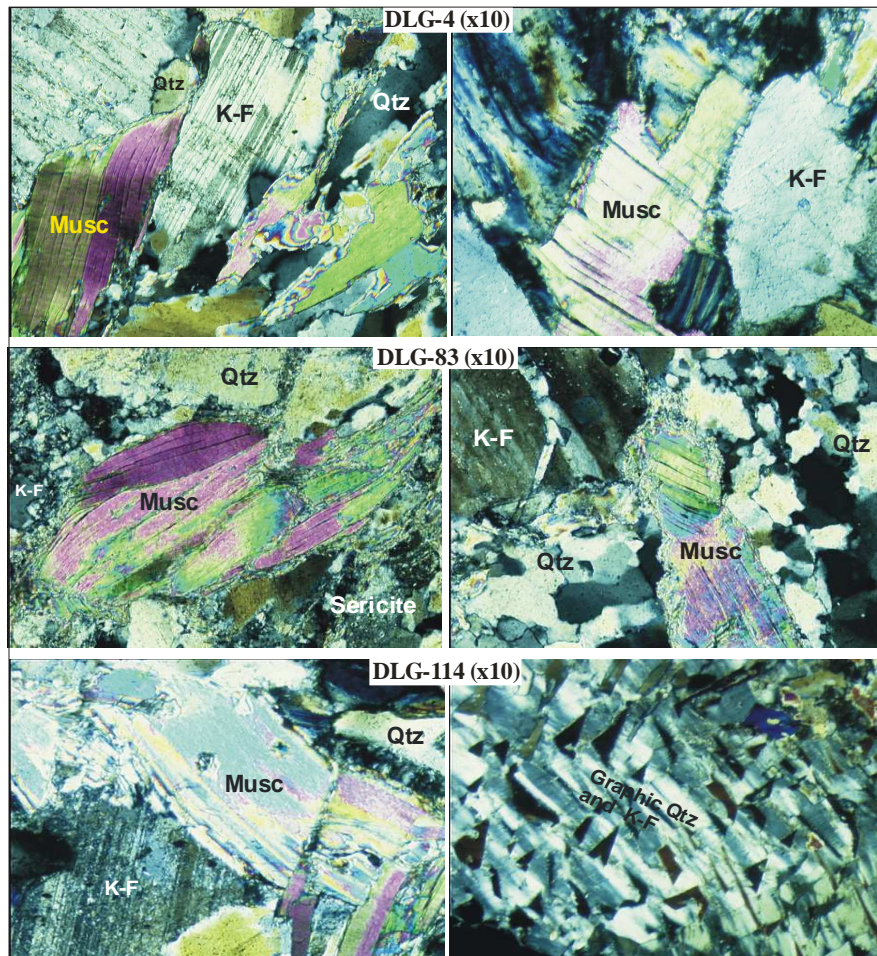


Fig. 3.3a- Representative microphotographs showing microstructures of Deliktaş granite rocks. Abbreviations: *K-F*, k-feldspar; *Bt*, biotite; *Musc*, muscovite; *Qtz*, quartz.

Deliktaş granite rocks are muscovite-rich monzogranites. Samples were collected from quarries and new roads, at a distance of ~500m around the Deliktaş (Ahiçay) village which is located on this pluton and DLG-114 near a pegmatite vein (Fig. 3.1). All of the Deliktaş rocks are leucocratic, predominantly coarse-grained displaying porphyritic texture with K-feldspar and muscovite phenocrysts (Fig. 3.3).

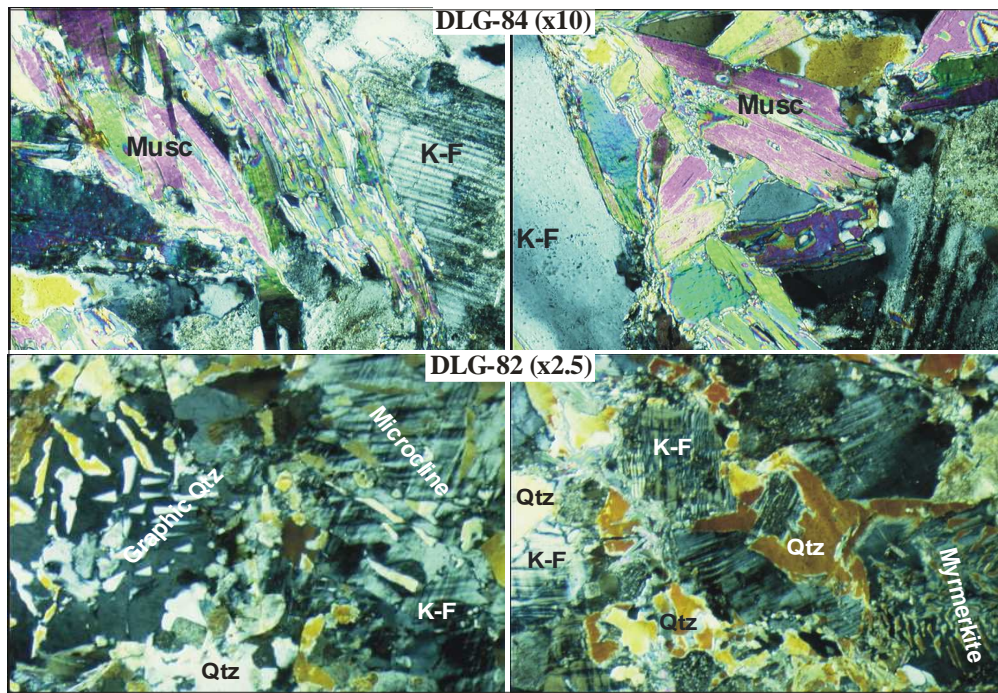


Fig. 3.3b- Representative microphotographs showing microstructures of Deliktaş granite rocks. *K-F*, k-feldspar; *Bt*, biotite; *Musc*, muscovite; *Qtz*, quartz.

In addition to quartz, K-feldspar (albite-orthoclase-microcline), muscovite and plagioclase, minor cordierite, calcite, apatite and zircon occur. Quartz occurs as anhedral crystals partially recrystallized as graphic quartz and myrmekite (Fig. 3.3). K-feldspar is cream-white and occurs as anhedral to subhedral crystals, often displays microcline twinning. Plagioclase is generally sub-euhedral, faintly zoned, twinned and mostly sericitized. Muscovite is coarse-grained, idiomorphic and “apparently primary” (Saavedra, 1978). Rare biotite occurs as minute flakes scattered throughout the rock.

3.2. GEOCHEMISTRY

3.2.1. Major and trace elements geochemistry

Representative geochemical analyses of samples are listed in Table 3.1. Generally the bulk -rock concentrations of the Sivrikaya and Deliktaş granites are characterized by high SiO₂ and low MgO, and low abundances of high-field strength elements (HFSE) (Nb, Th, Ta, Zr and Hf). These features are commonly considered as characteristics of subduction-related (e.g. Floyd and Winchester, 1975; Keppler, 1996). Major and trace elements variations are illustrated in Harker diagrams in Figures. 3.4 and 3.5.

Table 3.1- Major, trace and rare earth element analyses of Deliktaş (DLG) and Sivrikaya (SG) granitoids rocks.

Sample	DLG-82	DLG-83	DLG-4	DLG-84	DLG-114	SG-132	SG-124	SG-125	SG-276	SG-116	SG-115	SG-74	SG-88b	SG-72	SG-75a	SG-186a	SG-72a
SiO ₂	77.1	77.4	77.6	78.5	79.8	68.7	69.0	69.4	69.8	69.9	71.2	74.9	75.0	75.1	75.9	76.0	76.1
TiO ₂	0.04	0.04	0.04	0.03	0.07	0.39	0.39	0.34	0.15	0.36	0.23	0.34	0.07	0.19	0.34	0.04	0.58
Al ₂ O ₃	14.3	13.7	13.2	13.9	11.4	16.2	16.1	15.8	14.5	15.9	15.8	14.5	14.3	11.8	13.7	14.5	15.1
Fe ₂ O ₃	0.64	0.35	0.31	0.57	0.34	3.29	3.08	2.89	1.19	2.77	1.95	0.35	0.67	0.73	0.56	0.42	0.26
MnO	0.04	0.01	0.00	0.06	0.00	0.08	0.06	0.08	0.03	0.06	0.03	0.00	0.02	0.003	0.00	0.01	0.00
MgO	0.18	0.12	0.11	0.15	0.13	0.99	1.13	0.83	0.55	0.84	0.63	0.15	0.25	0.14	0.11	0.12	0.21
CaO	0.37	0.22	0.22	0.51	0.14	3.55	0.45	2.48	3.10	3.32	3.57	0.12	0.39	0.10	0.12	0.22	0.07
Na ₂ O	4.44	3.85	3.67	4.82	2.63	3.79	3.73	3.87	4.17	3.96	4.02	2.19	4.14	1.74	3.12	4.75	1.76
K ₂ O	3.67	5.16	5.16	2.14	4.66	1.54	3.36	3.01	3.04	1.94	1.80	5.48	3.98	4.55	5.28	3.43	4.87
P ₂ O ₅	0.08	0.06	0.05	0.11	0.03	0.11	0.17	0.16	0.07	0.14	0.15	0.04	0.09	0.05	0.03	0.06	0.04
LOI	0.84	0.54	0.83	0.85	0.81	1.67	2.20	1.46	3.78	1.46	0.73	1.63	1.18	1.58	1.28	1.05	2.48
Sum	101.7	101.5	101.3	101.7	101.9	100.6	101.8	102.0	102.2	100.7	100.1	100.2	100.5	100.5	100.7	100.7	100.0
ASI	1.20	1.11	1.10	1.25	1.18	1.13	1.52	1.12	0.92	1.08	1.05	1.49	1.21	1.5	1.24	1.21	1.82
Mg#	54.8	59.4	61.6	54.2	63.6	56.9	61.8	55.9	66.9	57.3	58.8	65.1	62.0	45.8	46.8	55.7	77.8
Cr	2.2	6.0	2.4	5.9	1.9	45.9	7	6.3	52.3	33	58	12	5	24.0	29	16.8	27
V	5	4	2	<0.1	4	29.0	37	31	15.9	28	16	19	2	50.9	14	4.2	39
Li	7.54	8.18	7.31	—	12.85	24.82	<0.1	28.16	<0.1	<0.1	<0.1	<0.1	5.34	7.52	<0.1	<0.1	<0.1
Rb	142	127	136	138	150	49.5	124	100.1	87.0	69	66	254	135	29.0	272	117.8	207
Sr	73	71	67	53	75	408.6	164	382.0	253.6	345	330	52	141	166.0	69	55.2	74
Y	14.7	9.0	18.0	10.5	18.2	12.4	19	18.4	13.7	14	15	28	15	32.7	29	20.1	27
Zr	93.4	79.2	86.5	90.3	133.9	224.5	172	181.2	115.6	197	203	206	94	122.4	196	100.1	247
Nb	15.4	19.1	10.6	12.7	14.8	10.0	16	20.8	0.0	0	0	13	19	7.1	13	8.4	14
Cs	2.67	0.86	0.78	—	1.36	3.25	<0.1	3.67	<0.1	<0.1	<0.1	<0.1	2.88	1.17	<0.1	<0.1	<0.1
Ba	306	430	341	56	418	457	629	872	990	488	491	287	448	558	318	185	334
La	13.5	14.3	32.0	16.0	27.1	50.9	31	40.0	20.7	44	22	46	17	33.0	41	17.4	42
Ce	11.4	6.3	4.8	<0.1	42.1	64.0	62	71.1	34.3	62	0	85	13	42.9	80	<0.1	82
Pr	1.35	0.82	0.59	—	5.16	6.19	—	7.94	<0.1	<0.1	<0.1	<0.1	1.44	5.05	<0.1	<0.1	—
Nd	13.9	23.3	4.1	14.0	24.8	31.5	29	33.3	10.4	30	14	30	16	20.2	42	9.1	37
Sm	3.0	4.9	0.9	3.9	5.2	5.7	6	5.87	3.1	4	<0.1	6	4	4.5	5	29.5	7
Eu	0.25	0.21	0.19	<0.1	0.27	1.15	0.70	1.20	0.70	1.00	0.30	0.70	0.31	0.78	0.20	<0.1	0.40
Yb	1.2	0.6	0.6	0.8	5.0	0.7	1.5	1.4	1.1	0.9	0.8	2.1	1.2	3.2	2.3	1.7	1.9
Gd	1.16	0.54	0.45	—	4.13	1.66	—	4.17	—	—	—	—	1.14	4.67	—	—	—
Tb	0.23	0.10	0.10	—	0.65	0.20	—	0.55	—	—	—	—	0.22	0.75	—	—	—
Dy	1.54	0.66	0.85	—	3.95	1.02	—	2.80	—	—	—	—	1.38	4.96	—	—	—
Ho	0.30	0.14	0.15	—	0.76	0.17	—	0.45	—	—	—	—	0.27	1.08	—	—	—
Er	1.00	0.50	0.48	—	2.15	0.42	—	1.12	—	—	—	—	0.79	3.30	—	—	—
Tm	0.17	0.07	0.08	—	0.32	0.06	—	0.16	—	—	—	—	0.13	0.50	—	—	—
Lu	0.17	0.06	0.08	—	0.30	0.04	—	0.12	—	—	—	—	0.15	0.49	—	—	—
Hf	1.13	0.39	0.61	—	1.16	0.70	—	1.54	—	—	—	—	1.67	1.25	—	—	—
Ta	3.34	0.43	0.21	—	1.52	0.38	—	1.73	—	—	—	—	4.89	0.37	—	—	—
Pb	33.2	33.2	36.3	25.3	27.9	14.3	23	52.6	27.4	11	15	34	44	9.0	30	26.0	11
Th	3.7	0.9	1.4	15.1	21.8	11.9	13	14.6	10.9	12	5	23	6	6.3	23	8.1	18
U	5.2	1.3	2.1	1.3	1.2	4.8	0	1.9	0.8	4	3	<0.1	15	0.9	<0.1	<0.1	<0.1
Co	0.0	0.0	0.0	0.0	0.0	3.3	4	3.1	0.0	3	1	<0.1	0	7.5	<0.1	<0.1	<0.1
Ni	0.0	0.0	0.0	0.0	0.0	15.6	0	0.0	10.7	2	16	<0.1	0	6.4	<0.1	<0.1	<0.1
Zn	0.0	0.0	0.0	0.0	2.4	51.6	63	54.3	10.5	36	21	<0.1	0	17.8	<0.1	<0.1	<0.1
Mo	0.20	0.18	0.00	—	0.00	6.00	—	0.14	—	—	—	—	0.07	3.16	—	—	—
Tl	0.46	0.58	0.62	—	0.67	0.19	—	0.53	—	—	—	—	0.59	0.06	—	—	—
Bi	5.54	0.02	0.02	—	0.03	0.14	—	0.33	—	—	—	—	0.98	0.05	—	—	—
Eu/Eu*	0.31	1.19	0.92	—	0.18	1.15	—	0.75	—	—	—	—	0.42	0.53	—	—	—
Nb/Ta	4.6	13.3	15.6	—	13.4	19.4	—	12.0	—	—	—	—	3.9	19.1	—	—	—
[La/Yb] _N	7.6	15.9	35.5	13.4	3.6	48.6	13.7	19.1	12.6	32.5	18.3	14.5	9.5	6.8	12.0	6.8	14.8
[Gd/Yb] _N	0.8	0.7	0.6	—	0.7	1.9	—	2.4	—	—	—	—	0.8	1.1	—	—	—
Sr/Y	5.0	7.9	3.7	5.0	4.1	33.0	8.7	20.8	18.5	24.0	22.8	1.9	9.4	5.1	2.4	2.7	2.7
Fe ₂ O ₃ /MgO	3.6	3.0	2.7	3.7	2.5	3.3	2.7	3.5	2.2	3.3	3.1	2.4	2.7	5.2	5.0	3.5	1.3
K ₂ O/Na ₂ O	0.83	1.34	1.41	0.44	1.77	0.41	0.90	0.78	0.73	0.49	0.45	2.50	0.96	2.76	1.69	0.72	2.76

- = not determined; ASI= aluminium saturation index= [molar Al₂O₃/(CaO+K₂O+Na₂O)];
Mg# = 100 x molar [MgO/(MgO+0.9xFe₂O₃)]; (Eu/Eu* = √[Sm_{cn}x Gd_{cn}])

The samples exhibit a narrow range of SiO₂ content, 68 to 79 wt % for the Sivrikaya and 77 to 78.5 wt % for Deliktaş (except for one pegmatite sample DLG-114, 79.8 wt %). MgO, Al₂O₃, Fe₂O₃ and CaO decrease slightly with increasing SiO₂, whereas K₂O remain nearly constant. SG rocks exhibit a cluster of data in two groups, the intermediate and felsic samples (Fig. 3.4).

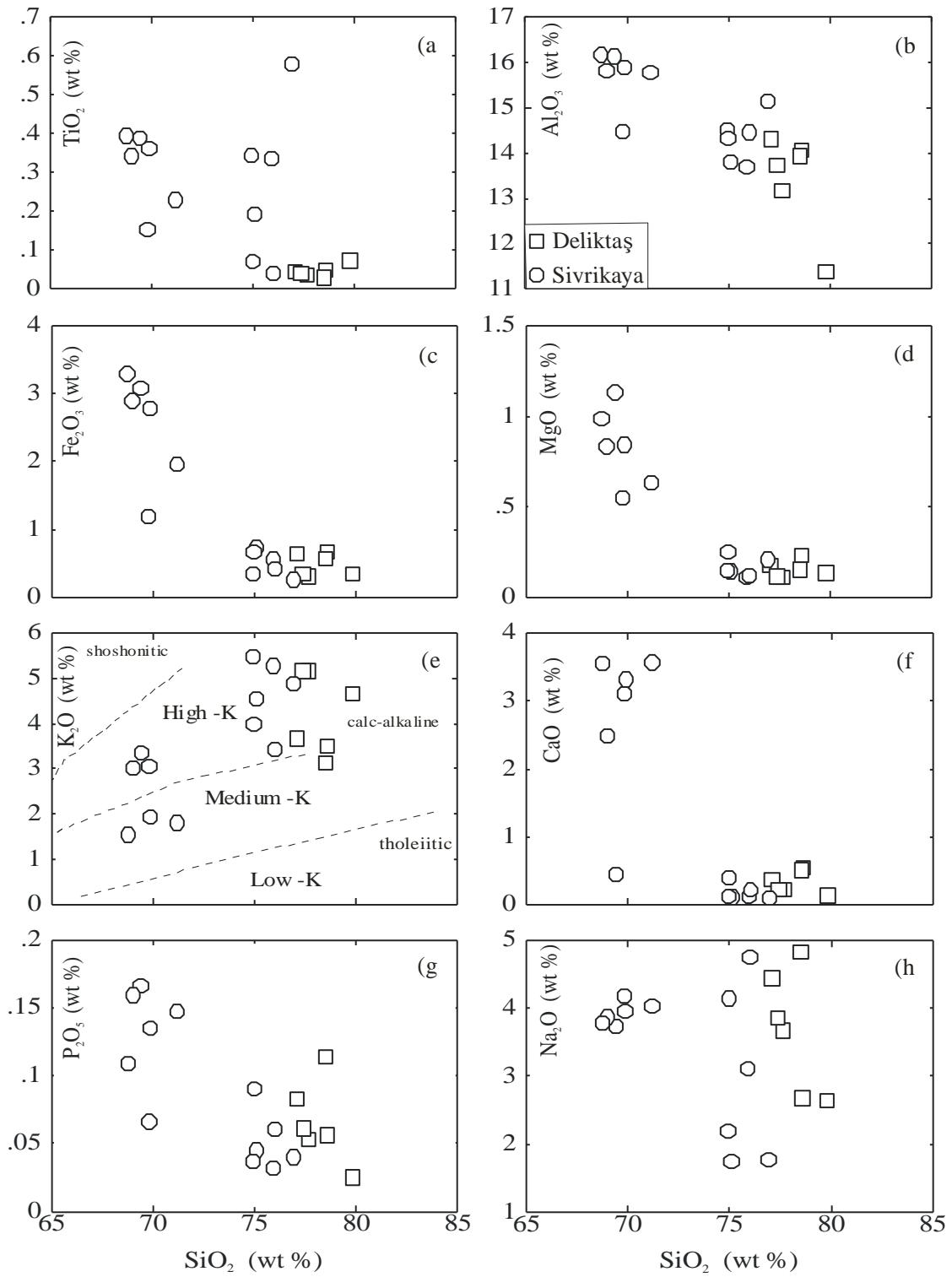


Fig. 3.4- Selected Harker variation plots of major elements (wt %) for Deliktaş and Sivrikaya granitoids samples. (e) Shows field boundaries between medium-K (normal calc-alkaline) and high-K series of Peccerillo and Taylor (1976)

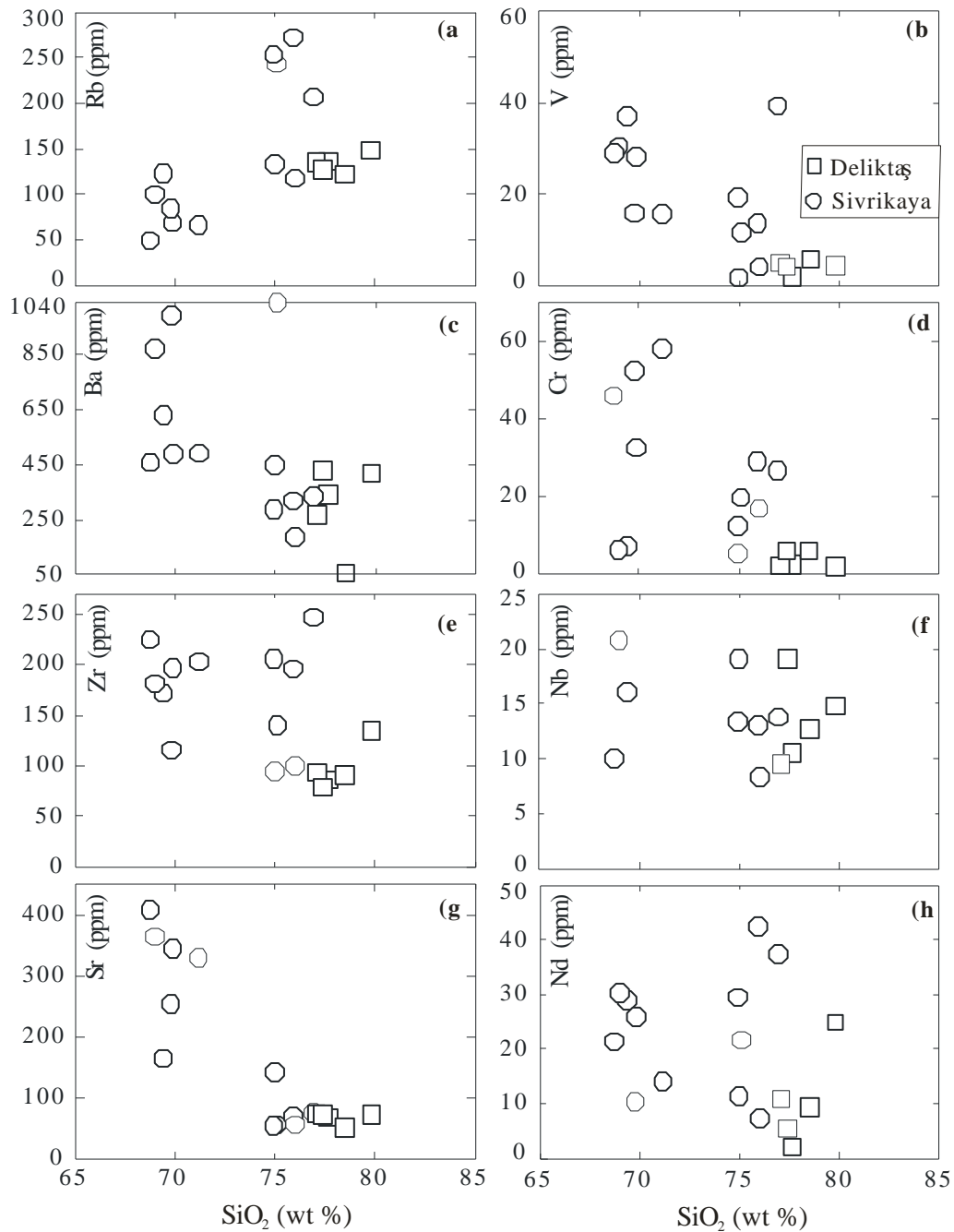


Fig. 3.5- Harker variation plots of selected trace elements for Deliktaş and Sivrikaya granitoids samples.

In terms of normative mineralogy, the Sivrikaya granite has tonalitic-granodioritic to granitic compositions (Fig. 3.6). In contrast, the Deliktaş granite melt approach minimum melt compositions (e.g. Tuttle and Bowen, 1958; Johannes and Holz, 1996). The molar A/CNK vs. A/NK diagram (Maniar and Piccolli 1989) defines the rocks as slightly metaluminous to strongly peraluminous, and of transitional to S-type character (Fig. 3.7a) (e.g Chappell, 1999).

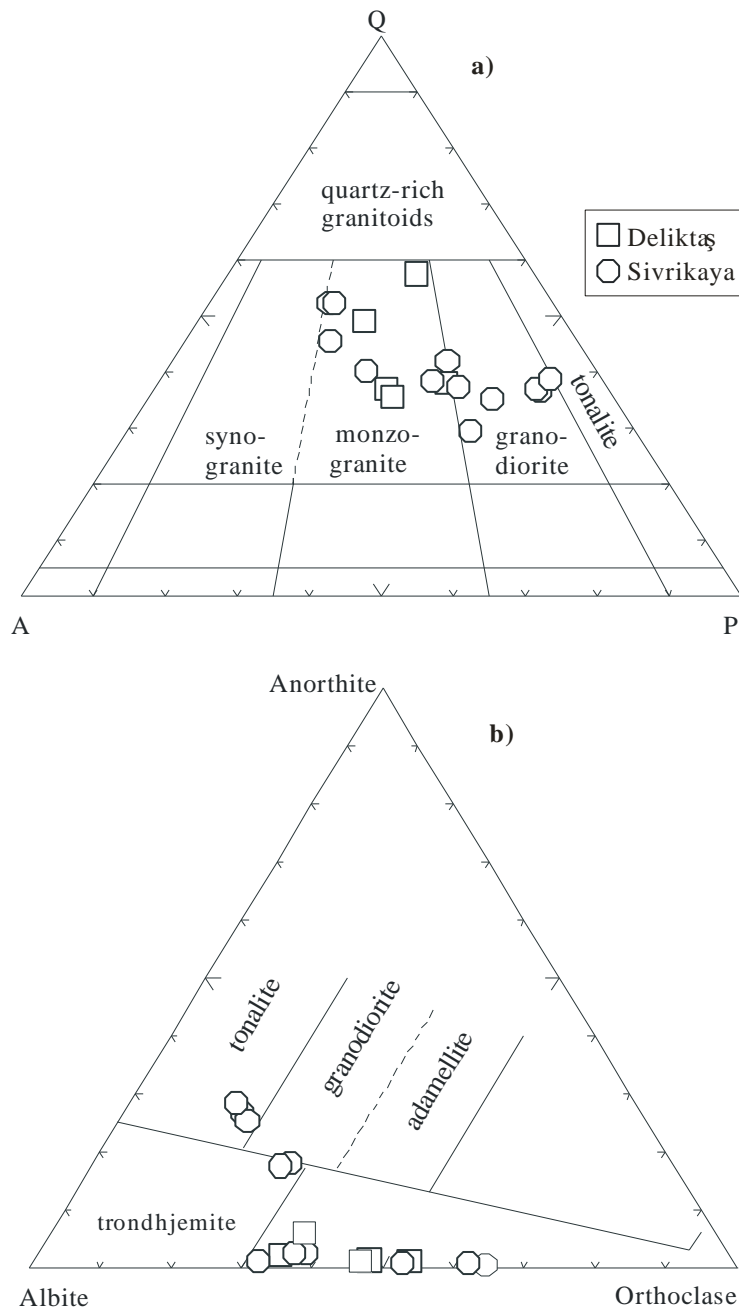


Fig. 3.6- (a) Ternary diagram illustrating the compositions of Deliktaş-Sivrikaya granites. Nomenclature from Le Maitre (1989): quartz (Q); alkali feldspar (A); plagioclase (P) and (b) The An-Or-Ab diagram of Baker (1979) and O'Connor (1965).

All samples are of sub-alkaline affinity, belong to the calc-alkaline series (Figs. 3.7b-c), and plot in the volcanic arc granitoids field of the Pearce et al. (1984) diagram. The K_2O vs. SiO_2 plot shows Deliktaş samples to be dominantly of high-K affiliation (Fig. 3.4e). Sr shows two groups of rocks for SG, but rather constant contents in the DLG (Fig. 3.5f). Although some rocks of both granitoids exhibit typical high-K, calc-alkaline compositions, the variation diagrams reveal some differences between them (Figs. 3.4, 3.5). The Deliktaş rocks exhibit a higher and smaller range in SiO_2 content. Among the trace elements, samples of Sivrikaya show a much larger range in concentration than those from Deliktaş granitoid, indicating that

the DLG was not derived by crystal-liquid fractionation processes from SG, but could represent a distinct group of rocks derived from different sources.

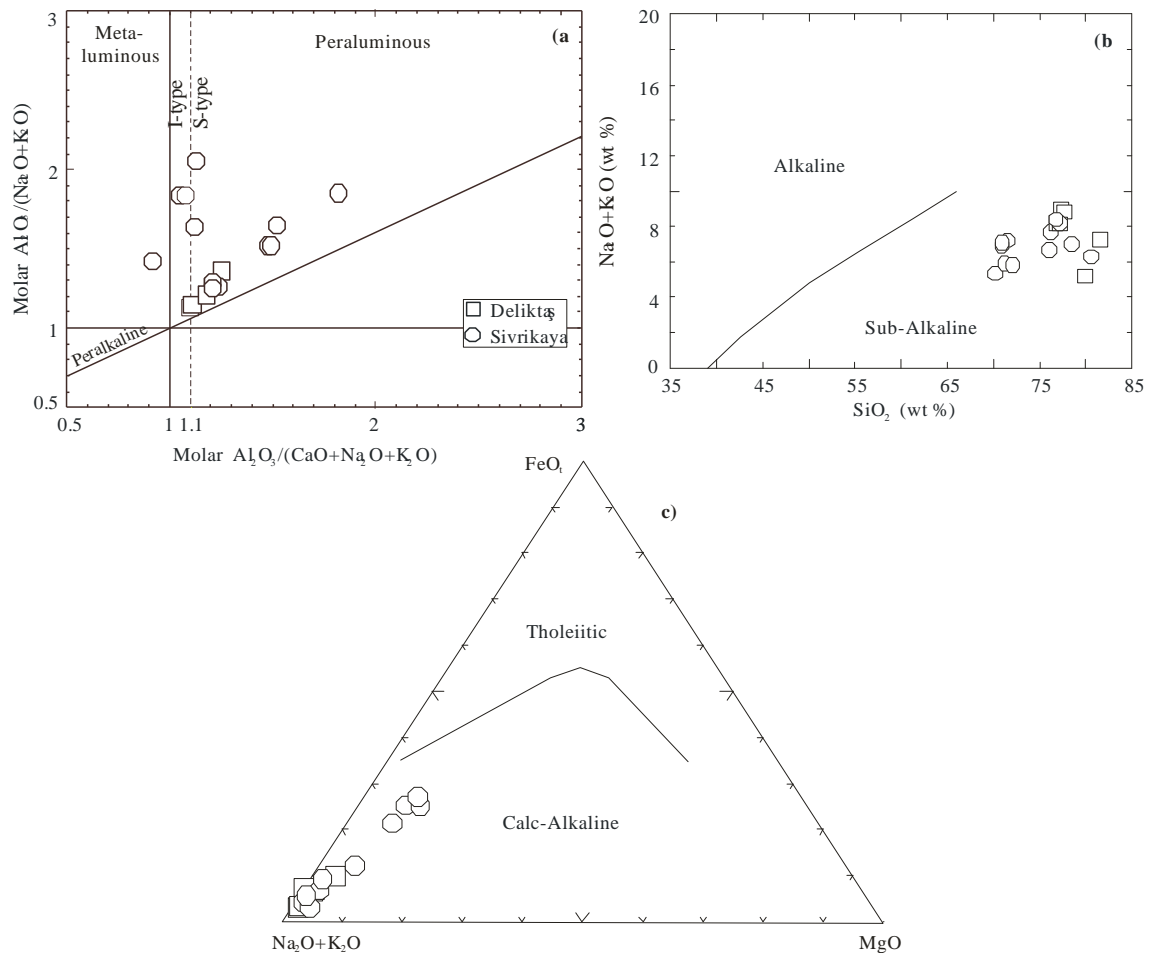


Fig. 3.7- Geochemical composition of Deliktaş and Sivrikaya plutons plotted on the (a) A plot of Shand's Index with fields of different granite-types after Maniar and Piccolli (1989), and (b) SiO_2 vs. alkaline and (c) Calc-alkaline diagrams of Irvine and Baragar (1971, 1989)

Some aspects of the chemical variations between the SG granitic samples and the DLG monzogranites could be interpreted as evidence for a comagmatic linkage between these granitoids. However, there are important differences, such as the higher Rb contents, and much higher Rb/Sr ratios, that precludes such an interpretation. Also, in terms of Sr, Nd and O isotopic compositions DLG has a more crustal signature. Taken together, this suggests that the protolith of the DLG was more crustally evolved and distinct from the SG. Jakes and White (1971, 1972) proposed that differences between calc-alkaline rocks from island arcs and continental margins have genetical significance. The main differences between the two series: SiO_2 range, K_2O/Na_2O ratio and K_2O , Rb, Ba, Sr, Th, U and Zr abundances are all thought to be higher in the continental margin calc-alkaline suite.

3.2.2. Rare earth elements

Chondrite-normalized (cn, Sun and McDonough, 1989) REE patterns are plotted in Fig. 3.8. The patterns of all samples from both plutons are characterized by fractionation of the light and heavy REEs. The Sivrikaya samples are characterized by moderately fractionated REE patterns ($[La/Yb]_{cn} = 6.8-49$) and flat to concave-upwards HREE ($[Gd/Yb]_{cn} = 0.76 - 2.37$) patterns, and have mostly very small Eu-anomalies ($Eu/Eu^* = 0.42 - 1.15$).

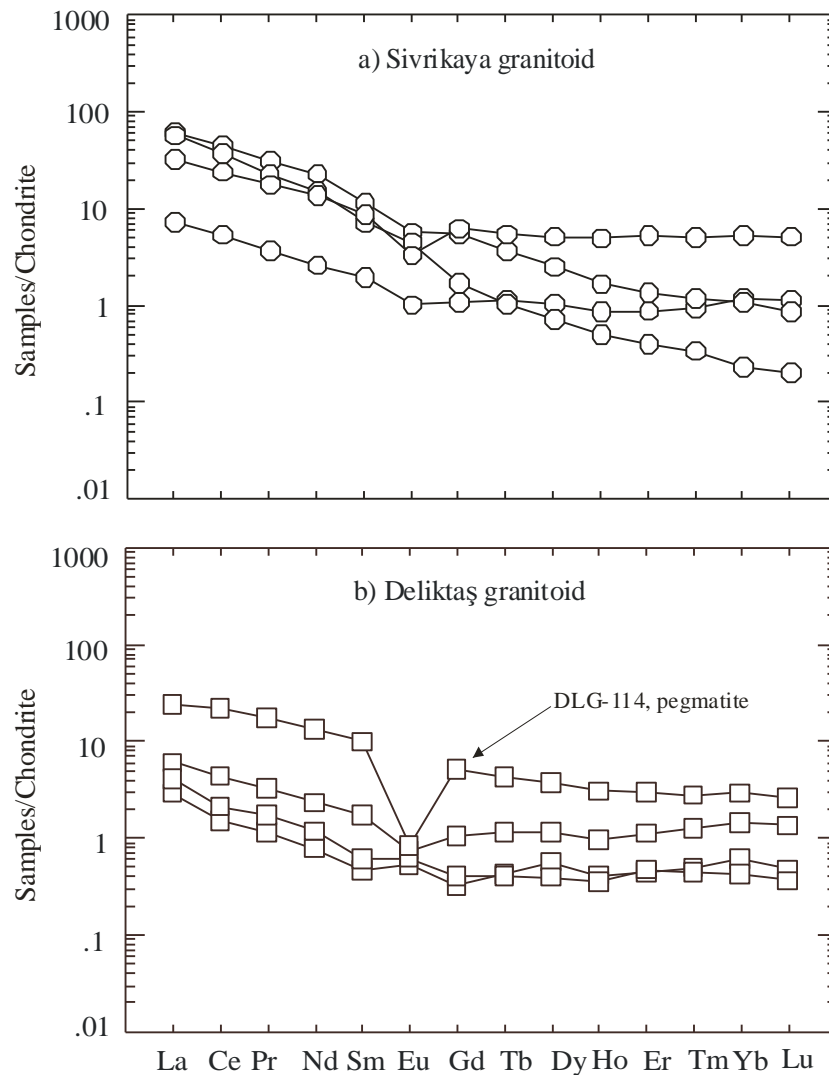


Fig. 3.8- Chondrite-normalized rare earth element abundances for Deliktaş and Sivrikaya granitoids. Normalizing values from Taylor and McLennan (1985).

The Deliktaş samples exhibit less fractionated REE patterns ($[La/Yb]_{cn} = 3.6 - 35.5$), flatter HREE ($[Gd/Yb]_{cn} = 0.59 - 0.78$), and have positive to negative Eu anomalies ($Eu/Eu^* = \sqrt{[Sm_{cn} \times Gd_{cn}]} = 0.18 - 1.19$). The pegmatite sample, DLG-114 has the highest absolute REE abundances but the lowest $[La/Yb]_{cn}$ ratio (3.6), which shows slight enrichment of middle REEs (Gd to Er) relative to the other HREEs. SG samples yielded moderate amount of zircons, while DLG samples are very poor in this mineral. As zircon has very high affinity for

HREE (Gromet and Silver, 1983), the different abundances of zircon may be sufficient to explain the different HREE patterns. From these considerations, it appears possible that the SG owe its origin to mantle-derived magmas that assimilated the amphibolitic basement rocks while undergoing fractionation. Primitive mantle-normalized (Sun and McDonough, 1989) trace elements show enrichment in large ion lithophile elements (LILE) (e.g. Cs, Rb, Th, K and U) and SG samples exhibit troughs for HFSE (Nb and Ti) (Fig. 3.9). Whereas, DLG samples virtually have no negative Nb anomalies but more distinct Ti depletion.

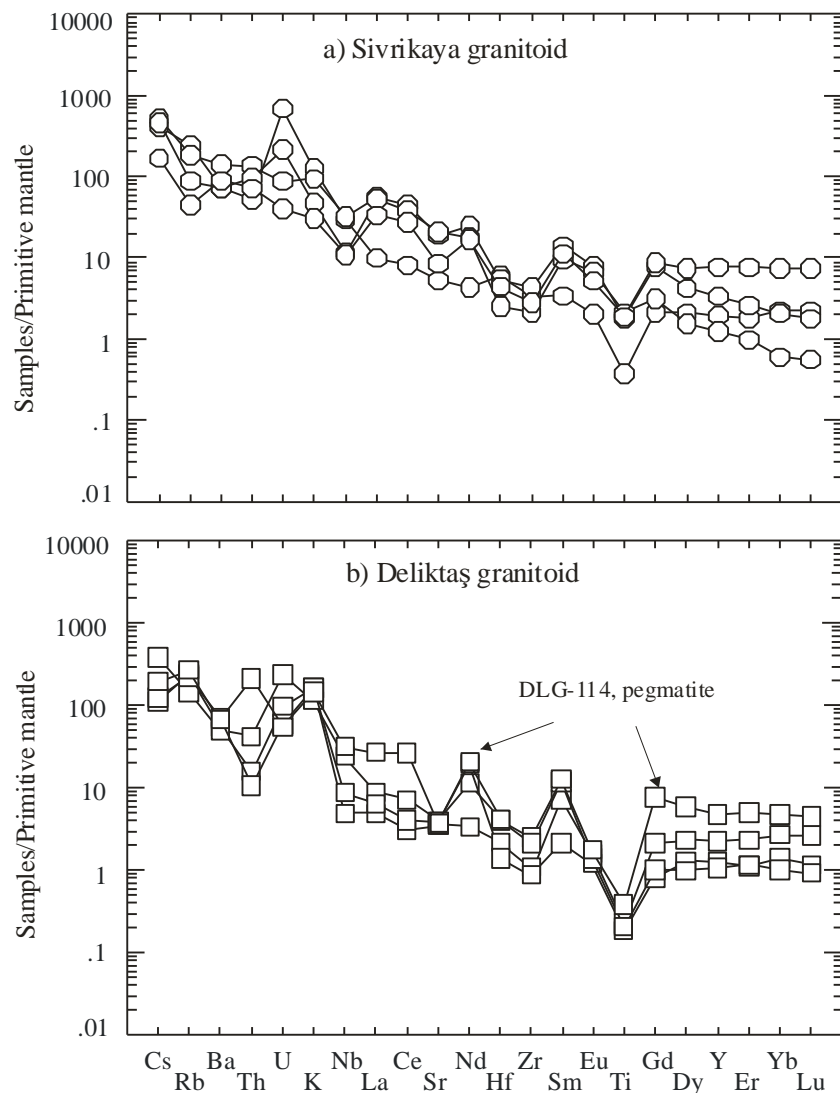


Fig. 3.9- Primitive mantle-normalized trace element abundances for the Deliktaş and Sivrikaya granitoids. Normalizing values are from Taylor and McLennan (1985).

Negative Ti anomaly can be attributed to fractional crystallization of accessory phases, e.g. allanite and titanite. Some samples show decoupling of Ba and Sr from Rb and K as indicated by the troughs for Ba and Sr. Geochemical and geochronological (U-Pb, see below) data indicate that the protolith for SG rocks were essentially of igneous origin, while those for DLG were sedimentary.

3.2.3. Sr-Nd-O isotopic compositions

The Nd, Sr and O isotope data are presented in Table 3.2. Calculated initial $^{87}\text{Sr}/^{86}\text{Sr}$ ($\text{Sr}_{(i)}$) and $^{144}\text{Nd}/^{143}\text{Nd}$ ($\epsilon\text{Nd}_{(t)}$) isotopic compositions are based on U-Pb and Pb-Pb zircon ages of 300 Ma for Sivrikaya and 295 Ma for Deliktaş. The isotopic data highlights the considerable crustal residence age of the source region and show that the granitoids magmas do and/or do not represent new additions to the crust. Possible protoliths could be lower crust, and consisting of amphibolites and metagreywackes. Figure 3.10a-b shows the variation of initial $^{143}\text{Nd}/^{144}\text{Nd}$ ($\epsilon\text{Nd}_{(t)}$) values with initial $^{87}\text{Sr}/^{86}\text{Sr}$ ($\text{Sr}_{(i)}$) isotopic ratios. For Deliktaş samples $\epsilon\text{Nd}_{(t)}$ values decrease with increasing $\text{Sr}_{(i)}$. Sivrikaya samples have similar $\epsilon\text{Nd}_{(t)}$ but lower $\text{Sr}_{(i)}$ values. Sivrikaya rocks show relatively large variations in isotopic composition ($\epsilon\text{Nd}_{(t)} = -1.0$ to -3.8 ; $\text{Sr}_{(i)} = 0.7040 - 0.7080$) further suggesting their derivation from heterogeneous and old sources. The wide range in $\epsilon\text{Nd}_{(t)}$ values and $\text{Sr}_{(i)}$ ratios of the SG samples, and high Sr content indicate low degree of partial melts of mantle and/or plagioclase fractionation. The relatively high $\epsilon\text{Nd}_{(t)}$ values shown by some samples (-1 to -2) further suggest involvement of mantle or mafic crustal sources. However, a young, more siliceous, LREE-enriched crustal source cannot be ruled out, such as detritus from young calc-alkaline arc-rocks which likely were part of the source region of this granitoid. Furthermore, the small to strong negative $\epsilon\text{Nd}_{(t)}$ values and low $\text{Sr}_{(i)}$ ratios, indicate significant input of mantle-derived component during magma generation. Young T_{DM} ages of SG rocks (0.75-1.08 Ga) indicate the presence in their source of a component with short crustal residence time. Such a source is compatible with young calc-alkaline arc-rocks (Ghosh and Lambert, 1989).

Sivrikaya $\delta^{18}\text{O}_{\text{whole-rock}}$ values are slightly lower and more variable in the range of 10.0 to 11.6 ‰, ~12 ‰ for quartz and ~6 ‰ for biotite. The wider range in $\delta^{18}\text{O}_{\text{whole-rock}}$ values of the Sivrikaya samples, reflect a heterogeneous source. There is a slight positive correlation between $\delta^{18}\text{O}$ and $\text{Sr}_{(i)}$ and SiO_2 values indicated for the Deliktaş samples (Fig. 3.10b-c). The $\delta^{18}\text{O}$ values of the Deliktaş samples are high with a narrow range from 11.5 to 12.1 ‰ for whole-rocks, restricted 13 ‰ for quartz and 11.5 ‰ for K-feldspar. These values are typical of intracrustal melts or “S-type” granites (e.g. Taylor, 1968; O’Neil and Chappell, 1977).

Table 3.2- Sm-Nd; Rb-Sr and O isotopic data of the Deliktaş and Sivrikaya granitoids

Samples	Sm	Nd	$^{143}\text{Nd}/^{144}\text{Nd}$	$^{147}\text{Sm}/^{144}\text{Nd}$	$^{143}\text{Nd}/^{144}\text{Nd}$	$\epsilon\text{Nd}_{(t)}$	T_{DM}	Rb	Sr	$^{87}\text{Rb}/^{86}\text{Sr}$	$^{87}\text{Sr}/^{86}\text{Sr}$	$^{87}\text{Sr}/^{86}\text{Sr}$	$^{87}\text{Sr}/^{86}\text{Sr}$	$\delta^{18}\text{O}_{(\text{VSMOW})}$			Age at $2\sigma_m$ (Ma)
														^{144}Nd	^{144}Nd	^{144}Nd	
Sivrikaya																	
SG-88b	4.4	16.4	0.512492 ± 09	0.2197	0.512058	-3.7	1.08	135	141	3.912 ± 10	0.72460 ± 11	0.70790	0.70790	11.6	-	-	-
SG-124	5.5	29.4	0.512300 ± 09	0.0773	0.512147	-2.0	0.83	123	164	2.185 ± 10	0.71423 ± 10	0.70451	0.70451	11.1	12.2	-	6.2
SG-125	5.9	33.2	0.512282 ± 09	0.1147	0.512056	-3.8	1.08	100	382	0.750 ± 10	0.71103 ± 11	0.70783	0.70783	10.2	11.9	-	-
SG-116								69	345	0.557 ± 10	0.73440 ± 10	0.73158	0.73158	-	-	-	-
SG-116 (KF)								152	345	1.276 ± 10	0.71110 ± 9	-	-	-	-	-	-
SG-116 (Bt>180 μm)								409	3.4	398.8 ± 10	2.24570 ± 19	-	-	-	-	-	-
SG-116 (Musc)								308	41.3	177.8 ± 10	1.44870 ± 11	-	-	-	-	-	-
SG-132	5.7	31.5	0.512335 ± 10	0.0689	0.512199	-1.0	0.75	50	409	0.342 ± 10	0.70840 ± 10	0.70694	0.70694	10.8	12.3	-	6.1
SG-132 (KF)								209	24.3	4.118 ± 10	0.71844 ± 9.5	-	-	-	-	-	-
SG-132 (Bt, 300-180 μm)								264	5.1	158.79 ± 10	1.33150 ± 12	-	-	-	-	-	276.5 ± 2.8
SG-132 (Bt>300 μm)								254	5.2	148.74 ± 10	1.28370 ± 13	-	-	-	-	-	272.6 ± 2.7
SG-186a	9.1	29.5	0.512529 ± 10	0.1865	0.512162	-1.7	1.00	118	55	5.884 ± 10	0.73246 ± 10	0.70642	0.70642	11.4	-	-	-
SG-186a (Musc)								561	2.4	971.6 ± 10	4.60007 ± 50	0.70642	0.70642	11.4	-	-	281.7 ± 2.8
SG-276	3.1	10.4	-	-	-	-	-	87	254	1.545 ± 10	0.71070 ± 10	0.70408	0.70408	12.4	-	-	-
Deliktaş																	
DLG-4	0.9	4.1	0.512349 ± 09	0.1285	0.512105	-2.8	1.23	136	67	5.889 ± 10	0.73554 ± 10	0.71124	0.71124	11.6	13.3	11.5	-
DLG-4 (Musc)								472	6.9	215.8 ± 10	1.58138 ± 19	-	-	-	-	-	283.2 ± 2.8
DLG-82	3.0	13.9	0.512394 ± 09	0.1312	0.512394	-2.0	1.28	142	73	5.720 ± 10	0.73261 ± 12	0.71101	0.71101	11.5	13.1	11.6	-
DLG-82 (Musc)								2896	250	139.20 ± 10	1.29110 ± 22	-	-	-	-	-	292.2 ± 2.9
DLG-83	4.9	23.3	0.512339 ± 11	0.1262	0.512099	-2.9	1.22	127	71	5.779 ± 10	0.73479 ± 12	0.71095	0.71095	11.7	13.1	11.5	-
DLG-83 (Musc)								455	9	159.04 ± 10	1.36617 ± 21	-	-	-	-	-	289.8 ± 2.8
DLG-83 (KF)								291	40	21.31 ± 10	0.79330 ± 10	0.71704	0.71704	11.7	-	-	273.8 ± 2.8
DLG-84	3.9	14.0	0.512312 ± 10	0.1607	0.512007	-4.7	2.15	138	53	7.563 ± 10	0.74231 ± 10	-	-	-	-	-	-
DLG-84 (Musc)								991	5	836.7 ± 10	4.23018 ± 40	-	-	-	-	-	-
DLG-114	15.2	41.9	0.512369 ± 09	0.1663	0.512053	-3.8	2.08	150	75	5.775 ± 10	0.74825 ± 10	0.71848	0.71848	12.1	13.2	-	295.2 ± 2.9

m = measured isotopic ratios; i = calculated initial isotopic ratios; $\epsilon\text{Nd}_{(t)}$ values were calculated using present day ($^{143}\text{Nd}/^{144}\text{Nd}$)_{CHUR} = 0.512638 and ($^{147}\text{Sm}/^{144}\text{Nd}$)_{CHUR}; CHUR = Chondrite uniform reservoir; $\lambda = 6.54 \cdot 10^{-12} \text{ a}^{-1}$ (Steiger & Jager, 1977). The ages of 295 Ma (Deliktaş) and 303 Ma (Sivrikaya) are used for the $\epsilon\text{Nd}_{(t)}$ and $\text{Sr}_{(t)}$ calculations. $[\text{Sr}_{(t)} = (^{87}\text{Sr}/^{86}\text{Sr})_m - \text{Rb}/^{86}\text{Sr}(e^{\lambda t} - 1)] \cdot 10^{-11} \text{ a}^{-1}$. -, not determined.

However, the SG and the surrounding basement rocks yield overlapping T_{DM} ages (e.g. basement, 0.6 1.3 Ga) suggesting that the SG may be strongly influenced by the Nd from these rocks.

High and nearly constant Rb/Sr ratios (~5.6) Deliktaş granite samples may be indicating derivation from a homogeneous source. However, the samples have variably high initial $Sr_{(i)}$ ratios (0.7326 - 0.7482) and low $\epsilon Nd_{(t)}$ values (-2.1 to -4.8) and Nd model ages of 1.2 - 2.2 Ga. These, and the positive to negative Eu anomalies, emphasizing that young and old crustal material contributed in their genesis. An origin through dehydration melting of homogeneous, felsic upper crust is regarded as the most viable model for generating the Deliktaş leucogranite, consistent with low Sr concentration (53 - 75 ppm, because plagioclase is residual) and some high negative $\epsilon Nd_{(t)}$ values (-4.8), which implies melting of a considerable proportion of old crustal material.

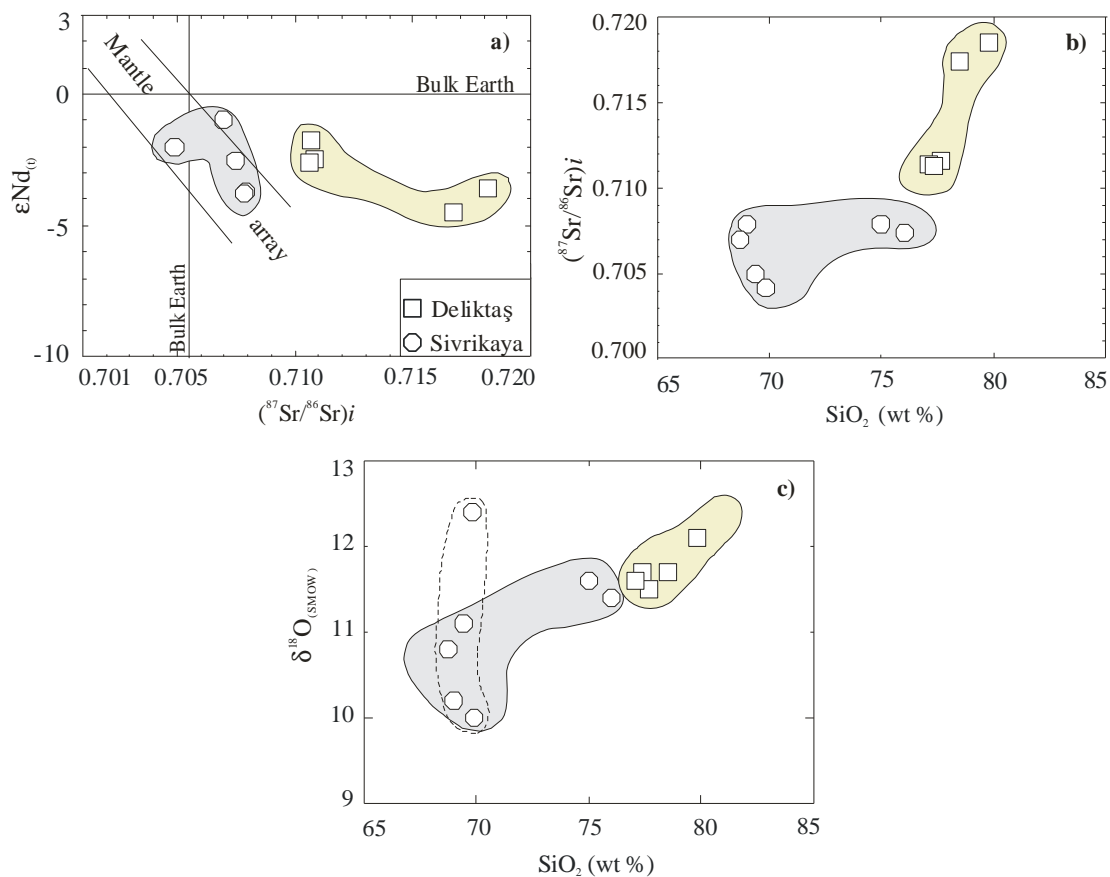


Fig. 3.10- Isotopic compositions of samples from Deliktaş and Sivrikaya granitoids **(a)** initial $\epsilon Nd_{(t)}$ values vs. initial Sr ratios, **(b)** and **(c)** initial Sr isotopic ratios and $\delta^{18}O$ values vs. SiO_2 respectively

Based on Sr, Nd and O isotope variations (Fig. 3.10), it would seem feasible that the Sivrikaya granite magmas were formed by variable degrees of mixing between mafic magmas and partial melts derived from older metasedimentary components (with high $Sr_{(i)}$, low $\epsilon Nd_{(t)}$ and high $\delta^{18}O$) in the lower crust, with additional crustal component. In either a mixing or a separate source model for the SG magmatism, the protoliths probably constrained variable amounts of a recycled crustal component that had been subjected to surface weathering as

suggested by $\delta^{18}\text{O}$ values (Table 3.2, Fig. 3.10c). Partial melting of crustal rocks was probably in response to heat input in the form of mantle-derived mafic magmas underplating (e.g. Davies and von Blanckenburg, 1985; von Blanckenburg and Davies, 1985; Dummond and Defant, 1990; Pearce and Parkinson, 1993 Schiano et al. 1995; Martin, 1997; Henk et al. 2000).

The relative mafic composition of the granodiorite-tonalite samples compared to the 2-mica granite coupled with dissimilar isotopic signatures, suggests derivation either from different protolith or that the granodiorite-tonalite samples represent a cumulate from the magma that also formed the granite (e.g. Roberts et al. 2000). However, petrological, geochemical and isotopic data show that the Sivrikaya 2-mica granites could represent a separate magma batch. The common association of the granodiorite-tonalite with the intermediate and basic basement rocks (Ösek and Büyükçay metabasic) suggests that the magmas may have inherited some of the signatures from the basement, the result of partial melting, assimilation, magma mixing during ascent to and emplacement in higher magma chamber (e.g. Collins, 1996). It should be noted that the 2-mica granites have marginally higher $\text{Sr}_{(i)}$ and lower $\epsilon\text{Nd}_{(t)}$ than the granodiorite-tonalite, which is expected from mixing.

The DLG and SG (KGB) rests on Precambrian-Palaeozoic granulite-amphibolite facies basement (gneisses, amphigneisses and amphibolites), which have variable Rb-concentrations (5 - 117 ppm) and initial Sr isotopic values in the range 0.70395 to 0.71256. It is noteworthy, that these values are compatible with those shown by SG and DLG, which are thought to be derived from these high-grade rocks. It seems most likely, therefore, that the isotopic compositions of the granitoids result from the mixing of old continental material with mantle-derived magmas, mafic continental crust or young LREE-enriched crustal rocks. The main question therefore is, whether the component with the mantle signature represents magma from the mantle that fractionated and assimilated continental crust, or whether this magma induced anatexis in a heterogeneous rock in the crust.

3.2.4. Discussion on geochemistry

3.2.4.1. *Petrogenetic considerations*

Petrogenetic models for the origin of arc magmas fall in two broad groups. Firstly, felsic arc magmas are derived from parent magmas of basaltic composition through fractional crystallization or AFC processes (e.g. Grove and Donnelly-Nolan, 1986; Bacon and Druitt, 1988). The second model is that basaltic magmas provide heat for partial melting of crustal rocks (e.g. Bullen and Clynne, 1990; Roberts and Clemens, 1993; Tepper et al. 1993; Guffanti et al. 1996). The first model is considered unlikely, because the Sivrikaya and Deliktaş granitoids rocks are voluminous (all samples have SiO₂ content > 60wt %). Furthermore, the rocks compositions do not represent a fractionation sequence from basalt-granodiorite-leucogranite. Such voluminous felsic magmas could not be generated solely by differentiation of mantle-derived mafic magmas. Rocks of Deliktaş and Sivrikaya granitoids show little or no variation in initial Sr-isotope ratios and $\delta^{18}\text{O}$ values with SiO₂ (Fig. 3.10b-c), which does not support derivation from mafic magmas through AFC processes. Experimental evidence (e.g. Wyllie, 1984) has shown that hydrous melting of basalt could produce tonalitic-trondhjemitic magmas that might evolve by fractional crystallization and/or crustal contamination towards more granitic compositions. Tepper et al. (1993) and Watson and Harrison (1982) reported that partial melting of the lower crustal metabasalt under variable H₂O conditions could yield a variety of granitoids. Similarly, Roberts and Clemens (1993), based on the results of experiments on partial melting of common crustal rocks stated that medium- to high-K, transitional- to S-type calc-alkaline granitoid magmas could be derived from partial melting of intermediate to felsic metamorphic rocks of the crust. Given the existing experimental constrains, the most reasonable model for the origin of the Sivrikaya and Deliktaş granitoids involves partial melting of crustal protoliths having different compositions, under variable H₂O activities, leaving restite with variable proportions of amphibole and plagioclase. This process combined with fractional crystallization and upper crustal contamination [as exemplified by basic to intermediate (amphibolitic) and felsic (gneissic-granitic) basement rocks], respectively could have generated the SG and DLG magmas. Fractional crystallization of the melts en route to higher crustal levels can generate the whole spectrum of rock types represented in the Sivrikaya granite. Some SG samples are transitional-types which could represent highly differentiated I-types which assimilated the metasedimentary (mafic-intermediate) basement rocks or the product of graywackes melting (e.g. Turpin et al. 1990) (Fig. 3.11a, b). The dispersion of the isotopic data for the SG and the high-grade metamorphic

basement rocks in the Sivrikaya area highlights the wide diversity of the material involved in the episodic differentiation.

The more evolved and less variable geochemical and isotopic characteristics of the Deliktaş rocks are similar to Moldanubian granites that are entirely derived from crustal sources (e.g. Liew and Hofmann, 1988). These characteristics further reflect low water activity and lower melt fraction, the most probably source lithology is a muscovite-rich metapelite (e.g. Thompson, 1996), which has sufficient volume to generate the observed proportion of the Deliktaş leucogranite. The parental magma characteristics, potential sources and crystal behaviour can be constrained by geochemical and isotope data.

3.2.4.2. *Fractional crystallization*

Small increases in SiO₂, K₂O, Rb and decreases in Al₂O₃, TiO₂, Fe₂O₃, CaO and MgO contents within both granitoids are compatible with very limited evolution through fractional crystallization processes (Figs. 3.4, 3.5). Slightly positive to strongly negative Ba and Sr anomalies of Deliktaş rocks are associated with small positive to huge negative Eu anomalies, indicating evolution by fractionation of K-feldspar (and plagioclase) either in the magma chamber or during magma ascent. This is also supported by negative correlations between CaO, Al₂O₃, and SiO₂. In contrast, fractionation of plagioclase has not played an important role in the petrogenesis of Sivrikaya granite, as indicated by small or no negative anomalies of Eu, Ba and Sr (Figs. 3.8a & 3.9a). Decreases in TiO₂ and P₂O₅ with increasing SiO₂ (Fig. 3.4) are attributed to fractionation of titanite and apatite, respectively. The fractionation of accessory phases such as zircon, allanite and titanium can account for depletion in zirconium. The Sivrikaya samples display moderate concave upward REE patterns and relative depletion of middle REEs with respect to HREE (Fig. 3.8a), which can be attributed to fractionation of amphibole and/or titanite (e.g. Romick et al. 1992; Hoskin et al. 2000). Some Sivrikaya samples have high SiO₂ contents and high values of Fe₂O₃/MgO ratios (Table 3.1) suggesting that the parental magma experienced magmatic differentiation (e.g. Whale et al. 1987).

The δ¹⁸O values range from 10 - 12.4 ‰ for Sivrikaya and 11.5 - 11.7 (12.1) ‰ for Deliktaş (Table 3.2, Fig. 3.10b-c). There is an increase in δ¹⁸O values of ~ 0.6 ‰ in the Sivrikaya granite, and this may be attributed to fractional crystallization (e.g. Matsuhisa, 1979). Without significant contamination by continental crust, since closed-system fractional crystallization is known to modify δ¹⁸O values by about 0.5-1 ‰ (e.g. Taylor 1978; Woodhead et al. 1987; Harmon and Grebe 1992). The wider range in δ¹⁸O values of the Sivrikaya samples (10 - 12.4 ‰) may reflect a heterogeneous source. In contrast, the high and narrow range in δ¹⁸O values (11.5 - 11.7 ‰) (Table 3.2) of the Deliktaş whole-rocks samples

and restricted values of ~13 ‰ and 11.5 ‰ respectively for quartz and K-feldspar could be attributed to significant contamination by continental crust (e.g. Taylor, 1978; O’Neil and Chappell, 1977).

The discontinuous and separate chemical variation trends illustrated in Harker diagrams (Figs. 3.4 & 3.5) and the considerable difference in emplacement time (Nzegge, in review), despite the close spatial and temporal association of both granitoids precludes the same magmatic source. To elucidate this problem, variation diagrams of the concentration of some oxides and elements, which are strongly affected by fractional crystallization process, have been plotted against Mg#. It is evident that the crystallization behaviour between the Sivrikaya and Deliktaş granites is different. Except for Mg# > 65, the Sivrikaya samples generally exhibit more coherent trends whereby TiO₂, P₂O₅, Fe₂O₃, MgO, CaO, and Sr decrease with increasing Mg# (Table 3.1, Fig. not shown). In contrast, the Deliktaş samples are less variable.

Nd model ages (T_{DM}) range from 0.75 - 1.08 Ga for the Sivrikaya and 1.2 - 2.2 Ga for the Deliktaş granitoids (Table 3.2). The Deliktaş granitoid has distinctly older T_{DM} age than Sivrikaya suggesting that they were derived from separate magmas or underwent different petrogenetic processes. Therefore, a comagmatic and continuous crystal fractionation relationship between the Sivrikaya and the Deliktaş plutons is unlikely. The slightly higher HREE concentrations, lower (La/Yd)_N and (Gd/Yb)_N ratios, but higher SiO₂ content of Deliktaş samples (Table 3.1) argue against a co-genetic relationship through crystal fractionation. The Deliktaş samples, in spite of some scatter, generally exhibit more coherent trends for most elements, but display less significant variation in Mg# (55-64). Differentiation of Sivrikaya parent magma alone to produce the Deliktaş granite rocks is excluded because the samples have overlapping Mg#.

The initial Nd and Sr isotopic compositions of Deliktaş samples lie outside the range of Sivrikaya rocks (Fig. 3.10a-b) and the concentration of trace elements (e.g. Ba, Sr & Zr) do not fall on a straight line between the samples of Sivrikaya and Deliktaş in Harker variation diagrams (Figs. 3.4, 3.5). Furthermore, rocks of the Deliktaş granite are all leucocratic and exhibit porphyritic textures, with “apparently” primary muscovite megacrysts, myrmekite and graphic quartz (Fig. 3.3), which are not observed for the Sivrikaya rocks. All these features preclude a comagmatic origin for the Sivrikaya and Deliktaş granites.

3.2.4.3. Nature of parental magma and possible sources

Rocks of both granites are high-K, calc-alkaline, are characterized by negative Ba, Sr, Nb and Ti anomalies, and are enriched in Rb, Th, K and La. These features are typical for crustal melts, e.g., granitoids of the Lachlan Fold belt (Chappell and White, 1992) and Himalayan leucogranites (Harris et al. 1986, Searle and Fryer, 1986). Hence a derivation from crustal sources is apparent. The crustal source, the crystalline basement that was intruded by the Kastamonu granitoids, is exposed and is locally called the Devrekani metamorphic unit. This basement comprises amphibolites, gneisses and granites (*see basement chapter below*).

Compositional diversity among crustal magmas may arise in part from different source compositions, in addition to conditions such as H₂O-activity, pressure, temperature and oxygen fugacity (e.g. Vielzeuf and Holloway, 1988; Wolf and Wyllie, 1994; Patiño Douce 1996, 1999; Thompson, 1996; Borg and Clynne, 1998). Compositional differences of magmas produced by partial melting conditions of different crustal source rocks such as amphibolites, gneisses, metagreywackes and metapelites, may be visualized in terms of major oxides ratios.

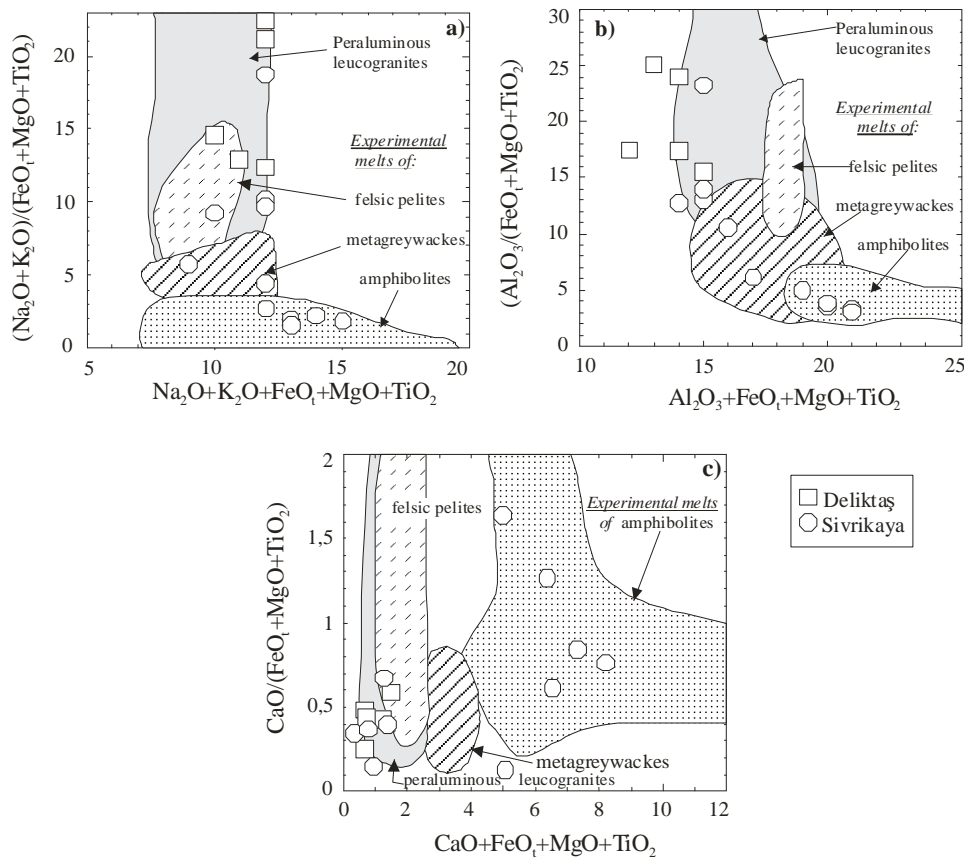


Fig. 3.11- Plots showing compositional fields of experimental melts derived from partial melting of felsic pelites, metagreywackes and amphibolites (Patiño Douce, 1999) and the composition of studied samples from Deliktaş and Sivrikaya granitoids

Partial melts originating from mafic source rocks, for example, have lower $\text{Al}_2\text{O}_3/(\text{FeO}_t+\text{MgO}+\text{TiO}_2)$ and $(\text{Na}_2\text{O}+\text{K}_2\text{O})/(\text{FeO}_t+\text{MgO}+\text{TiO}_2)$ than those derived from felsic metapelites (Fig. 3.11). Sivrikaya rocks have moderate $\text{Al}_2\text{O}_3/(\text{FeO}_t+\text{MgO}+\text{TiO}_2)$, $(\text{Na}_2\text{O}+\text{K}_2\text{O})/(\text{FeO}_t+\text{MgO}+\text{TiO}_2)$ and a rather wide range of $\text{CaO}/(\text{FeO}_t+\text{MgO}+\text{TiO}_2)$ ratios. These features, in combination with relatively high and wide range of Mg# values (61-28), suggest a derivation from felsic pelite, metagreywackes and amphibolite rocks. On the Na_2O vs. K_2O diagram (Fig. not shown) the Sivrikaya transitional samples (SG-115, -116, -125, -132) plot in the field outlined for typical I-type granite of the Lachlan Fold Belt (White and Chappell, 1983). High contents of CaO, Sr, and negligible Eu/Eu* depletion in the REE patterns of these samples all suggest melting of a plagioclase-bearing source. Some of the Sivrikaya samples fall in the range of felsic pelite (Fig. 3.11), as these samples contain secondary muscovite. Muscovitization of feldspar and chloritization of biotite in these samples suggest hydrothermal alteration. Partial melting models, e.g., incongruent melting of muscovite and biotite (Clemens and Vielzeuf, 1987; Vielzeuf and Holloway 1988; Patiño Douce and Johnston 1991), suggest partial melting of metabasic rocks might generate rocks which exhibit transitional- to S-type geochemical characteristics. The fact that some Sivrikaya samples are compositionally transitional between the I- and S-type granites implies that the Sivrikaya granitoid might have been derived from partial melting of acid to intermediate igneous rocks or immature sediments, consistent with the relatively large variations in isotopic composition ($\epsilon\text{Nd}_{(t)} = -1.0$ to -3.8 ; $\text{Sr}_{(i)} = 0.7040 - 0.7079$; $\delta^{18}\text{O} = 10 - 12.4$ ‰), underlining their derivation from heterogeneous sources. The slight to strong negative $\epsilon\text{Nd}_{(t)}$ values, low Sr_i ratios, and young Nd model ages ($T_{\text{DM}} = 0.75 - 1.08$ Ga) indicating significant input of mantle-derived component during magma generation. The Sivrikaya basement consists of gneissic rocks and amphibolites with variable isotopic compositions, similar $\text{Sr}_{(i)}$ ratios (0.704 - 0.706), higher $\epsilon\text{Nd}_{(t)}$ values (-1.4 to 6.8) and lower $\delta^{18}\text{O}$ values (8.2 to 10.3 ‰) (Table 3.2) compared to Sivrikaya granitoid samples. However, the young model Nd ages of the SG samples indicate that the petrogenesis of this granitoid involved the input of juvenile component (e.g. DePaolo et al. 1992). Therefore, a mixture of juvenile material and old continental crust may characterize the petrogenesis of this granitoid. In this case, the Nd model ages represent the average crustal residence time for the Sivrikaya granitoid (e.g. De Paolo et al. 1991, 1992). Furthermore, the rocks show the concave-upward REE patterns and are depleted in MREE relative to HREE (Fig. 3.9a) indicating that amphibole played a more significant role than garnet during magma segregation. The MREE depletion and the negative Ti anomaly can also be attributed to fractional crystallization of allanite and titanite (e.g. Weaver 1990; Hoskin et al. 2000).

Muscovite and/or biotite dehydration melting produces melts that strongly peraluminous, K-rich, and very poor in Fe, Mg, and Ti (Clemens and Vielzeuf, 1987; Patiño Douce and Johnson, 1991); incompatible with the slightly metaluminous and high Na₂O/K₂O nature of SG rocks. Amphibole dehydration melting can produce large volumes of metaluminous to slightly peraluminous granitoid magma with high Na₂O/K₂O ratios (Ellis and Thompson, 1986), and this process may have been important in SG. A combination of biotite and amphibole dehydration melting from a plagioclase (albite component) and quartz-bearing crustal rocks can explain the general high Na₂O/K₂O values.

All plots in Figure 3.11 indicate an origin of the Deliktaş magmas by dehydration melting of felsic pelite-type source rocks. The Deliktaş samples have high initial Sr ratios (0.7109 - 0.7185), variably lower εNd_(t) values and older Nd model ages (T_{DM}= 1.2 - 2.2 Ga). These, emphasizing that mature crustal material played a very important role in their petrogenesis. The high and nearly constant Rb/Sr ratios (5.6 - 5.7) indicating derivation from a rather homogeneous melt that underwent closed-system fractional crystallization as indicated by high δ¹⁸O values (11.5 to 12.1 ‰) of the rocks. Excluding sample DLG-114 (porphyroid), the Deliktaş granite samples show less HREE depletion (Fig. 3.8b) predicted for melts that equilibrated with residual garnet (e.g. Tepper et al. 1993). The basement rocks (gneisses and granites) of the Deliktaş granitoid have similar εNd_(t) in the range of -6.6 to -3.4 and δ¹⁸O values ranging from 10 to 11.3 ‰, lower but similar Sr_(i) ratios (0.707 - 0.712) and Nd model ages (T_{DM}= 1.1-1.3 Ga) (Table 3.3), compared to the granitoid samples. All these characteristics indicate the contribution of the basement to the genesis of Deliktaş granitoid.

3.2.4.4. *Tectonic implications*

Both granitoids rocks are high-k, calc-alkaline enriched in LILEs such as Cs, K, Rb, U, and Th with respect to HFSEs, especially Nb and Ti (Fig. 3.9). Magmas with these chemical features are typically generated in subduction (collision-related) environment (e.g. Pearce et al. 1984; Harris et al. 1986; Rogers and Hawkesworth 1989; Sajona et al. 1996). Numerous studies suggest that trace elements could be used as discriminatory tools to distinguish among different tectonic settings of granitoids magmas. Pearce et al. (1984) used the elements Rb, Y and Nb as the most efficient discriminants amongst oceanic-ridge granitoids (ORG), within-plate granitoids (WPG), volcanic arc granitoids (VAG) and syn-collisional granite (syn-COLG). Applying their discrimination criteria, the Deliktaş granitoid is classified as volcanic arc granitoid (VAG) (Fig. 3.12a-b).

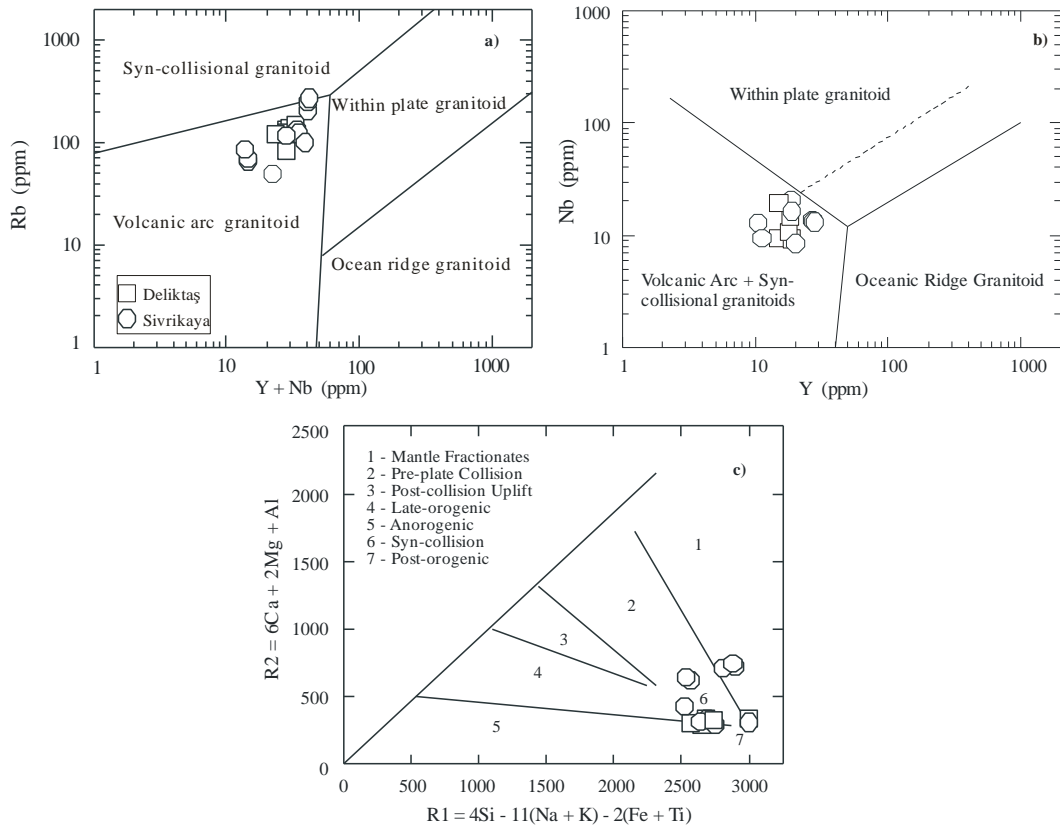


Fig. 3.12. Geochemical compositions of Deliktaş and Sivrikaya samples plotted in tectonic setting discrimination diagrams: **(a)** Rb vs. Y+Nb and **(b)** Nb vs. Y (Pearce et al. 1984), and **(c)** R1 vs. R2 (De La Roche et al. 1980) the fields boundary based on Batchelor and Bowen (1985)

The high silica content (75-79 wt % SiO₂) samples from the Sivrikaya granitoid plot around the boundary between VAG and syn-COLG fields (Fig. 3.12a). This is likely due to progressive differentiation (e.g. Förster et al. 1997). Crossing of the VAG and syn-COLG boundary as observed for the Sivrikaya samples could be the results of a magmatic differentiation trend. On the R1 vs. R2 diagram (De La Roche et al. 1980) Sivrikaya samples fall in the pre-plate collision and the syn-COLG fields (Fig. 3.12b). In contrast all the Deliktaş samples plot in the post-orogenic field. Collisional tectonic setting commonly involves an early syn-collisional stage of thrusting and folding, resulting in crustal thickening followed by a late post-collisional stage of strike-slip and extensional faulting, reflecting adjustments of accreted blocks (Sylvester, 1998). Pitcher (1982, 1983) revealed that granite types broadly correlate with geological environment and tectonic regimes, his view has been substantiated by studies of the relationship between trace element abundance patterns and tectonic setting (e.g. Floyd and Winchester, 1975; Pearce et al. 1984; Thompson et al. 1984; Harris et al. 1986). Using the Pitcher-Pearce-Harris scheme, the strongly peraluminous (ASI ≥ 1.1) assemblage of DLG would undoubtedly be classified as post-collisional, that is, were

emplaced after the climax of crustal thickening (e.g. Sylvester, 1998). In this tectonic setting the granites are often recognizably S-type, i.e., ultimately derived from sedimentary lithologies (Miller, 1985). Increase in K- and Sr-contents, high Rb/Sr ratios and initial Sr values and low $\epsilon\text{Nd}_{(t)}$ of the DLG samples, are clearly related to crustal thickening and the involvement of more crustal material in their genesis (e.g. Bennett and De Paolo, 1987). K-rich peraluminous granitoids are generally considered to be post-orogenic (e.g. Lameyer et al. 1980; Pitcher, 1983; Pearce et al. 1984; Harris et al. 1986). In addition Deliktaş monzogranites have K-feldspar megacrysts and apparently “primary” muscovite, common in the leucogranites of Variscan belts of western and central Europe (e.g. Pagel and Laterrier, 1980; Lameyer et al. 1980; Liew et al. 1989; Barbarin, 1999; Fernandez-Saúrez et al. 2000). The isotope systematics (Table- 3.2, Fig. 3.10a) in combination with the REE pattern of Deliktaş granite (Fig. 3.8b) are therefore considered as products of post-collisional magmatism.

The geochemical data of the Deliktaş and Sivrikaya granitoids can be summarized as follows: the SG group ultimately derived from a sub-arc mantle wedge enriched by silica-rich melts and fluids from escaping subducting slab (e.g. Hawkesworth et al. 1993), and crustally derived high-K Deliktaş leucogranites resulting from partial melting of crustal material, indicating a major crustal thickening episode (e.g. Boztuğ et al. 1995) that followed subduction and collision of Gondwana-derived micro-continental plates with South Eurasian active margin (e.g. Şengör 1984; Robertson and Dixon 1984; Ustaömer and Robertson 1993). The activity of the Eurasia-Pontides convergent zone probably consisted of successive periods of compression and piling of the crustal fragments on one hand and tension on the other hand, to permit respectively genesis of magmas and alternating emplacement of (1) mixed (crust and mantle) origin (e.g. Sivrikaya granitoid), the result of subduction, transitional regimes and continental collision; and (2) peraluminous granitoids (cordierite-bearing, and muscovite- and K-rich peraluminous granites, associated with the climax of orogenesis) dominantly of crustal origin (e.g. Deliktaş granite). Deliktaş rocks were probably emplaced during the relaxation phases (e.g. Barbarin, 1999) where anatectic complexes formed are commonly porphyritic-K-feldspars-rich (e.g. Wyllie, 1977).

3.2.4.5. *Conclusions on geochemistry and isotopic systematics*

Overall geochemical signatures, a wide range of Sr-O isotopic compositions and geochronological data preclude a comagmatic origin of the Sivrikaya and Deliktaş magmas. An origin through dehydration melting of homogeneous, felsic upper crust is regarded as the most viable model for generating the Deliktaş leucogranite, whereas, the Sivrikaya magmas

composition are intermediate between crustal and mantle sources. In contrast, the Sivrikaya magmas originated by partial melting of heterogeneous pelite-amphibolite-greywackes-type sources. The lowermost crust must have been hot, implying extensive heating by mantle-derived mafic magmas.

Individual K-feldspar from Sivrikaya granitoid yield Permo-Carboniferous ages 5 to 30 Ma younger than the crystallization age of the host rock. Further minerals from the same samples but with different closure temperatures (Rb-Sr biotite, muscovite, and hornblende) (Table 3.5, Appendix) show similar young ages, thereby, making it likely that these rocks achieved post-crystallization isotopic homogenisation. The homogenisation of the strontium isotopic signature probably took place under thermo-metamorphic and/or hydrothermal conditions. The mineralogical and geochemical data and isotopic characteristics of the Sivrikaya and Deliktaş granitoids are therefore, predominantly the consequences of melting, mixing and assimilation of crustal rocks, and the compositions of the source regions rather than large-scale, post-emplacement differentiation. Major and trace element compositions suggest the Sivrikaya granitoid to be syn-collisional to subduction-related, while the Deliktaş granite may be post-orogenic, with inherited arc-related signatures. However, the spatial and temporal relationships appear to indicate a convincing genetic link amongst the basement, granitoids emplacement and the subduction processes in this area.

The occurrence of peraluminous primary muscovite-rich S-type monzogranites along with a somewhat less peraluminous suite of hornblende granodiorites-tonalites and two-mica-granites is a situation common to many segments of the European Variscan. Therefore, the SG and DLG correspond to magmatic activities which bear analogy with Variscan magmatism documented in the domain extending from central Europe (e.g. Finger et al. 1997; Stampfli et al. 2002; Hann et al. 2003; Liew and Hofmann 1988; Liew et al. 1989), through the Balkans (e.g. Chatalov, 1988; Carrigan et al. 2005; Cherneva and Georgiova 2005; Okay et al. 2006), and beyond the Variscan suture systems, to the Lesser Caucasus (Şengör et al. 1993). The Variscan evolution of northern Turkey and the Balkans, therefore, appears to be similar to that of central Europe, with the Istanbul-Moesia-Scythian block (Fig. 3.13) corresponding to Avalonia, and the Sakarya-Strandja to Amorica (e.g. Stampfli et al. 2002).

In the east, such intrusions appear in the so-called Variscan-Cimmeride transition region, where it is uncertain whether they are collisional-related (Variscan) or subduction-related (Cimmeride, Şengör et al. 1993). In fact, this difficulty also occurs in the central Pontides (this study) and in the Greater Caucasus (Şengör et al. 1993).

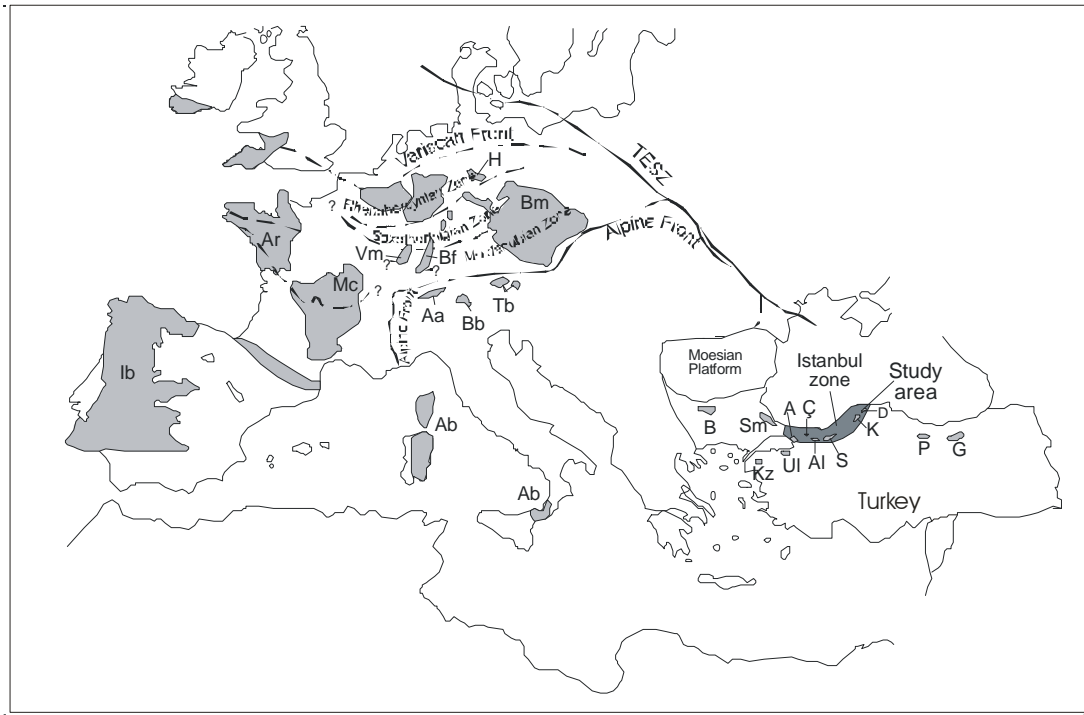


Fig. 3.13- Simplified geographic locations of the Variscan massifs in Europe and Turkey. *Ib*, Iberian massif; *Ar*, Armorican massif; *Mc*, Massif Central; *Vm*, Vosges massif; *Bf*, Black Forest massif; *H*, Harz massif; *BM*, Bohemian massif; *Aa*, Aar batholith; *Bb*, Bernina batholith; *Tb*, Tauern batholith; *Ab*, Alboran massif; *B*, Balkans; *Sm*, Strandja massif; *Kz*, Kazdağ massif; *Ul*, Uludağ massif; *A*, Armutlu massif; *Ç*, Çamdağ massif; *Al*, Almacık massif; *S*, Sünnicedağ massif; *K*, Karadere- Kastamonu region; *D*, Devrekani massif; *P*, Pulur massif; *G*, Gümüşhane massif (adapted from von Raumer et al. 2002, Carrigan et al. 2005)

3.3. GEOCHRONOLOGY

3.3.1. Zircon internal structure

CL photos of typical zircon population of granitoids are displayed in figures 3.14 and 3.15.

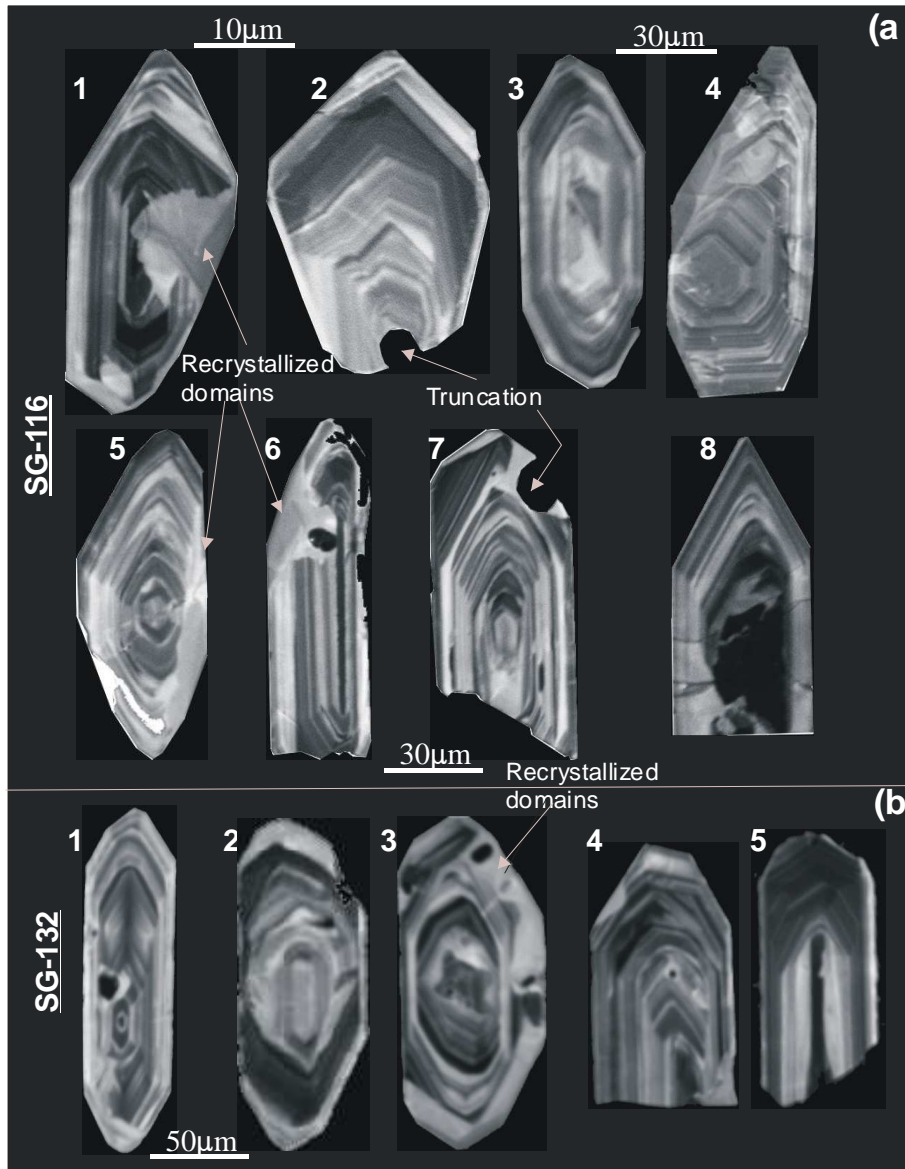


Fig. 3.14- Cathodoluminescence (CL) photographs of characteristic zircon population from Sivrikaya granite (a) SG-114 and (b) SG-132. The crystals are ca. 100-125µm long and 60-100µm wide. Zircon grains typically have prismatic morphology and oscillatory zoning, indicating magmatic origin. Truncation of some zircons (grains 2, 7 from sample SG-116) show they were not armoured in other minerals (e.g. biotite, quartz)

Zircons of the Sivrikaya granite rocks (Figs. 3.14) are all euhedral and reveal typical igneous zonation. Xenocrystic cores and overgrowth are not commonly observed; however, some SG-116 zircons show truncation of zoning (Figs. 3.14a, grains 2, 7) and recrystallized domains (Figs. 3.15a, grains 1, 5, 6). Such truncated grains show that they were not armoured in other

minerals and that partial dissolution occurred prior to rim growth. Rare very small xenocrystic cores occur (Fig. 3.14b, grains 2-3), truncated zoning and post-magmatic overprint are absent in SG-132 zircons.

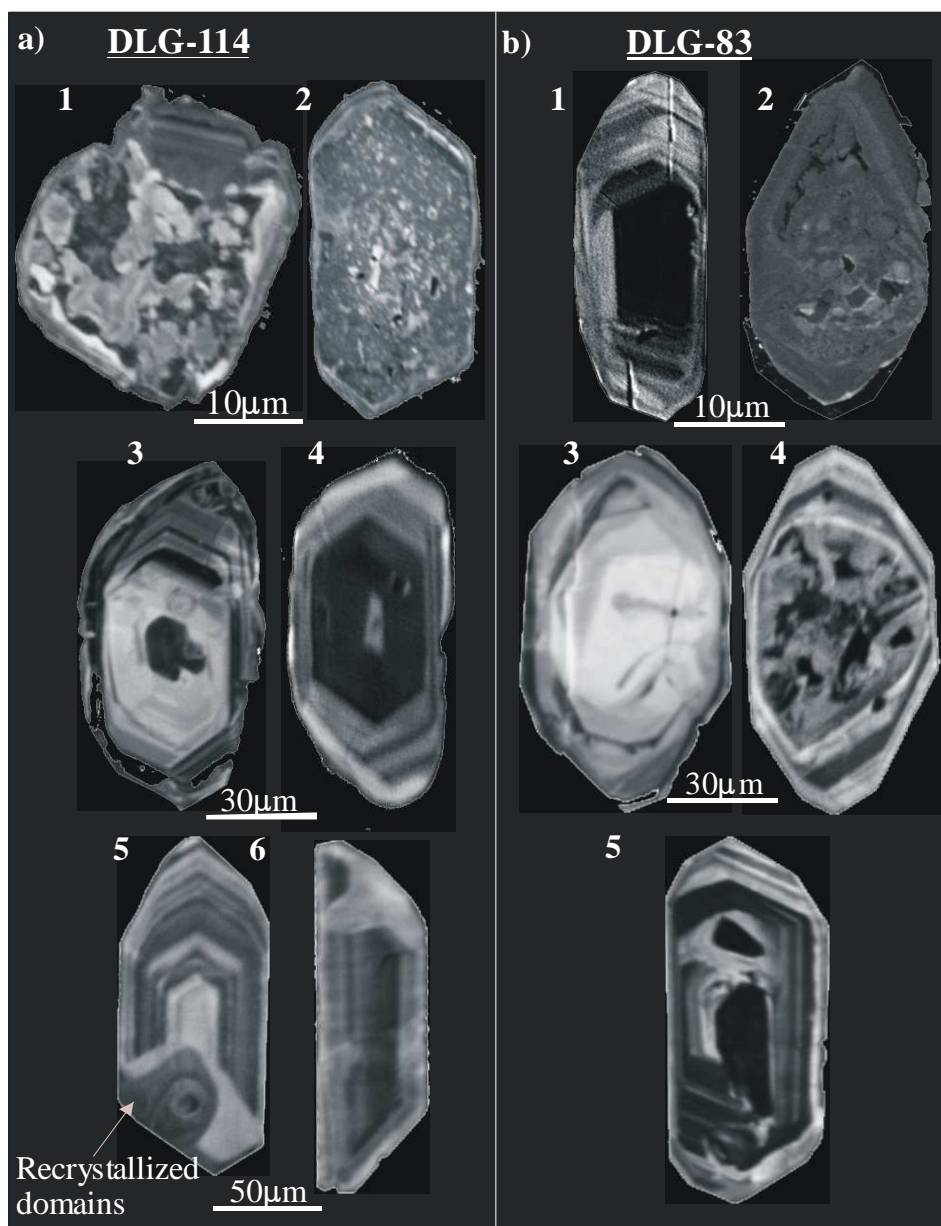


Fig. 3.15- Cathodoluminescence (CL) photographs of characteristic zircon population from Deliktaş granite: (a) DLG-114 and (b) DLG-83. The crystals are ca. 90-125 µm long and 60-80 µm wide. CL images reveal two morphological grain-types; elongated, euhedral with oscillatory zoning of igneous origin, and multi-faceted stout, euhedral, with a pre-existing inherited detrital and altered (metamict) core rimmed by magmatic zoning.

The Deliktaş leucogranite samples (DLG-83 and DLG-114) are zircon-poor (typical of felsic melts, e.g. Paquette et al. 1985) and the zircon grains are very fragile. This could be due to the combined effects of metamictization, recrystallization and replacement processes. The CL images (Fig. 3.15) reveal a heterogeneous population made up of two contrasting

morphological grain-types: elongated, euhedral, long prisms with oscillatory zoning (grains 3.15a, grains 3-6 & 3.15b grains 1, 5) and multi-faceted stout, euhedral grains with an inherited/endogenic detrital core more or less altered enclosed by a faintly zoned thin rim (grains 3.15a 1, 2 & 3.15b 2-4). Some DLG-114 zircons show partly re-crystallized domains (Fig. 3.15a, grains 5-6).

3.3.2. U-Pb, Pb-Pb and Rb-Sr data

1. Sivrikaya granitoid (SG)

Tonalite sample, SG-116. Five zircon fractions were analysed from this sample (Table 3.2, Fig. 3.16), three are concordant at ~303 Ma and one at ~ 345 Ma, and one fraction has an older Pb-component, although inherited cores were not identified in the CL images. Regressing the fractions at 303 Ma and the one with relic core yields an upper intercept age of 1846 ± 65 Ma (MSWD= 1.7), indicating the presence of a Proterozoic component.

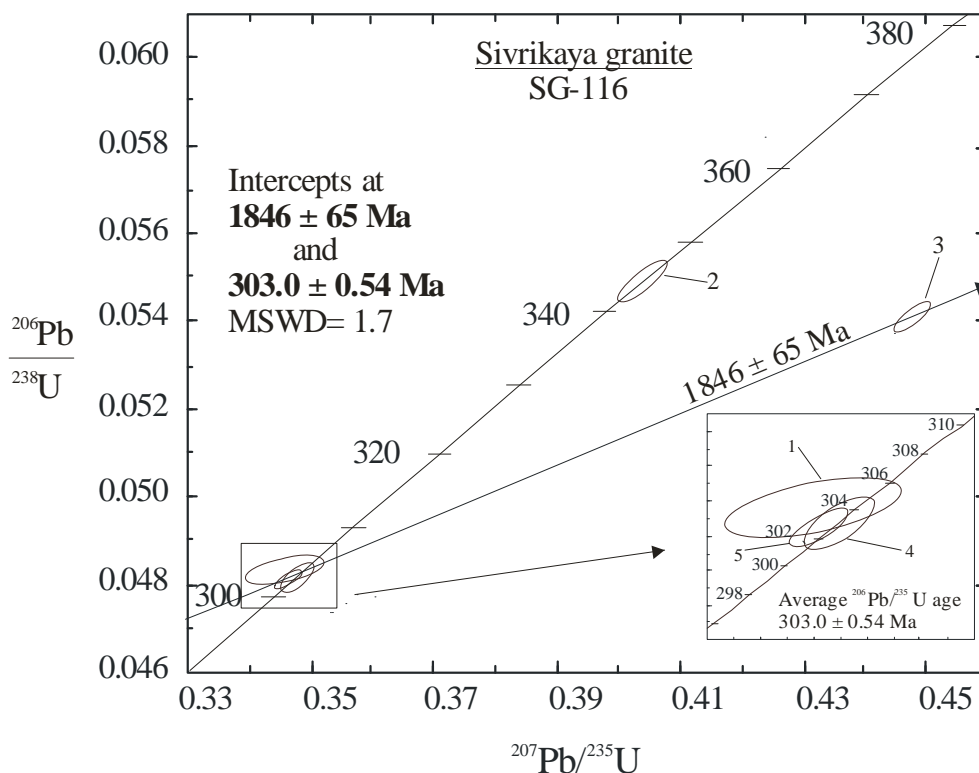


Fig. 3.16- Concordia plot showing U-Pb zircon isotope dilution analyses from Sivrikaya sample, SG-116. The upper intercept age of 1846 ± 65 Ma is given by a discordia through 303 ± 0.54 Ma defined by three concordant data points and one fraction with relic core; the inset is an enlargement of the lower intercept of the discordia. Error ellipses are $2\sigma_m$.

Table 3.3. U-Pb-zircon isotope dilution analytical results of Sivrikaya (SG) and Deliktaş (DLG) granitoid samples.

Fraction	Zircon description	Weight (mg)	Concentration (ppm)			Isotopic ratios			Apparent ages (Ma)				
			U	Pb _{tot}	Pb _{rad}	$\frac{^{206}\text{Pb}}{^{204}\text{Pb}}$	$\frac{^{207}\text{Pb}}{^{238}\text{U}}$	$\frac{^{207}\text{Pb}}{^{206}\text{Pb}}$	$\frac{^{207}\text{Pb}}{^{238}\text{U}}$	$\frac{^{207}\text{Pb}}{^{206}\text{Pb}}$	Rho		
SG-116													
1	lg, thk, ly, euh, lpr, cl, 1:6	0.0523	463	23	23	1904	0.04833±59	0.34596±156	0.05151±134	306	301	264	0.570
2	s, str, lbr, lpr, euh, cl, 1:2	0.0378	400	24	21	6089	0.05490±71	0.40401±81	0.05304±36	343	349	385	0.783
3	st, thk, y, spr, euh, cl, 1:2	0.0381	546	30	29	2029	0.05406±52	0.44736±56	0.06001±18	339	375	604	0.817
4	lg, m, ly, euh, lpr, cl, 2:5	0.0732	233	11	11	3813	0.04815±55	0.34794±63	0.05241±52	303	304	310	0.590
5	lg, th, lbr, lpr, euh, tr, 1:3	0.0231	459	23	21	553	0.04809±37	0.34637±51	0.05275±36	295	298	318	0.712
SG-132													
1	ndl, y, lpr, euh, cl, 1:3	0.0350	391	19	19	1942	0.04816±46	0.35285±49	0.05314±15	303	307	335	0.951
2	st, thk, ly, lpr, euh, cl, 1:2	0.0515	272	29	15	82	0.05424±39	0.48987±144	0.06550±131	341	405	791	0.471
3	m, lg, lbr, lpr, euh, tr, 1:5:3	0.0613	318	15	16	3250	0.04856±69	0.35989±70	0.05375±12	306	312	361	0.901
4	thk-hlf, ly-lbr, euh, lspr, cl	0.0632	269	13	13	1761	0.04832±82	0.35278±82	0.05295±10	304	307	327	0.992
5	lg, thk, lbr, lpr, euh, cl, 2:5	0.0897	395	20	20	4834	0.04926±0.7	0.38042±72	0.05490±16	316	327	408	0.978
6	m, lg, ly, lpr, euh, tr, 5:3	0.2050	255	14	12	241	0.04851±205	0.35364±229	0.05029±93	305	308	323	0.914
DLG-114													
1	ndl, lbr, lpr, euh, cl, 1:3	0.0507	244	32	31	1164	0.11721±49	2.10161±50	0.13005±06	715	1149	2099	0.982
2	m, br, spr, euh, tr, 1:1:5	0.0270	2129	68	63	784	0.06011±60	0.44327±98	0.05417±18	381	380	378	0.698
3	st, thk, lbr, spr, euh, tr, 2:4	0.0740	3258	150	142	1133	0.04658±238	0.33876±238	0.05275±16	293	296	318	0.990
4	th, lg, lbr, spr, euh, tr, 2:3	0.0298	1075	69	54	584	0.04885±54	0.35166±56	0.05221±14	307	306	295	0.967
5	st, thk, lbr, euh, spr, tr, 2:4	0.0250	1332	28	26	782	0.05957±58	0.44003±72	0.05357±94	373	370	353	0.543
6	s, th, lbr, lpr, tr-cl, 1:2	0.0180	458	30	84	1025	0.05982±87	0.43989±87	0.05147±37	387	369	262	0.906
7	m, st, br, lpr, euh, tr, 2:3	0.0360	1372	63	58	835	0.04494±53	0.32903±53	0.05310±11	283	289	333	0.977
8	s, st, br, spr, euh, cl, 1:2	0.0108	3192	101	94	832	0.04671±53	0.33917±58	0.05266±23	294	297	314	0.921
9	lg, th, dbr, euh, lpr, tr, 1:3	0.0199	698	43	41	677	0.05934±54	0.44488±61	0.05477±28	369	374	403	0.889
DLG-83													
1	lg, grt-lk, dbr, euh, lpr, tr, 2:3	0.0311	2656	119	112	1060	0.04647±47	0.33834±49	0.05281±17	293	296	320	0.984
2	m, lg, br, lpr, euh, tr, 1.5:3	0.0324	3354	141	133	1019	0.04362±37	0.31781±38	0.05284±09	275	280	322	0.971
3	b, grt-lk, dbr, spr, euh, tr, 1:3	0.0577	1833	81	77	1224	0.04599±73	0.33657±73	0.05307±11	288	290	305	0.966
4	s, grt-lk, br, spr, euh, tr, 1:2	0.0160	928	37	35	804	0.04581±55	0.32902±63	0.05209±29	289	289	289	0.892
5	s, st, dbr, spr, euh, tr, 1:2	0.0377	5084	205	196	1463	0.04241±47	0.30317±49	0.05185±13	268	269	279	0.966
6	b, grt-lk, br, euh, spr, tr, 2:3	0.0453	2980	124	118	1187	0.04380±36	0.30917±46	0.05120±28	276	274	250	0.801
7	s, grt-lk, br, spr, euh, tr, 1:2	0.0402	5547	224	215	1574	0.04264±68	0.30987±68	0.05271±11	269	274	316	0.987
8	s, br, lpr, euh, tr, 1:2	0.0231	8067	320	304	1301	0.04142±170	0.29957±175	0.05241±72	262	266	304	0.974
9	b, st, cl, lpr, euh, tr, 1:3	0.0144	5507	207	192	878	0.03833±157	0.27747±161	0.05220±34	242	249	308	0.977

Isotope dilution U-Pb zircon analytical results of Sivrikaya and Deliktaş calculated with ISOPLoT (Ludwig, 2000). *Rho*, correlation coefficient. *b*, big; *l*, long; *m*, medium; *s*, small; *sh*, short; *st*, stout; *th*, thin; *thk*, thick; *euh*, euhedral; *flt*, flat; *lpr*, long prism; *frag*, fragment; *spr*, short prism; *tr*, transparent; *trl*, translucent; *ndl*, needle; *y*, yellow; *ly*, light yellow; *cl*, clear; *chrls*, colourless; *m-fac*, multi-facet; *br*, brown; *lbr*, light brown; *l:l*, width : length ratio.

Granodiorite sample, SG-132. For this sample the Pb-evaporation and U-Pb isotope dilution methods were employed. Three out of six analysed zircon fractions are nearly concordant at ~304 Ma (Fig. 3.17a, inset). Two fractions are discordant indicating old Pb-component, which can be observed in CL images in the form of small inherited cores with brighter luminescence (Fig. 3.14, grain 3). A regression of all data points define intercept ages of 301.1 ± 1.4 and 2383 ± 87 Ma (MSWD= 0.89) (Fig. 3.17a).

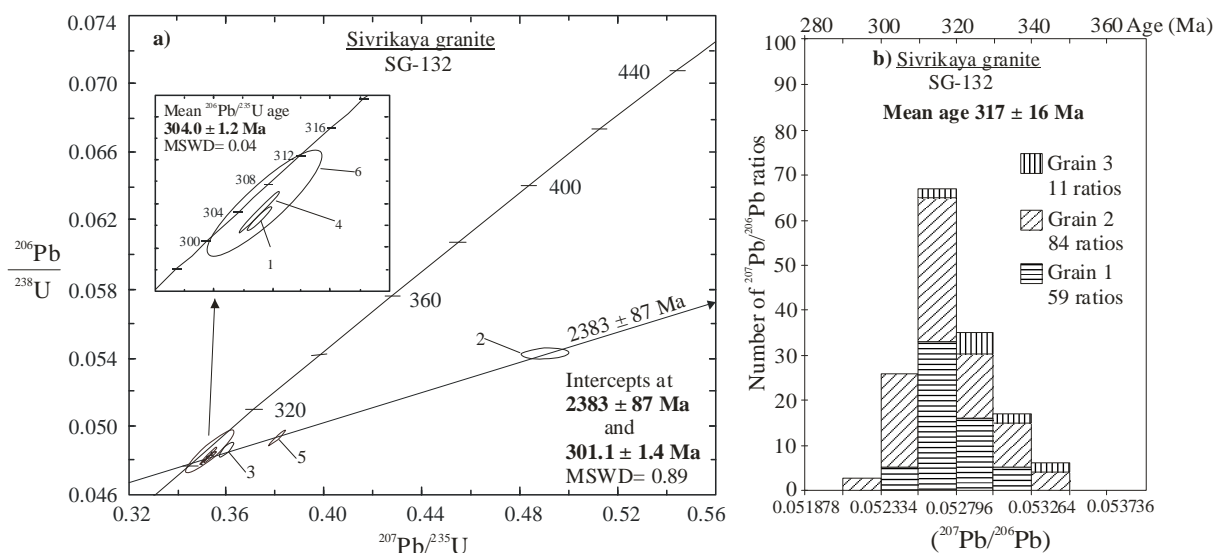


Fig. 3.17- Zircon ages for the Sivrikaya granitoid sample SG-132. **(a)** U-Pb concordia plot for isotope dilution analyses; discordia through the data points give intercepts at 301.1 ± 1.4 Ma and 2383 ± 87 Ma. The inset is an enlargement of the three nearly concordant data points at ~304 Ma. Error ellipses indicate $2\sigma_m$. **(b)** Histogram showing the frequency distribution of radiogenic $^{207}\text{Pb}/^{206}\text{Pb}$ ratios of single zircon Pb-Pb evaporation. The spectrums for three idiomorphic grains, integrated from 308 ratios give an age of 317 ± 16 Ma.

Three separately evaporated SG-132 zircon grains yield a mean $^{207}\text{Pb}/^{206}\text{Pb}$ evaporation age of 317 ± 16 Ma (Table 3.4, Fig. 3.17b). This age agrees within analytical error with the U-Pb age.

Table 3.3- Radiogenic $^{207}\text{Pb}/^{206}\text{Pb}$ ratios of evaporation of single zircon grains and corresponding ages

Sample	Grain	Zircon features	Number of $^{207}\text{Pb}/^{206}\text{Pb}$ ratios	Mean of $^{207}\text{Pb}/^{206}\text{Pb}$ ratios	$^{207}\text{Pb}/^{206}\text{Pb}$ age (Ma)
SG-132, granodiorite	1	medium, stout, brown	59	0.052500 ± 22	307 ± 10
	2	long, thick, brown	84	0.053125 ± 37	322 ± 16
	3	long, thin, yellow	11	0.052795 ± 28	320 ± 12
Weighted mean no. Of ratios and mean age			51	0.052810 ± 29	317 ± 13

All the U-Pb zircon analyses from SG-116 and SG-132 calculated together on the same concordia diagram, yield a discordia with a lower intercept age of 303 ± 1.4 Ma (Fig. 3.18), which is well defined by six nearly concordant fractions at ~ 303 Ma, most likely the age of the Sivrikaya granite.

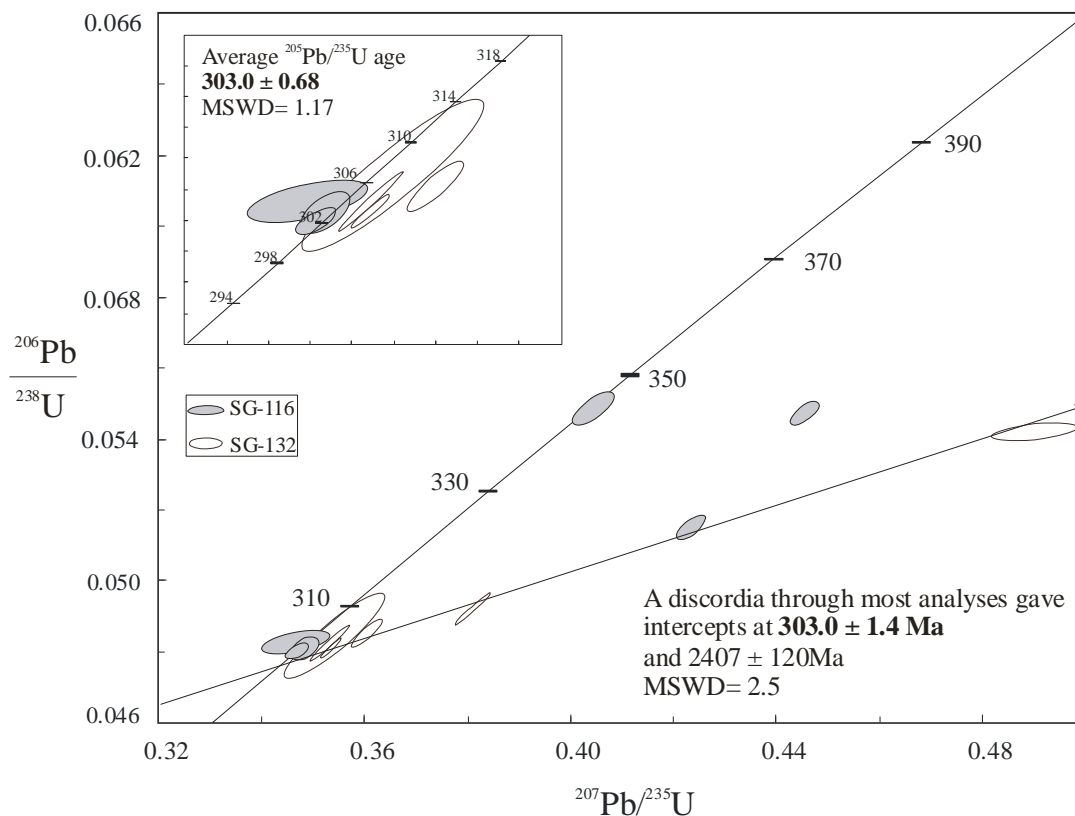


Fig. 3.18- Summary U-Pb concordia plot for zircon analyses of two Sivrikaya granitoid samples (SG-116 and SG-132). Data points ellipse are 2σ .

From samples SG-116, SG-132 SG-125 and SG-186a minerals were separated for Rb-Sr analyses (Tables 3.2 & 1, Appendix). The whole-rock data of samples SG-88b, SG-125, SG-132 and SG-186a yield an isochron age of 302 ± 32 Ma (MSWD= 3.4, $\text{Sr}_{(i)} = 0.7075 \pm 0.0016$) (Fig. 3.20a). However, Rb-Sr whole-rock and mineral (micas, K-feldspar, hornblende) analyses of sample SG-116 give an age of 275 ± 21 Ma (very high MSWD, $\text{Sr}_{(i)} = 0.717 \pm 0.046$) (Fig. 3.20b). Whole-rock, K-feldspar and two biotite fractions from SG-132 yield a Rb-Sr age of 275.4 ± 9.7 Ma (MSWD= 90, $\text{Sr}_{(i)} = 0.705 \pm 0.011$) (Fig. 3.19c). Two biotite fractions from this sample yield a mean Rb-Sr age of 274.6 ± 2.7 Ma and one muscovite gives an age of 281.6 ± 2.8 Ma (Table 1, Appendix). The young mica ages of SG could either mean slow cooling or rejuvenation during the intrusion of the younger granitoid-generation (see below).

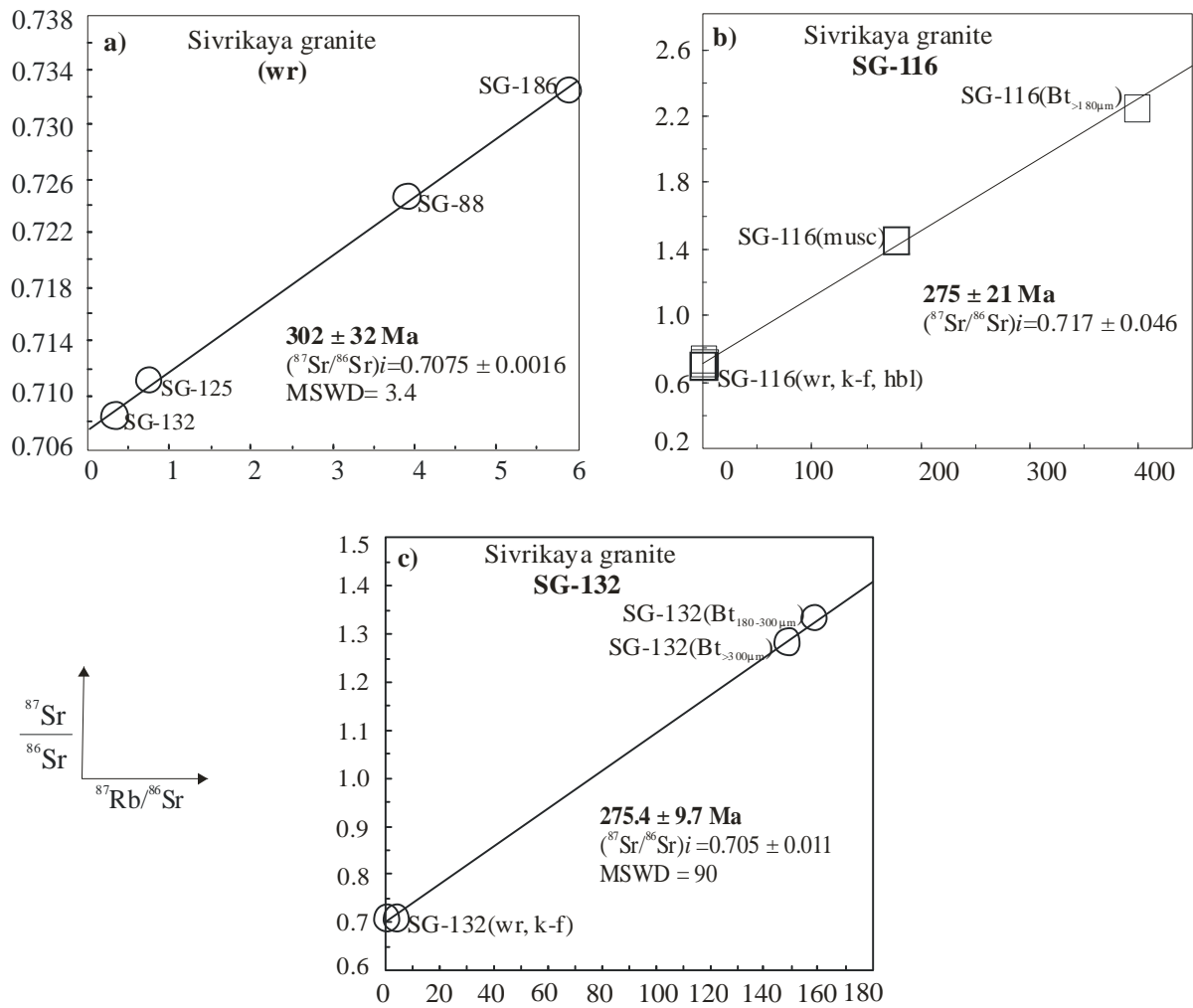


Fig. 3.19- $^{87}\text{Sr}/^{86}\text{Sr}$ vs. $^{87}\text{Rb}/^{86}\text{Sr}$ whole-rock and mineral isochron plots of data from Sivrikaya granitoid (samples SG-88, SG-132, and SG-186).

2. Deliktaş leucogranite (DLG)

Monzogranite sample DLG-114. Nine zircon fractions were analysed from this sample (Table 3.3). Uranium concentrations range from 244 up to 3258 ppm. Four zircon fractions with variably small degrees of Pb loss plot close to the concordia curve at ~295 Ma and two are concordant at ~375 Ma. The latter age indicate the presence of a xenocryst which can be observed in the CL images as turbid/metamict cores or endogenic zircons (Fig. 3.15a-b), which had earlier lost Pb and/or U during a Devonian event. The presence of two morphological types of zircons in this sample as revealed by CL images (Figs. 3.15a, b) is clearly visible in the result, for example, the clustering of the data points in two groups (~375 & 295 - 298 Ma) (Fig. 20). Meanwhile, one other fraction (DLG-114-1) is discordant indicating the presence of an old Pb-component. This zircon fraction has significantly low U (244 ppm) and Pb (32 ppm) concentrations than the other fractions. A discordia calculated

through DLG-114-1 and the fractions concordant at ~300 Ma yielded an upper intercept age of 2682 Ma (Fig. 3.20).

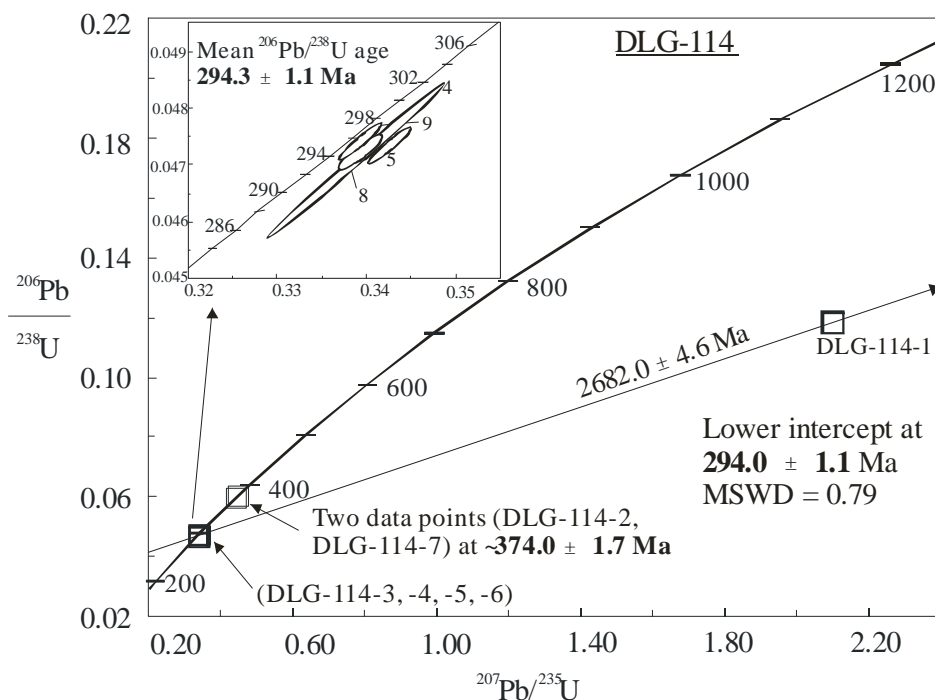


Fig. 3.20- Concordia plot showing U-Pb zircon isotope dilution analyses from Deliktaş sample DLG-114. The upper intercept age of 2682.0 ± 4.6 Ma is given by a discordia calculated through the data points nearly concordant at ~295 Ma (inset) and one fraction with relic core. Error ellipses are $2\sigma_m$.

Monzogranite sample, DLG-83. $^{206}\text{Pb}/^{238}\text{U}$ and $^{207}\text{Pb}/^{235}\text{U}$ ages of nine zircon fractions show a large scatter, the discordant analyses cluster at $^{206}\text{Pb}/^{238}\text{Pb}$ ages of ~275 Ma and 295 Ma (Fig. 3.21). Only one fraction is concordant at ~290 Ma. The discordance in these zircons most likely resulted from Pb-loss combined with minor contribution of preexisting grains (e.g. the homogeneous and metamict crystals without pronounced zoning patterns, Fig. 3.15b, grains 2, 3). Uranium concentrations are very high, ranging from 928 to 8067 ppm (Table 3.2). Zircon grains with the highest U content (8067 ppm) yield the lowest $^{206}\text{Pb}/^{238}\text{U}$ age (~260 Ma) indicating Pb loss related to radiation damages and metamictization process (e.g. Davis and Krogh 2000; Nasdala et al. 1996). It is impossible to draw a discordia line through the data points and to find a precise age for this sample.

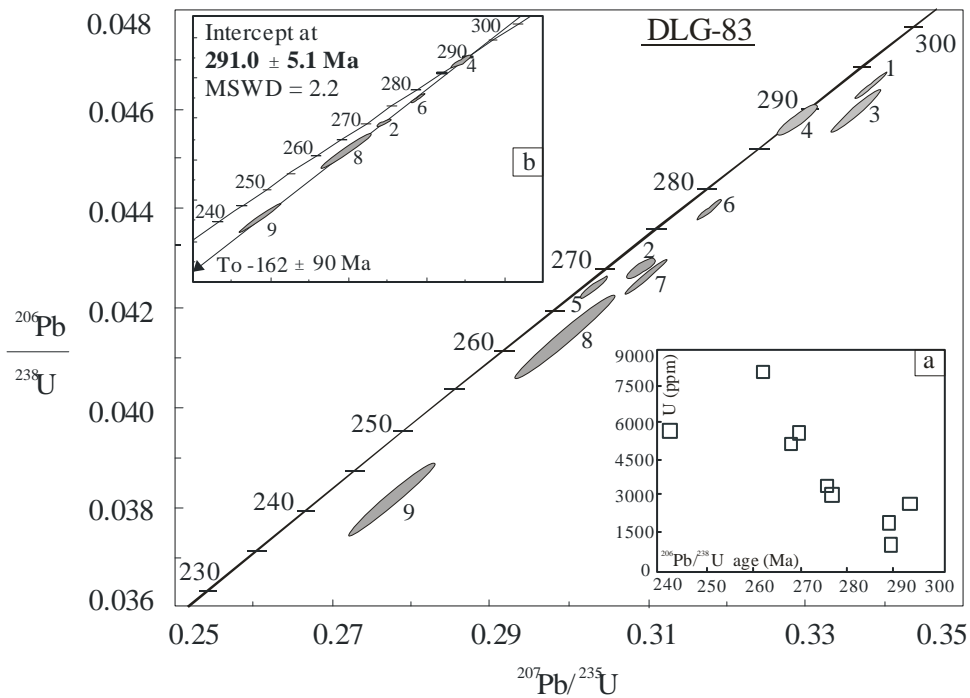


Fig. 3.21- U-Pb concordia plot for zircon analyses from sample DLG-83. A discordia through five data points yields 291.1 ± 5.1 Ma (inset). Error ellipses indicate $2\sigma_m$.

A plot of all the U-Pb data from the two DLG samples on a concordia diagram further shows two groups of ages (Fig. 3.22). However, six fractions are nearly concordant and define an average $^{206}\text{Pb}/^{238}\text{U}$ age of ~ 295 Ma. Considering the Rb-Sr muscovite age (Fig. 3.23) I tentatively interpret the age 295 Ma as the crystallization time of main bulk of the Deliktaş granite.

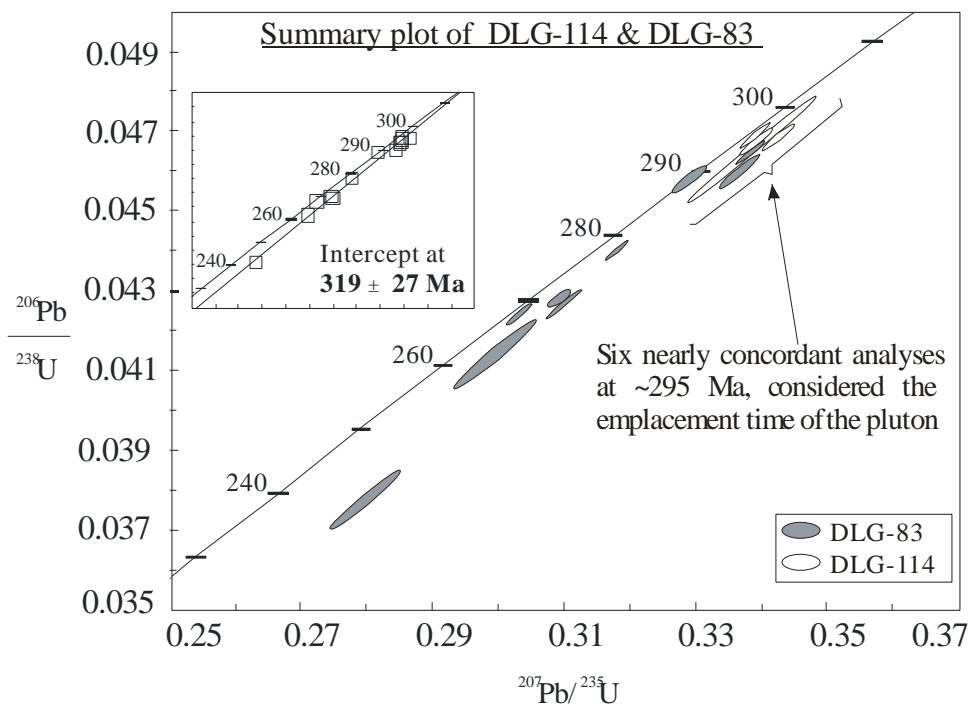


Fig. 3.22- Summary U-Pb concordia plot for zircon analyses of Deliktaş granite samples (DLG-114 and DLG-83)

Most of the Deliktaş (DLG-83, DLG-114) zircons show very high U-concentrations, high radiogenic and total Pb-content, as was observed in U-rich metamict zircons by Wiedenbeck et al. (1995), Mattinson et al. (1996) and Corfu (2000), for example, fractions 3, 4 and 9 from DLG-114 (2000-3200 ppm U) and DLG-83 (928-8100 ppm U). Abrasion of the outer rims of zircons did not reduce the discordance in Deliktaş samples (DLG-83). Therefore, Pb-loss also occurred in the zircon cores, which show altered interior and totally destroyed zonation (Fig. 3a-b). This attests that Palaeo-weathering caused the Pb-loss in the Deliktaş zircons (e.g. Black, 1987). I therefore, think that the zircon age pattern of the DLG monzogranites reflects a syn-magmatic-metamorphic and sedimentary source.

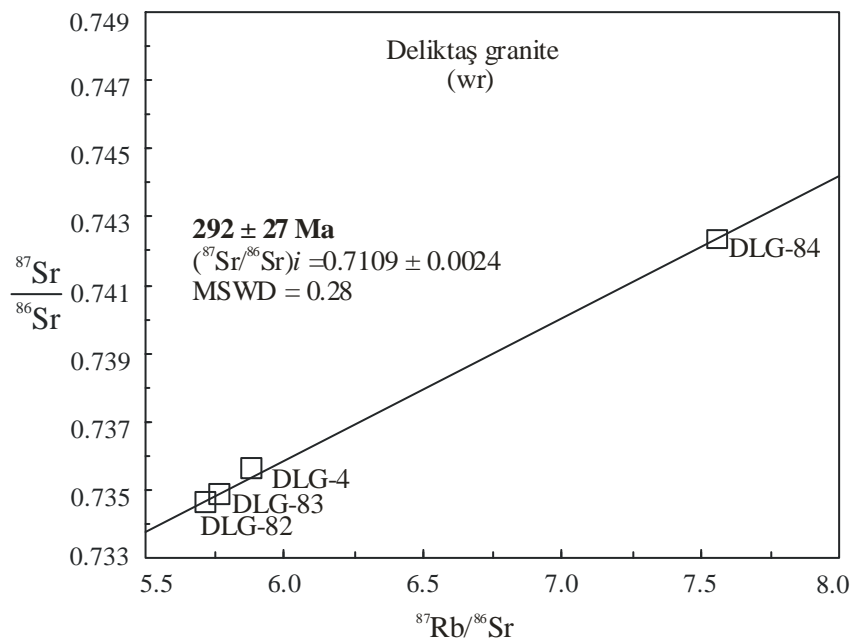


Fig. 3.23- $^{87}\text{Sr}/^{86}\text{Sr}$ vs. $^{87}\text{Rb}/^{86}\text{Sr}$ whole-rock isochron plots of data from Deliktaş granite.

Rb-Sr whole-rock analyses from the Deliktaş monzogranites define an isochron age of 292 ± 27 Ma (MSWD= 0.28 and $\text{Sr}_{(i)} = 0.7109 \pm 0.0024$) (Fig. 3.23). The Rb-Sr age, although with large error is similar to the U-Pb ages.

Four muscovite separates give an average Rb-Sr age of 290.1 ± 2.9 Ma and one K-feldspar gives an age of 273.8 ± 2.8 Ma. The muscovite in these samples is coarse-grained and euhedral, the blocking temperature for coarse-grained muscovite may reach 600-650°C (Cliff 1985), i.e., are close to the crystallization temperature of a granite. Therefore, the Rb-Sr muscovite age of 290.1 ± 2.9 Ma is considered to be close to the crystallization time of this pluton. Probably a post-intrusive event had rejuvenated the Rb-Sr-system of the K-feldspar.

3.3.3. Discussion and conclusions on geochronology

The zircon ages presented in this study provide the first reliable age constraints on the magmatism in the Kastamonu area and have significant regional implications. From the new data the following tentative conclusions can be drawn:

- The ages from the different radiometric methods allows us to suggest that the emplacement times of the Sivrikaya and Deliktaş plutons were between 303-300 Ma, and 295-270 Ma respectively, much older than the previously estimated Middle Jurassic ages. Three zircon fractions from Sivrikaya and Deliktaş granitoids contain relic cores that yield Precambrian protolith ages. These ages, in conjunction with the Nd average crustal residence time although younger indicate the contribution of recycled Precambrian material. This reiterates the observation by former workers that the central Pontides constitutes fragments of Gondwana and Laurasian Superterrane. The difference in age between the Sivrikaya and the Deliktaş is also accompanied by a change in the magmatism, from slightly metaluminous transitional-type to peraluminous S-type. The Late Carboniferous-Early Permian ages justify the conclusion that Variscan plutonism (until now, unidentified in the central Pontides), despite the tectonic setting, is a common feature of the Tethysides (Şengör et al. 1993), co-existing with Middle Mesozoic plutons in the Kastamonu granitoid belt (Boztuğ et al. 1995; Yılmaz and Boztuğ 1986).

- The geodynamic setting of the Carboniferous-Permian granitoids in the Central Pontides is complicated, and they could be explained by subduction of the Palaeotethys beneath Eurasia or Gondwana. Such pre-Jurassic granitoids are common in other parts of the Pontides and have been interpreted to be of Gondwanan origin. The Sivrikaya and Deliktaş granites therefore, indicate the Central Pontides is contiguous with the Sakarya and the Istanbul Zones.

- The Central Pontides is a juxtaposition of the Precambrian-Palaeozoic Istanbul and the Sakarya Zones, with distinct Devonian-Palaeozoic-Mesozoic metamorphic and magmatic histories (e.g. Chen et al. 2002b; Görür et al. 1997; Haas 1968; Stampfli 2000). The 375-345 Ma event recorded in some zircons is a common feature of pre-Variscan metamorphism and magmatism (e.g. Matte 2001; Warr 2002). This means that, the magma-source inherited Devonian zircons from the heterogeneous Central Pontides basement that did not have enough residence time in the small dyke to develop growth zonation.

- The Late Carboniferous-Early Permian ages for the Sivrikaya and Deliktaş granitoids and the geochemical and isotopic data of the granitoids and basement, suggest that they were components of the Variscan orogenic belt.

The geochemical and isotopic signatures of the Sivrikaya and Deliktaş granitoids in combination with the protolith ages, therefore, could be interpreted to indicate an evolution from Eurasian continental arc magma-type represented by the Sivrikaya granitoid, to entirely anatectic Gondwana-Eurasian continental post-collisional magma-type, as crystallized in the Deliktaş monzogranite. The younger ages, the high U-content of the zircons and the highly evolved nature of the rocks, the Deliktaş leucogranite appears to represent the final stage of the magmatism linked to the Late Palaeozoic subduction of the Palaeotethys beneath south Eurasian margin (e.g. Chen et al. 2002b; Okay et al 2006). Apart from continental convergent zones, both granite types can be expected in mature continental magmatic arcs to sit on continental crust. In this light, the Late Carboniferous-Permian magmatism can be considered as the consequence and culmination of a long-lasting active margin setting that has occurred since the Palaeozoic.

*Granites are not simply chemical numbers but are
representative of central geological processes.*

4. DEVREKANI GRANITOID (DG)

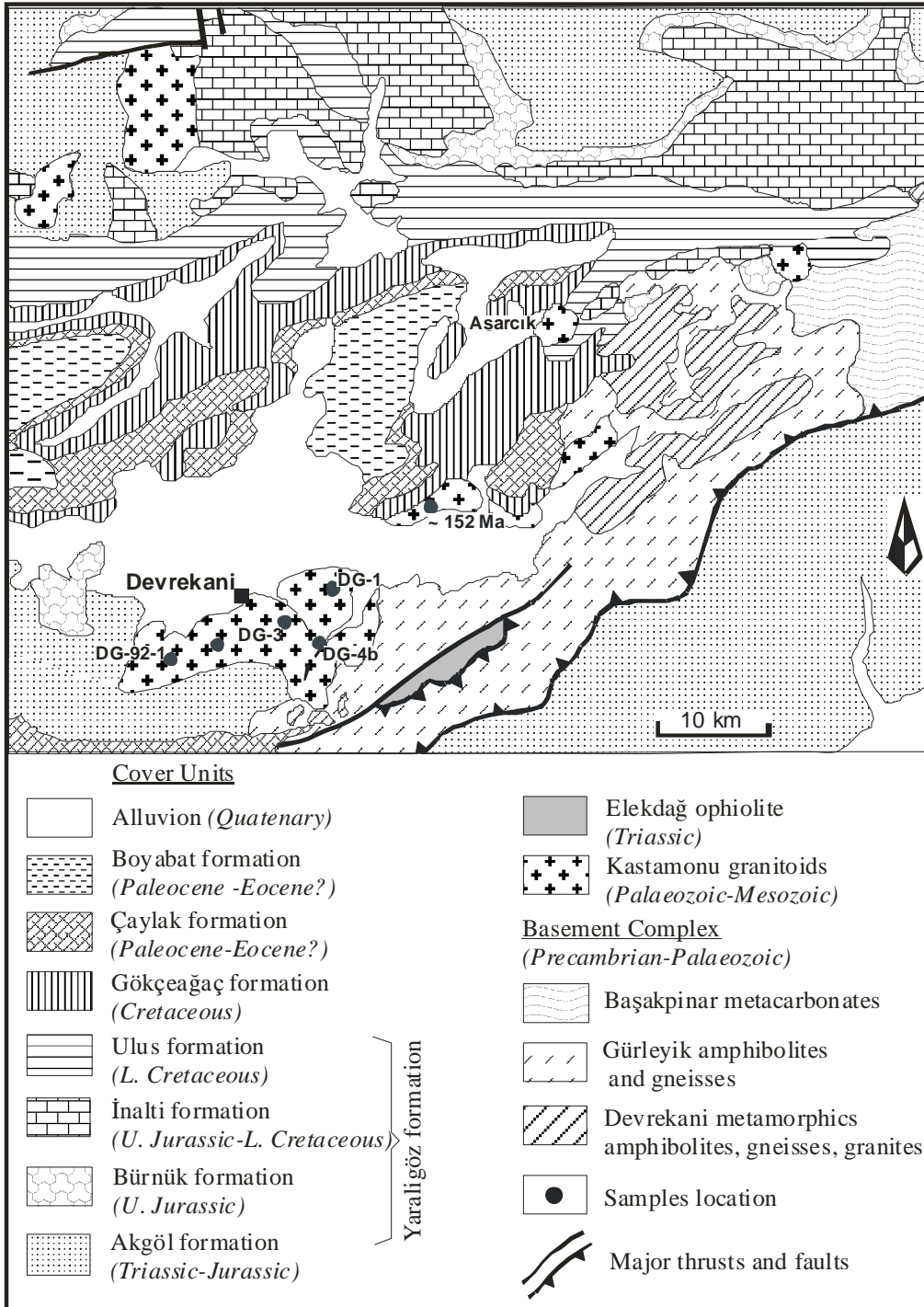


Fig. 4.1- Sketch map of Devrekani granitoids and basement Complex (modified from Şengün et al., 1990; Tüysüz et al., 1999)

4.1. PETROGRAPHY

The Devrekani granitoid is geochemically zoned (with a more mafic core), and highly tectonized indicating the emplacement before the Early Cretaceous collision-accretion-extension regime that followed the south-dipping subduction of the Palaeotethys Küre marginal basin (e.g. Okay, 2000; Okay et al., 2006; Ustaömer and Robertson, 1997). It crops out for ~60-70 km² in the Devrekani town, Kastamonu province, where it intrudes the Proterozoic-Palaeozoic (Tüysüz, 1990; Yılmaz, 1980; own unpublished data) Eurasian-derived continental basement (e.g. Aydin et al., 1995; Ustaömer and Robertson, 1993, 1994, 1997), and the Triassic-Early Jurassic flyschoid country-rocks (İnalti/Börümce formation) (Fig. 4.1). A low grade contact aureole developed between the intrusion and the flyschoid country-rocks (Yılmaz et al., 1996, 1997). The association of Kastamonu granitoids with contemporaneous volcanic rocks shows that the plutons were emplaced at high level (Peccerillo and Taylor, 1976; Ustaömer and Robertson, 1992, 1993).

DG samples were collected from around Devrekani town and at the Musa valley (Fig. 4.1, DG-4b). Petrographically the rocks are plagioclase-hornblende-biotite diorites, and quartz and minor tonalitic-diorites. Generally, the Devrekani granitoid rocks are medium to coarse-grained occasionally with micro-granular enclaves. They display porphyritic textures with euhedral plagioclase, hornblende, and pyroxene megacrysts set in a medium-grained subhedral-anhedral groundmass of latter minerals, biotite and quartz (Fig. 4.2). The major rock-forming mineral assemblage is plagioclase (albite + Ca-rich anorthite 40 to >50% in DG-2a, DG-2b and DG-3), dark-green pleochroic subhedral to euhedric hornblende (basal sections) and subhedral pyroxene (enstatite) make up >45 % of rocks. Accessory zircon, calcite, magnetite, dark-brown biotite, clinopyroxene (augite), quartz (interstitial), magnesite and ilmenite occur in variable proportions. Temperatures of granitoids magmas may be estimated from apatite and zircon saturation temperatures that can be calculated from chemical composition of rock samples (Harrison and Watson, 1984; Hanchar and Watson, 2003). For any given melt, saturation temperatures for apatite and zircons components depend on both melt composition and temperature, whereby the solubilities of both components increase with temperature. Apatite and zircon saturation temperatures calculated from bulk-rock chemical analyses will therefore correspond to maximum or minimum temperature limits for the intruding magma depending on whether the melt was saturated or undersaturated in these components. Zircon is abundant and euhedral, and does not occur as inclusions in other minerals. Inferring crystallization took place together with other minerals and at high temperatures. The dominance of hornblende throughout the rocks suggests that the magmas were either hydrous at the onset or became hydrated through contamination in the crust.

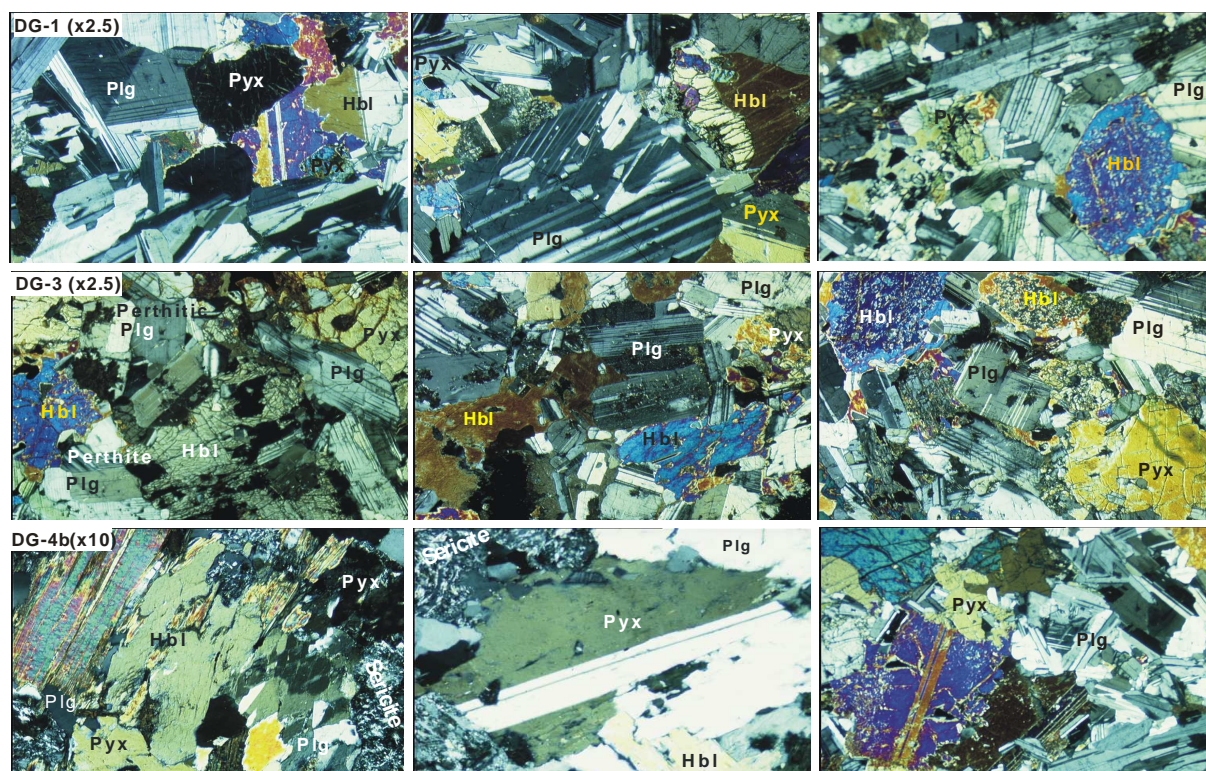


Fig. 4.2a- Representative microphotographs of Devrekani granitoid rocks (DG-1, DG-3, DG-4b). Note the late magmatic formation of hornblende (*Hbl*) (DG-4b). Plagioclase (*Plg*) and *Hbl* are at times sericitized (*Se*). Abbreviations: *Qtz*, quartz; *Pyx*, pyroxene.

With accessory K-feldspar (orthoclase, DG-1, DG-4b, DG-92-1, DG-134 in DG-3) chromite, apatite, titanite, allanite and secondary hematite. The plagioclase phenocrysts are euhedral, twinned and zoned, rarely altered (sericitized, e.g. Fig. 4.2b, DG-92-1, DG-134) and at times exhibit microperthitic to perthitic texture with K-feldspar (DG-1, DG-3, DG-2, DG-134). In some cases the pyroxene is twinned and well zoned, and rarely with hour-glass zonation (DG-1, DG-4b) indicating that the clinopyroxene have relatively high Ti-content. Microphotographs of sample DG-134 show magmatic growth of hornblende at the expense of plagioclase. Locally, biotite and amphibole are partially chloritized and epidotized, and usually contain zircon or apatite inclusions. The epidote is secondary, and occurs as fine-grained aggregates replacing plagioclase. Some rock (DG-2a, DG-2b, and DG-3) thin-sections show evidence of biotite and hornblende sericitization.

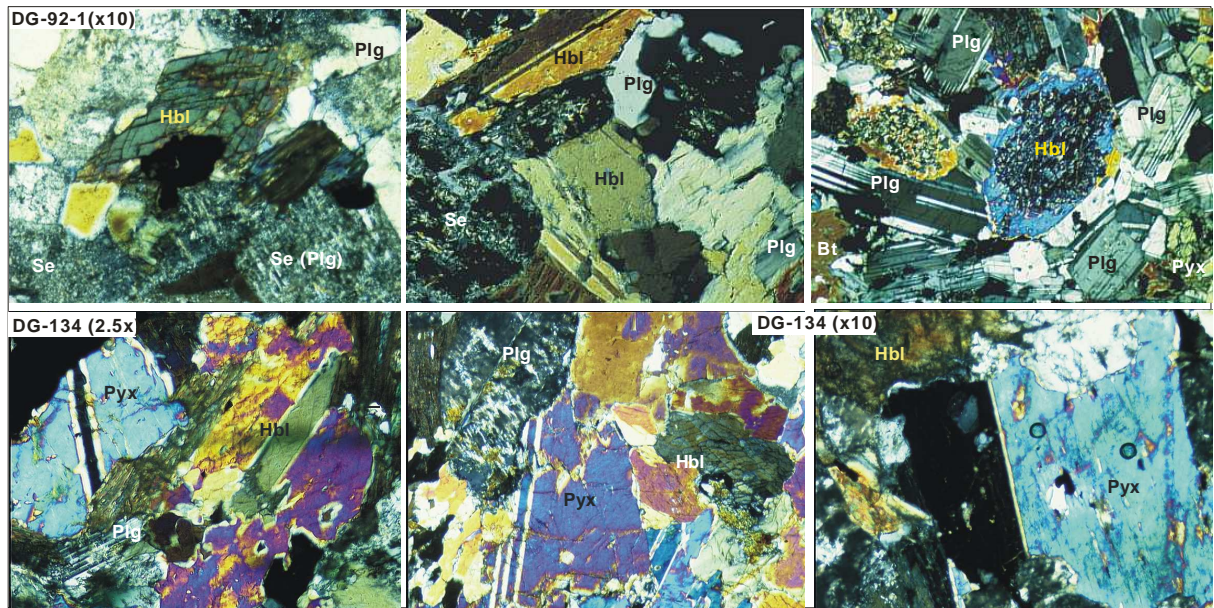


Fig. 4.2b- Representative microphotographs of Devrekani granitoid samples (DG-92-1, DG-134). Note the formation of hornblende (*Hbl*) at the expense of pyroxene (*Pyx*) (DG-134). The plagioclase (*Plg*) is strongly sericitized (*Se*).

4.2. GEOCHEMISTRY

4.2.1. Major and trace elements

Representative chemical analyses of samples are listed in Table 4.1. The bulk whole-rock concentrations of the Devrekani granitoid is characterized by low SiO_2 (49-59 wt %). Harker variation plots (Figs. 4.3) show a cluster of data points in two groups of rocks; diorites (e.g. DG-2a, DG-2b and DG-3) characterized by high Al_2O_3 , FeO, MgO, CaO and Co concentrations but low Na_2O , K_2O , Rb, Ba and REE contents (Figs. 4.4) and tonalites (DG-1, DG-92-1, DG-01-1, DG-4b, DG-4c, DG-134). These geochemical differences are reflected in the DG-1, DG-2a, DG-2b and DG-3, composed largely of plagioclase (>60%), hornblende and pyroxene megacrysts, and more porphyric texture (Figs. 4.2).

Table 4.1- Major (wt %) and trace (ppm) element abundances of Devrekani granitoid samples.

Sample	DG-01-1	DG-1	DG-92-1	DG-2a	DG-2b	DG-3	DG-4b	DG-4c	DG-134
SiO ₂	58.37	56.74	55.81	49.97	50.41	49.92	55.52	59.94	55.54
TiO ₂	1.14	1.05	0.60	1.89	1.54	0.43	0.83	0.81	0.88
Al ₂ O ₃	15.81	16.11	16.25	20.13	19.16	19.06	16.27	16.35	18.26
Fe ₂ O ₃	6.53	7.01	5.44	8.15	7.72	6.53	6.71	5.25	6.49
MnO	0.14	0.14	0.10	0.17	0.16	0.13	0.13	0.10	0.13
MgO	4.55	5.56	5.27	6.05	6.21	8.91	5.76	3.50	4.45
CaO	4.26	6.70	6.11	10.81	11.70	12.24	7.01	5.13	7.07
Na ₂ O	4.03	3.38	3.70	2.91	2.77	1.93	3.34	4.02	3.66
K ₂ O	2.01	1.29	2.31	0.18	0.17	0.20	1.22	1.49	1.22
P ₂ O ₅	0.133	0.135	0.100	0.137	0.067	0.031	0.139	0.179	0.020
LOI	2.17	1.86	5.40	0.32	0.36	0.76	2.08	1.63	0.76
Sum	99.3	100.8	103.8	100.9	101.2	100.8	100.6	101.5	99.7
ASI	0.94	0.83	0.82	0.82	0.73	0.76	0.85	0.92	0.88
Mg#	58.0	60.8	66.0	58.8	61.8	73.1	62.6	57.3	57.6
Cs	<0.1	<0.1	<0.1	<0.1	<0.1	0.25	1.77	<0.1	2.20
Rb	86	56	102	8	6	10	52	53	61
Ba	468	242	327	126	120	58	179	225	237
Sr	290	248	332	307	303	271	365	269	123
Y	27	25	22	12	14	10	18	18	19
Pb	12	8	12	6	3	10	15	20	10
Zn	61	66	56	70	65	62	61	41	89
V	127	150	119	223	240	228	135	94	107
Cr	170	229	140	210	228	461	173	117	117
Li	<0.1	<0.1	<0.1	<0.1	<0.1	7.36	19.8	<0.1	8.1
Nb	<0.1	4.0	<0.1	7.0	6.0	0.5	6.0	8.0	6.5
La	21	25	36	8	15	4	14	31	10
Ce	23	23	37	<0.1	<0.1	9	30	28	17
Nd	17	12	17	8	<0.1	6	15	16	7
Sm	4.9	4.9	5.0	3.0	3.6	1.5	3.4	3.9	1.2
Eu	—	—	—	—	—	0.98	1.13	—	0.79
Yb	2.5	2.5	2.1	1.1	1.1	1.0	1.8	1.6	0.5
Th	6.1	5.0	6.9	0.1	<0.1	<0.1	10.0	9.2	6.1
U	<0.1	<0.1	<0.1	<0.1	<0.1	0.18	1.23	<0.1	<0.1
Co	24	24	20	28	26	32	25	16	18
Ni	2.5	11	18	24	14	45	32	38	30
Pr	—	—	—	—	—	1.19	3.69	—	1.81
Gd	—	—	—	—	—	1.72	3.32	—	0.99
Zr	114	99	103	25	24	31	84	118	92
Tb	—	—	—	—	—	0.28	0.52	—	0.14
Dy	—	—	—	—	—	1.81	3.27	—	0.81
Ho	—	—	—	—	—	0.38	0.67	—	0.16
Er	—	—	—	—	—	1.08	1.90	—	0.45
Tm	—	—	—	—	—	0.16	0.28	—	0.07
Lu	—	—	—	—	—	0.15	0.27	—	0.08
Hf	—	—	—	—	—	0.64	0.99	—	2.31
Ta	—	—	—	—	—	0.07	0.47	—	0.95
Sr/Y	10.8	9.9	5.6	25.6	21.7	27.1	20.3	15.0	6.5
Zr/Y	4.2	3.9	4.7	2.1	1.7	3.1	4.7	6.6	4.8
Ce/Yb	9.1	9.1	17.5	—	—	8.8	16.5	17.5	37.4
Eu/Eu*	—	—	—	—	—	1.84	1.04	—	2.22
[La/Yb] _N	—	—	—	—	—	2.6	5.0	—	14.0
[Gd/Yb] _N	—	—	—	—	—	1.35	1.44	—	1.70
K ₂ O/Na ₂ O	0.50	0.38	0.63	0.06	0.06	0.10	0.37	0.37	0.33
Fe ₂ O ₃ /MgO	1.44	1.26	1.03	1.35	1.24	0.73	1.17	1.5	1.46

— = not determined; *ASI* = Aluminium Saturation Index [molar Al₂O₃/CaO+K₂O+Na₂O];
LOI = loss on ignition; *Mg#* = 100 x molar [MgO/(MgO+0.9Fe₂O₃)]

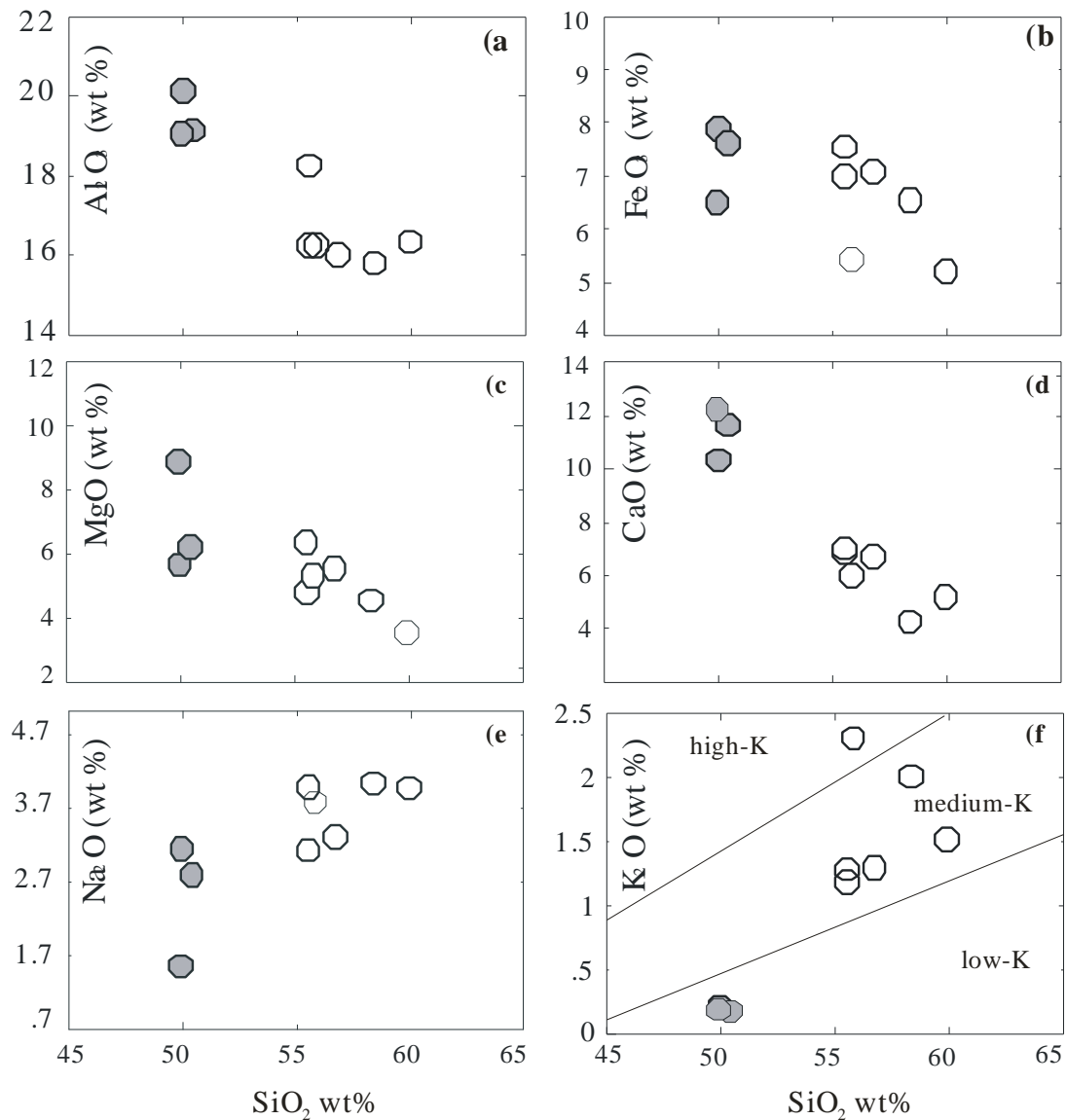


Fig. 4.3- Selected Harker variation plots of major elements for Devrekani granitoid, (f) shows field boundary between medium-K(normal calc-alkaline) and high-K series of Peccerillo and Taylor (1976)

Low aluminium saturation index (ASI= 0.73 - 0.94) describe the rocks as metaluminous I-type (e.g Chappell (1999); Chappell and White, 1974; Maniar and Piccolli, 1989) (Figs. 4.6c). The rocks are tholeiitic (DG-3) to calc-alkaline (Irvine and Baragar, 1971). Chappell and White (1974); Arculus and Johnson (1978); Saunders et al. (1980) suggested that many arcs showed temporal progression from tholeiitic through calc-alkaline rocks. The (Y + Nb) vs. Rb diagram (Pearce, 1982) define the rocks as volcanic arc granitoid (VAG) field. However, on the R1 vs. R2 diagram (De La Roche et al.; 1980) they spread from the mantle fractionates to pre-collision fields (Figs. 4.8a, b, d).

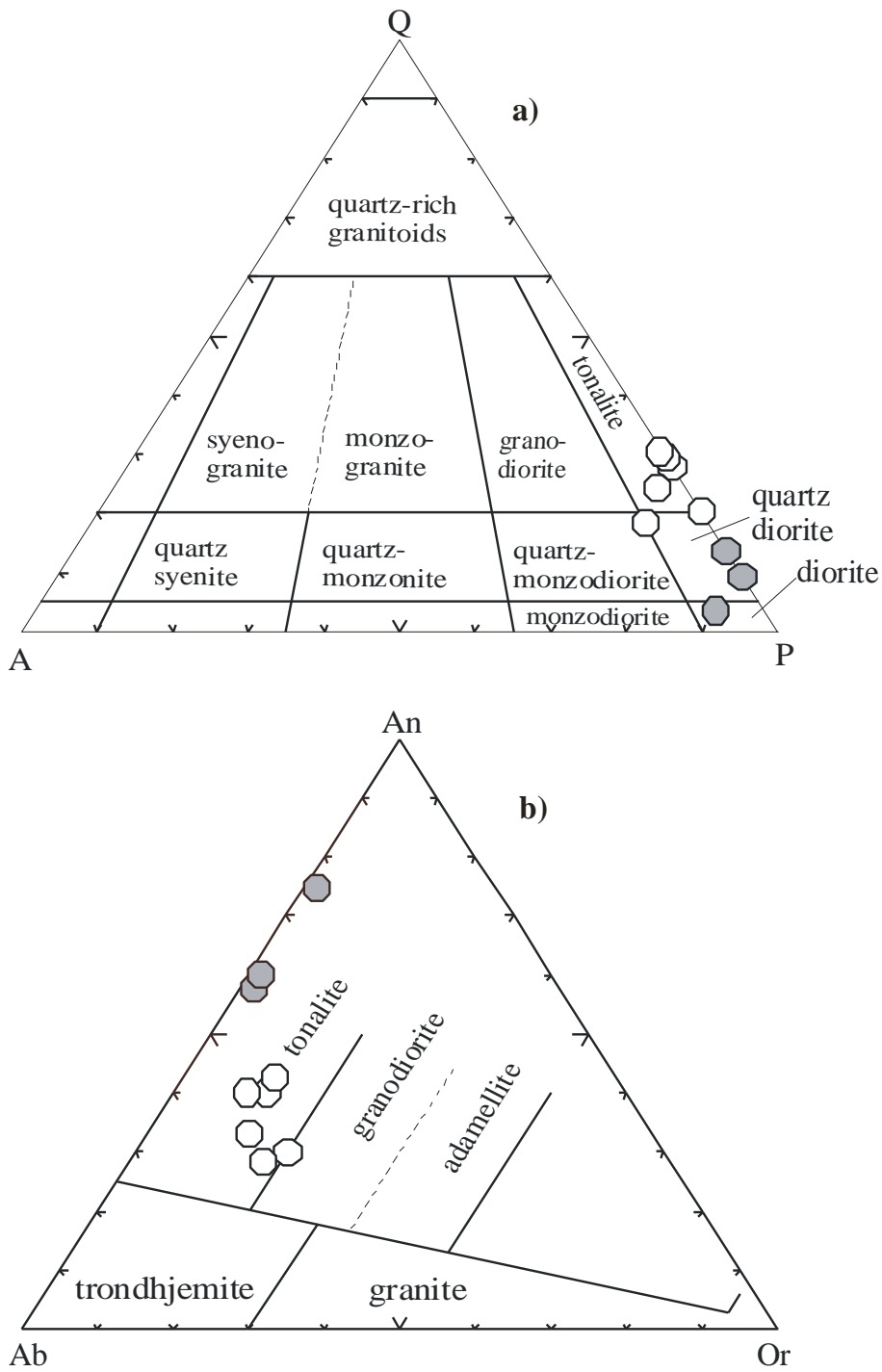


Fig. 4.4- Normative classification of Devrekani granitoid rocks according to modal mineral contents using (a) the QAP diagram of Streckeisen (1976) and Le Maitre (1989) and (b) the An-Or-Ab diagram of Baker (1979) and O'Connor (1965)

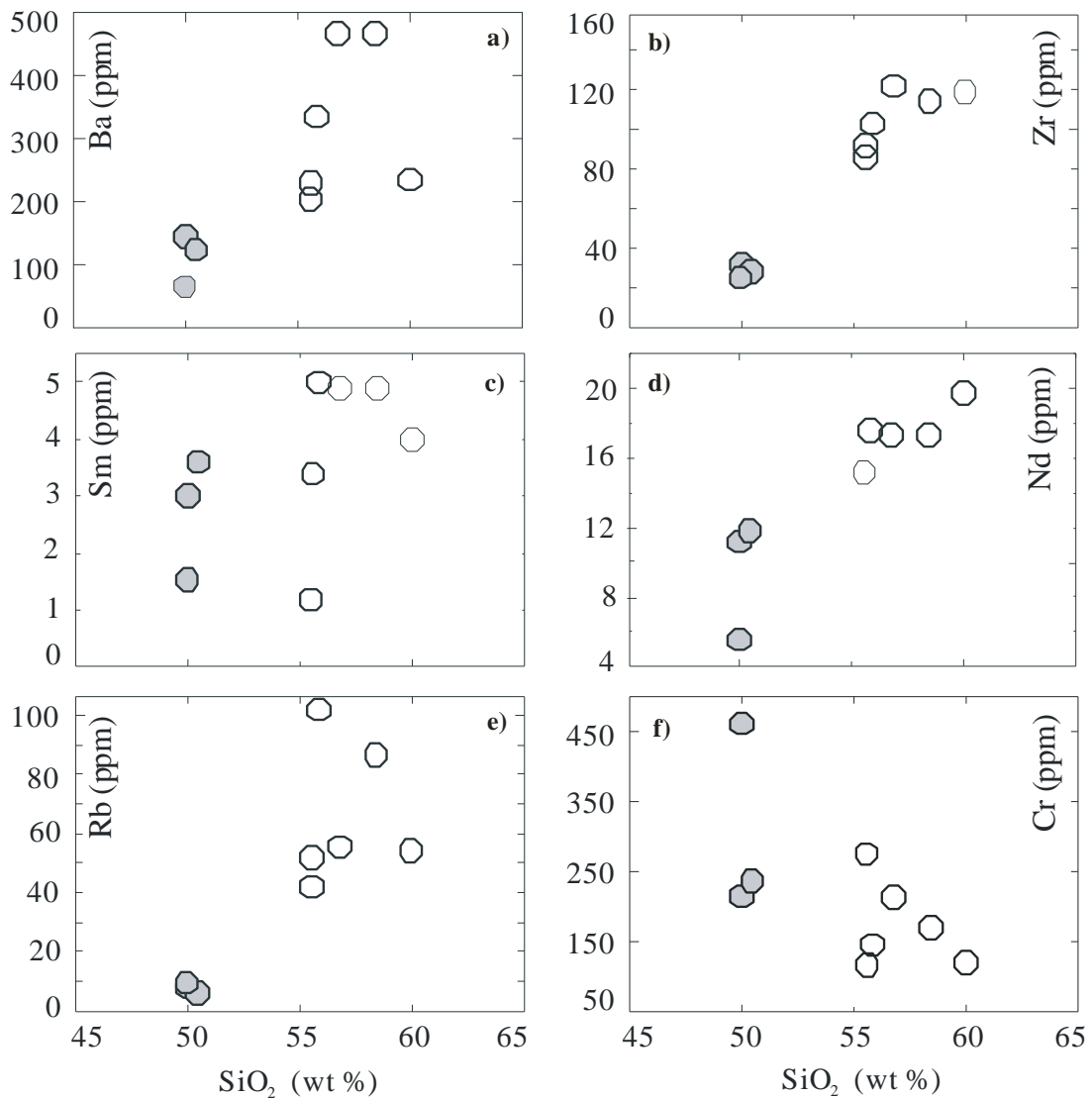


Fig. 4.5- Harker variation diagrams of selected trace elements for Devrekani granitoid

Geochemical features such as low K_2O/Na_2O ratios, high Ni, Cr and Sr contents, fractionated REE patterns and low Sr/Y, high La/Yb and Sr/Yb ratios (Table 4.1) are similar to modern adakites/ mantle-derived arc magmas, which formed in subduction environments, where the subducted slab is young and still hot, therefore, capable of undergoing partial melting (Dummond and Defant, 1990; Schiano et al. 1995; Martin, 1997; Davies and von Blackenburg, 1995; von Blackenburg and Davis, 1995; Kampunzu et al. 2003).

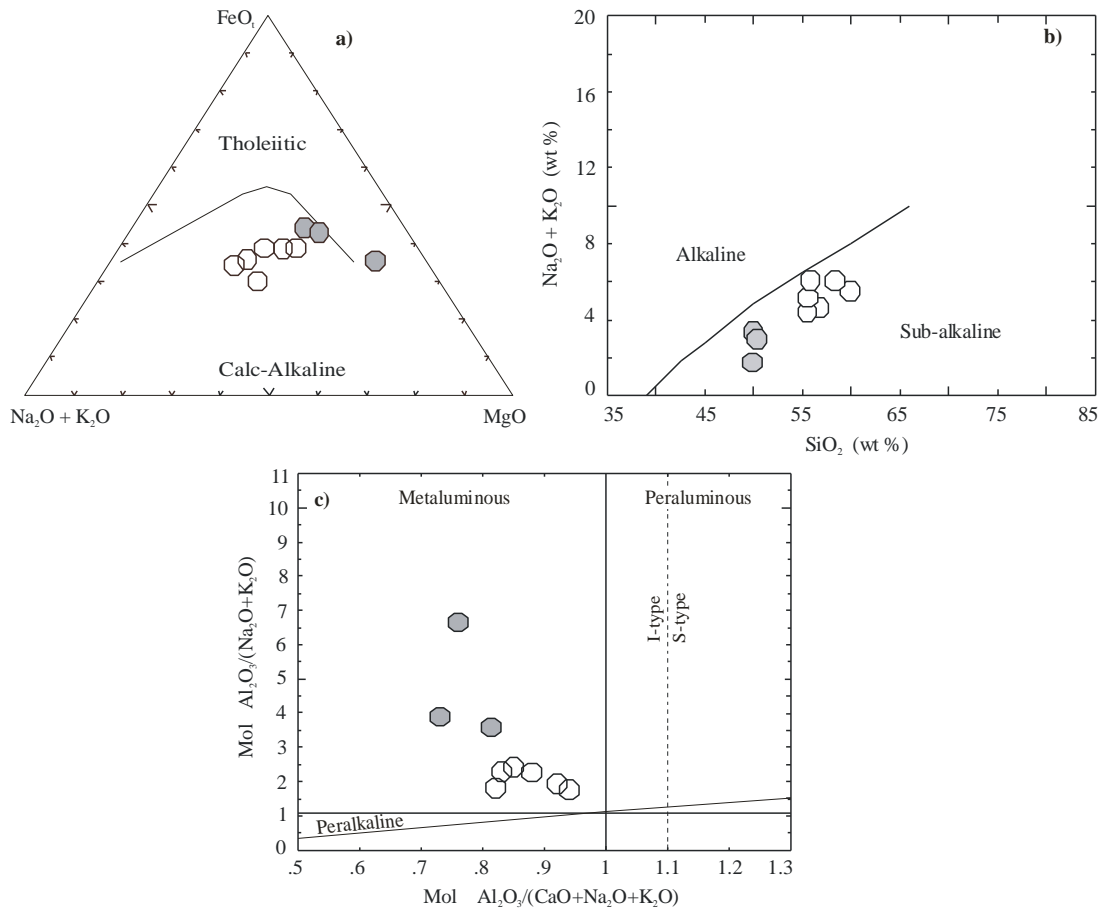


Fig. 4.6- Geochemical composition of Devrekani granitoid samples plotted on the (a) Calc-alkaline and (b) Silica vs. alkaline diagrams of Irvine and Baragar (1971, 1989), and (c) A plot of Shand's Index with fields of different granite-types after Maniar and Piccolli (1989)

4.2.2. Rare earth elements

Generally, all the Devrekani granitoid samples show enrichment in large ion lithophile elements (LILE) such as Cs, Rb, Ba and K, and depletion in Cr and Ni and depletion in high field strength elements (HFSE, Nb, and Ti) with respect to MORB. These features are commonly considered as characteristics of subduction-related magmatism (e.g. Floyd and Winchester, 1975; Keppler, 1996; Tatsumi and Kogiso, 1997). Sample DG-3 contains 461 ppm Cr and 44.5 ppm Ni at Mg# of 73, is tholeiitic and represents the most primitive near-primary magma.

Chondrite-normalized REE (cn, Sun and McDonough 1989) plots show broad spectrum of sub-parallel patterns characterized by little enrichment in light rare earth elements (LREE) (10-50x Chondrite values) and display flat heavy rare earth elements (HREE, 6-12x Chondrite) patterns with a small negative (DG-4b) to distinct (DG-3, DG-134) positive Eu anomaly ($Eu/Eu^* = \sqrt{[Sm_{(cn)} \times Gd_{(cn)}]} = 1.04$ to 2.22), and mildly fractionated REE patterns (Table 4.1,

Fig. 4.7a). The flat REE patterns and slight to moderate Eu anomaly may be related to plagioclase accumulation.

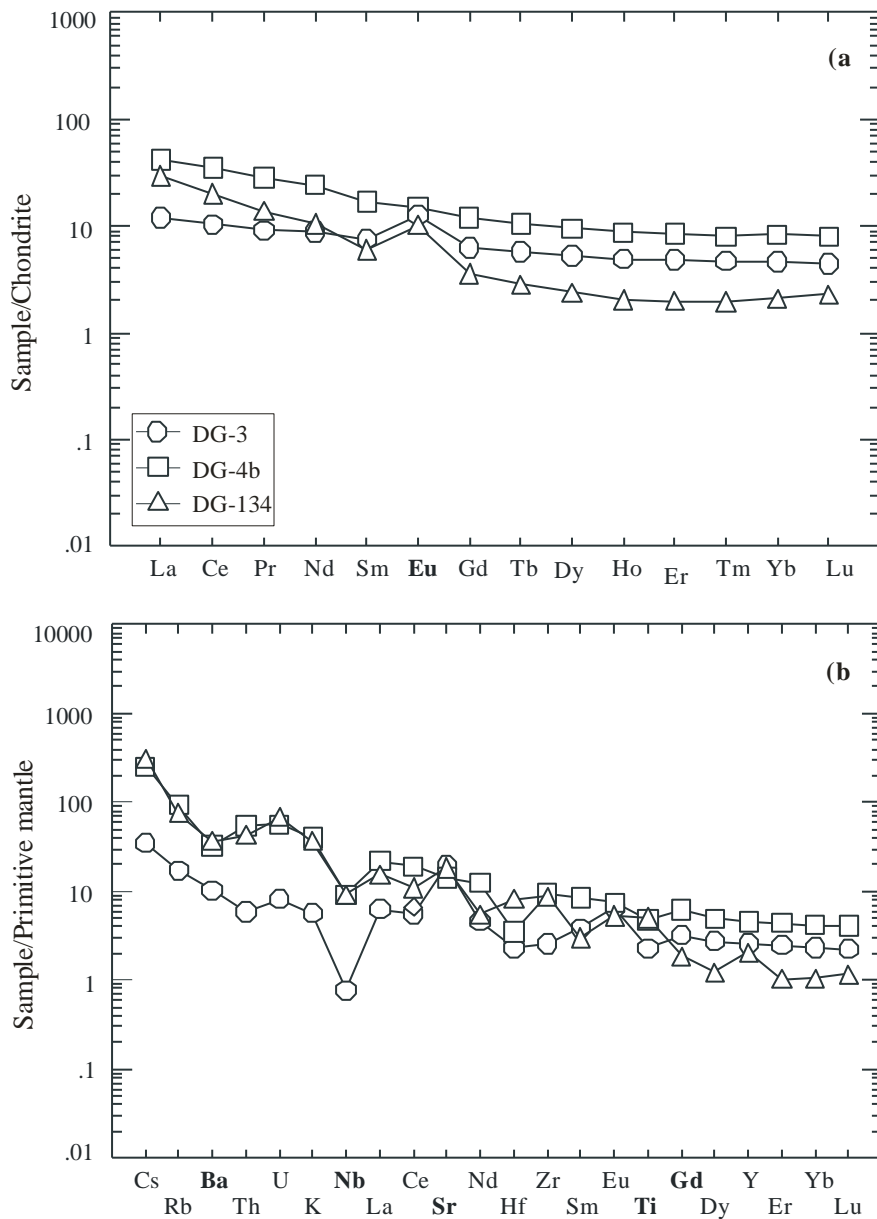


Fig. 4.7- (a) Chondrite-normalized rare earth element abundances and (b) Primitive mantle-normalized trace element abundances for the Devrekani granitoid. Normalizing values are from Sun and McDonough (1989)

Primitive mantle-normalized (Sun and McDonough, 1989) trace element patterns (Fig. 4.7b), similarly show two groups of samples with the diorites (e.g. DG-3) having lower concentrations and more pronounced Nb depletion. These features and slightly high V contents (94-240 ppm) are typical of less evolved I-type granitoids and suggest involvement of mantle material in the DG magmas genesis. Comparison of the normalized trace element patterns of DG samples allows the distinction into two groups of rocks. Low Rb contents (troughs) and variable Sr contents, suggesting derivation from plume-like mantle source; and

negative Nb and Rb anomalies, and restricted Sr concentration, which are usually interpreted as derived from mantle lithospheric sources. This is supported by the isotopic signatures which show a compositional range from OIB-like ratios to highly radiogenic MORB-like compositions (Fig. 8c). However, the linear relationships observed in the trace element data (Fig. 4.5) and the Sr-Nd plots probably invoke a binary mixture between two components crustal and enriched lithospheric mantle sources (e.g. McDonough and Sun, 1995; Sun and McDonough, 1989).

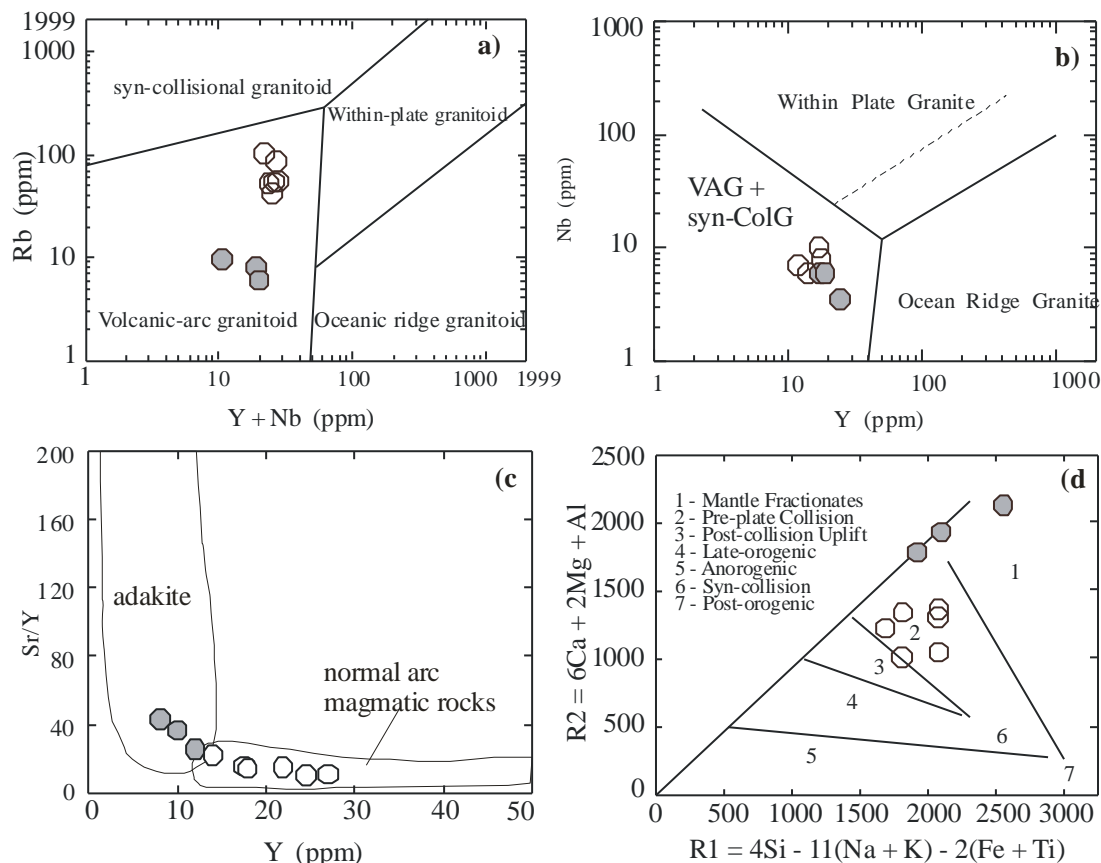


Fig. 4.8- Geochemical composition of Devrekani granitoid rocks plotted in the tectonic discrimination diagrams (a) Rb vs. Y+Nb and (c) Y vs. Nb (Pearce et al. 1984) and (e) Sr/Y vs. Y, fields from Martin et al. (2005); and (d) R1 vs. R2 (Batchelor and Bowden, 1985)

The elemental compositions and the inter-element ratios of DG rocks are similar to values documented in arc igneous provinces linked to three main processes: (1) mantle wedge enrichment by sediments recycled in the mantle along subducting slabs (e.g. Plank and Langmuir, 1993); (2) mantle wedge enrichment by fluids from the dehydration of a subducting slab (e.g. Keppler, 1996; Tatsumi and Kogiso, 1997) and (3) enrichment of the sub-arc mantle by slab-derived melts (e.g. Kelemen, 1995; Yogodzinski et al. 1995; Kepezhinskias et al. 1996; Sajona et al. 2000). The studies related to the mobility of elements in aqueous fluids escaping from the subducting slab (e.g. Stolper and Newman, 1994; You et

al. 1996) showed that more than 95% by mass are made of LILE and other highly compatible elements. LREE have low to moderate mobility whereas HREE are the least mobile. Therefore, arc magmas derived from partial melting of a mantle wedge enriched by fluids escaping from a subducting slab will be characterized by a strong enrichment in LILE (e.g. Sr, Pb, and Hf) versus a moderate enrichment in LILE/LREE in the melt. Mafic magmas generated in a sub-arc mantle source enriched by slab-derived fluids are generally marked by high Sr/Ce values ($>>20$), low Sr/Ce and low Ce/Pb ratios (<20) (e.g. Chauvel et al. 1995; Kapenda et al. 1998). However, Sajona et al. (2000) emphasized that the same enrichment style characterize mantle wedge sections metasomatized by slab melts. In contrast, mafic magmas originating from a sub-arc mantle enriched by subducting sediment melts are marked by low Sr/Ce, Ce/Pb and Sr/Y values. The large variation of ratios between incompatible trace elements, indicate a heterogeneous mantle source. This interpretation is supported by the coexistence of enriched rocks with both flat (DG-4b) and fractionated (DG-3 and DG-134) REE patterns. The flat REE patterns of some Devrekani granitoid samples and their relatively high Y and Yb contents indicate a garnet-free source. High Mg# and transition metal contents of the rocks are acquired during interaction of slab-derived melt with the overlying mantle and this is consistent with the following geochemical features of DG: (1) an increase of SiO₂ from diorites to tonalitic-diorites, and a correlative increase of [Gd/Yb]_{cn} and [La/Yb]_{cn}; (2) mild to no LREE and HREE fractionation in the diorites (Fig. 4.7a) and (3) high Ni and Cr abundances requiring an ultramafic source.

4.2.3. Sr-Nd-O isotopic compositions

The Devrekani granitoid Sr_(i) ratios range from 0.7052 to 0.7061 and the εNd_(t) values of -0.8 to -2.2 (Table 4.2, Fig. 9).

Table-2 Sm-Nd; Rb-Sr and O isotopic data of the Devrekani granitoid (DG)

Sample	Rb	Sr	[⁸⁷ Rb/ ⁸⁶ Sr] _i	[⁸⁷ Sr/ ⁸⁶ Sr] _m	[⁸⁷ Sr/ ⁸⁶ Sr] _i	Sm	Nd	[¹⁴⁷ Sm/ ¹⁴⁴ Nd] _m	[¹⁴³ Nd/ ¹⁴⁴ Nd] _m	[¹⁴³ Nd/ ¹⁴⁴ Nd] _i	εNd _(t) T _{DM}	δ ¹⁸ O _(VSMOW)	
	(ppm)					(ppm)					(Ga)	(‰)	
DG-1	54	283	0.547	0.70713±10	0.70584	4.1	17.1	0.147	0.512529±12	0.512370	-1.1	1.16	8.8
DG-2a	5	304	0.041	0.70544±9.3	0.70534	1.9	6.8	0.166	0.512566±09	0.512385	-0.8	1.51	8.2
DG-2b	3	296	0.029	0.70546±10	0.70539	3.5	11.6	0.183	0.512574±09	0.512376	-0.9	0.00	8.2
DG-3	10	365	0.074	0.70523±10	0.70523	1.6	5.7	0.170	0.512570±09	0.512385	-0.8	1.64	7.2
DG-4b	52	270	0.427	0.70692±9.4	0.70591	3.4	15.1	0.139	0.512479±23	0.512328	-1.9	1.14	8.4
DG-4c	54	266	0.558	0.70747±8.5	0.70616	3.5	16.3	0.130	0.512452±08	0.512311	-2.2	1.07	8.8
DG-134	44	348	0.366	0.70691±10	0.70605	3.6	16.6	0.129	0.512457±10	0.512317	-2.1	1.05	8.7
DG-01-1	86	290	0.565	0.70764±20	0.70631	4.3	17.8	0.145	0.512537±10	0.512380	-0.9	1.11	9.5
DG-92-1	96	327	0.852	0.70743±26	0.70542	4.0	17.7	0.138	0.512523±11	0.512374	-1.0	1.04	9.1

m = measured isotopic ratios; *i* = calculated initial isotopic ratios; εNd_(t) values were calculated using present day (¹⁴³Nd/¹⁴⁴Nd)_{CHUR} = 0.512638 and ¹⁴⁷Sm/¹⁴⁴Nd_{CHUR} = 0.1967; CHUR = Chondrite Uniform Reservoir; λ = 6.54 · 10⁻¹² a⁻¹ (Steiger & Jäger, 1977). The age of 165 Ma is used for the Nd_(i) and Sr_(i) calculations. [Sr_(i)] = (⁸⁷Sr/⁸⁶Sr)_i = (⁸⁷Sr/⁸⁶Sr)_m - ⁸⁷Rb/⁸⁶Sr(e^{λt} - 1); λ = 1.42 · 10⁻¹¹ a⁻¹

Young Nd model ages (T_{DM}) in the range of 1.6 to 1.0 Ga, indicate short crustal residence time compatible with young calc-alkaline arc-rocks (e.g. Ghost and Lambert, 1989), and the input of recycled Precambrian material in DG genesis. Figure 4.9a shows a variation of $\epsilon Nd_{(t)}$ versus $Sr_{(i)}$, whereby $\epsilon Nd_{(t)}$ values decrease slightly with increasing $Sr_{(i)}$ relative to mantle values, suggest mantle origin for all the DG rocks, with the diorite samples distinctly situated in the OIB field (e.g. Zhang et al. 2005). In the $^{87}Sr/^{86}Sr$ vs. $^{143}Nd/^{144}Nd$ plot of Machado et al. (2005) (Fig. 4.9c) the samples plot between the EMI and EMII fields, with the diorites situated closer to the EMI field.

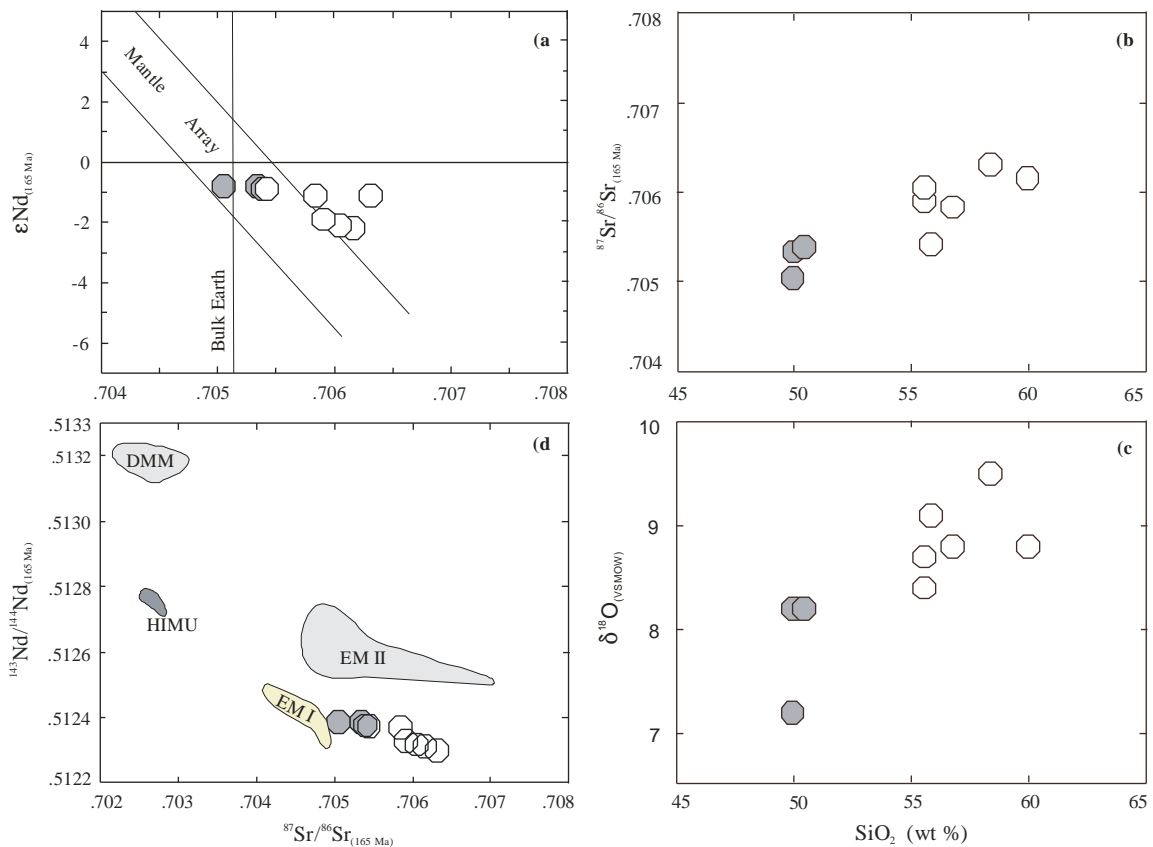


Fig. 4.9- Isotopic compositions of Devrekani granitoid samples (a) Initial $\epsilon Nd_{(t)}$ vs. initial Sr isotopic ratios; (b) and (c) SiO_2 and $\delta^{18}O$ values vs initial Sr isotopic ratios respectively. (d) Initial $^{143}Nd/^{144}Nd$ vs. initial $^{87}Sr/^{86}Sr$ isotopic ratios, fields of DMM (depleted mantle), HIMU, EMI (enriched mantle I) and enriched mantle (II) from Machado et al. (2005)

The $\delta^{18}O_{\text{whole-rock}}$ values of the Devrekani rocks are low with a narrow range from 7.2 to 9.1 ‰ is representative of a mantle and mixed origin respectively for the diorites and the quartz/tonalitic diorites. The nearly uniform $\delta^{18}O_{\text{whole-rock}}$ values (within uncertainties) for groups of rocks suggest that these rocks have not been severely affected by subsolidus $^{18}O/^{16}O$ alteration, and requires that any material assimilated during crystallization must have been similar to the magma in $^{18}O/^{16}O$ or only moderately enriched in ^{18}O . A positive

correlation between $\delta^{18}\text{O}$ and $\text{Sr}_{(i)}$ and SiO_2 values observed for the quartz/tonalitic diorite samples further indicate crustal contamination (Fig. 4.9d).

High and narrow range in $\text{Sr}_{(i)}$ ratios and $\epsilon\text{Nd}_{(t)}$ values, and high Sr content (mantle signature) for DG rocks, indicate recycled juvenile continental crust and/or small proportions of recycled older crust, consistent with the lack of inherited Precambrian zircons in all the samples.

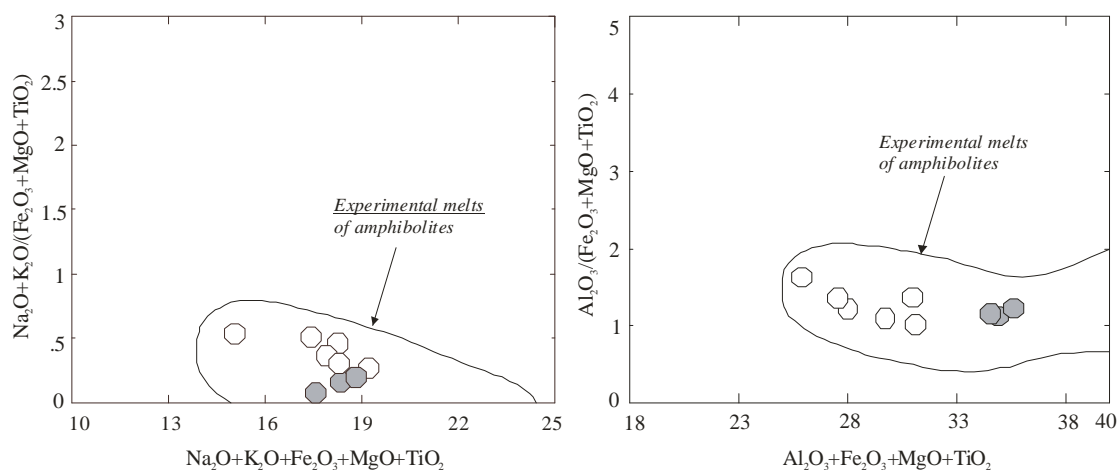


Fig. 4.10- Plots showing compositional fields of experimental melts derived from partial melting of amphibolites (Patiño Douce, 1999) and the composition of studied samples from Devrekani granitoid.

The composition of the DG supports its derivation from tholeiitic magma (amphibolite, e.g. Fig. 4.10). The HREE is flat suggesting garnet and zircon accumulation/formation. The DG crops out in a major extensional shear zone related to gravitational collapse of the Late Carboniferous orogeny. Because the intrusion is late syn-tectonic with respect to the shear fabric it is reasonable to assume that its generation in some way is related to the extension-collapse events. According to Dewey (1988) large volumes of mantle partial melts are injected into the lower crust during gravitational collapse of mountain chains by detachment faulting. I speculate that during the collapse event the geotherm crossed the garnet-lherzolite solidus and mafic melts were produced. The melt may have little interaction with the felsic lower crust, accumulated plagioclase, and intruded in the shear zones, giving rise to DG.

4.2. GEOCHRONOLOGY

4.2.1. Zircon internal structure

Devrekani samples are rich in zircons. Generally zircons from all the analysed samples are relatively large and of good quality, with relatively low U-content. The CL images reveal a population made up of euhedral grains with different morphologies (Fig. 4.11): long prism and stout multifaceted with combination of prism $\{(100)\}$ and $\{(110)\}$ and pyramid forms

{(211)}, {(101)}, and {(301)}, predominantly yellow to light brown, and variations between the two types. Inherited cores and overgrowth are not commonly observed.

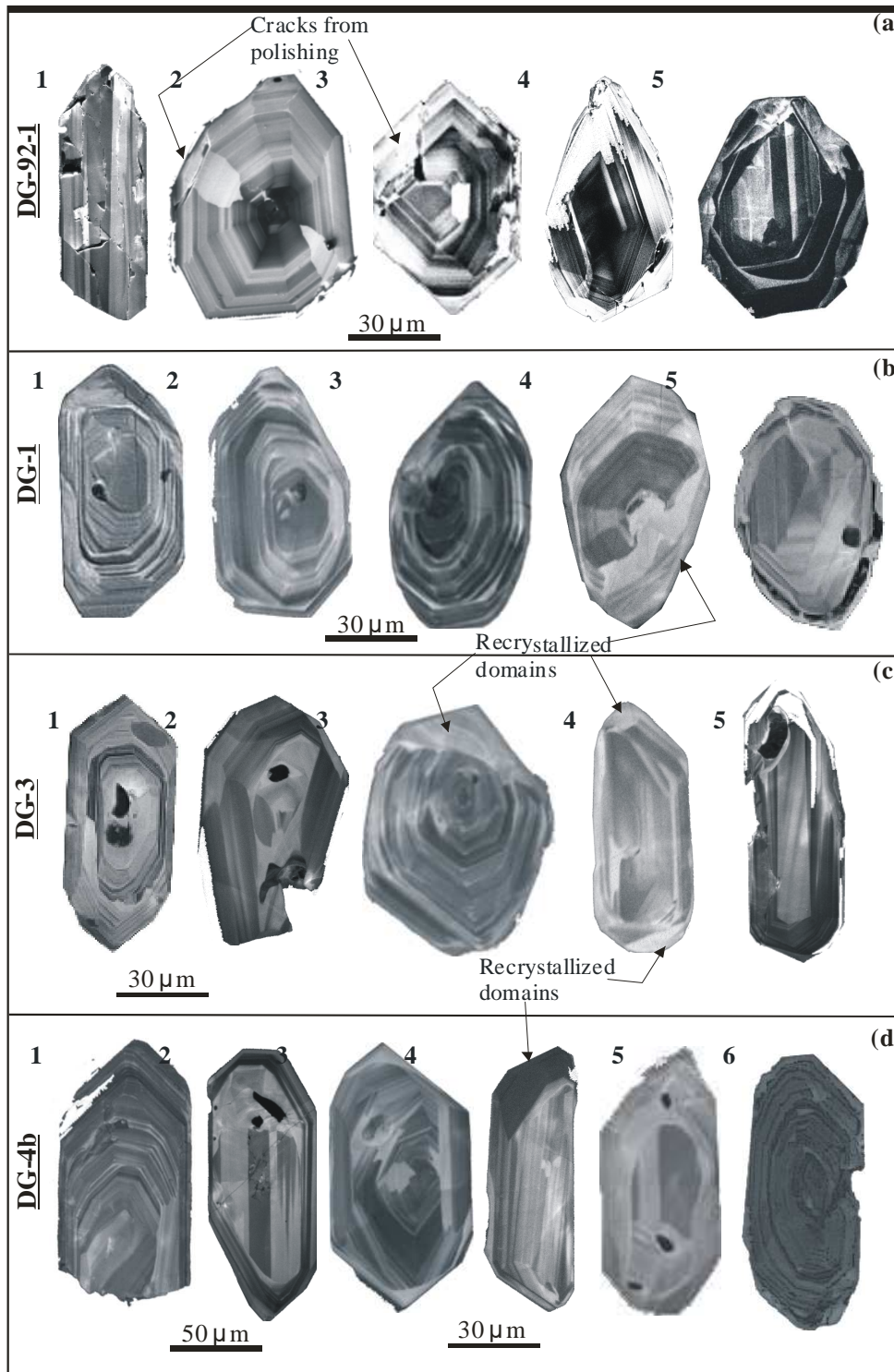


Fig. 4.11- CL photographs of characteristic zircon populations from Devrekani granitoid. Absence of xenocrystic cores and post-magmatic overprint. Rare recrystallized domains are observed. The crystals are 100-125 μm long and 60-100 μm wide. (a) DG-92-1 zircons show three grain-types; euhedral long-prism, multi-faceted and mixed crystals. Zircons internal structure show sector and oscillatory zoning; (b) DG-1 zircon population is homogeneous comprising stout multi-faceted crystals with different combination of prisms. Zircons internal structure show magmatic zoning. (c) DG-3 and (d) DG-4b zircons show a heterogeneous population made up of two contrasting grain-types; elongated, euhedral and multi-faceted stout, with oscillatory and sector zoning

This implies that the zircons grew in a melt and had not experienced alteration after crystallization. Such zircons usually yield concordant U-Pb ages (e.g. Poller et al. 1997).

DG-92-1 zircons are all light brown. CL analyses show three grain-types; simple euhedral long-prism, stout multifaceted with combination of prisms and mixed crystals (Fig. 4.11a). Zircons internal structure show sector and oscillatory zoning (grains 1-5). DG-1 zircon population is homogeneous comprising stout multi-faceted crystals with different combination of prisms. CL images show magmatic zoning (Fig. 4.11b, grains 1-5) and rare recrystallized domains (grains 3-5). The style of zoning (oscillatory and broad) may indicate differentiation of the pluton from diorite through quartz-diorite to more felsic compositions (e.g. Corfu et al. 2003). DG-3 zircons have long prisms and are multifaceted. CL images of zircons are similar, more commonly oscillatory and sector zoning (Fig. 4.11b). Rare recrystallization domains (e.g. Pidgeon, 1972) can be observed (Fig. 4.11c, grains 3-5). DG-4b zircons are yellow to brown, big, have very similar morphologies, consisting of euhedral, prismatic crystals rarely multifaceted (Fig. 4.11d). CL images reveal two types of grains: entirely oscillatory zoned zircons (grains 1, 3, 5) and grains with a sector-zoned inherited core surrounded by rims of magmatic overgrowth resulting in the euhedral shape (grains 2, 4).

4.2.2. U-Pb, Pb-Pb and Rb-Sr data

Tonalitic-diorite, DG-92-1: Eleven single zircons yield nearly concordant U-Pb ages between 164 Ma and 190 Ma (Fig. 4.12a). Regression of all eleven data points define an intercept age of 172.0 ± 9.7 Ma (MSWD= 7.9).

Quartz Diorite, DG-1: The U-contents in the range of 317 to 655 ppm are low. Nine data points from this sample plot close to and/or on the concordia between 164-175 Ma (Fig. 4.12b). Two fractions are reversely discordant at ~172 Ma and ~175 Ma. Regression of all the analytical points give a lower intercept age of 165.0 ± 5.3 Ma (MSWD=23). Four concordant fractions yield a mean $^{206}\text{Pb}/^{238}\text{U}$ age of 168 ± 0.73 Ma (MSWD=0.73), interpreted as the crystallization time of this rock (Fig. 4.12b, inset).

Diorite sample, DG-3: U-contents range from 351 up to 1294 ppm (Table 3). One fraction with minor surface related Pb-loss is discordant at ~164 Ma and two other fractions are reversely discordant at ~180 Ma (Fig. 4.12c). Regression of all the analyses define an intercept age of 170.0 ± 1.8 [± 3.3] Ma (MSWD= 1.6), considered the crystallization time of this rock.

Table 4.3- U-Pb-zircon isotope dilution analytical results of Devrekani granitoid samples.

Fraction	Zircon description	Concentration (ppm)				Isotopic ratios				Apparent ages (Ma)				
		Weight (mg)	U	Pb _{tot}	Pb _{ex}	$\frac{^{206}\text{Pb}}{^{238}\text{U}}$	$\frac{^{207}\text{Pb}}{^{235}\text{U}}$	$\frac{^{206}\text{Pb}}{^{207}\text{Pb}}$	$\frac{^{206}\text{Pb}}{^{238}\text{U}}$	$\frac{^{207}\text{Pb}}{^{235}\text{U}}$	$\frac{^{206}\text{Pb}}{^{207}\text{Pb}}$	$\frac{^{206}\text{Pb}}{^{238}\text{U}}$	$\frac{^{207}\text{Pb}}{^{235}\text{U}}$	Rho
DG-92-1	*1	0.0215	882	23.5	23.5	2193	0.026479±2777	0.180640±278	0.049479±22	168.5	170.5	168.5	170.5	0.997
	2	0.0165	1258	32.9	32.6	1219	0.026021±70	0.177462±73	0.049462±19	165.6	165.9	165.6	169.8	0.965
	*3	0.0296	202	5.7	5.7	472	0.026778±48	0.181019±85	0.049027±67	170.4	168.9	149.1	149.1	0.627
	4	0.0295	432	12.4	12.2	780	0.027301±46	0.184775±60	0.049087±37	173.6	172.2	151.9	151.9	0.785
	5	0.0119	469	17.7	13.6	145	0.028284±115	0.192151±158	0.049272±102	179.8	178.5	160.8	160.8	0.764
	*6	0.0200	274	7.9	7.8	453	0.027116±44	0.185725±58	0.049676±38	172.5	173.0	179.8	179.8	0.754
	7	0.0169	374	20.1	10.1	72	0.026717±37	0.183543±147	0.049826±141	170.2	171.1	186.8	186.8	0.284
	8	0.0227	765	20.4	20.2	1034	0.026416±44	0.179496±50	0.049282±23	168.1	167.6	161.2	161.2	0.889
	*9	0.0213	330	9.6	9.4	546	0.028699±59	0.197127±125	0.049817±109	182.4	182.7	186.4	186.4	0.494
	10	0.0590	312	10.6	9.1	116	0.029209±79	0.203996±148	0.050652±120	185.6	188.5	225.0	225.0	0.586
DG-1	*11	0.0111	473	13.5	13.0	336	0.027612±71	0.190488±87	0.050035±49	175.6	177.0	196.6	196.6	0.824
	1	0.1021	516	14.3	14.0	1511	0.026178±53	0.178157±54	0.049359±15	166.6	166.5	164.9	164.9	0.989
	2	0.1006	502	13.2	13.1	2695	0.025892±83	0.176513±105	0.049444±65	164.8	165.1	168.9	168.9	0.789
	3	0.0994	549	17.2	14.5	323	0.026397±72	0.180782±76	0.049670±37	168.0	168.7	179.5	179.5	0.950
	4	0.1766	421	11.8	11.4	1223	0.026349±70	0.180341±71	0.049640±17	167.7	168.4	178.1	178.1	0.992
	5	0.1124	498	13.3	13.3	2772	0.026525±56	0.180821±56	0.049441±10	168.8	168.8	168.7	168.7	0.996
	6	0.0841	384	10.7	10.5	1155	0.026888±52	0.182899±53	0.049335±12	171.0	170.6	163.8	163.8	0.957
	7	0.1142	384	10.5	10.4	2674	0.026386±52	0.180000±52	0.049476±08	167.9	168.1	170.4	170.4	0.996
	8	0.1968	317	8.3	8.3	3189	0.025692±50	0.175350±51	0.049500±06	163.5	164.1	171.5	171.5	0.998
	9	0.0717	356	9.6	9.5	1692	0.026263±51	0.178514±52	0.049298±19	167.1	166.8	162.0	162.0	0.981
DG-3	10	0.1078	655	18.3	18.0	1887	0.027445±52	0.187164±52	0.049460±07	174.5	174.2	169.6	169.6	0.997
	1	0.0496	645	16.6	16.6	3509	0.026446±74	0.180610±75	0.049617±29	167.9	168.5	177.0	177.0	0.981
	2	0.0490	1294	35.2	35.0	3166	0.028076±121	0.191285±123	0.049473±12	178.1	177.5	170.3	170.3	0.998
	3	0.0488	776	20.9	20.8	2202	0.027303±62	0.185542±63	0.049357±31	173.3	172.7	164.8	164.8	0.924
	4	0.0962	351	9.7	9.7	2741	0.028351±53	0.192949±54	0.049450±19	179.8	179.1	169.2	169.2	0.984
	5	0.0970	616	15.5	15.5	3078	0.026206±55	0.178869±56	0.049503±12	166.8	167.1	171.7	171.7	0.975
	6	0.0787	366	9.5	9.5	1916	0.026491±52	0.180552±53	0.049353±22	168.8	168.5	164.6	164.6	0.977
	7	0.0889	615	16.3	16.2	2523	0.026749±57	0.182612±58	0.049513±16	170.2	170.3	172.2	172.2	0.991
	8	0.0666	683	17.0	16.9	2497	0.025644±53	0.175243±55	0.049649±24	162.9	163.9	178.6	178.6	0.976
	DG-4b	1	0.0130	3901	99.5	98.5	2012	0.026087±162	0.179042±163	0.049777±12	166.0	167.2	184.5	184.5
2		0.0540	1272	43.3	41.3	944	0.033347±57	0.237643±57	0.051684±11	211.5	216.5	271.4	271.4	0.983
3		0.0575	449	23.4	23.3	3257	0.053079±53	0.392092±53	0.053575±06	333.4	335.9	353.2	353.2	0.993
4		0.0320	566	13.1	12.9	964	0.025947±60	0.179264±65	0.050107±24	165.1	167.4	199.9	199.9	0.932
5		0.2006	176	4.3	4.3	2341	0.025146±55	0.173296±57	0.049982±16	160.1	162.3	194.1	194.1	0.959
6		0.1680	419	10.9	10.8	2086	0.026518±84	0.182029±85	0.049786±14	168.7	169.8	184.9	184.9	0.986
7		0.0184	997	27.0	26.8	1338	0.027193±59	0.182879±128	0.048775±113	173.0	170.5	137.0	137.0	0.442
8		0.0187	1346	33.8	32.7	786	0.024863±109	0.171435±252	0.050009±226	158.3	160.7	195.3	195.3	0.443
9		0.0308	451	15.7	15.5	1074	0.035045±205	0.238166±232	0.049290±106	222.0	216.9	161.6	161.6	0.889
10		0.0318	756	19.3	19.0	1089	0.025863±67	0.176728±91	0.049559±02	164.6	165.2	174.3	174.3	0.734
11		0.0407	578	14.9	14.6	940	0.026029±72	0.176659±125	0.049225±100	165.6	165.2	158.5	158.5	0.596
12		0.0320	544	14.1	13.8	818	0.025963±53	0.176285±87	0.049246±69	165.2	164.9	159.5	159.5	0.611
13		0.0432	416	10.9	10.8	1017	0.026774±56	0.185553±151	0.050264±140	170.3	172.8	207.2	207.2	0.388

All errors are two-sigma standard deviation (2σ). Common Pb isotopic compositions from Stacey and Kramers (1975) were used for correction. The data were calculated with ISOPLOT (Lugwig, 1993). *m-fac*=multi-facet; *s*=small; *st*=short; *st*=stout; *c*/*rl*=colourless; *l*=long; *frag*=fragment; *lg*=large; *tr*/*l*=translucent; *tr*=transparent; *euh*=euhedral; *pr*=prism; *ndl*=needle; *l*=light; *y*=yellow; *br*=brown; *lbr*=light brown; *b*=big; ***=unabraded; *w*=weighing error=0.001 mg

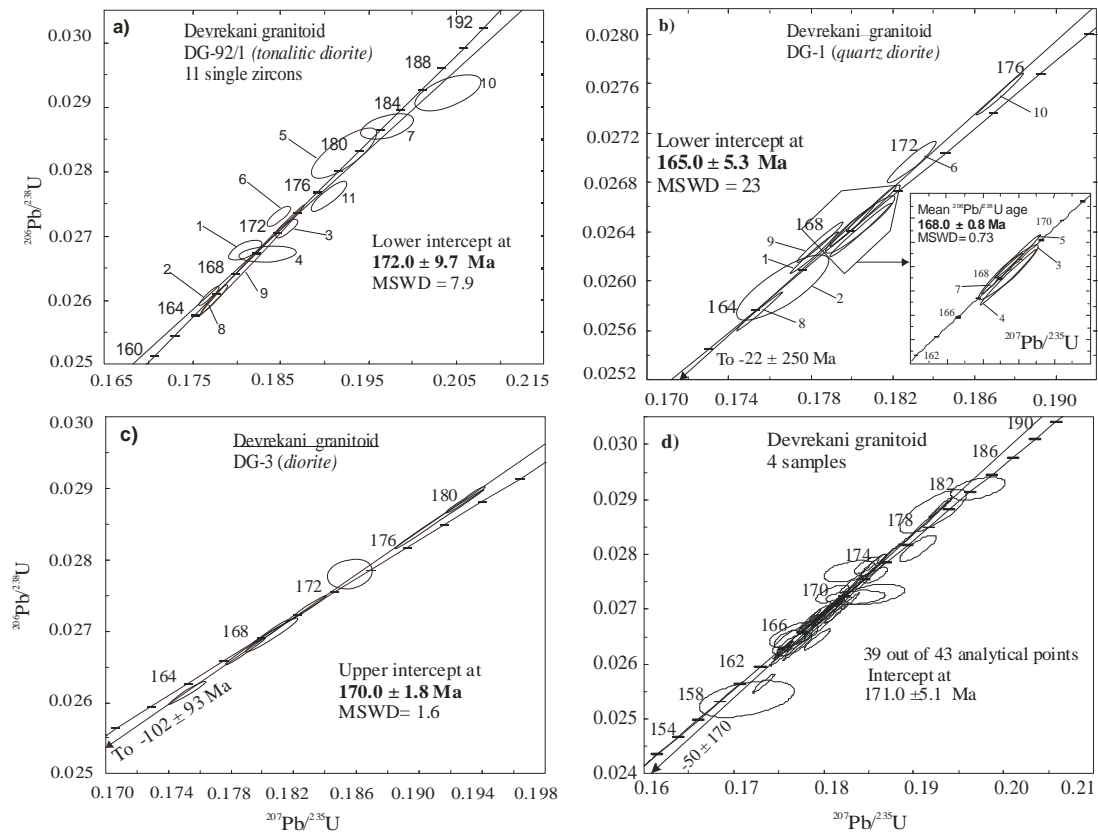


Fig. 4.12- Concordia plot showing data points of U-Pb isotope dilution analyses from the Devrekani granitoid; (a) sample DG-92-1, 11 single zircons, (b) DG-1 and (c) DG-3 and (d) Summary plot of all four (analyzed samples). Error ellipses represent $2\sigma_m$.

Quartz diorite sample, DG-4b: U concentrations are in the range of 176-3901 ppm (Table 4.3). Most zircons analysed are concordant between 160-172 Ma (Fig. 4.13a). Four zircon fractions with variable small degrees of Pb-loss plot close to the concordia curve at 162-172 Ma and 220 Ma. Although xenocrystic cores were not discerned in the CL images, one fraction has a small inherited Pb-component and plot close to 330 Ma. One fraction is reversely discordant at ~220 Ma. Three fractions are concordant at 165.0 ± 0.54 Ma (MSWD= 0.67) (Fig. 4.13a, inset).

Table 4.4 Radiogenic $^{207}\text{Pb}/^{206}\text{Pb}$ ratios of evaporation of single zircon grains and corresponding age

Sample	Grain/Zircon features	Number of $^{207}\text{Pb}/^{206}\text{Pb}$ ratios	Mean of $^{207}\text{Pb}/^{206}\text{Pb}$ ratios	$^{207}\text{Pb}/^{206}\text{Pb}$ (Ma)
DG-4b, quartz-diorite	1 thick, multi-facet, clair	16	0.048853 ± 35	141 ± 17
	2 long, thick, brown	81	0.049400 ± 28	167 ± 13
	3 medium, thick, brown	73	0.049160 ± 19	156 ± 09
	4 medium, multi-facet, brown	125	0.049310 ± 30	163 ± 14
	5 thick, multi-facet, brown	116	0.049470 ± 28	171 ± 13
Weighted mean no. of ratios and mean age		82	0.049239 ± 28	166 ± 16

Five separately evaporated DG-4b zircons yield a mean $^{207}\text{Pb}/^{206}\text{Pb}$ age of 166 ± 16 Ma (Table 4.4, Fig. 4.13b), which is within the error limit similar to the average $^{206}\text{Pb}/^{238}\text{U}$ age. The lack of inherited zircons in DG zircons is due to either derivation from juvenile (volcanic arc, back-arc development [$\epsilon\text{Nd}_{(t)}$ -2.2 to -0.8] material or complete resetting of the pre-existing zircon.

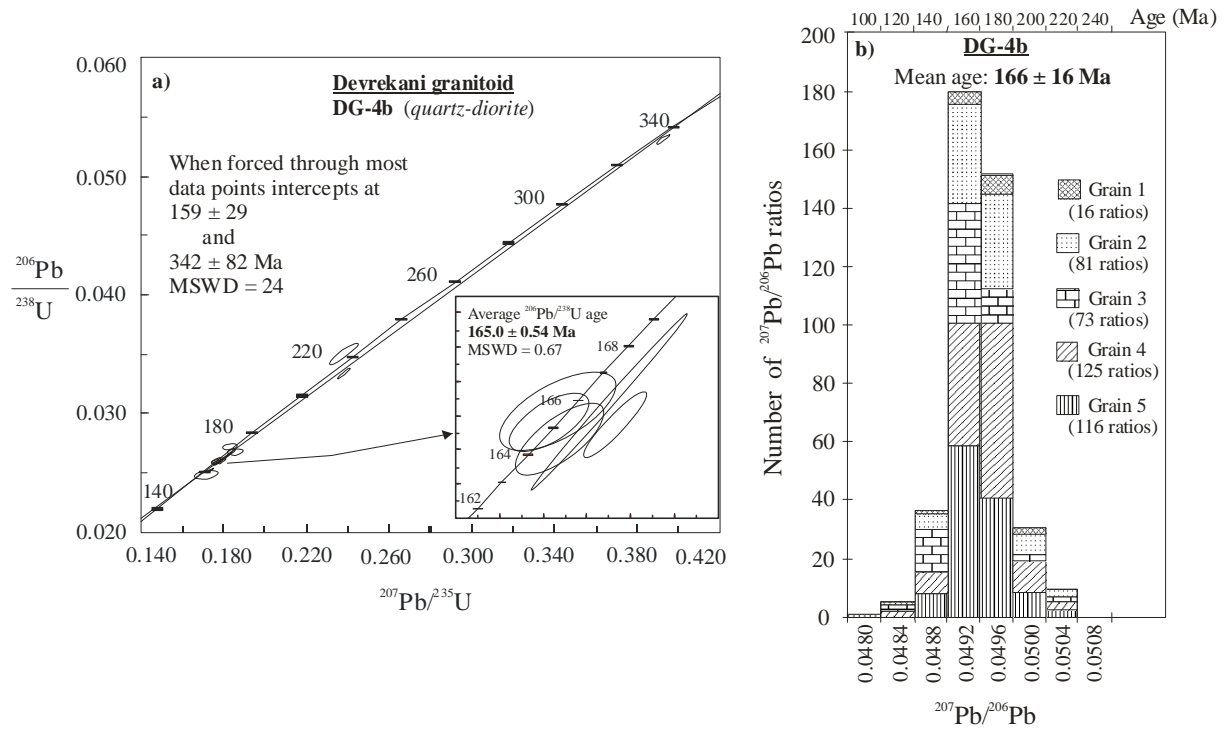


Fig. 4.13- Zircon data from the Devrekani granitoid, quartz diorite sample DG-4b. (a) U-Pb concordia plot for zircon analyses. Ellipses indicate $2\sigma_m$ error. (b) Histogram showing the frequency distribution of radiogenic $^{207}\text{Pb}/^{206}\text{Pb}$ ratios derived from single zircon Pb-evaporation. The spectrum for five idiomorphic grains, integrated from 411 ratios give a mean $^{207}\text{Pb}/^{206}\text{Pb}$ age of 166 ± 16 Ma.

Rb-Sr whole-rock analyses from the Devrekani granitoid define an isochron age of 176 ± 43 Ma (MSWD= 0.041 and $\text{Sr}_{(i)} = 0.70538 \pm 0.00028$) (Fig. 4.14). The Rb-Sr age, although with very large errors are similar to the U-Pb age (Figs. 4.12 & 4.13).

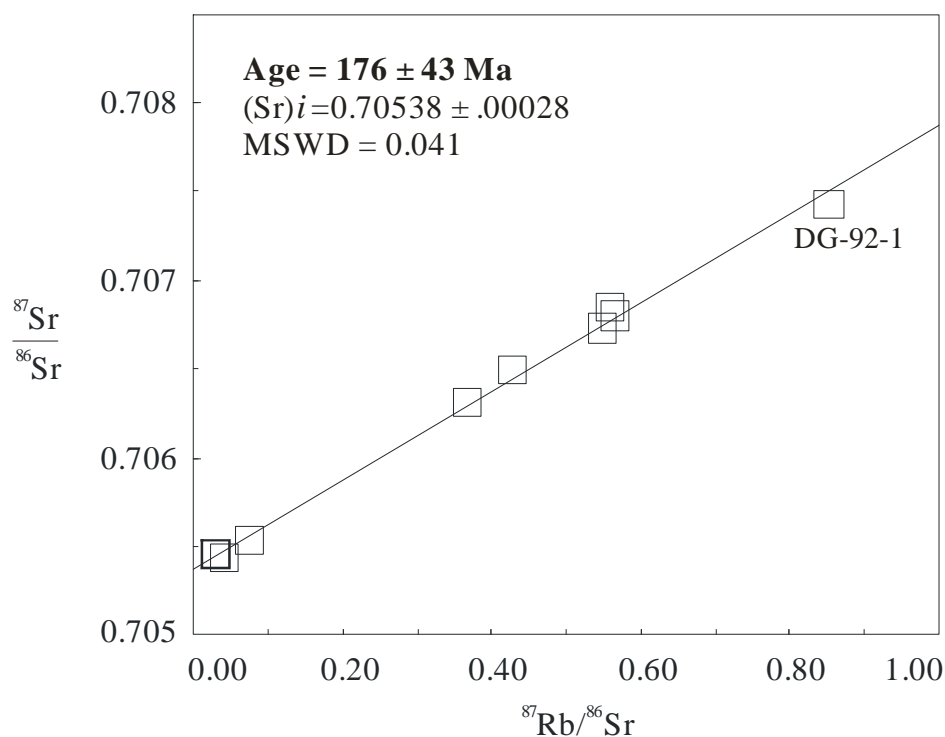


Fig. 4.14- $^{87}\text{Rb}/^{86}\text{Sr}$ vs. $^{87}\text{Sr}/^{86}\text{Sr}$ whole-rock isochron plots of data from Devrekani granitoid

The Middle Mesozoic basic magmatism is documented by Rb-Sr_(whole-rock) and zircon ages of 175-165 Ma from four samples. Xenocrystic cores were not discerned in zircons of these samples. Zircons of four rocks have similar ages and internal morphologies displaying primary magmatic structures (oscillatory zoning) and minor secondary structures (recrystallization domains). Ages from all samples are similar within the error range and show little spread. The pooled age 165 Ma is interpreted as the crystallization time of this pluton.

4.3. DISCUSSION

4.3.1. *Magma genesis and possible sources*

Devrekani (DG) rocks are rich in Ca-plagioclase, hornblende, biotite, orthopyroxene and \pm clinopyroxene, implying an origin through partial melting of mafic source rocks. Experiments by Patiño Douce (1995, 1996) have shown that dehydration melting of amphibolite at ~0.4 GPa can produce a melt assemblage dominated by Ca-rich plagioclase (An₇₇) and orthopyroxene with subordinate clinopyroxene. Devrekani rocks have moderate Na₂O/K₂O ratios (2-17), low Al₂O₃/(FeO_t+MgO+TiO₂), (Na₂O+K₂O)/(FeO_t+MgO+TiO₂) and narrow range CaO/(FeO_t+MgO+TiO₂) ratios (Fig. 4.10). These features combined with very high Mg# values (75-86), suggest derivation from an amphibolitic source rock close to primary mantle melts (e.g. Patiño Douce, 1995, 1996, 1999). High CaO (5-14 wt%) and

moderate Sr (271-370 ppm) contents, and positive Sr and Eu anomalies further suggest melting of a plagioclase-bearing source and/or slab melting outside the plagioclase stability field (e.g. Martin, 1999), and the magma crosscutting a thicker hotter mantle wedge or mafic plutons, having efficient interactions with it, resulting in MgO, Ni and Cr enrichment (e.g. Sajona, 1995; Sajona et al. 2000; Tatsumi et al. 1986), and slightly adakitic signature for the diorites (e.g. Martin, 1999; Condie, 2005).

Although Sr- and Nd-isotopic ratios are within the mantle array (Fig. 4.9a), slight shift of the data to more radiogenic Sr isotopic compositions may be interpreted as the result of Sr-rich slab fluid mixed into the mantle wedge (e.g. Churikova et al. 2001; Dorendorf et al. 2000; Prouteau et al. 2001; Rapp and Watson, 1995; Rapp et al. 1999; Smithies, 2000). The high $\epsilon\text{Nd}_{(t)}$ values (-0.8 to -2.2) and the low $\text{Sr}_{(i)}$ ratios (0.7052-0.7061) of the samples reflect the involvement mantle material and/or mafic crustal source in their genesis. The fact that older Pb-components are almost absent in the analyzed zircons (Figs. 4.11, 4.12, 4.13) further ascertain the lack of important old continental material contribution in the DG magmas. These characteristics and the fact that this pluton is geochemically zoned (batches of magma intruding each other) suggest coeval magmas generated from different mafic sources, consistent with the isotopic data indicating OIB-EMI- type source for the diorites and the EMII-type source represented in the dioritic-tonalitic rocks (Fig. 4.9c). Generally the main difference between the EMI and EMII enriched mantle source types is that the former may include recycled oceanic crust, pelagic sediments and/or metasomatized subcontinental lithospheric mantle (i.e., low $^{143}\text{Nd}/^{144}\text{Nd}$ and $^{87}\text{Sr}/^{86}\text{Sr}$ ratios, Table 4.2) and the latter recycled oceanic crust and continentally-derived sedimentary rocks (i.e., low $^{143}\text{Nd}/^{144}\text{Nd}$ and slightly elevated $^{87}\text{Sr}/^{86}\text{Sr}$ ratios) (e.g. Hart et al. 1986; Hoffman, 1988; McKenzie and O'Nions, 1983; Zindler and Hart, 1986). As has been suggested by many authors adakitic melts can be derived from the partial melting of the mafic oceanic crust (Defant and Drummond, 1990; Drummond and Defant, 1990; Kay et al. 1993), could interact with the metasomatized mantle wedge (Stern and Kilian, 1996; Rapp and Watson, 1995; Rapp et al. 1999; Smithies, 2000; Prouteau et al. 2001).

Albeit slightly elevated $\delta^{18}\text{O}_{\text{whole-rock}}$ values (8.2 to 9.1 ‰) compared with mantle melt composition, they signal differentiation from a mantle source with only minor crustal contribution (Fig. 4.9d), most probably subduction-related. Accordingly, it could be assumed that the composition of the analysed rocks have not been significantly modified by crustal contamination, rather they reflect the variations in chemical and isotopic compositions of different sources and magmatic processes in the mantle.

In conclusion, the geochemical and isotopic data suggest the generation of Devrekani magmas involved both active continental-margin melting of the metasomatized mantle lithospheric plate and asthenospheric mantle (e.g. Henk et al. 2000; Pearce and Parkinson, 1993).

4.3.2. *Subduction versus mantle wedge components*

Slab fluids are known to be enriched in LILEs and LREEs but depleted in HFSEs and HREEs (e.g. Ayers, 1998; Brenan et al. 1995; Tatsumi et al. 1986). Melting in subduction zones is triggered by the interaction between the mantle wedge and slab-derived hydrous fluids and melts. So that, typical volcanic arc granitoid rocks are characterized by high LILE/HFSE and LREE/HREE ratios, which are commonly attributed to mantle metasomatism. These elements can migrate with the dehydrating fluid phase, whereas the HFSEs and HREEs are retained in the slab and subducted to the deeper mantle (Keppler, 1996; Tatsumi et al. 1986). Devrekani granitoid samples plot in VAG field on the Y+Nb vs. Rb diagram (e.g. Pearce, 1982) and on the R1 vs. R2 diagram (De La Roche et al. 1980), they trend from the mantle fractionates (diorites, DG-3) to pre-plate collision (quartz diorites) and post collision (tonalitic diorites) uplift fields (Fig. 4.8b, d). However, active continental margin magmas normally show greater degree of enrichment in incompatible elements compared to those of Devrekani rocks. Implying, the VAG chemical signatures shown by the samples only reflect the arc environment in which they were generated (e.g. Harris et al. 1986; Pearce et al. 1984; Rogers and Hawkesworth, 1989; Sajona et al. 1996). Low TiO₂ contents, low Sr_(i), high εNd_(t) ratios and flat HREE patterns of the samples are consistent with derivation from mafic lower crustal source, where HREE-bearing mineral phases are unstable. Positive Eu-anomalies, shows the activity of Eu increased in the melt, may be due to elevated temperatures, hence increased feldspars breakdown. Such conditions are possible during high-temperature hydrothermal processes in subduction zones (e.g. Uysal and Golding, 2003). The δ¹⁸O values are lower than continental crustal values, but trends on the Sr_(i) vs. δ¹⁸O diagram show that the source was contaminated by some limited amount of continental crust. These trends could have resulted from mantle wedge-derived magma and the continental crust interaction. Negative correlation observed between the ¹⁴³Nd/¹⁴⁴Nd and ⁸⁷Sr/⁸⁶Sr ratios strongly indicates two mantle reservoirs involved in the genesis of these rocks: asthenospheric MORB-like source with a fairly high ¹⁴³Nd/¹⁴⁴Nd (εNd_(t)) and low ⁸⁷Sr/⁸⁶Sr, and another component, the EMI source of Zindler and Hart (1986). The primary magma of the rocks might be the product of partial melting of either enriched subcontinental lithospheric mantle or a mixture of this enriched source with an MORB-type asthenospheric source. In either case, subcontinental lithospheric mantle made a

significant contribution to these rocks. After the previous subduction in the Late Palaeozoic and Earliest Mesozoic continent-continent collision, (Ustaömer and Robertson, 1997, 1999; Okay et al. 2006; Nzegge et al. *in review*), it was possible to derive a greater proportion of such melts from an enriched mantle reservoir.

4.3.3. *Tectonic evolution: evidence for slab break-off/detachment*

The Late Palaeozoic-Early Triassic evolution of the NW Turkey was dominated by the subduction of the Palaeotethys oceanic plate beneath the Eurasian plate. The thermal effect of subduction might have caused asthenospheric currents beneath the Central Pontides, NW Turkey and the resultant lithospheric stretching, crustal thickening/thinning and extensive magmatism intruding the Palaeotethyan subduction-accretion complex. Therefore, the major sources of the magma are the subcontinental lithospheric mantle and the MORB-like asthenosphere. The Kastamonu granitoids are located at the juxtaposition of the Eastern and Western Pontides, where the very complicated tectonic setting can be summarized as follows: (1) The Palaeotethys oceanic plate transporting Gondwana-derived continental fragments subducted beneath Eurasia and continental rifting and strike-slip movements (Istanbul Zone and Devrekani Unit) during the Latest Palaeozoic-Earliest Triassic (e.g. Robertson and Dixon, 1984; Ustaömer and Robertson, 1991, 1997; Robinson et al. 1992, 1995; Okay et al. 2006); (2) During the Latest Palaeozoic-Earliest Mesozoic, collision of Gondwana- and Eurasia-derived fragments led to accretion, large-scale extension by gravitational orogenic collapse, and the development of marginal basins (e.g. the Küre marginal basin) (e.g. Dewey et al. 1989; Robertson and Dixon, 1984; Yılmaz and Boztuğ, 1986; Aydın et al. 1986, 1995; Banks and Robinson, 1997; Ustaömer and Robertson, 1993, 1994, 1999; Boztuğ et al. 1984, 1995; Robinson et al. 1995); (3) The post-collisional regional extension probably triggered slab detachment or lithospheric delamination (e.g. von Blanckenburg and Davies, 1995; Davies and von Blanckenburg, 1995; Henk et al. 2000;). This resulted in Early-Middle Jurassic regional metamorphism (e.g. Boztuğ et al. 1984, 1995; Yılmaz and Boztuğ 1986); (4) subduction reversal (i.e. the southward dipping of the Küre marginal basin) in the Earliest Triassic (e.g. Ustaömer and Robertson, 1994, 1997, 1999), and the Middle Mesozoic emplacement of I-type mafic granitoids (Devrekani granitoid, this study and Boztuğ et al. 1984, 1995) in the south of KGB.

It could be concluded that, the post-collisional extensional tectonics that started at ~190 Ma ago with regional metamorphism (Yılmaz and Boztuğ, 1986; Yılmaz et al. 1996) was accompanied by granitoids emplacement and fast tectonic exhumation till 165-155 Ma. This

was followed by deposition of polygenic basal conglomerate of the Bürnük formation, the İnalti limestone formation, and finally deep sea sediments of the Çağlayan formations. Therefore, the regional metamorphism, the emplacement of the plutons in the south of KGB, and the exhumation can be interpreted as the product of post-collisional lithospheric detachment of the subducted Palaeotethys oceanic lithosphere from the continental lithosphere during collision of Gondwana- and Eurasia-derived fragments. Such post-extensional tectonics could have brought hot asthenospheric mantle into direct contact with the earlier metasomatized lithospheric mantle of the overriding plate, and induced melting (e.g. McKenzie and Bickle, 1988). The contemporaneity of shearing, magmatism and metamorphism at ~185-165 Ma suggests the processes (Palaeotethyan subduction, continent-continent collision (Eurasian-Gondwana-derived fragment) and post-collisional extension) in the Kastamonu region, Central Pontides, were closely related geodynamically.

4.4. CONCLUSIONS

The Devrekani granitoid encompasses diorites to low-Si tonalitic-diorites were emplaced in a volcanic arc environment comprising accreted Eurasian-Gondwana-derived and oceanic fragments fragments, during the Middle Jurassic.

Geochemical and isotopic data reveal two magma types low-K tholeiitic and medium-K calc-alkaline metaluminous I-type. The isotopic composition of Sr and Nd suggests that the Devrekani granitoid rocks represent either mantle-derived magma that experienced slight if any assimilation of isotopically different crust, or were generated from mafic sources in the lower crust. High MgO, CaO, Cr, and Ni contents are supportive of derivation from a mantle source. Other characteristics such as low-Ti, moderate K₂O of some samples indicate the rocks may represent two distinct magmas (EMI and EMII), which were probably derived from variably enriched mafic sources including the upper mantle with high $\epsilon\text{Nd}_{(t)}$ values, and a high radiogenic Sr source, with a moderate time-integrated Rb/Sr such as ancient amphibolitic lower crust. Enrichment is interpreted to be related to metasomatic processes in response to previous Late Palaeozoic Palaeotethys subduction.

Post-collisional extension-induced slab break-off must have contributed to a major extend after the closure of Palaeotethys oceanic basins, as indicated by the presence of basaltic magmatism in the south of the Kastamonu belt. From the geochemical and isotopic signatures we think Devrekani magmatism represent a juvenile stage of an active margin evolution, formation in an extensional tectonic setting and/or genesis in an oceanic arc underlined by a 'recently' thinned continental crust. Relatively low negative $\epsilon\text{Nd}_{(t)}$ values (-2.2 to -0.8) point to magma sources with variably small proportion of old continental crustal material,

consistent with the lack of inherited zircons. The associated metabasites of Bekirli metamorphics (BM) showing enriched MORB signatures (very low Rb content 0.5 - 2.1 ppm, $Sr_{(i)}$, ~ 0.70525 ; $\epsilon Nd_{(t)}$, +0.8 to +1.2, own unpublished data) is presumably derived from subcontinental lithospheric mantle source. Geochemical signatures of the Devrekani granitoid samples and the Bikirli metabasites therefore, suggest development within the back-arc basin of an active continental margin, for the Middle Mesozoic magmatism in the south of the Kastamonu belt.

The Precambrian-Palaeozoic basement rocks of the Central Pontides had a complex thermo-tectonic history, with Mid-Carboniferous (Variscan), Late Triassic (Cimmeride), and Oligo-Miocene (Alpide) thermal events. It is noteworthy that the Devrekani granitoid (except for one), has no inherited zircons of Variscan age, although it is in direct contact with the Variscan basement (Devrekani metamorphics), suggesting major Middle-Upper Jurassic crustal shortening. Pb loss and/or U loss at 220-200 Ma probably reflect the time of regional metamorphism associated with the extensional tectonics, basins opening and deposition of the deep-Sea formations.

Our Middle Mesozoic ages and $\sim 152.0 \pm 1.9$ Ma (own unpublished data) for the small pluton NE of Devrekani town, along with reported K-Ar hornblende and biotite ages of 146 ± 6 to 176 ± 7 Ma and 162 ± 5 Ma respectively, from the Asarcık granitoid in the southeast of KGB, document a “short” period of mafic (unimodal) magmatism, which may be interpreted in terms of south-dipping subduction and closure of the Küre MORB-type marginal basin.

4.5. **General conclusion on granitoids:** *Geodynamic interpretation of Palaeozoic and Mesozoic plutonism*

Earlier studies were mostly based on stratigraphy and whole-rock major and trace element geochemistry which are very sensitive to later tectonic/thermal events, alteration and other secondary processes. However, the geochemical and Sr-Nd-O isotopic features, and zircon and Rb-Sr ages in this study, allows a reassessment of the geological evolution of the Kastamonu granitoid belt and the surrounding area in the central Pontides.

When the data herein for the Sivrikaya (~303-300 Ma) and Deliktaş (~295-270) are considered together with those of central European Variscan granitoids, (e.g. Finger et al. 1997; Hann et al. 2003, Carrigan et al. 2005, Okay et al. 2006), it could be conclude that the Sivrikaya granitoid magma was derived either through renewed subduction and/or from decompression melting near the crust-mantle boundary in a syn- to post-collisional extension-related geodynamic setting as described by Finger et al. (1997). Or part of the Late Viséan-Namurian post-collisional, collapse-related or lithospheric delamination-related granitoid magmatism (e.g. Hann et al. 2003). As for the Deliktaş granitoid, it is very similar to post-collisional, strongly peraluminous (SP), S-type granites common in the Hercynides (e.g. Sylvester (1998). The latter author asserted that the strongly peraluminous S-type granites of the Hercynides (Variscides) and the Lachlan Fold belt (Chappell and White 1974, 1992; White and Chappell 1983) originated not solely through syn-collisional crustal thickening processes rather predominantly through crustal anatexis related to “high-temperature” post-collisional lithospheric delamination and upwelling of hot asthenospheric material, producing large volumes of SP, S-type granitic melts.

All the data above in conjunction with published data on the geodynamic interpretation of Variscan granitoids in the central Europe (e.g. Finger et al. 1997; Hann et al. 2003) and in Bulgaria (e.g. Carrigan et al. 2005), allow us to suggest the following geodynamic model for the genesis of Sivrikaya and Deliktaş granitoids from the Devrekani-Kastamonu region, Central Pontides-Turkey (Fig. 4.15, below): (1) Palaeotethys is situated between the Sakarya continent (Gondwana fragment) and Laurasia with an intra-oceanic arc constituting the supra-subduction zone (SSZ) type Domuzdağ and Çangaldağ ophiolite complexes. The oceanic crust northward subducted underneath Laurasia forming arc magmatism in the active margin of Laurasia during Silurian-Devonian time (Fig. 4.15, below). Continued northward underthrusting of Palaeotethys oceanic crust beneath Laurasia margin during the Early Carboniferous produced a magmatic arc (Çangaldağ complex), followed by collision of continental fragments (Sakarya continent and Devrekani metamorphics, DM) and back-arc

marginal basins formation (e.g. Küre basin) in the Latest Carboniferous time. (2) Late Carboniferous collision between the Sakarya continent and Laurasia probably provoked slab break-off and/or lithospheric delamination and the genesis of metasomatized mantle-derived magma and subsequent incorporation of upper crustal-derived felsic melt to produce the Sivrikaya granitoid magma source (Fig. 4.15, below). The geochemical and isotopic features of the Deliktaş granitoid suggest derivation of the magma predominantly from crustal sources, through partial melting in an extensional geodynamic setting following lithospheric delamination as proposed by Sylvester (1998) for the SP, S-type granites of Hercynides.

In Turkey, the incoming Eurasian continental fragments were narrow, with substantial subsequent shortening, so that the Carboniferous collisional 'suture-crossing' magmatism became later the site of the later continental margin arc and related magmatic episode (e.g. Şengör et al. 1993; Okay et al. 1996, 2006). This resulted in the intermixing of collisional- and subduction-related magmatism, aided by extensive conjugate strike-slip faulting that frequently follows collisions. Although this scenario may not be wholly compatible with many currently held ideas on the evolution of the Palaeotethys in the Central Pontides it is partly compatible with the works of Şengör et al. (1984, 1993); Aydın et al. (1986); Okay et al. (2006), and the data herein that support a Late Carboniferous orogeny related to the Late Palaeozoic subduction of the Palaeotethys beneath south Eurasian.

Such a geodynamic model is particularly similar to those of Late Variscan granitoids in the Balkans and Sredna-Gora terranes in central Bulgaria (315 to 285 Ma e.g. Carrigan et al. 2005), which are spatially close, and having mineralogical and geochemical compositions very similar to those of Sivrikaya and Deliktaş granitoids. Furthermore, the latter authors contended that these Late Variscan granitoids as well as those in the Iberian and the intra-Alpine massifs were all post-collisional and generated after the main compressional and high-grade metamorphic events during the Variscan Orogeny.

Geochemical and isotopic compositions suggests that the Middle Jurassic Devrekani metaluminous I-type granitoid rocks represent either mantle-derived magma that experienced slight if any assimilation of isotopically different crust, or were generated from mafic sources in the lower crust. Post-collisional extension-induced slab break-off must have contributed to a major extend after the closure of Palaeotethys oceanic basins, as indicated by the presence of basaltic magmatism in the south of the Kastamonu belt. From the geochemical and isotopic signatures we think Devrekani plutonism represent a juvenile stage of an active margin evolution, formation in an extensional tectonic setting and/or genesis in an oceanic arc underlined by a 'recently' thinned continental crust.

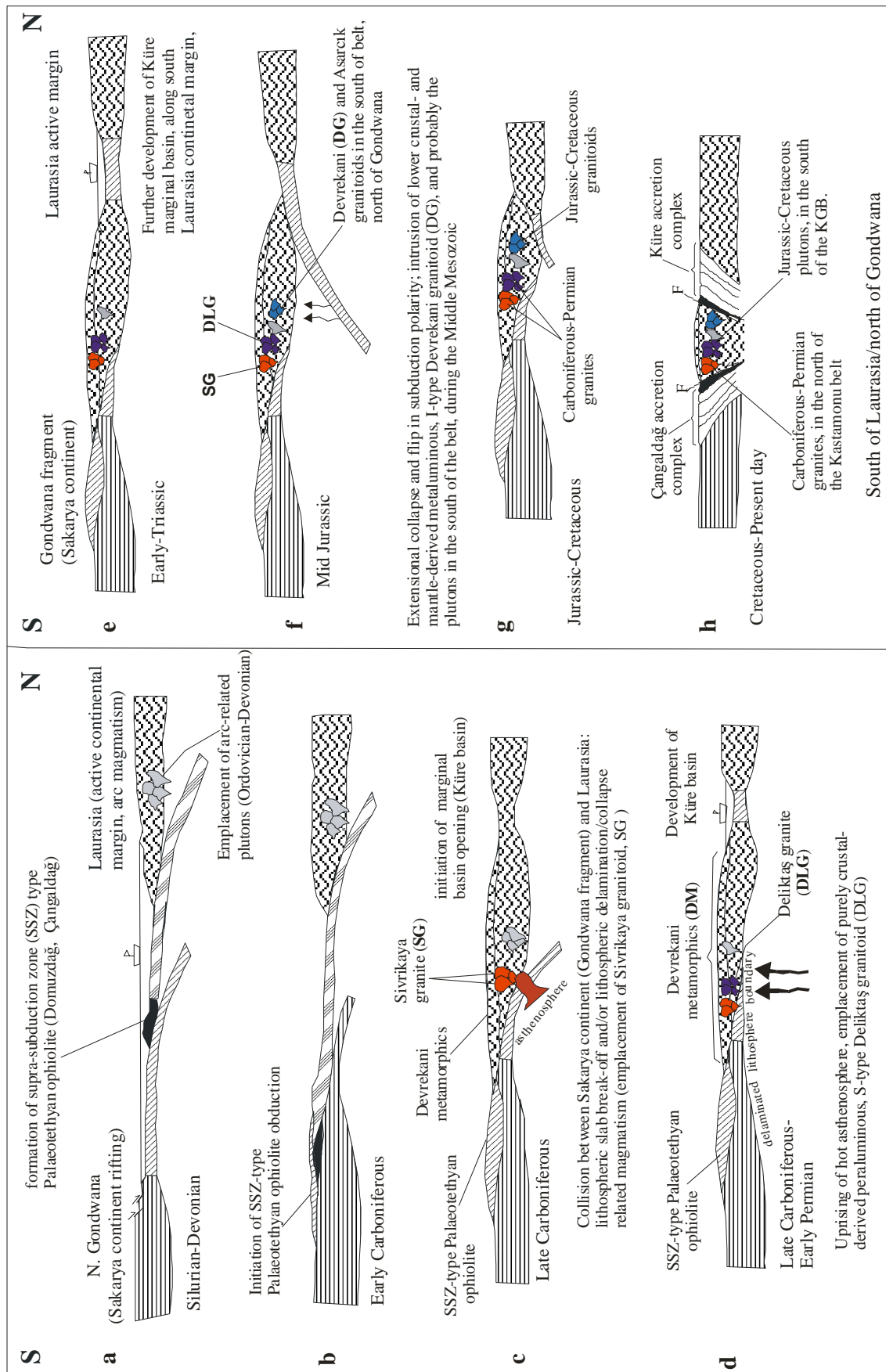


Fig. 4.15-SUG-gested geodynamic model for the genesis of the Late Palaeozoic Sivrikaya (SG), Deliktaş, (DLG) and the Middle Jurassic Devrekani granitoids (DG) from the Kastamonu granitoid belt, Central Pontides (Turkey) (Nzege et al. in review, JAES and IJES).

It noteworthy is that the Devrekani granitoid (except for one), has no inherited zircons of Variscan age, although it is in direct contact with the Variscan basement (Devrekani metamorphics), suggesting major Middle-Upper Jurassic crustal shortening. Pb loss and/or U loss at 220-200 Ma probably reflect the time of regional metamorphism associated with the extensional tectonics, basins opening and deposition of the deep-Sea formations. Our Middle Mesozoic ages and $\sim 152.0 \pm 1.9$ Ma (own unpublished data) for the small pluton NE of Devrekani town, along with reported K-Ar hornblende and biotite ages of 146 ± 6 to 176 ± 7 Ma and 162 ± 5 Ma respectively, from the Asarcık granitoid in the southeast of KGB, document a “*short*” period of mafic (unimodal) magmatism, which may be interpreted in terms of south-dipping subduction and closure of the Küre MORB-type marginal basin (Fig. 4.15).

The data herein from the Sivrikaya, Deliktaş and Devrekani granitoids indicate that a “*long-lasting*” Carboniferous-Permian bimodal magmatism commenced probably in the north and gradually migrated to the south followed by “*short-lived*” Middle Mesozoic unimodal plutonism in the Devrekani area, in the south of the Kastamonu granitoid belt. The possible rearrangement of the original locations of the Kastamonu plutons by later tectonic events and incomplete age information on all the 15 plutons makes such a conclusion only preliminary.

5. EURASIAN-DERIVED BASEMENT

The Pre-Jurassic basement of the Central Pontides comprises a thick subduction-accretion complex, amalgamated since the Late Palaeozoic (Ustaömer and Robertson 1997). Detailed structural, sedimentological and geochemical studies reveal four E-W tectonic units, assembled through plate tectonic processes, and exposed beneath Late Jurassic-Tertiary cover units (Fig. 1c). The first, the Devrekani metamorphic unit (DM), gneisses and amphibolites at the base, transgressively overlain by metamorphosed carbonates, interpreted as basement of a rifted south Eurasian margin fragment. The Palaeozoic of İstanbul Zone and the Early Mesozoic sequences of the Western Pontides may represent the cover of the Devrekani unit. The second unit, the Çangaldağ Complex, thick, imbricated pile of evolved volcanics and volcanoclastics, overlying oceanic basement, comprising sheeted dykes and basic lavas. The Çangaldağ unit is interpreted as a south-facing oceanic arc. The northern oceanic basin, the Küre Complex, a structurally thickened (>29 km) wedge of thrust-imbricated siliciclastic turbidites, interleaved with dismembered, subduction zone ophiolites; in which Late Palaeozoic-Mid Jurassic fossils have been identified (Aydin et al. 1986). The Küre Complex is interpreted as Triassic-Early-Jurassic subduction-accretion complex of southward polarity. The southerly basin represented by the Domuzdağ-Saraycıkdağ Complex, is a Palaeozoic-Early Mesozoic subduction-accretion complex of northward polarity, comprising an ophiolitic melange in the north and an accretionary prism in the south, both metamorphosed to blueschist facies. This basement was affected by Alpine metamorphism, that resulted in retrogressive effects inprinted on the rocks (e.g. Boztuğ and Yılmaz, 1995).

Available data suggest Palaeotethys was subducted northward beneath the active south Eurasian margin (long-lived Pacific type, Robertson and Dixon, 1984), during the Late Palaeozoic time resulting in continental margin arc and rifting off a continental crustal sliver (Devrekani metamorphic unit) (e.g. Ustaömer and Robertson, 1990), related to transform fault and/or active margin processes, opening the Küre back-arc basin, in the Latest Palaeozoic-Earliest Mesozoic.

The the Devrekani metamorphic unit (DM) is exposed (in the Musa-Ousman river valley, ENE of the Devrekani granitoid), as a WSW-ENE fault-bound tectonic window sandwiched between the Küre and the Çangaldağ Complexes respectively to the north and south (Ustaömer and Robertson, 1991) (Fig. 1c). This high-grade metamorphic assemblage comprises gneisses and amphibolites at the base, transgressively overlain by metacarbonates. The Devrekani metamorphic unit is divided into two groups: the Precambrian Devrekani

metasedimentary group, made up of basic to felsic high-grade granulite to amphibolite-facies (Ustaömer and Robertson, 1991, 1997; Boztuğ et al. 1984, 1995) and the Lower-Middle Palaeozoic Samatlar group (epicontinental) made up of low grade metamorphic rocks. The Devrekani Unit is lithologically and stratigraphically very similar to the Precambrian basement of continental units of the Rhodope-Pontides belt and in the Caucasus (Ustaömer and Robertson, 1991). Based on stratigraphic correlation with the Cambrian to Silurian sequence of the Palaeozoic of Istanbul Zone (Okay, 1989, 2000; Okay et al. 1994; Okay and Tüysüz, 1999; Tüysüz, 1990), both Precambrian (Yılmaz, 1980) and Lower Palaeozoic ages (Tüysüz, 1990) were proposed for the Central Pontides basement. The Devrekani metamorphic unit is intruded by Late Palaeozoic to Middle Jurassic plutons (Nzegge et al. 2006, 2007, in review).

The rocks are medium to coarse-grained, granular and displaying foliated texture with at times augen formation. The amphibolite and granulite facies metamorphic rocks include ortho- and para-amphibolites, gneisses and gneissic-granites, and meta-basalts and -andesite.

Granulite facies rocks are important in the reconstruction and evaluation of orogenic processes as they represent crustal material transformed at highest grade (i.e. temperature) of metamorphism at conditions where melting (i.e. magmatic) processes prevail. These conditions can be those of a stable lower crustal geotherm or, alternatively, those attained during the peak of regional metamorphism. Many of the large exposed granulite domains around the world were formed in the Precambrian, but most were exhumed by much later tectonism and so yield long-term information pertaining to conditions and processes in the lower continental crust. The most voluminous of the scattered granulite relics in the crystalline core of the European Variscides are high pressure (HP), kyanite-k-feldspar varieties of granitic composition (e.g. Pin and Vieléuf, 1983; Fiala et al. 1987).

Although a Precambrian age was proposed for the Central Pontides Eurasian-derived basement (e.g. Yılmaz, 1990), our geochronological studies have produced Palaeozoic, and in many cases Carboniferous, ages for the metamorphism consistent with the works of Tüysüz (1990). U-Pb zircon dating of a metabasic sample (BÜ-20, amphibolite) define Cambro-Ordovician events from 502 Ma to 488 Ma within the Pontides belt. Interpreted as magmatic protolith formation. The detection of pre-Variscan ages within the basement of the Central Pontides must reflect a complex history involving significant pre-Variscan activity.

An understanding of the formation, modification and preservation of the granulite-facies rocks will provide important information for the interpretation of the Palaeozoic, and especially Variscan evolution of the European basement. The purpose of the present study is to investigate the formation and the age of the rocks in the basement units. To accomplish this

I have determined geochemical and isotopic compositions, U-Pb and Pb-Pb zircon and Rb-Sr whole-rock ages.

5.1. PETROGRAPHY

The *Deliktaş basement* samples (MN-1, MN-3, MN-5, MN-11, MN-12, MN-72) were collected from the south of Deliktaş, Hürsü Gököy (Ülukoy) towns and between Hacibrahim and Kirazsoku villages (Fig. 3.1). The samples are quartz-rich granites and gneisses, with adamellitic tendencies. They are all holocrystalline, coarse to very coarse-grained, granular, porphyric to granoblastic, and more or less foliated. Textures range from gneissic to granitic, with the micas forming bands around the more competent quartz and feldspars. The plagioclase and k-feldspar (orthoclase, microcline) are xenocrystic and rarely perthitic.

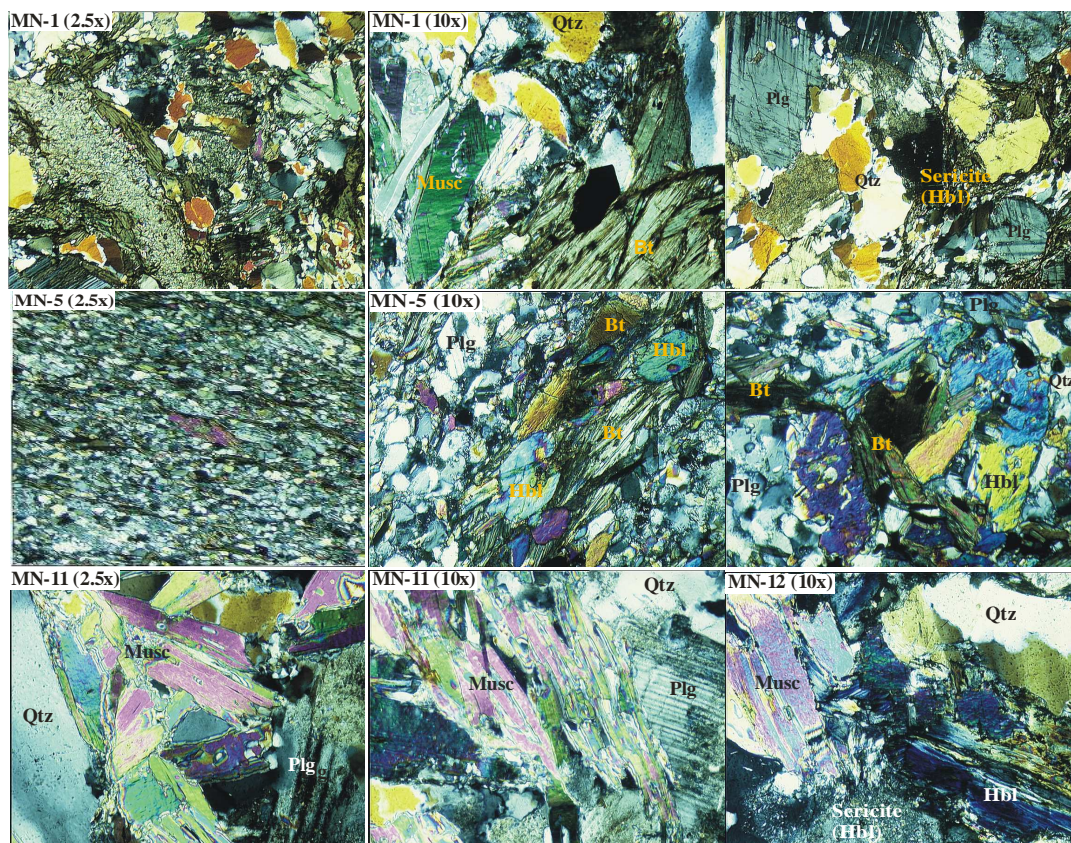


Fig. 5.1- Representative microphotographs of Deliktaş basement samples (para-gneisses and granitic- gneisses). *K-F*, k-feldspar; *Bt*, biotite; *Musc*, muscovite; *Qtz*, quartz; *pyx*, pyroxene; *Hbl*, hornblende; *Ep*, epidote; *Se*, sericite; *Plg*, plagioclase

The typical rock-forming minerals quartz, euhedric plagioclase, k-feldspar, biotite lamellae, pink idiomorphic garnet often skeletal, muscovite (more or less chloritized), ± hornblende and ± orthopyroxene (hypersthene, e.g. MN-1, MN-5, MN-12) occur in different proportions. Quartz forms aggregates between the other mineral and at times vermicular intergrowths

(myrmekite, e.g. MN-11, MN-12, MN-72) with feldspars. Accessory phases include opaques from garnet alteration, zircon, calcite, apatite, hematite and ilmenite.

The *Sivrikaya basement* crops out in Ösek (ÖS) (and between Göynüdağı and Dikmentürbet towns) and in the Büyükçay (BÜ) river valley (Fig. 3.1). The Ösek metabasic (ÖS) rocks (ortho-amphibolites) are rich in green minerals, e.g. epidote and plagioclase with amphibolitic to gabbroic compositions, and metamorphic texture (foliated). Minerals are granular and euhedral and undeformed. The original magmatic and sedimentary textures are still preserved in the ortho-amphibolites/gneisses (amphigneiss). The grain-size is medium to coarse and minerals are elongated.

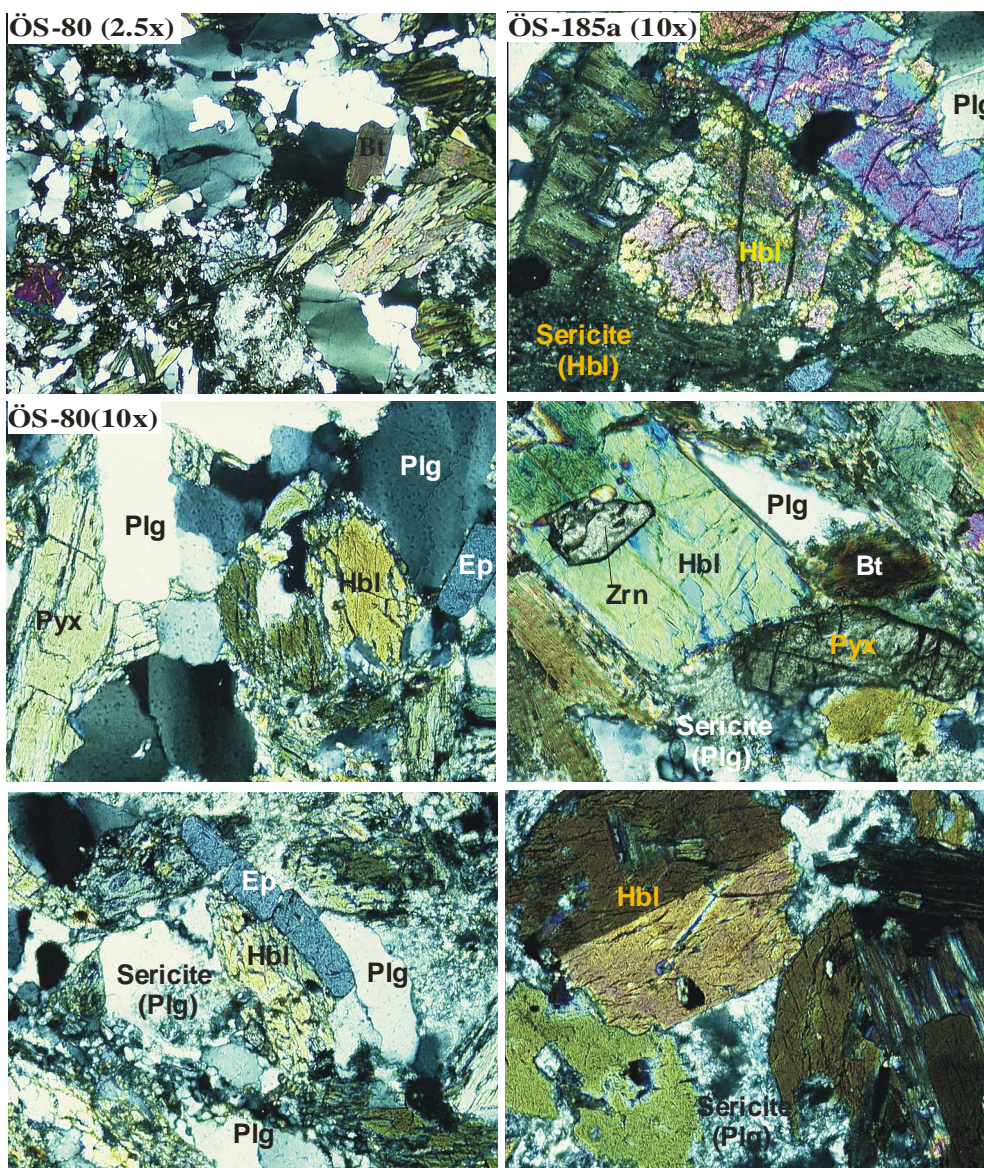


Fig. 5.2- Representative microphotographs of Sivrikaya basement samples collected around Ösek town (ÖS). Samples are typically hornblende and the plagioclase are mostly sericitized and/or replaced by hornblende. Symbols as in Fig. 5.1.

The rock types include amphibolites and gneisses. Samples are quartz-poor and the feldspars (plagioclase > K-feldspar) constitute 50-62 % of the rocks. The minerals plagioclase (albite-anorthite), green hornblende, biotite, epidote, and k-feldspar (orthoclase), olivine, pyroxene (hypersthene, 3-11 %) and garnet (mostly altered to dark brown-opaque mineral) occur in variable proportions. Plagioclase occur as megacrysts and often zoned. Zircon, calcite apatite and ilmenite are the minor components. Büyükçay (BÜ) metaigneous rocks, mainly epidote-garnet ortho-amphibolites (plagioclase gneiss or amphigneiss?) are green, porphyric and foliated with rudimentary granular/sedimentary texture.

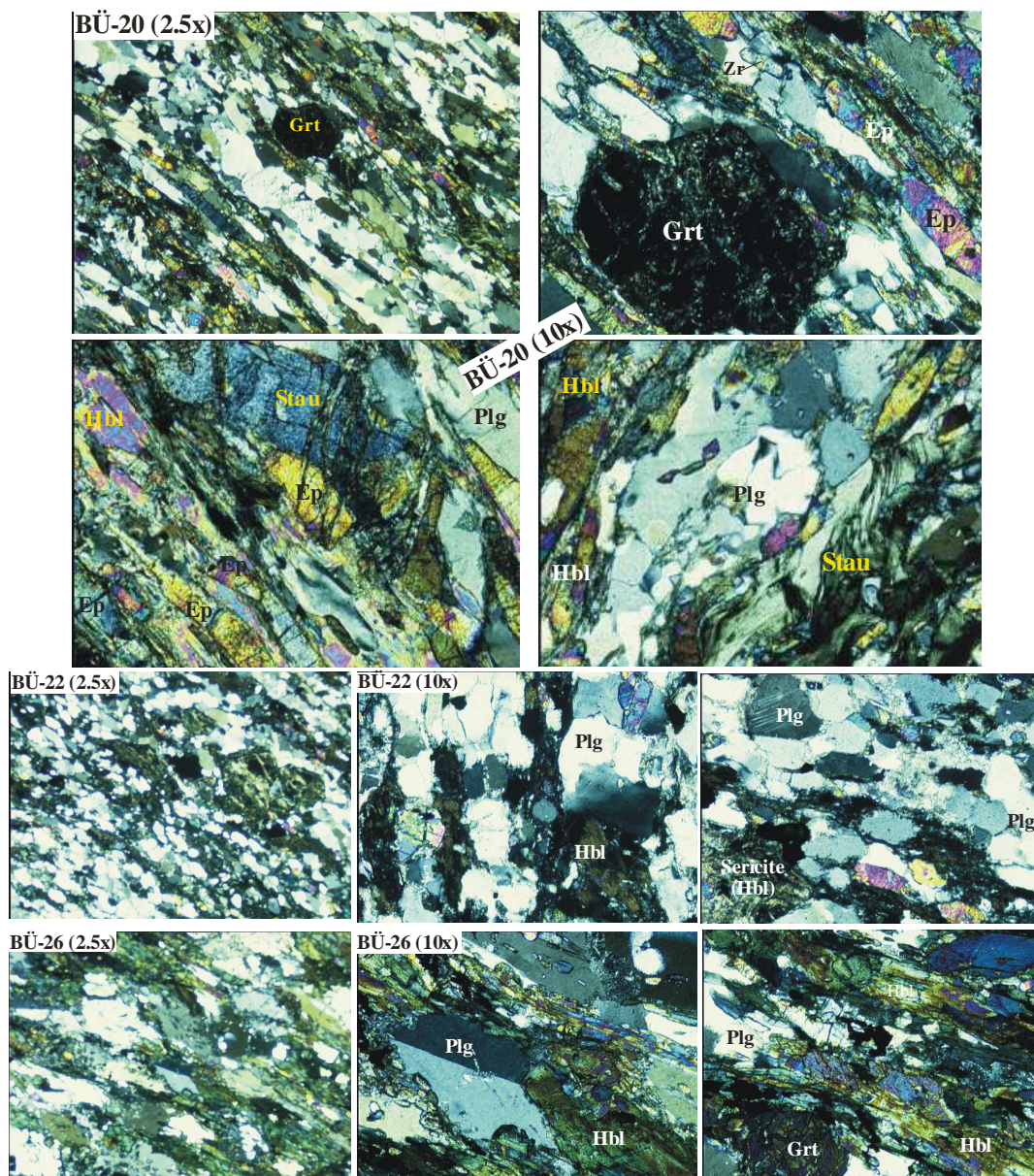


Fig. 5.2b- Representative microphotographs of Sivrikaya basement rocks collected around Büyükçay(BÜ) river valley. Samples (ortho-amphigneiss) are *Ep*, epidote, *Grt*, garnet, *Stau*, staurolite and *Plg*, plagioclase rich. Plagioclase and *Hbl*, hornblende are mostly sericitized. Abbreviations: *K-F*, k-feldspar; *Bt*, biotite; *Musc*, muscovite; *Qtz*, quartz; *Pyx*, pyroxene

The rocks are foliated with the light band made up of quartz aggregates and feldspars, and dark band the mafic minerals, which at times form boudinage. The samples comprise, plagioclase (>40 %), hornblende, garnet, biotite, k-feldspar (orthoclase 1-5 %), pyroxene (hypersthene, diopside), ±olivine and ±phengite in BÜ-20. The garnet is more or less altered to opagues. Hematite, zircon, apatite, calcite and ilmenite are accessory.

The *Devrekani granitoid basement* (Osman valley) forms a transition zone between the Devrekani granitoid and the Devrekani metamorphics (Musa valley). This basement comprises mainly banded gneisses (augen gneisses) and mylonitized grano-diorite sample (DG-4b, basement of DG-4a). The mylonitized (sheared) contact between Devrekani basement and granitoid crops out in the Osman valley east of the Devrekani town.

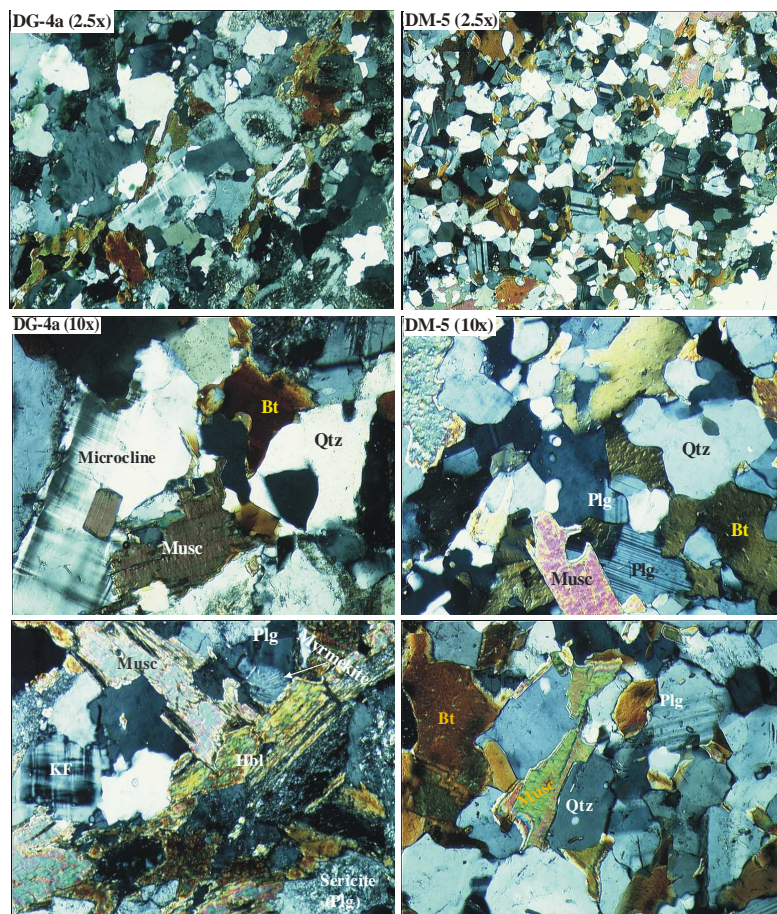


Fig. 5.3a- Representative microphotos of Devrekani pluton basement rocks [granodiorites (DG-4a) and granites (DM-5)] taken from around Devrekani town and in the Musa valley. The convex boundary of myrmekite (DG-4b) suggest texture formed through the replacement of k-feldspar (*K-F*) by *Plg*, Plagioclase in the solid state. *Bt*, biotite; *Musc*, muscovite; *Hbl*, hornblende; *Qtz*, quartz

This basement is comparable to the Devrekani metamorphic unit [(ortho and para), amphibolites and gneisses, grano-diorites and granites], which is well exposed in the Musa valley between the Küre and Çangaldağ complexes (Fig. 4.1).

The rocks are fine to coarse-grained, micro-granular to granular and foliated, with the stretched quartz and feldspars surrounded by bands of micas, resulting in “eyes”. The main rock forming minerals are quartz, feldspars [(plagioclase (albite) > K-feldspar (orthoclase)], muscovite, biotite, hornblende and skeletons of garnet. The quartz is porphyric, graphic, deformed (lenticular/boudinaged), intersitial and at times forms myrmekite with feldspar (Fig. 5.3b, DM-30, DM-33). Magnesite and hematite occur in variable proportions. Subordinate phases include opagues (from biotite and garnet alteration), zircon, calcite, apatite and ilmenite.

Some rocks (gneissic-granites, DM-5, DM-21, DM-25 and DM-30) show start of melting and segregation of amphiboles and garnet (migmatization), and boudinage formation. The main rock forming minerals of the amphibolites are green hornblende, occurring as subeuhedric to euhedric phenocrysts: plagioclase (oligoclase, andesine), k-feldspar, epidote often altered, green biotite more or less chloritized, pink garnet, pyroxene (augite) quartz, ±muscovite and ±olivine. In samples DM-32 (meta-andesite) a reaction rim can be observed between plagioclase and pyroxene, and biotite forms aggregates. In samples DM-21, DM-28 and DM-33 (granites in an amphibolitic country-rock) quartz occurs as anhedral crystals partially recrystallized as graphic quartz and the plagioclase (albite) and k-feldspar (orthoclase) are perthitic. Additionally, hematite/ilmenite, zircon, calcite, opagues, apatite and chromite occur as accessory phases.

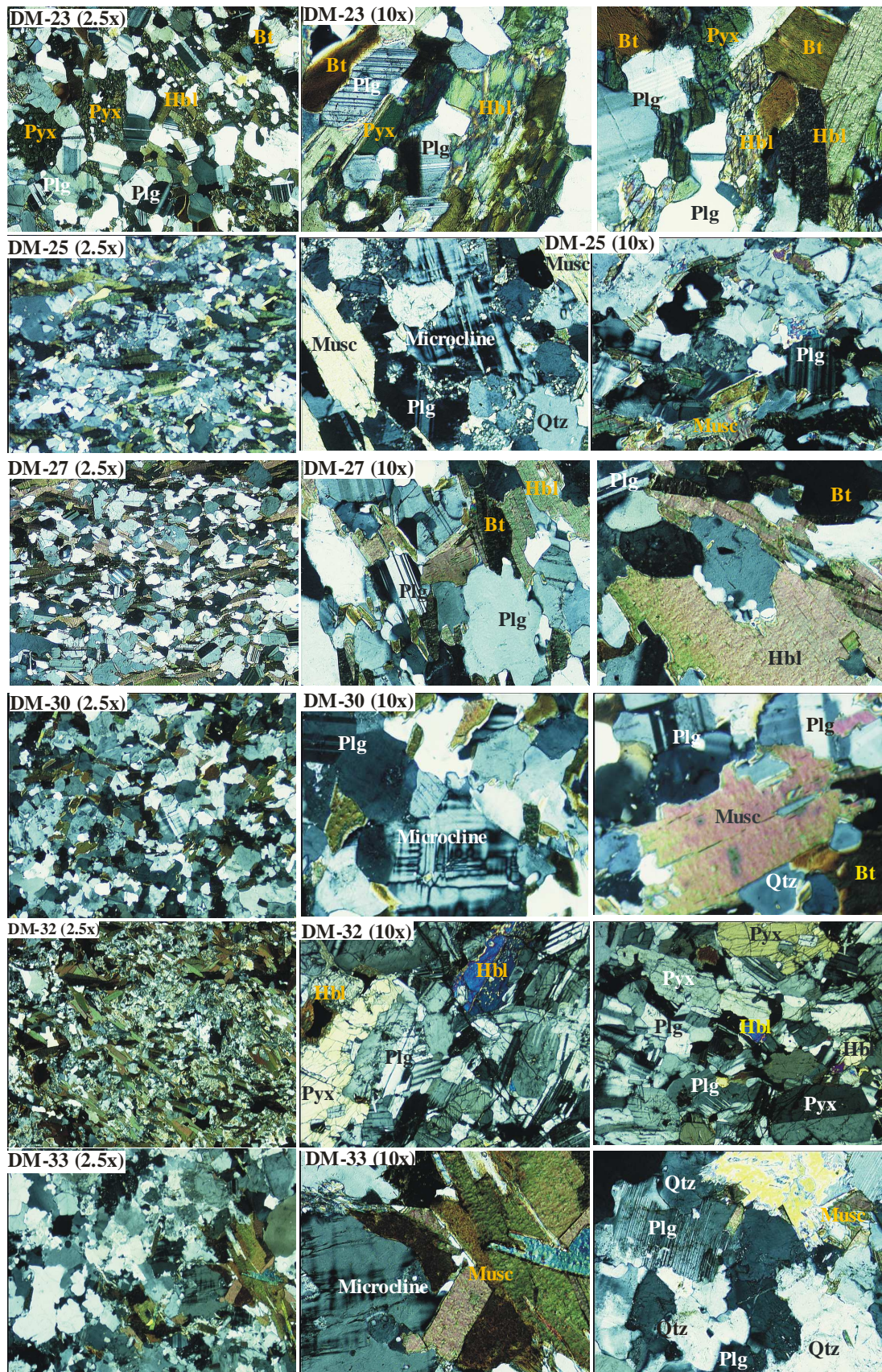


Fig. 5.3b- Representative microphotographs of Devrekani granitoid basement samples from around the Devrekani town [granodiorites (DG-4a) and granites (DM-5)]. Convex boundary of the myrmekite (DG-4b) suggest this texture formed through replacement of k-feldspar (*K-F*) by Plagioclase (*Plg*) in the solid state. *Bt*, biotite; *Musc*, muscovite; *Qtz*, quartz; *Hbl*, hornblende; *pyx*, pyroxene.

5.2. GEOCHEMISTRY

5.2.1. Major and trace element

Major and trace element concentrations of samples are listed in Table 2, Appendix. In the Ternary anorthite-albite-orthoclase normative compositions diagram (O'Connor, 1965), (Fig. 5.4a), as well as in the ternary quartz-plagioclase-K-feldspar modal compositions diagram (LeMaitre, 1987 based on Streckeneisen, 1976), the samples from the Deliktaş-Sivrikaya basement plot in the tonalite, granodiorite and granite fields (Fig. 5.4b), while those of the Devrekani are defined as trondjemite, tonalite, granodiorite and granite. Generally samples form a diagonal variation field that is nearly continuous from quartz diorite through tonalite, granodiorite to granites (monzo- and quartz-rich).

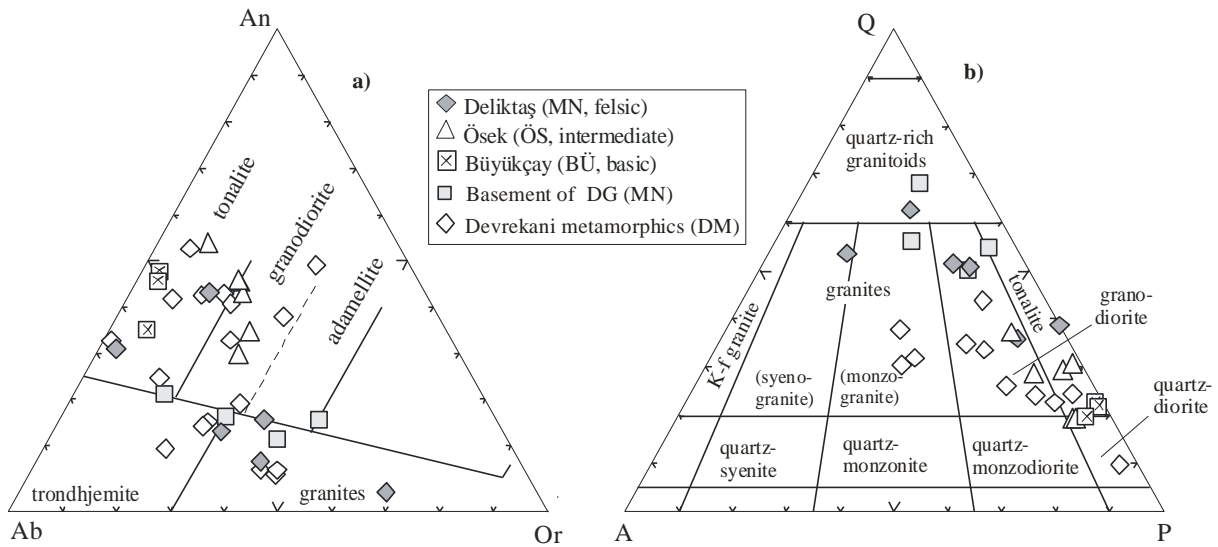


Fig. 5.4- Normative compositions plots: (a) Q-A-P (after LeMaitre, 1987; Streckeneisen, 1976) and (b) An-Ab-Or (after O'Connor, 1982) of Deliktaş-Sivrikaya and Devrekani metamorphics.

The bulk-rock concentration of the basement samples is characterized by a wide range in SiO₂ content, 52 to 75 wt % and 47 - 75 wt % for Deliktaş-Sivrikaya and Devrekani respectively (except the leucogranite sample MN-11, 79.8 wt %). The low aluminium saturation index (ASI= 0.58 - 2.20) and high aluminium index (AI= 1.0 - 3.5) ratios of samples indicate a metaluminous I-type, transitional and peraluminous S-type (e.g Chappell (1999); Chappell and White, 1974; Maniar and Piccolli, 1989) (Fig. 5.5) compositions, consistent with an origin from basaltic to felsic precursors (e.g. Drummond and Defant, 1990). In order to get information on the geotectonic setting the basement samples were plotted the on the Pearce et al. (1986) diagram (Fig. not shown), and nearly all the samples plot in the volcanic arc granites field.

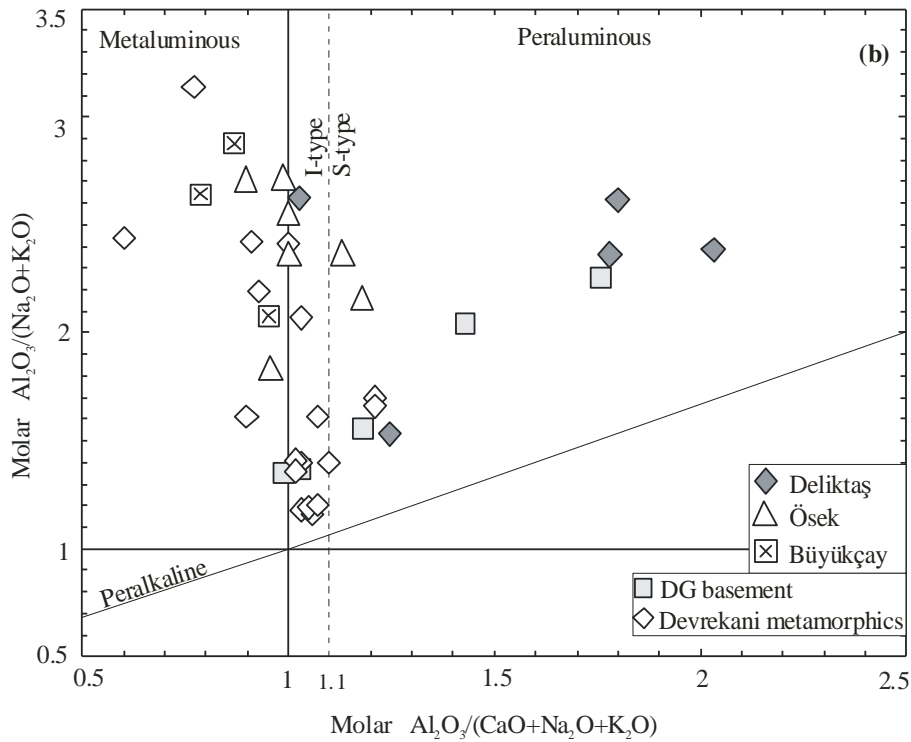


Fig. 5.5- Geochemical compositions of the Devrekani metamorphic unit; Deliktaş, Sivrikaya and Devrekani basements plotted in the ASI vs. AI, Shand's Index (1927) discrimination diagram, with fields of the different rock types after Maniar and Piccolli (1989) shown.

Samples show a wide range in trace elemental concentrations (Table 2, Appendix), with the highest values in mafic samples and the lowest in felsic rocks, indicating they could be derived from similar sources by crystal-liquid fractionation processes. Chondrite-normalized (Sun and McDonough 1989) REE patterns are plotted in Fig. 5.6. The patterns are sub-parallel and show moderate to strong fractionation between the LREE and HREE ($[La/Yb]_{cn} = 10 - 24$), and concave-upwards HREE ($[Gd/Yb]_{cn} = 0.93 - 2.7$) patterns. The mafic samples (BÜ) have small negative Eu anomalies ($Eu^*/Eu = \sim 0.90$), but better developed in the more evolved samples ($Eu^*/Eu = 0.76 - 0.96$). The moderate to strong fractionated REE patterns and small to large Eu-anomalies in samples support melting of amphibolite-type protoliths (e.g. Patino Douce, 1999) and different roles for garnet and plagioclase. Furthermore, samples show distinct troughs in the high-field-strength elements (HFSE) Ba, Nb, Hf and Ti, which is consistent with a subduction-related origin of the protoliths (e.g. Floyd and Winchester, 1975; Keppler, 1996).

The Devrekani metamorphics (DM) samples similarly show a broad spectrum of sub-parallel REE patterns characterized by moderate fractionation between the LREE and HREE ($[La/Yb]_{cn} = 6.4 - 27.6$), small concave-upwards LREE ($[Gd/Yb]_{cn} = 0.93 - 2.7$) and almost flat

HREE patterns. Moderate fractionated REE patterns and no to small negative Eu-anomalies ($Eu^*/Eu = 0.62 - 0.87$) in rocks support melting of mafic protoliths and subordinate or no role for garnet and plagioclase.

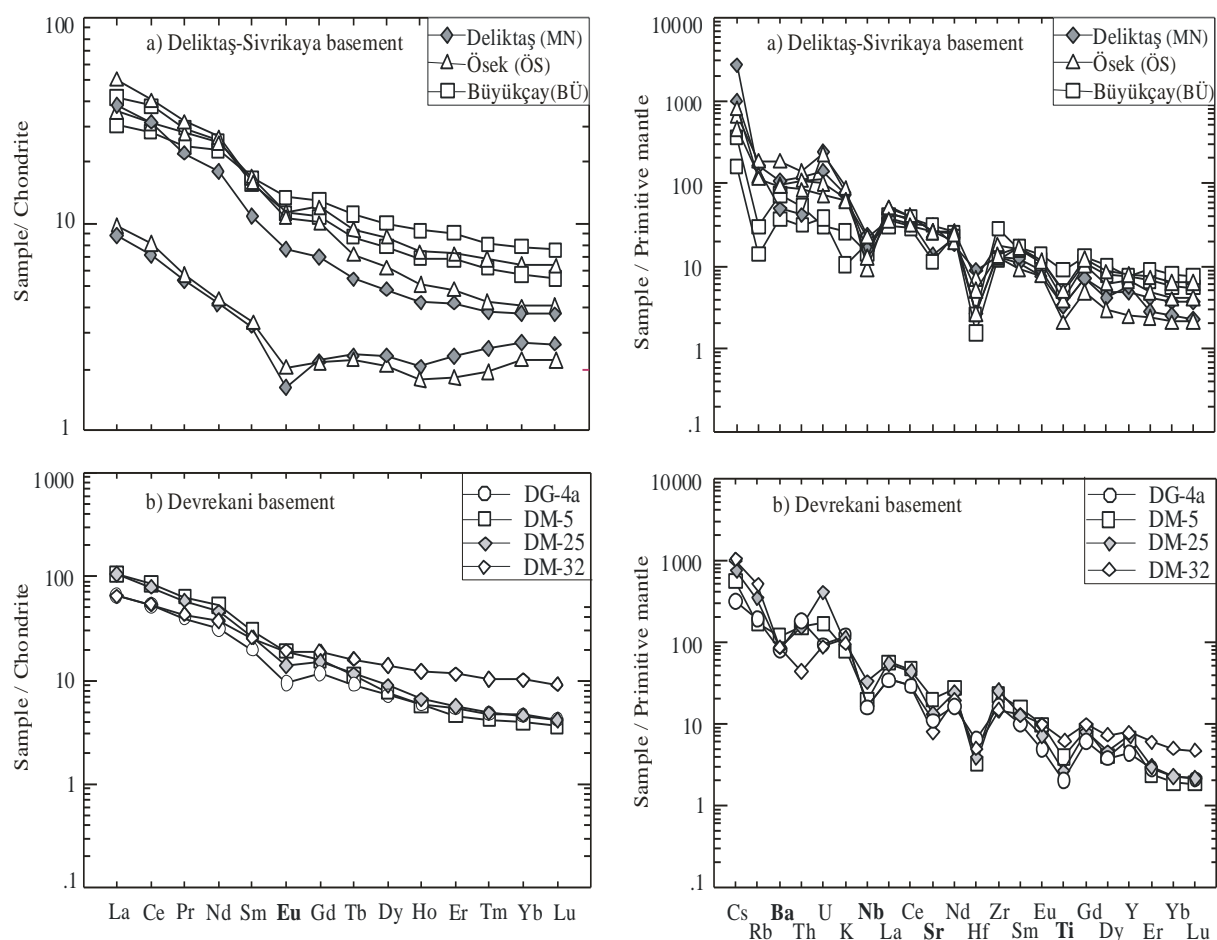


Fig. 5.6- (a) Chondrite-normalized REE spidergrams and (b) Primitive mantle-normalized plots of basement complex samples: Deliktaş (MN), Sivrikaya (ÖS, BÜ) and Devrekani metamorphics (DM). Normalizing values from Sun and Mc-Donough (1989).

All the basement samples show enrichment in large ion lithophile elements (LILE) such as Cs, Rb, Ba, Th, U and K, and depletion in high field strength elements (HFSE, Ba, Nb, Sr, Hf and Ti), consistent with subduction-related origin of the protoliths (e.g. Floyd and Winchester, 1975; Keppler, 1996; Tatsumi and Kogiso, 1997).

5.2.2. Sr-Nd-O isotopic compositions

The Nd, Sr and O isotope data are presented in Table 3, Appendix. Calculated initial $^{87}\text{Sr}/^{86}\text{Sr}$ (Sr_i) and $^{144}\text{Nd}/^{143}\text{Nd}$ ($\epsilon\text{Nd}_{(t)}$) isotopic compositions are based on U-Pb ages. The isotopic data highlights the considerable crustal residence age of the source region and show that protolith magmas represent new additions to the crust. Possible protoliths could be lower crust, and consisting of pelites, amphibolites and metagreywackes. Figures 5.7 show the

variation of initial $^{143}\text{Nd}/^{144}\text{Nd}$ expressed as $\epsilon\text{Nd}_{(t)}$ values with initial $^{87}\text{Sr}/^{86}\text{Sr}$ ($\text{Sr}_{(i)}$) isotopic ratios for the Deliktaş-Sivrikaya and Devrekani basement respectively. The $\epsilon\text{Nd}_{(t)}$ values decrease with increasing $\text{Sr}_{(i)}$ from the mafic to the felsic samples (exception of two quartz-rich samples with high $\text{Sr}_{(i)}$), indicating mantle origin for the protolith of basement rocks. Sivrikaya mafic and intermediate basement rocks have similar $\epsilon\text{Nd}_{(t)}$ and $\text{Sr}_{(i)}$ values (e.g. ÖS, $\epsilon\text{Nd}_{(t)} = -1.4$ to -2.7 ; $\text{Sr}_{(i)} = \sim 0.706$; BÜ, $\epsilon\text{Nd}_{(t)} = 6.8$ to 2.6 ; $\text{Sr}_{(i)} = \sim 0.704$) but the evolved samples show relatively large variations in isotopic composition (MN, $\epsilon\text{Nd}_{(t)} = -3.4$ to -6.6 ; $\text{Sr}_{(i)} = 0.706$ to 0.712) (Fig. 5.7a). Negative to positive $\epsilon\text{Nd}_{(t)}$ values, low $\text{Sr}_{(i)}$ ratios (Fig. 5.7a), and young Nd model ages ($T_{\text{DM}} = 0.6 - 1.3$ Ga) for the Deliktaş-Sivrikaya basement indicate significant input of mantle-derived component during protolith magma formation.

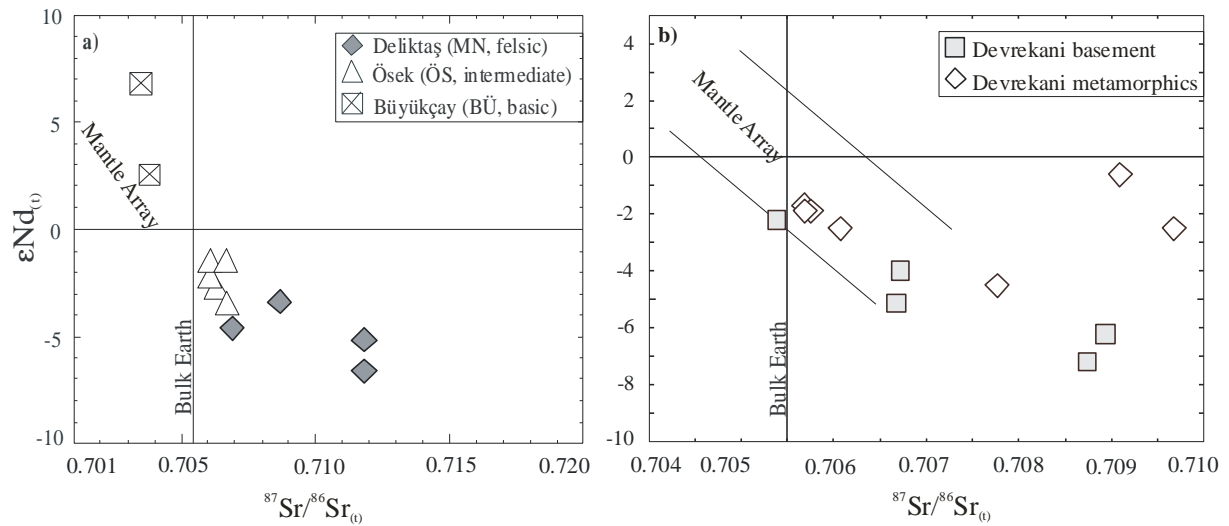


Fig. 5.7- $\text{Sr}_{(i)}$ vs. $\epsilon\text{Nd}_{(t)}$ plots of Devrekani metamorphic unit: (a) Deliktaş (MN), Sivrikaya (ÖS, BÜ) and (b) Devrekani (DM) basements.

The $\epsilon\text{Nd}_{(t)}$ and $\text{Sr}_{(i)}$ values range from 0.2 to -5.4 and $0.7002 - 0.7097$ respectively for Devrekani basement, with the most evolved samples (DM-21, DM-33) having higher values (Fig. 5.7b). The small positive (0.2) to large negative (-5.4) $\epsilon\text{Nd}_{(t)}$ values, variable $\text{Sr}_{(i)}$ ratios, and young Nd model ages ($T_{\text{DM}} = 0.9 - 1.3$ Ga) indicate variable proportions of juvenile and old, recycled continental crust-material contribution during protolith genesis.

The basement $\delta^{18}\text{O}_{\text{whole-rock}}$ values are very variable in the range of 8 to 12 ‰, is representative of mantle and mixed origin. The basement samples from all three outcrops plotted on the same diagram show a strong positive correlation between $\delta^{18}\text{O}$ and SiO_2 values, indicating crustal contamination (Fig. 5.8).

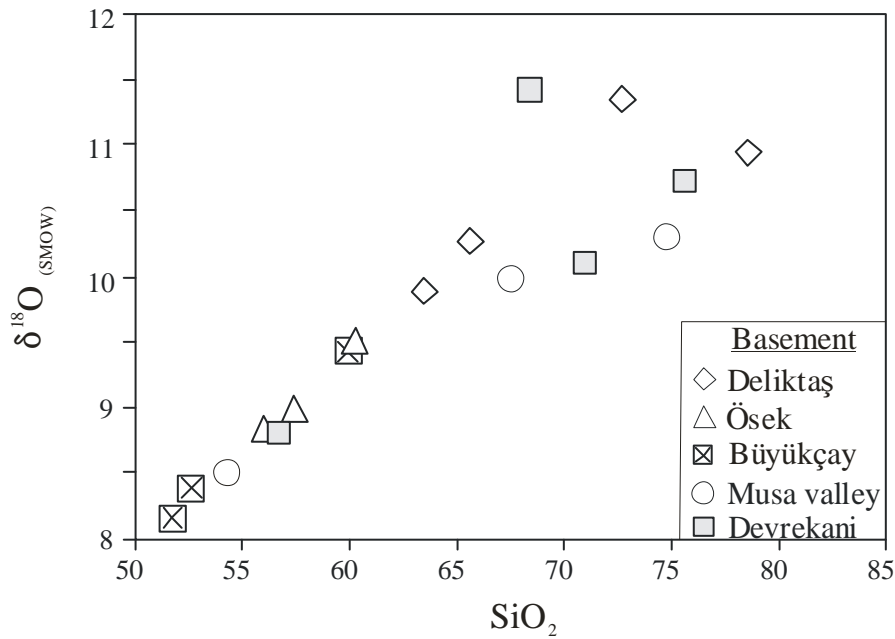


Fig. 5.8- $\delta^{18}\text{O}$ vs. SiO_2 plots of Devrekani metamorphic unit: Deliktaş, Sivrikaya (Ösek and Büyükçay) and Devrekani (Ousman and Musa valley) basement illustrating the effect of source (mantle) and crustal contamination

Very high, negative $\epsilon\text{Nd}_{(t)}$ values (-4.1 to -6.6) are shown by some basement samples, strongly indicate melting of, or contamination of by old continental crust or sediments derived from such crust. In contrast, more intermediate $\epsilon\text{Nd}_{(t)}$ values (-1.4 to -3.5) shown by Sivrikaya basement rocks (ÖS), may be explained by mixing old continental and mantle materials or young LREE-enriched arc-rocks. Evidence for the involvement of old continental material includes inherited Precambrian zircons in some samples. Although the trends on the $\epsilon\text{Nd}_{(t)}$ vs. $^{87}\text{Sr}/^{86}\text{Sr}$ and $\delta^{18}\text{O}$ vs. SiO_2 diagrams may show that the basement rocks could be derived from a single source, the narrow range in Sr, Nd and O isotopic compositions of the whole-rock samples and the small to distinct negative Eu-anomalies, reflect derivation of the basement rocks protoliths from heterogeneous sources with variable immature and old crustal material contribution.

The evolution of the Variscan Belt in Carboniferous times was characterized by contemporaneous formation of sedimentary basins and migmatites, by the intrusion of granitoids, and the formation and exhumation of granulites (e.g. Finger and Clemens, 1995; Kröner et al. 1998; Schaltegger et al. 1996). The magmatic rocks show chemical signatures that refer to remobilized mantle and lower crustal sources in variable proportions (Hegner et al. 1996; Langer et al. 1995; Liew and Hoffmann, 1988; Michard-Vitrac et al. 1981; Reischmann and Anthes, 1996). Compressional deformation, magmatism, exhumation of high-grade rocks and sedimentation in basins during extension were successive or spatially associated contemporaneous processes. The temporal resolution can only be achieved by

precise dating tools such as the conventional U-Pb and Pb-Pb techniques using zircon and monazite, which provides analytical uncertainties of better than $\pm 0.5\%$ of age results.

5.3. GEOCHRONOLOGY

5.3.1. Zircon internal structure

The closure temperature of zircon for the U-Pb system is probably well above 900°C (e.g. Mezger and Krogstad, 1997; Kröner et al. 2000) as documented by the survival of zircon xenocrysts in a variety of igneous rocks, notably basalt (Compston et al. 1986). Zircon can also survive regional metamorphism and partial melting (e.g. Gulson and Krogh, 1973; Pankhurst and Pidgeon, 1976; Harrison et al. 1987). This makes it almost certain that metamorphic zircon records the isotopic composition near or at its growth stage (Kröner et al. 2000). Survival of magmatic zircon and preservation of original crystallization age information in rocks that experienced high temperature overprint is shown by Möller et al. (2002), implying that resetting of zircon by diffusion during high-grade metamorphism is negligible. The composition of metamorphic zircon in equilibrium with an anatectic melt does not differ greatly from igneous zircon (Hoskin and Schaltegger, 2003), the only apparent systematic distinction is the Th/U ratio, which is very low for the former (<0.07 ppm, Rubatto, 2002). U-Pb isotopic ages can be linked with specific P-T conditions but allowing direct assessment of the rate of tectonic and metamorphic processes (Hoskin and Schaltegger, 2003). Concordant U-Pb ages for such zircons can therefore be interpreted as dating the peak of pressure, and the observed highly variable diffusive Pb loss is probably due to the very short exposure of such rocks to extreme depths. These two factors, resistance to resetting and protection of inclusion, make metamorphic zircon probably the best currently available mineral to allow precise dating of regional high-grade metamorphism (Krogh, 1993; Kröner and Jaeckel, 1995; Mezger and Krogstad, 1997). Zircons that grew in high-grade metamorphic rocks often shows a distinct sequence of internal structures: an initial low-luminescence growth zone (sometimes overgrowing an inherited core) sequentially overgrown by sector zoned domains. These textures are commonly followed by oscillatory zoned domains (Vavra et al. 1996, 1999; Schaltegger et al. 1999). The discordance in zircons could result from multiple episodes of growth indicating thermal events, variably small degrees of younger Pb loss that moves the points toward the origin, combined with minor contribution from preexisting grains (xenocrystic cores) that move the data point to the upper right on the concordia diagram (e.g Todt and Büsch, 1981). Linear distribution of the data points could be ascribed to the derivation of the zircons from a cogenetic suite that underwent

an episodic Pb loss or from averaging of the zircon population during sample selection by sizing, combined with the effects of an isotopic disturbance.

Two explanations for the negative value of lower intercept age of some samples: The studied zircon fractions may be comprised some grains with an inherited Pb component, which caused different discordant and nearly concordant starting points before the Pb loss event. Different degrees of subsequent Pb loss may have caused a negative lower intercept without significantly influencing the geological relevance of the upper intercept. The data points provide a relatively small spread of isotopic ratios and cluster at the higher end of the discordia line. As a consequence, the upper intercept is well anchored and of geological significance, whereas the lower intercept is vaguely defined.

5.3.2. U-Pb and Pb-Pb zircon data

No geochronologic data have been previously published for the Central Pontides basement. In order to constrain the timing of the high-grade metamorphism that produced the granulite facies metamorphic zircons were analyzed from samples from four basement outcrops. The results will be presented and discussed in three groups: Deliktaş and Sivrikaya basement, Devrekani basement/Devrekani metamorphics. I now present and discuss the individual results of U-Pb and Pb-Pb zircon analyses combined with cathodoluminescence study.

Deliktaş-Sivrikaya basement

Ortho-amphibolite sample BÜ-20. Ep+Grt(alm)+Stau+Hbl±Pyx±Qtz-Amphibolite. Albite-epidote-amphibolite facies regional metamorphism rock formed under P-T conditions of 3-7 kbar and 250-450°C respectively, and high shearing stress, or in the outer contact metamorphic zone. BÜ-20 zircon population is homogeneous. A date of this rock would provide an important time mark and greatly aid in determining the chronology of the pre-variscan events in this region and/or region of origin of the Central Pontides.

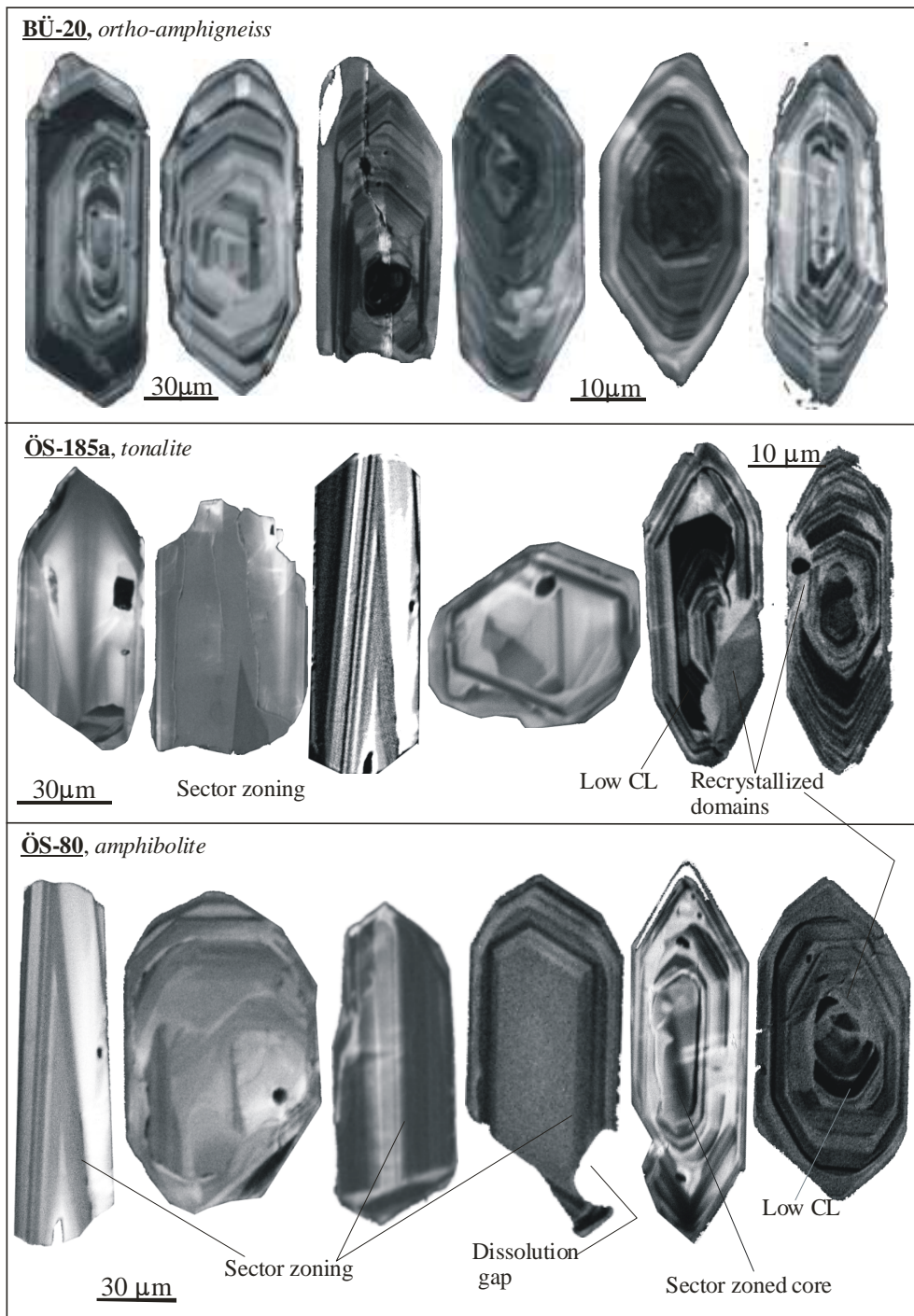


Fig. 5.9- CL photographs of characteristic zircon population from Deliktaş-Sivrikaya basement; Büyükçay river valley (BÜ-20) and Ösek area (ÖS-80 and ÖS-185a). Note the dissimilar morphological grain-types from both outcrops.

There is a problem in plotting the Rb-Sr whole-rock data, may be because of the thermal influence of the younger events, conditions under which Sr is mobilized and/or rehomogenized. The U-Pb-dating method on zircons of polymetamorphic rocks (Gebauer and Grünenfelder, 1979a,b) shows that it is possible to date first event of a polymetamorphic history, if the younger metamorphic overprints did not reach temperatures high enough to open the U-Pb-system completely.

Abundant medium (63-80 μm), euhedral, clear, short and at times stout zircons were separated from BÜ-20. CL images reveal two prismatic grain-types (Fig. 5.9), short and long prisms. The core may be surrounded by a small non-luminescent domain. Xenocrystic cores which are visible in all the zircons are of two types: in the prismatic grains multi-faceted core with oscillatory zoning, and prismatic core with sector zoning rimmed by magmatic zoning and over growth. This could be taken to represent many growth stages, as indicated by zones of high and low CL intensity and/or recrystallized domains.

Six (3 abraded) out of ten zircon analyses are nearly concordant to concordant at ~ 502 Ma (Fig. 5.10, inset), is interpreted as the crystallization time of the magmatic precursor. Two zircon fractions with variable small degrees of Pb-loss plot close to the concordia curve at ~ 450 Ma and 575 Ma. Two other fractions are reversely discordant at ~ 450 Ma and 800 Ma.

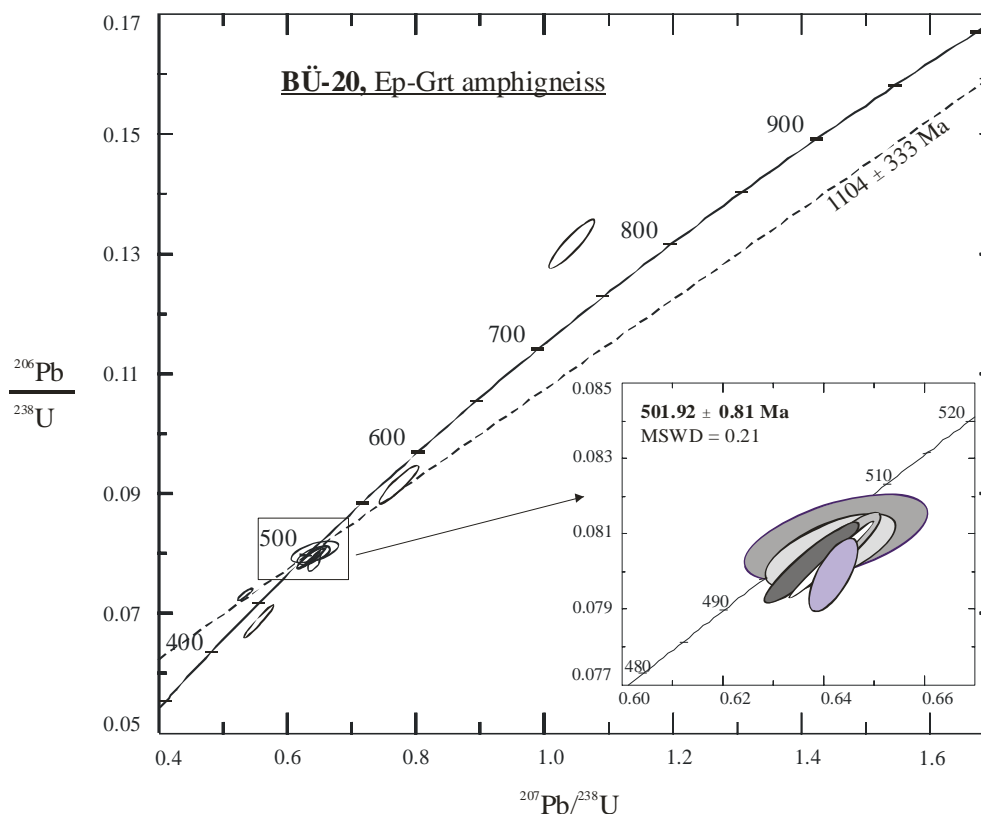


Fig. 5.10- U-Pb concordia plot for isotope dilution analyses for BÜ-20. Six analyses are concordant to nearly concordant at ~ 502 Ma (inset). A discordia through most of the data points yield an upper intercepts at 1104 ± 333 Ma. Error ellipses are $2\sigma_m$.

The analysis at ~ 800 Ma may represent a Proterozoic inherited component and analysis at ~ 575 Ma is probably a mixture between inherited component and radiogenic Pb loss since the

closure or the zircon U-Pb geochronometer. Reverse discordia may be due to geologic events such as high-grade metamorphism, so are not considered for age calculation. A discordia forced through most fractions yield a Precambrian protolith age. The linear distribution of the data points could be ascribed to the derivation of the zircons from a cogenetic suite that underwent an episodic Pb loss.

The age 501.92 ± 0.81 Ma is interpreted as the primary age (time of crystallization). This age is equivalent to that of several Cambrian rocks found in the Hercynian belt (e.g. Pin and Ducrot, ; Maurel et al. 2002; Paquette et al. 1999) in the Schwarzwald (e.g. Hofmann and Köhler, 1973; Steiger et al. 1973; Todt and Büsch, 1981; Gebauer and Grünenfelder, 1979b). There are no evidence of regional and Variscan (320-344-370 Ma) tectonometamorphic overprint, and intrusion of the Kastamonu granitoids on the zircons. In contrast, upper Ordovician Pb loss event is documented. Therefore, this outcrop may be one of the rare preserved relics of the continental crust that was subducted northward during the Variscan orogeny (Matte, 1986, 1998; Ziegler, 1989, Carboniferous collision between Gondwana and Laurentia-Baltica). *Additional Pb-Pb zircon age and microprobe data is required for further evaluation of the significance of this 502 Ma age cluster!*

Ösek samples (ÖS-80 and ÖS-185a). Contain near-spherical metamorphic zircons as well as long-prismatic, magmatic zircons with pointed termination. Zircon grains are euhedral, clear to light pink and/or light brown, with darker terminations. Zircon grain-sizes range from 63-200 μm , are beautiful, clear to light brown (dark ends), euhedral, transparent and inclusion free. CL images show very heterogeneous zircon population (Fig. 5.9): (1) long needles with V-shaped sector zoning; (2) prismatic grains with a compositional zoned core rimmed by regular magmatic zoning, with dissolution gaps and recrystallized domains; (3) magmatic zircons with oscillatory zoning, sector- as well as magmatic-zoned cores and rounded low CL core followed by a very luminescent portion, (4) stout near-spherical grains with kidney-shape zoned cores; (5) thick halves with faint broad-band zoning surrounded by a thin rim of magmatic zoning. Recrystallized domains and dissolution gaps are common.

Amphibolite sample ÖS-80. Pb and U contents respectively range from 600 to 1700 ppm and 17 to 86 ppm. Ten data points cluster in two groups of ages ~ 298 Ma and ~ 305 Ma with variable degrees of discordance and/or Pb loss, corresponding to the emplacement of the Deliktaş and Sivrikaya granites. Two further fractions with inherited Pb-component plot below the concordia line. A discordia calculated through the first group of data points gives U-Pb ages of 949 ± 96 Ma and 295.0 ± 1.7 [± 2.4] Ma (MSWD= 2.3).

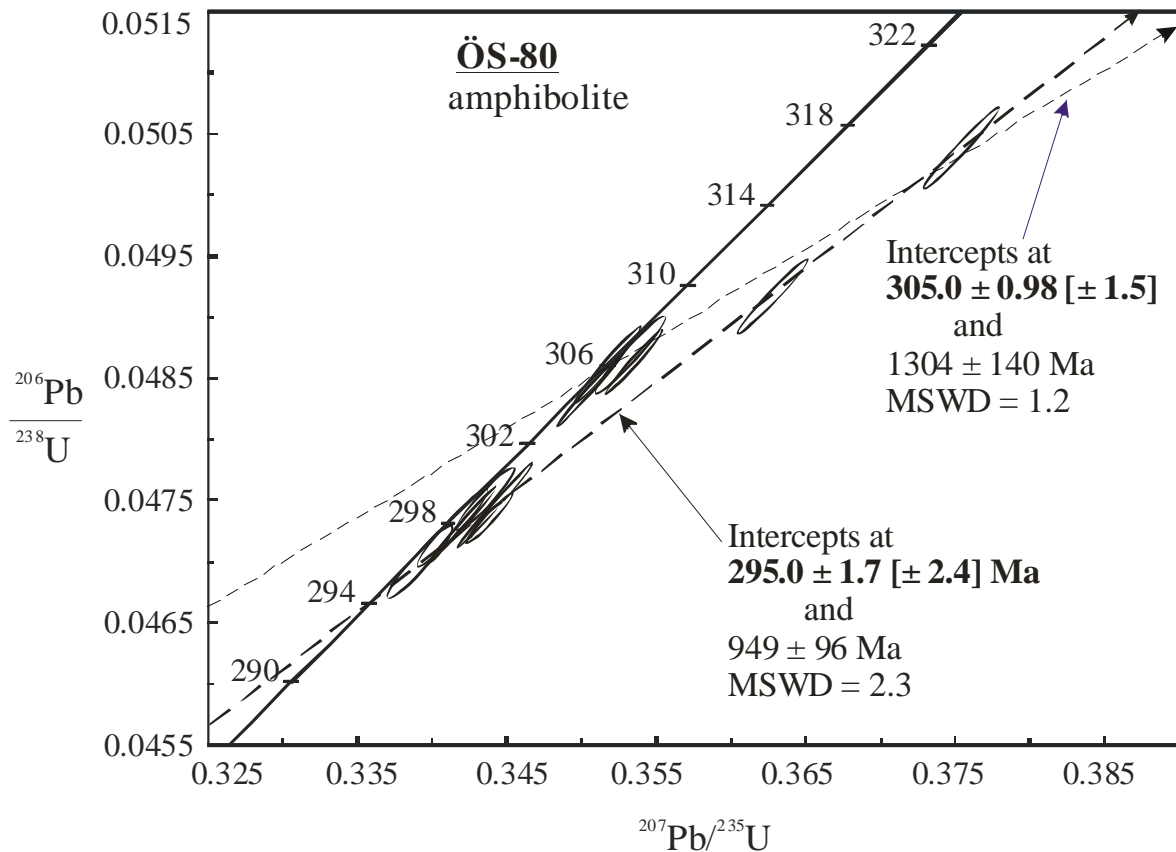


Fig. 5.12- U-Pb concordia plot for isotope dilution analyses for ÖS-80. Two separate discordia through the cluster of data points and the fractions with old Pb-components intercept the concordia respectively at 1304 ± 140 Ma and 305.0 ± 0.98 [± 1.5] Ma, and 949 ± 96 Ma and 295.0 ± 1.7 [± 2.4] Ma. Error ellipses are $2\sigma_m$.

The second group of analyses yielded an upper intercept age of 1304 ± 140 Ma and lower intercept of 305.0 ± 0.98 [± 1.5] Ma (MSWD= 1.2). Similarly, nine zircon analyses from another sample (ÖS-185a) plot on a well-defined line of Pb loss, that intercept the concordia at 310.0 ± 1.6 [± 3.9] Ma (MSWD= 4.2), however, four data points are nearly concordant yield a mean $^{206}\text{Pb}/^{238}\text{U}$ age of 306 ± 4.4 (MSWD= 0.52) (Fig. not shown). The results are supported by the CL images of zircons revealing three grain-types. The upper intercept ages indicate Precambrian components. The linear distribution of the data points could be ascribed to the derivation of the zircons from a cogenetic suite with an original age of 1340 Ma that underwent an episodic Pb loss ~ 300 Ma ago or from averaging of the zircon population during sample selection by sizing, combined with the effects of an isotopic disturbance.

Tonalitic-amphibolite sample ÖS-185. Ten zircon fractions were analyzed from this sample. The analyses cluster in two groups. Four data points are nearly concordant at ~306 Ma (Fig. 5.13, inset) and four others are reversely discordant between 320-335 Ma. All the analyses plot on a well-defined line of Pb loss (Fig. 5.13, inset) intercepting the concordia at $310.0 \pm 1.6 [\pm 3.9]$ Ma (MSWD= 4.2). The 320-325 Ma Pb loss may indicate either partial resetting or new components (overgrowth) as the result of Carboniferous metamorphism. Different degrees of subsequent Pb loss may have caused a negative lower intercept.

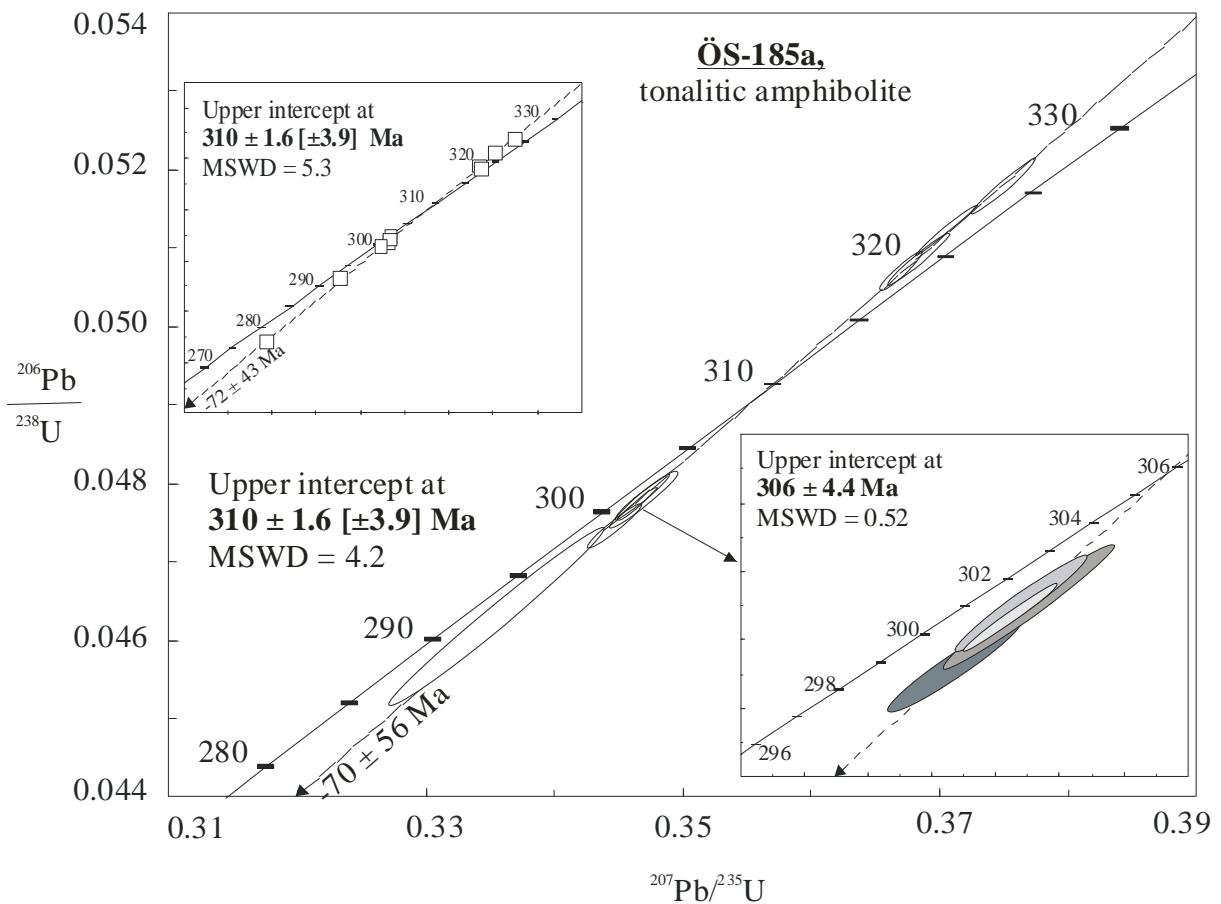


Fig. 5.13- Concordia plot showing U-Pb zircon isotope dilution analyses from Ösek metabasic sample, ÖS-185a. The lower intercept age of 310 ± 1.6 Ma is given by a discordia line calculated through all nine data points. The inset is an enlargement of four slightly concordant fractions. Error ellipses are $2 \sigma_m$.

Devrekani granitoid basement/Devrekani metamorphic

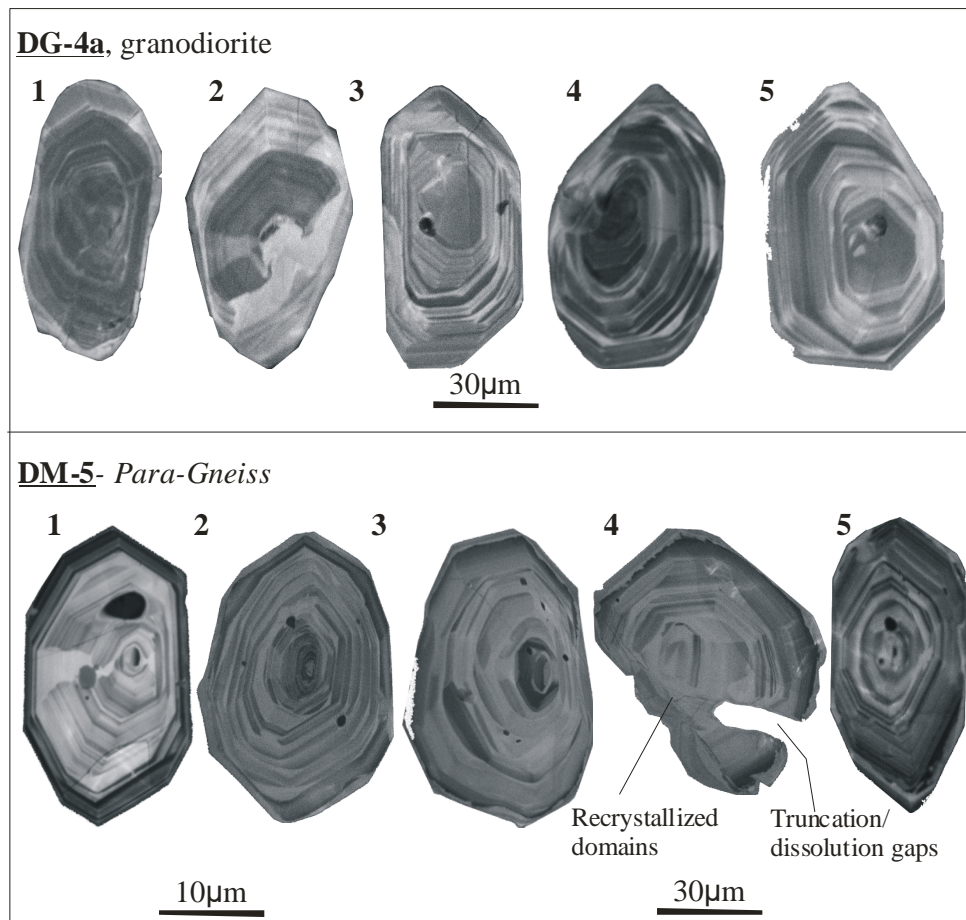


Fig. 5.14- CL photographs of characteristic zircon population from Devrekani basement samples (Osman valley) DG-4a and DM-5. Note the similar morphological grain- types, presence of two-three growth stages, rounded relic cores and recrystallized domains

Quartz diorite sample, DG-4a. Zircon grains are idiomorphic, large and colourless to light yellow/brown. Two morphological grain-types make up the zircon population of this sample: euhedral, prismatic crystals with well developed [100] and [101] phases and more abundantly multifaceted grains. The grain-size ranges from 123 to 200 µm in length. CL images reveal that the prismatic zircons consist of detrital core and recrystallized domains, rimmed by magmatic overgrowth resulting in euhedral grains (Fig. 5.14). This rock occurs as an apophysis in the Devrekani granitoid.

From DG-4a (Fig. 5.15), eight zircon grains were analysed by U-Pb isotope dilution method. Three data points are nearly concordant at ~220 Ma and three other fractions with small Pb loss plot close the concordia at ~ 195 Ma. A discordia calculated through all the data points yielded an upper intercept of 2070 ± 24 Ma (inset, Fig. 5.15) may indicate the presence of

older cores of Proterozoic age. A further unabraded zircon analyses plots below the concordia line at ~ 190 Ma, probably Jurassic overgrowth or substantial Pb loss.

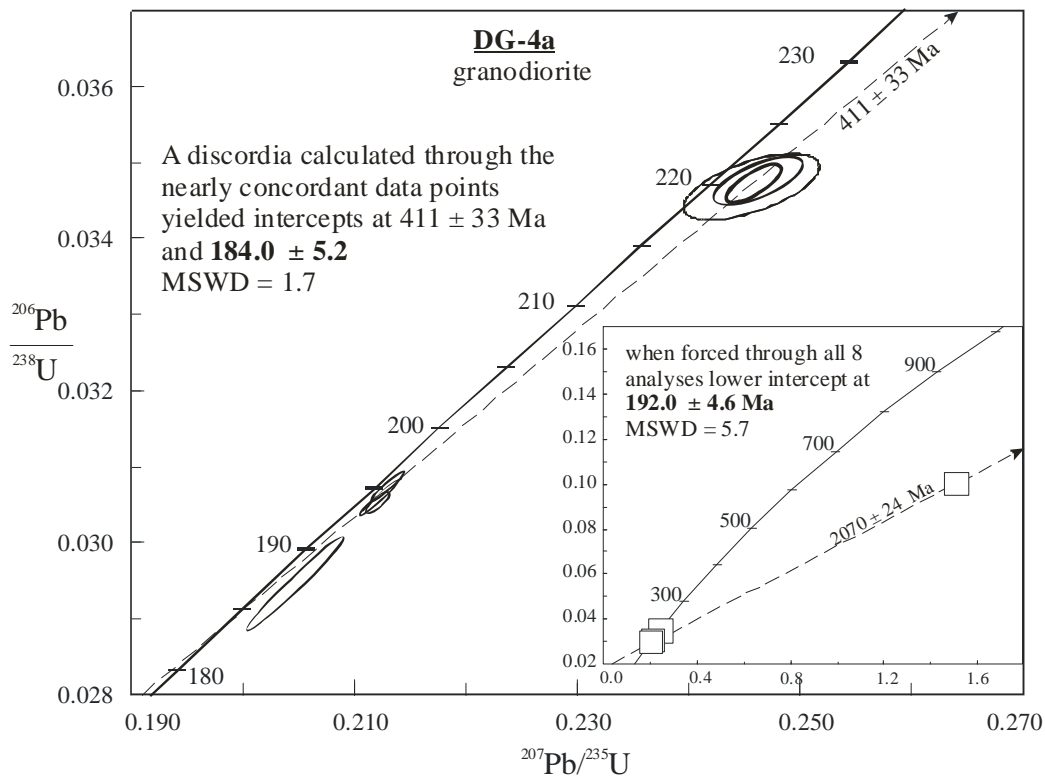


Fig. 5.15- U-Pb concordia plot for isotope dilution analyses for DG-4a. A discordia through all the nearly concordant data points cuts the concordia at 444 ± 33 Ma and 184.0 ± 5.2 Ma. Inset is a plot of the fraction with relic core and the other 7 fractions. Error ellipses are $2 \sigma_m$.

Para-gneiss sample, DM-5. sample contains beautiful, large/thick and clear to light brown garnet-shaped euhedral zircon grains. CL photographs of zircons reveal a population made up of euhedral grains multi-faceted habit with two morphologies: stout and prismatic with combination of prism $\{(100)\}$ and $\{(110)\}$ and pyramid forms $\{(211)\}$, $\{(101)\}$, and $\{(301)\}$. Zircons internal structure show a rounded relic core, two-three magmatic growth stages followed by a small overgrowth. Recrystallized domains and truncated zoning are common. (Fig. 5.14) This may imply the zircons grew in a melt and experienced alteration after crystallization. Such zircons usually yield discordant U-Pb ages (e.g. Poller et al. 1997).

The $^{206}\text{Pb}/^{238}\text{U}$ and $^{207}\text{Pb}/^{235}\text{U}$ ages of nine zircon fractions show a large scatter (Fig. 5.16). The scattered U-Pb data suggest multiple sources for the protolith of the para-gneisses. Four fractions are concordant between 290 Ma, 360 Ma and 400 Ma. It is not possible to draw a discordia line through the data points and to find a reasonable age. The discordance in these zircons most likely resulted from variably small degrees of younger Pb loss that moves the points toward the origin, multiple episodes of growth indicating thermal events, combined

with minor contribution from preexisting grains (rounded xenocrystic cores, Fig. 5.14) that move the data point on the concordia diagram to the upper right.

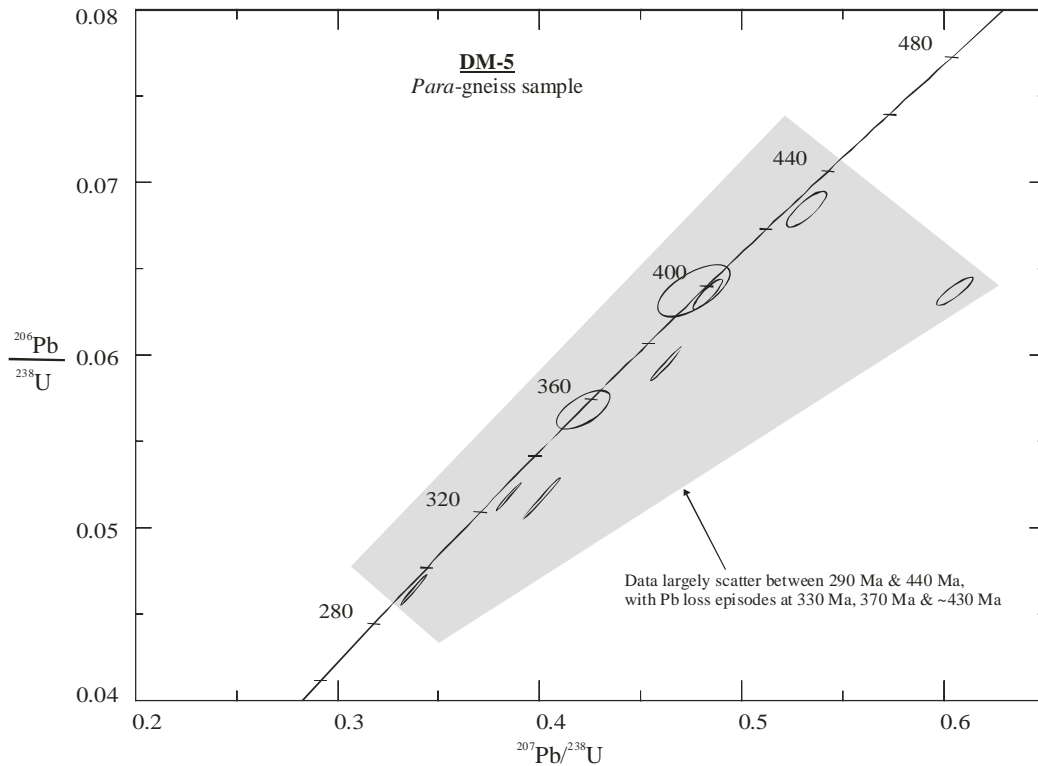


Fig. 5.16- Osman valley, large spread of ages between 290 - 440 Ma and small inherited core at ~430 Ma

The linear distribution of the data points could be ascribed to the derivation of the zircons from a cogenetic suite that underwent an episodic Pb loss ~300 Ma ago. It is also likely that this metasedimentary zircon suite is comprised of zircons of different origins and ages. A linear distribution of data points on a concordia plot could result from averaging of the zircon population during sample selection by sizing, combined with the effects of an isotopic disturbance (e.g. Pidgeon et al. 1970), and the lower interception of the discordia will give the approximate age of the isotopic disturbance (e.g. Todt and Büsch, 1981).

Ortho-amphibolite sample, DM-23. Abundant small (63-125µm) euhedral zircon grains were extracted from this sample. The crystals are prismatic, clear to light brown (dark tips), transparent and devoid of inclusions. Two to three growth stages can be recognized in CL images (Fig. 5.17). A characteristic feature of the zircons is oscillatory zoned core with high luminescence, indicating a magmatic origin. A thick low CL intensity overgrowth or recrystallized domain, probably resulting from magmatic overprint, is observed in all grains.

The radiogenic Pb and U contents respectively range from 24 to 90 ppm and 460 to 1640 ppm (Table 4, Appendix). Of the twelve zircon fractions analyzed, ten (8 abraded and 2 unabraded) are concordant to nearly concordant between 285 Ma and 300 Ma (Fig. 5.18).

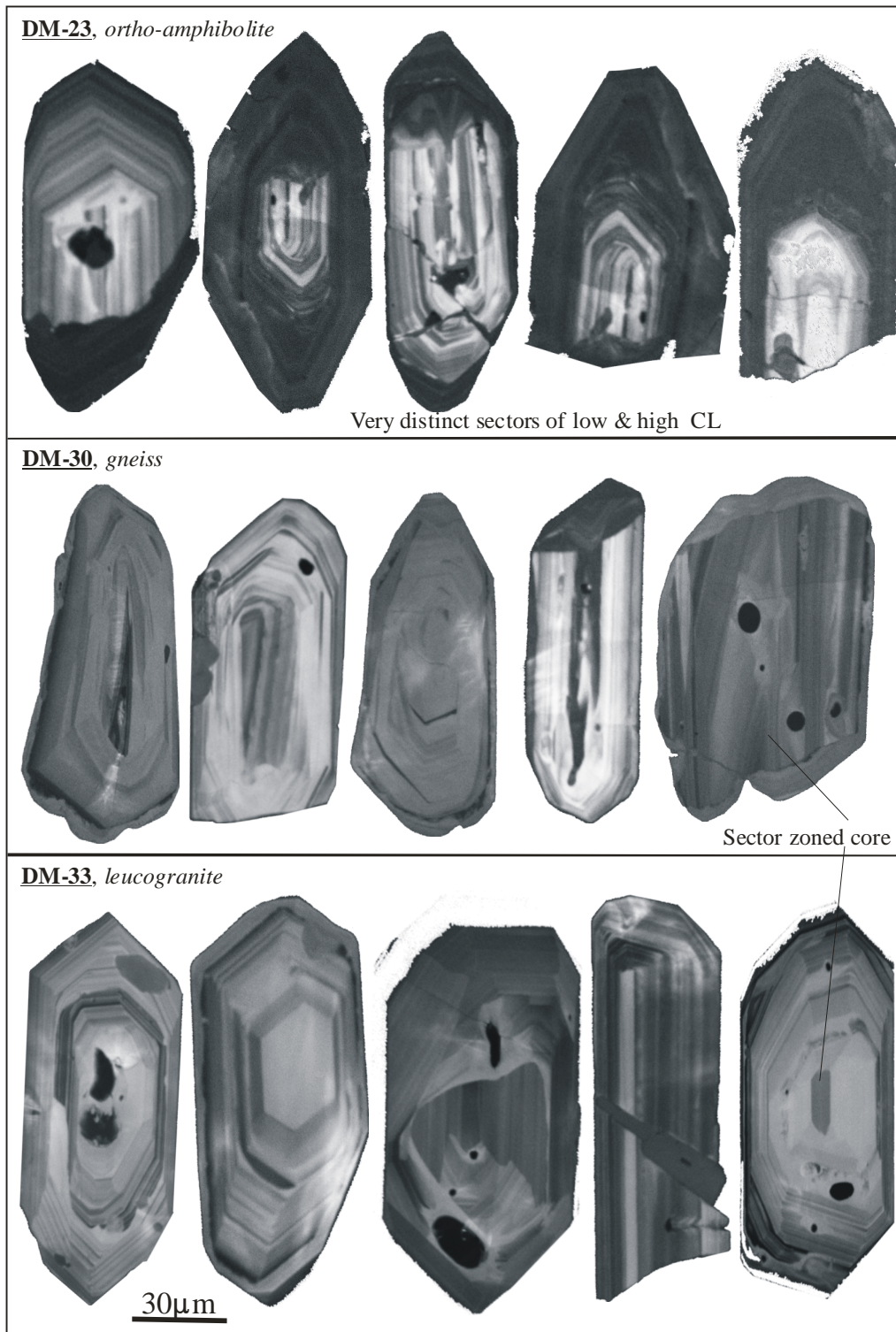


Fig. 5.17- CL photographs of characteristic zircon population from Devrekani basement samples (Musa valley). Noteworthy are the dissimilar morphological grain-types, internal structure shows many growth stages and recrystallized domains. Sample DM-23 is very peculiar with high luminescence magmatic

zoned parts and low CL intensity overgrowth or recrystallized domains with on/faint zoning

Two fractions variable degrees of Pb loss plot close to the concordia at 290 Ma and 300 Ma. But five data points cluster at ~300 Ma. A discordia line forced through most of the analyses gives intercept ages of 1203 ± 821 Ma and 291.5 ± 6.8 Ma. The upper intercept age corresponds within the error limit to the Nd model age ($T_{DM} = 1.2$ Ga) of this sample (Table 3, Appendix).

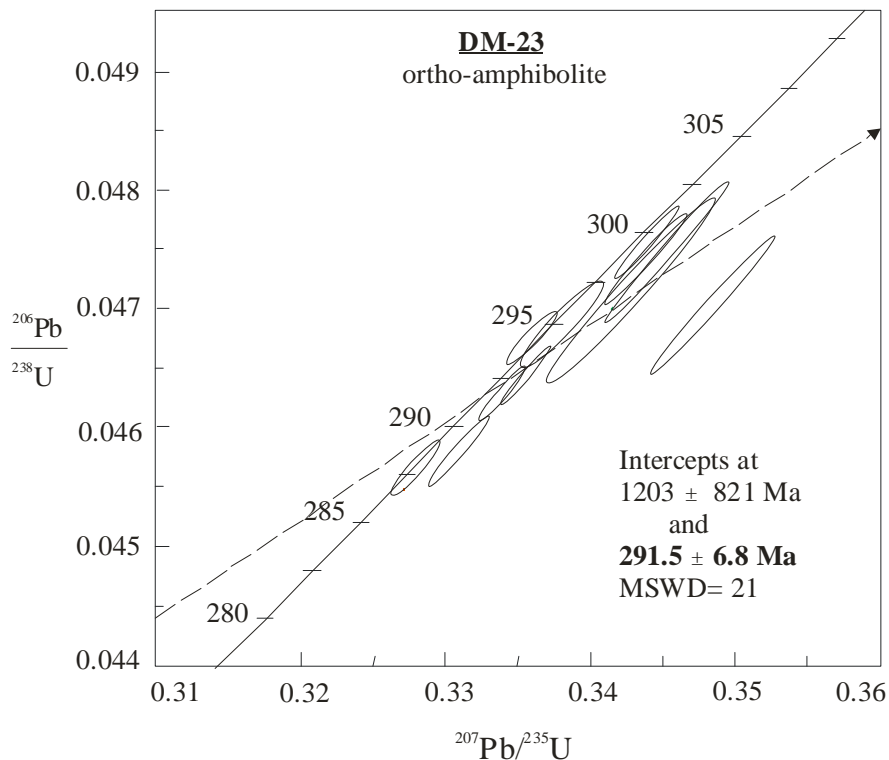


Fig. 5.18- Concordia plot of U-Pb zircon isotope analyses from Devrekani metamorphics (Musa valley), sample DM-23. Error ellipses are $2 \sigma_m$.

Granite samples, DM-33. Zircons from this sample have similar morphology and consist of euhedral prismatic crystals. The grains are colourless to light brown, transparent and translucent with dark brown points. CL reveals internal structures with at least two growth periods, simply oscillatory zoning, compositional zoned cores with and without magmatic overgrowth or recrystallized domains (Fig. 5.17). Uranium concentrations range from 602-2062 ppm (Table 4, Appendix). U-Pb analyses of nine fractions yielded U-Pb ages with variable degrees of discordance (Fig. 5.19a). U-Pb data provide evidence for Palaeozoic zircon growth and/or Pb-loss episodes at 290-300 Ma and ~ 370 Ma. When eight data are regressed together on the same discordia line, they yield intercept ages of 509 ± 43 Ma and 225 ± 23 Ma. The latter age is similar to the one got from sample DG-4a (Fig. 5.15), while the

upper intercept age correspond to the concordant data points of the sample BÜ-20. Evaporation of five euhedral zircon grains yielded a mean $^{207}\text{Pb}/^{206}\text{Pb}$ age of 310 ± 9 Ma with thermal events at ~ 360 Ma (Fig. 5.19b), Table 5, Appendix). The former age is similar to the U-Pb 300 Ma episode of new growth. The young lower intercept age might be a thermal overprint/resetting related to the intrusion of the middle Mesozoic Devrekani granitoid.

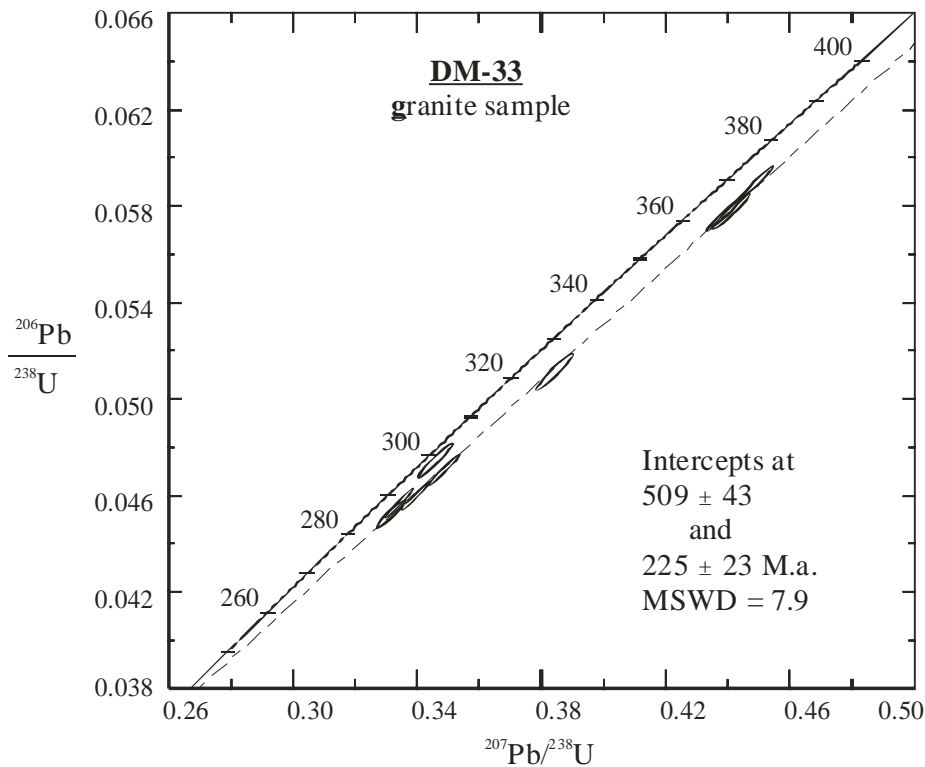


Fig. 5.19a- U-Pb concordia plot for isotope dilution analyses for granite sample DM-33, from the Devrekani metamorphics (Musa valley). A line forced through eight of the nine data points yield intercepts at 225 ± 23 Ma and 509 ± 43 Ma. Error ellipses indicate $2\sigma_m$.

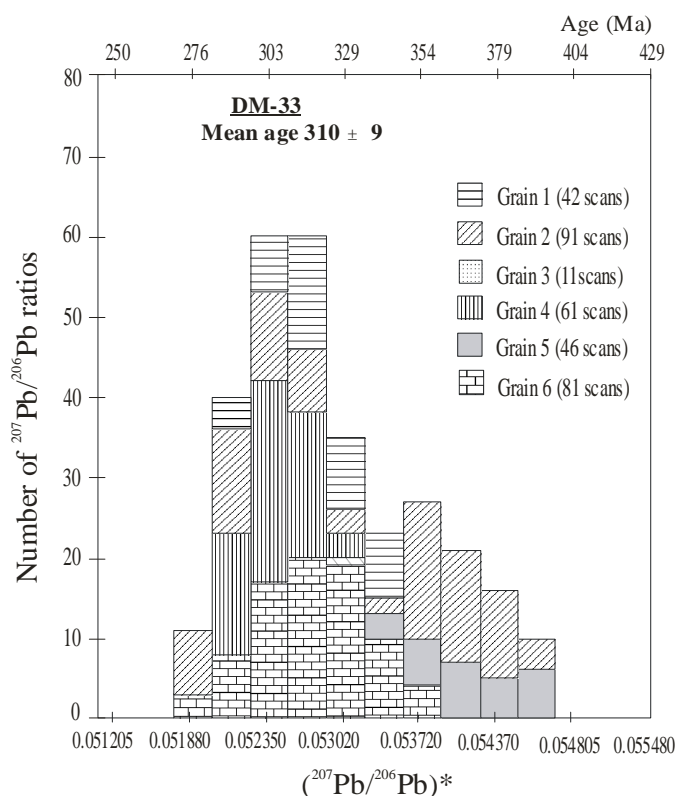


Fig. 5.19b- Histogram showing the frequency distribution of radiogenic $^{207}\text{Pb}/^{206}\text{Pb}$ ratios of single zircon Pb-Pb evaporation from sample DM-33. The spectrums for six idiomorphic grains, integrated from 332 ratios give an age of 310 ± 9 Ma

5.3.3. Rb-Sr whole-rock data

Rb-Sr whole-rock analyses from the Deliktaş-Sivrikaya basement define an isochron age of 314 ± 15 Ma (MSWD= 1.2 and $\text{Sr}_{(i)} = 0.70698 \pm 0.00029$) (Fig. 5.20a). The Rb-Sr age, although with large error is similar to the U-Pb ages (Figs. 5.12, 5.13). Similarly, the whole-rock data of samples DG-4a, DM-5, DM-23, DM-25, DM-27, DM-30, DM-32, DM-33 and MN-32 yield an isochron age of 301 ± 8.4 Ma (MSWD= 1.03, $\text{Sr}_{(i)} = 0.706474 \pm 0.00030$) (Fig. 5.20b).

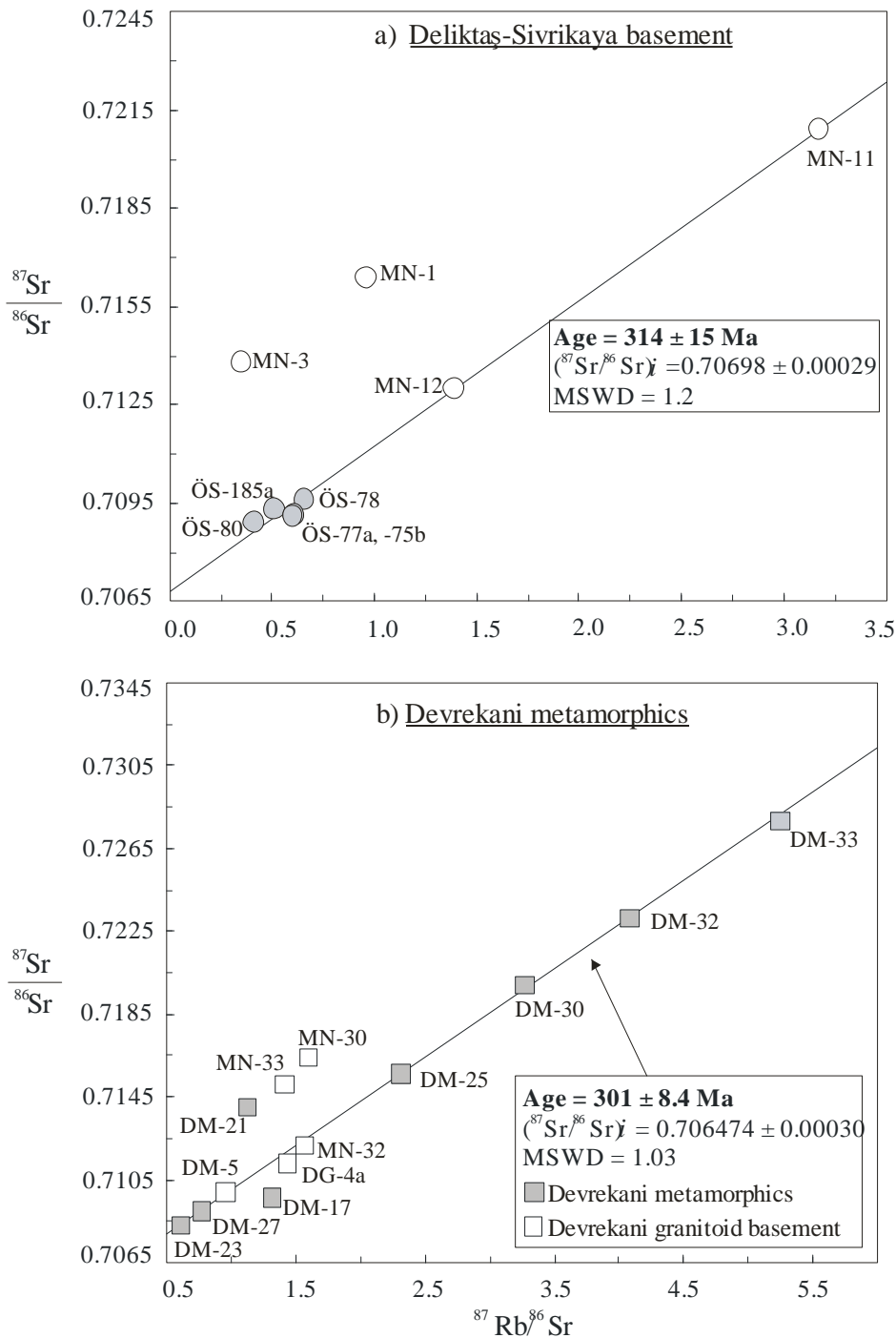


Fig. 5.20- $^{87}\text{Sr}/^{86}\text{Sr}$ vs. $^{87}\text{Rb}/^{86}\text{Sr}$ whole-rock isochron plots, samples from the different basement outcrops. **(a)** Deliktaş-Sivrikaya and **(b)** Devrekani

The Rb-Sr whole-rock ages, although with big error is similar to the zircon ages (Figs. 5.15, 5.16, 5.18 & 5.19). The Rb-Sr whole-rock ages from both basement outcrops are regarded as the cooling ages. These ages confirms a Late Carboniferous metamorphism and deformation in the Pontides, and forms a link between the Variscan orogeny in Central Europe and the Uralides of Eastern Europe.

5.4. DISCUSSION

The basement largely includes Proterozoic-Palaeozoic gneisses, granites, amphibolites and meta-volcanics. The steep REE patterns shown by some samples, confirms the presence of garnet in the source because this phase strongly concentrates HREE (Hanson, 1978). Some samples have steep LREE and flat HREE patterns, resulting in a change in slope at Tb. This feature suggests fractionation of sphene or amphibole (Hanson, 1978; Fourcade and Allégre, 1981; Witt and Swager, 1989). The very high concentrations of Sr (117-588 ppm) in the samples are also important for petrogenetic considerations because crust-derived melts most likely have low Sr concentrations whereas the concentration in mantle-derived melts may be high. Subsequent fractionation of hornblende, for example, from mantle-derived melts may further increase the Sr-concentration (Dempsey et al. 1990). According to Halliday et al. (1985) melt composed of 50 % mantle-derived magma and 50 % crust-derived magma may obtain 90 % of its Sr from the mantle. Calc-alkaline rocks are frequently enriched in Sr and Ba (Hawkesworth et al. 1979; Meen and Egger, 1987), suggesting that the rocks calc-alkaline or detritus from such rocks may have been involved in their generation. If the protoliths are derived by partial melting of a heterogeneous crustal source, consisting of components with different crustal residence time, this would reflect in the Nd-model ages (T_{DM}). The basement samples yield T_{DM} ages ranging from 0.6 to 1.7 Ga suggesting Proterozoic and possibly Archean crust as the Nd model ages will always give the minimum values. These ages, in some cases, are compatible with the inherited U-Pb ages of the granitoids and basement.

The relatively high $\epsilon Nd_{(t)}$ values shown by some of the rocks (-0.6 to -4) suggest involvement of mantle or mafic crustal sources. However, a younger, more siliceous LREE-enriched crustal source cannot be ruled out, such as detritus from the young calc-alkaline arc-rocks which likely were part of the source region. More intermediate $\epsilon Nd_{(t)}$ values (-4 to -6) may be explained by mixing old continental material with mantle material or young LREE-enriched arc rocks, consistent with Proterozoic zircons upper intercept ages. The heterogeneity of initial Sr isotope ratios, and wide range in $\epsilon Nd_{(t)}$ could also reflect varying influence of xenocrystic accessory mineral phases on the Sm-Nd isotope system.

From geochemical and isotope results it seems most likely that at least two sources, mantle-derived and old continental crust are necessary to explain the isotopic compositions of the basement rocks of the Central Pontides. There is also strong evidence that the source with mantle signature was rich in LREE. These characteristics are compatible with a subduction-related calc-alkaline source. Overall, the geochemistry of the basement rocks indicates a subduction zone setting for their protolith, in the Palaeozoic.

Zircon U-Pb and Pb-Pb, and Rb/Sr whole-rock data from the investigated basement samples indicate the protoliths to be of Proterozoic to Palaeozoic ages, which is a characteristic feature of the Variscan belt. The age data and the protolith ages in this study further indicate Cadomian and Variscan tectonometamorphic events within the basement. The 360-340-320 episodes of Pb-loss document regional metamorphism, migmatization and granitoid magmatism, widespread in the entire Variscan belt. The Carboniferous age for metamorphism from zircons coincides with the results from Rb-Sr whole-rock investigations which yielded Late Palaeozoic isochron ages. All the basement rocks were overprinted during Variscan cycle and regional metamorphism. The postmagmatic Early Variscan amphibolite-facies metamorphism and mylonitic shear/deformation had variable affected the U-Pb isotopic system of zircons.

5.5. CONCLUSIONS

5.5.1. *Regional geological implications*

The region between the Eastern Mediterranean and the Black Sea consists of several small continental fragments/terrane bearing evidence for various periods of deformation, metamorphism and magmatism, associated with Variscide, Cimmeride and Alpidic orogeny, (the strongest). The Alpidic orogeny started with the convergence between Africa-Arabia and Eurasian plates during the Late Mesozoic, and resulted in the amalgamation of the continental fragments which were situated on the margins of the Tethyan oceans, into a single landmass in the Tertiary. Pre-Alpidic orogenic events are especially strong and well documented in the Pontides.

In the Early Palaeozoic, the east European craton formed part of the Baltica plate, which collided in the west with Laurentia, Avalonia and Armorica creating Laurasia in the Late Palaeozoic (e.g. Pharaoh, 1999; Matte, 2001; Warr, 2002; Okay et al. 2006). In contrast, Africa and the Arabian Platform constituted part of the Gondwana, which preserved its unity until the Early Mesozoic opening of the southern Atlantic (e.g. Okay et al. 2006). Large areas in the northern margins of Gondwana are characterized by Neoproterozoic-Cambrian plutonism and metamorphism forming part of Pan-African/Cadomian orogenic cycle (e.g. Stern, 1994), and are therefore easily distinguished from the Palaeoproterozoic basement of the East European Craton. During the Late Palaeozoic and Mesozoic, Tethyan oceanic basins separated Laurasia from northeast Africa-Arabia. Parts of the present Eastern Mediterranean Sea represent a Triassic to Jurassic remnant of a Tethyan oceanic crust (e.g. Şengör and Yılmaz 1981; Garfunkel, 1998).

The pre-Alpide geological history of northern Turkey-Balkan region involved episodic growth of Laurasia by accretion of oceanic and Gondwana-derived continental fragments, interrupted by the opening of narrow back-arc basins on the southern margin of Laurasia. The continental terranes were accreted to Laurasia during the Late Ordovician-Early Silurian and Late Carboniferous, whereas a major accretion of oceanic crustal material occurred during the Late Triassic-Early Jurassic. The ensuing suture is probably an extension of the Rheic suture in central Europe (Ziegler and Stampfli, 2001). The Carboniferous accretion of the Strandja-Sakarya terrane to Laurasian margin resulted in strong deformation, Mid Carboniferous high-grade regional metamorphism, and latest Carboniferous-Early Permian post-orogenic plutonism.

The Late Carboniferous orogeny in the Pontides forms a link between the Variscan orogen in Central Europe and the Uralides of Eastern Europe. The Variscan orogeny comprises Carboniferous to Early Permian deformation, metamorphism and magmatism linked to the collision and amalgamation of Gondwana, Laurasia and the intervening terranes (e.g. Matte, 2001). It is marked in the Pontides by high-grade regional metamorphism, deformation and post-orogenic latest Carboniferous-Early Permian plutonism. The East European Craton is bordered in the south by a narrow tectonic belt, called the Scythian Platform, which is generally considered as a Late Palaeozoic (Early Carboniferous) orogen (e.g. Nikishin et al. 2001). During the Devonian and Carboniferous the İstanbul Zone (Western Pontides) and the Moesian Platform were adjacent to the Scythian platform, and formed a south-facing passive continental margin (Fig. 1.2).

The Late Carboniferous deformation in the İstanbul Zone is coeval with the high-grade metamorphism in the Sakarya Zone (Eastern and Central Pontides). The deformation and regional metamorphism is related to the collision of the Laurasia margin with a continental arc represented by the basement rocks of Sakarya and Strandja zones. The ocean between the Laurasia margin and the Sakarya-Strandja microplate started to close by the Early Devonian, producing a magmatic arc represented by the Çamlık granite in the Sakarya zone (e.g. Okay et al. 2007). The Late Carboniferous collision was followed by the latest Carboniferous-Early Permian plutonism in the centre of the orogen in the Strandja and Sakarya zones (e.g. Deliktaş and Sivrikaya) linked to crustal thickening (e.g. Nzegge et al. 2006). The latest Carboniferous-Early Permian molasse deposition in the Eastern Pontides and the Caucasus marked the end of the Variscan orogeny in northern Turkey. The intra-Pontides suture between the İstanbul and Sakarya zones links up the Late Carboniferous Rheic suture in the central Europe (e.g. Ziegler and Stampfli 2001). The Variscan evolution of northern Turkey

and the Balkans appears to be similar to that of NW Europe, with the Istanbul-Moesian-Scythian Block corresponding to Avalonia, and the Sakarya-Strandja to Armorica (e.g. Stampfli et al. 2002; Okay et al. 2006).

5.5.2. *Precambrian basement*

Evidence for Precambrian basement in the Central Pontides comes from sample BÜ-20, from inherited zircons (U-Pb upper intercept ages) and model Nd ages. Analyses from two DM samples (DG-4a and DM-33) roughly align on a regression line with upper intercept ages between 411 Ma (MSWD= 1.7, Fig. 5.15) and 509 Ma (MSWD= 7.9, Fig. 5.19a) respectively. The latter age is comparable to the concordant age of the oldest group of the abraded zircons (BÜ-20, 502 Ma), which is taken as a tentative estimate for the magmatic formation of these zircons. Most discordant zircons point to upper intercept ages of 1.0 Ga to 2.2 Ga (Figs. 5.10, 5.12, 5.15, 5.18). From the pattern of ages and the contrasting internal morphology of the different basement outcrops zircons, it could be assumed that Late Cambrian-Early Ordovician Büyükçay zircons crystallized in a ~502 Ma magmatic event as part of the widespread subduction-related Cadomian magmatism in the Gondwana-derived terranes (e.g. Linnemann et al. 2000; Nance and Murphy, 1996; Nance et al. 1991), and that recrystallized, originally ~1.0 - 2.2 Ga old zircons suffered Pb loss while being incorporated in the Cadomian magmas at ~502 Ma.

The ~1.0 and 2.2 Ga old xenocrystic zircons fit into the range of inherited and detrital zircon ages known from the Schwarzwald, Bayerischer Wald and Bohemian massif (Todt and Büsch, 1981; Quadt, 1997; Gebauer and Friedl G, 1994; Gebauer et al. 1989; Grauert et al. 1973; Kröner et al. 1988; Dörr et al. 1992, 1998; Wendt et al. 1993; Teipel et al. 2004), from the Hercynian belt of Massif Central, France (Matte, 1998, 2001; Maurel et al. 2002; Pin and Ducrot, ; Paquette et al. 1999), they are also direct evidence of Precambrian in the Eurasian-derived basement of Central Pontides. The Büyükçay metabasics may be related to the wide spread thermal event in Europe, an expression of the Early Palaeozoic continental break-up recorded in the Cadomian basement across the Variscan belt from Spain to the Polish Sudetes (Pin and Martini, 1993 and references therein).

Overall geochemical and isotope signatures [low $\delta^{18}\text{O}$ (~8.4 ‰) and high positive $\epsilon\text{Nd}_{(t)}$ values (2.6 to 6.8), and low and narrow range in initial $^{87}\text{Sr}/^{86}\text{Sr}$ ratios (0.70352 - 0.70445)] indicate a position at an active continental margin, probably with back-arc development, for the Upper-Cambrian-lower Ordovician magmatism. Possible source rocks for the inherited zircons are located at the northern Gondwana margin (e.g. Nance and Murphy, 1996; Söllner et al. 1997), consistent with the Mesoproterozoic inherited zircon ages and Nd model ages

(~1.0 to 1.69 Ga). Upper-Cambrian-lower Ordovician, ~502 Ma zircons are seen as evidence for the wide-spread, subduction-related Cadomian magmatism and are very important for the evolution of the Tethys. *However, additional microprobe, age and CL data is required for further evaluation of the significance of this 502 Ma age cluster!*

The new ages, combined with the overall geochemical variation in the basement samples, indicate the existence of rock assemblages representing both Eurasian and relics of pre-Variscan basement (Gondwana active margin). The recognition of Neoproterozoic (zircon protolith and Nd model ages) and Palaeozoic subduction-related basement rocks and Late Palaeozoic plutonism (DLG and SG) provides additional arguments for the hypothesis that equivalents of Variscan domain are exposed in the Central Pontides. Earlier workers had suggested that the Central Pontides represents a composite tectonic entity that juxtaposes elements of Variscan (\pm pre-Variscan relics) basement, intruded by Upper Palaeozoic and Middle Mesozoic granitoids (Nzegge et al. in review).

REFERENCES

- Adamia SHA, Lordkipanidze, MB and Zakariadze GS, 1977. Evolution of an active Continental margin as exemplified by the Alpine history of the Caucasus. *Tectonophysics* **40**, pp. 183–199.
- Adamia S, Bayraktutan S and Lordkipanidze M, 1995. Structural correlation and Phanerozoic evolution of the Caucasus-Eastern Pontides. *In*: Erler, A., Ercan, T., Bingöl, E. and Orcen, S. (eds) Proceedings of the International Symposium on the Geology of the Black Sea Region. *Mineral Research and Exploration Institute of Turkey (MTA) Publication* pp.

69-75.

Arculus RJ and Johnson RW, 1978. Criticism of generalized models for the magmatic evolution of arc-trench systems. *Earth and Planetary Science Letters* **39**: 118-126.

Aydin M, Şahintürk HS, Serdar Y, Özçelik I, Akarsus A, Üngör R, Çokuğra S, Kasar S, 1986. The Geology of the region between Ballıdağ and Çangaldağı (Kastamonu), Türkiye Jeoloji Kurumu Bull 29:1-16 (in Turkish).

Aydin M, Demir O, Özçelik Y, Terzioğlu N and Satir M, 1995. A geological revision of İnebolu, Devrekani, Aglı and Küre areas: new observations in Palaeotethys-Neotethys sedimentary successions. *In*: Erler A, Ercan T, Bingöl E and Orcen S. (eds.) *Geology of the Black Sea Region. Proceedings of the International Symposium on the Geology of the Black Sea and surrounding region.* AAPG Memoir. **68**, pp. 53-62.

Ayers J, 1998. Trace element modelling of aqueous fluid-peridotite interaction in the mantle wedge of subduction zones. *Contribution to Mineralogy and Petrology* **132**, 390-404.

Banks C and Robinson AG, 1997. Mesozoic strike-slip back-arc basins of the western Black Sea Region. *In*: Robinson, A.G. (ed.) *Regional and Petroleum Geology of the Black Sea and Surrounding Region.* *American Association of Petroleum Geologist Memoir* **68**, pp. 53-62.

Black LP, 1987. Recent Pb loss in zircon: a natural or laboratory-induced phenomenon? *Chemical Geology* **65**: 25-33

Bonhomme MG and Yılmaz O, 1984. First K-Ar data from the Daday-Devrekani and Ilgaz massifs and the Kastamonu granitoids belt, northern Turkey: *Terra Cognita* 4/2:199-200

Boztuğ D, 1992. Lithostratigraphic units and tectonics of the south western part of Daday-Devrekani massive, western Pontides, Turkey. *Mineral Research Exploration Bulletin* **114**:1 22.

Boztuğ D, Debon F, Le Fort P and Yılmaz O, 1984. Geochemical characteristics of some plutons from the Kastamonu granitoids belt (Northern Anatholia, Turkey): *Schweizer Mineralogie und Petrologie Mitteilung* **64/3**: 53-62.

Boztuğ D, Debon F, Le Fort P and Yılmaz O, 1995. High compositional diversity of the Middle Jurassic Kastamonu Plutonic Belt, Northern Anatolia, Turkey: *Turk J Earth Sci* **4/2**: 67-86

Boztuğ D and Yılmaz O, 1991. K-Ar geochronology of fractions from the Göynükdağı contact aureole: A mixed age due to inherited muscovite, Kastamonu N Turkey. *Proceedings of the Mahmut Sayin Clay Symposium.* Çukurova Univ, Adana. 74-86.

Boztuğ D and Yılmaz O, 1995. Metamorphism and geological evolution of the Daday-Devrekani massif, Kastamonu region, Western Pontides, N Turkey. *Geological Bulletin of*

Turkey **38/1**: 33-48.

Bebout GE, 1995. The impact of subduction-zone metamorphism on mantle-ocean chemical cycling, *In*: Staudigel, H., Albarede, F., Hilton, D. and Elliott, T. (eds) *The Mantle-Ocean Connection*. Chemical Geology, Elsevier, Amsterdam. **126**: 191-218.

Boztuğ D, Debon F, Le Fort P and Yılmaz O, 1984. Geochemical characteristics of Some plutons from the Kastamonu granitoid belt (Northern Anatolia, Turkey). *Schweizer Mineralogie und Petrographie Mitteilung* **64**: 389-403.

Boztuğ D, Debon F, Le Fort P and Yılmaz O, 1995. High compositional diversity of the Middle Jurassic Kastamonu plutonic belt (Northern Anatolia, Turkey). *Turkish Journal of Earth Sciences* **4**: 67-86.

Brenan JM, Shaw H.F, Ryerson FJ, Phinney D.L, 1995. Mineral-aqueous fluid partitioning of trace elements at 900°C and 2 GPa: constraints on the trace element chemistry of mantle and deep crustal fluids. *Geochimica et Cosmochimica Acta* **59**: 3331-3350.

Bullen TD and Clyne MA, 1990. Trace element and isotopic constraints on magmatic evolution at Lassen volcanic centre. *Journal of Geophysical Research* **95**: 19671-19691.

Burchfield BC, 1980. Eastern European Alpine system and the Carpathian orocline as an example of collision tectonics. *Tectonophysics* **63**: 31-61.

Cahen L, Snelling NJ, Delhal J, Vail JR, Bonhomme M and Ledendt D, 1984. *The geochronology and evolution of Africa*: Oxford, Clarendon Press pp. 512.

Çapkınoğlu Ş, 2003. First records of conodonts from “the Permo-Carboniferous of the Demirözü (Bayburt), Eastern Pontides, NE Turkey. *Turkish Journal of Earth sciences* **12**: 199-207.

Chappell BW, 1999. Aluminium saturation in I- and S-type granites and the characterization of fractionated haplogranite. *Lithos* **46**, pp. 531-551.

Chappell BW and White AJR, 1974. Two contrasting granite types. *Pacific Geology* **8**: 173-174.

Chappell BW and White AJR, 1987. The importance of residual source material (restite) in granite petrogenesis *Journal of Petrology* **28**: 1111-1138.

Chappell BW and White AJR, 1992. I- and S-type granites in the Lachlan Fold Belt. *Transaction of the Royal Society of Edinburgh, Earth Sciences* **83**: 1-26.

Chatalov GA, 1988 Recent developments in the geology of the Strandzha Zone in Bulgaria. *Bulletin of the Technical University of Istanbul* **41**: 43-465.

Chauvel C, Goldstein SL and Hofman AW 1995. Hydration and dehydration of oceanic crust controls Pb evolution in the mantle. *Chemical Geology* **126**: 65-75.

Chen F, Siebel W and Satir M, 2002a. Zircon U-Pb and Pb-isotope fractionation during

stepwise HF-acid leaching and geochronological implications. *Chemical Geology* 191:153-162.

Chen F, Siebel W, Satir M, Terzioğlu N, Saka K, 2002b. Geochronology of the Karadere basement (NW Turkey) and implications for the geological evolution of the Istanbul Zone: *International Journal of Earth Sciences* **91**: 469-481.

Chen F and Siebel W, 2004. Zircon and titanite geochronology of the Fürstentein granite massif, Bavarian Forest, NW Bohemian Massif: pulses of late Variscan magmatic activity. *European Journal of Mineralogy* **16**: 777-788.

Cherniak DJ, Hanchar JM and Watson EB, 1997. Diffusion of tetravalent cations in zircon. *Contribution in Mineralogy and Petrology* **127**: 383-390.

Cherniak DJ and Watson EB, 2001. Pb diffusion in zircon. *Chemical Geology* 172: 198-207.

Churikova T, Dorendorf F and Wörner G, 2001. Sources and Fluids in the Mantle Wedge below Kamchatka, evidence from across-arc geochemical variation. *Journal of Petrology* **42**: 1567-1593.

Clayton RN and Mayeda TK 1963. The use of bromine pentafluoride in the extraction of oxygen from oxides and silicates for isotopic analyses. *Geochimica et Cosmochimica Acta* **27**: 43-52.

Clemens JD and Vielzeuf D, 1987. Constraints on melting and magma production in the crust. *Earth and Planetary Science Letters* **86**: 287-306.

Cliff RA, 1985. Isotopic dating in metamorphic belts. *Journal Geological Society of London* **142**: 97-110.

Cocherie A, Guerrot C and Rossi PH, 1992. Single-zircons dating by step-wise Pb evaporation: Comparison with other geochronological techniques applied to the Hercynian granites of Corsica, France. *Chemical Geology* **101**: 131-141.

Çoğulu E, Krummenacher D (1967) Problème géochronologiques dans la partie NW de L`Anatolie Centrale, Turquie. *Schweizer Mineralogie und Petrographie Mitteilung* **47**:825-831.

Çoğulu E, Delaloye M and Chessex R, 1965. Sur l`age de quelques roches plutoniques acides dans le région D`Eskişehir, Turquie. *Archives des Sciences, Genève* **18**: 692-699.

Cohen AS, O`Nions RK and O`Hara MJ, 1991. Chronology and mechanism of depletion in Lewisian granulites. *Contribution to Mineralogy Petrology* **117**: 421-434.

Condie KC, 1993. Chemical composition and evolution of the upper continental crust: contrasting results from surface samples and shales. *Chemical Geology* **104**: 1-37.

Corfu F (2000) Extraction of Pb with artificially too-old ages during stepwise dissolution experiments on Archean zircon. *Lithos* **53**: 279-291.

Corfu F, Hanchar JM, Hoskin PWO and Kinny P 2003. Atlas of Zircon textures. In: Hanchar

- JM, Hoskin PWO (Eds) ZIRCON. *Reviews in Mineralogy and Geochemistry* **53**: 27-55.
- Corfu F and Davis DW, 1991. Comments on “Archean hydrothermal zircon in the Abitibi greenstone belt: constraints on the timing of gold mineralization” by Claoué-Long JC, King RW and Kerrich R. *Earth and Planetary Sciences Letters* **104**: 545-552.
- Davis DW and Krogh TE, 2000. Preferential dissolution of ^{234}U and radiometric Pb from a-recoil-damaged lattice sites in zircon: implications for thermal histories and Pb isotopic fractionation in the near surface environment. *Chemical Geology* **172**: 41-58.
- Davies JH and Von Blanckenburg F, 1995. Slab breakoff: A model of lithosphere detachment and its test in the magmatism and deformation of collisional orogens. *Earth and Planetary Science Letters* **129**: 85-102.
- Defant, M.J. and Drummond, M.S., 1990. Derivation of some modern arc magmas by melting of young subducted lithosphere. *Nature* **347**: 662-665.
- Delaloye M and Bingöl E, 2000. Granitoids from western and north-western Anatolia: Geochemistry and modelling of geodynamic evolution. *International Geological Reviews* **42**: 241-268.
- De La Roche H, Leterrier J, Grandeclaude P and Marshal M, 1980. A classification of volcanic and plutonic rocks using R1-R2-diagrams and major elements analyses- its relationships with current nomenclature. *Chemical Geology* **29**: 183-210.
- DePaolo DJ and Daley EE, 2000. Neodymium isotopes in basalts of the southwest basin and range and lithospheric thinning during continental extension. *Chemical Geology* **169**: 157–185.
- Dercourt J, Zonenshain LP, Ricou LE, Kazmin VG, Le Pichon X, Knipper AL, Grandjacquet C, Sbortshikov IM, Geysant J, Lepvrier C, Pechersky DH, Boulin J, Sibuet JC, Savostin LA, Westphal M, Basenov ML, Lauer JP and Biji-Duval B, 1986. Geological evolution of the Tethys belt from the Atlantic to the Pamirs since the Lias. *Tectonophysics* **123**: 241-315.
- Dercourt J, Zonenshain LP, Ricou LE and Vrielynck B, 1993. Atlas of Tethys Palaeo-environmental Maps. Gauthier-Villars, Paris.
- Dewey JF, 1988. Extensional collapse of orogens. *Tectonics* **6**: 1123-1139.
- Dewey JF and Burke KCA, 1973. Tibetan, Variscan, and Precambrian basement and reactivation: Products of continental collision. *Journal of Geology* **81**: 683-692.
- Dewey JF and Windley B, 1981. Growth and differentiation of the continental crust. *Philosophical Transactions of the Royal Society of London* **A301**: 105-123.
- Dewey JF, Shackleton RM, Chang CF and Sun YY, 1988. The tectonic evolution of the Tibetan plateau. *Philosophical Transactions of the Royal Society of London* **A327**: 379-413.

- Dewey JF, Helman ML, Turco E, Hutton DHW and Knott SD, 1989. Kinematics of the western Mediterranean. In: Coward MP, Dietrich D and Park RG. (eds) *Alpine Tectonics*, Geological Society, Special Publication **45**: 265-283.
- Dixon JE and Robertson AHF, 1999. Are multiple plumes implicated in the Triassic break-up of the Gondwana margin in the Eastern Mediterranean region? *J Conference Abs* 4: 314.
- Dörr WE, Zulauf G, Fiala J, Franke W and Vejnar Z, 2002. Neoproterozoic to Early Cambrian history of an active plate margin in the Teplá-Bohemian unit—a correlation of U-Pb isotopic-dilution-TIMS ages (Bohemia, Czech Republic) *Tectonophysics* 352: 65-85.
- Dorendorf F, Wiechert U and Wörner G, 2000. Hydrated sub-arc mantle: a source for the Kluchevskoy volcano, Kamchatka/Russia. *Earth and Planetary Science Letters* **175**: 69-86.
- Dostal J, Baragar WRA and Dupuy C, 1986. Petrogenesis of the Natkusiak continental basalts, Victoria Island, NWT. *Journal of Canadian Earth Sciences* **23**: 622-632.
- Dostal J, Dupuy C and Caby R, 1994. Geochemistry of the Neo-Proterozoic Tilemsi Belt of Iforas (Mali, Sahara): a crustal section of an oceanic island arc. *Precambrian Research* **65**: 55-59.
- Drummond MS and Defant MJ, 1990. A model for trondhjemite-tonalite-dacite genesis and crustal growth via slab melting: Archean to modern comparisons. *Journal of Geophysical Research* **95**: 21503-21521.
- Ellis DJ and Thompson AB, 1986. Solidus and partial melting reactions in the quartz-excess CaO+MgO+Al₂O₃+SiO₂+H₂O system under water-excess and water-deficient conditions to 10kb: some implications for the origin of peraluminous melts from mafic rocks. *Journal of Petrology* **27**: 91-121.
- Eren Y, 2001. Polyphase Alpine deformation at the northern edge of the Menderes-Taurus block, North Konya, Central Turkey. *Journal of Asian Earth Sciences* **19**: 737-749.
- Evans Y, Sarıbudak MA and Aykol A, 1991. Preliminary palaeomagnetic results from Palaeozoic rocks of the Istanbul-Zonguldak region, NW Turkey. *Bulletin of the Technical University of Istanbul* **44**: 165-190.
- Finger F and Clemens JD, 1995. Migmatization and secondary granite magmas: effects of emplacement and crystallization of “primary” granitoids in Southern Bohemia, Austria. *Contribution to Mineralogy and Petrology* **120**: 311-326.
- Floyd PA and Winchester JA, 1975. Magma type and tectonic setting discrimination using immobile elements. *Earth and Planetary Science Letters* **27**: 211-218.
- Franke W, 2001. The mid-European segment of the Variscides: tectono-stratigraphic units, terranes boundaries and plate tectonic evolution *J Geol Soc London* **197**: 35-61.
- Franke W, 1995. Stratigraphy. In: Dallmeyer RD, Franke W and Weber K. (Eds) *Pre-Permian*

- geology of Central and Eastern Europe. Springer Berlin 33-49.
- Franke W, Dallmeyer RD and Weber K, 1995. Geodynamic evolution. In: Dallmeyer R D, Franke W and Weber K (Eds) Pre-Permian geology of Central and Eastern Europe. Springer Berlin pp.579-593.
- Garfunkel Z. 1998. Constrains on the origin and history of the Eastern Mediterranean basin. *Tectonophysics* **298**: 5-35.
- Gebauer D and Grunenfelder M (1979a) U-Th-Pb dating of minerals. In: Lectures in Isotope Geology (Ed. Jäger and Hunziker), Springer, pp. 105-131.
- Gebauer D and Grunenfelder M (1979b) U -Pb zircon and Rb-Sr mineral dating of eclogites and their country rocks. Example: Münchberger Gneiss Massif. Northeastern Bavaria. *Earth Planetary Science Letters* **42**: 35-44.
- Gebauer D, Schertl HP, Brix M and Schreyer W, 1997. 35 Ma old ultra high-pressure metamorphism and evidence for very rapid exhumation in Dora Maira Massif Western Alps. *Lithos* **41**: 5-24.
- Gebauer D and Friedl G, 1994. 1.38 Ga protolith age from the Dobra orthogneiss (Moldanubian zone of southern Bohemian Massif, NE Austria): evidence from ion-microprobe (SHRIMP) dating of zircon. *Journal of the Czech Geological Society* **39**: 34-35.
- Gebauer D, Williams IS, Compton W and Grünenfelder M, 1989. the development of the Central European continental crust since the Early Archean based on conventional and ion-microprobe dating of up to 3.84 Ga old detrital zircons. *Tectonophysics* **157**: 81-96.
- Gehmlich M, 2003. Die Cadomiden und Varisziden des Saxo-Thurigischen Terranes. *Geochronologie magmatischer Ereignisse. Freiburger Forschungshefte C500*, pp. 129.
- Geisler T, Pidgeon RT, Van Bronswijk W and Kurtz R, 2002. Transport of U, Th and Pb in metamict zircon under low temperature hydrothermal conditions.
- Ghosh DK and Lambert RSt.J, 1989. Nd-Sr isotopic study of Proterozoic to Triassic sediments from southeastern British Columbia. *Earth and Planetary Science Letters* **94**: 29-44.
- Görür N, Monod O, Okay AI, Sengör AMC, Tüysüz O, Yiğibaş E, Sakıncı M and Akkök R, 1997. Palaeogeographic and tectonic position of the Carboniferous rocks of the Western Pontides (Turkey) in the frame of the Variscan belt. *Bulletin de Société Géologique la France* **168**: 197-205.
- Grauert B, Hännly R, and Soptrajanova M, 1973. Age and origin of detrital zircons from the pre-Permian basement of the Bohemian Massif and the Alps. *Contribution in Mineralogy and Petrology* **40**: 105-130.
- Gromet LP and Silver LT (1983) Rare earth element distributions among minerals in a granodiorite and their petrogenetic implications. *Geochimica Cosmochimica Acta* **47**:925-939.

- Gulson BL and Krogh TT, 1973. Old lead components in the young Bergell Massif, south-east Swiss Alps. *Contribution to Mineralogy and Petrology* **40**: 239-252.
- Haas W, 1968. Das Alt-Paläozoikum von Bithynien (Nordwest Türkei). *Neues Jahrbuch für Geologie und Paläontologie, Abhandlungen* **131**: 178-242.
- Halliday AN, Stephens WE, Hunter RH, Menzies MA, Dickin AP and Hamilton PJ, 1985. Isotopic and geochemical constraints on the building of the deep Scottish lithosphere. *Scottish Journal of Geology* **21**:465-491.
- Hanchar JM and Miller CF, 1993. Zircon zonation patterns as revealed by Cathodoluminescence and back-scattered electron images: implication for interpretation of complex crustal histories. *Chemical Geology* **110**: 1-13.
- Hanchar JM and Rudnick RL, 1995. Revealing hidden structures: application to CL and BSE imaging to dating zircons from lower crustal xenoliths. *Lithos* **36**: 289-303.
- Hanchar JM , Finch RJ, Hoskin PWO, Watson EB Chernaik DJ and Mariano AN, 2001. Rare elements in synthetic, and zircon: Part I. Synthesis, and rare-earth element and phosphorous doping of zircon. *American Mineralogy* **86**:667-680.
- Hanchar JM and Watson EB (2003) Zircon saturation thermometry. In: Hanchar JM and Hoskin PWO (Eds.), *ZIRCON. Reviews in mineralogy and geochemistry* **53**: 27-55.
- Harrison TM and Watson EB (1983). Kinetics of zircon dissolution patterns and zirconium diffusion in granitic melts of variable water content. *Contribution to Mineralogy and Petrology* **84**:66-72.
- Harrison TM and Watson EB (1984) The behaviour of apatite during crustal anatexis: equilibrium and kinetic considerations. *Geochimica Cosmochimica Acta* **49**: 2461-2468.
- Harris NBW, Pearce JA and Tindle AG, 1986. Geochemical characteristics of collision- zone magmatism. *In: Collision Tectonics*. Coward MP and Ries AC (eds.) Geological Society of London **19**: 67-81.
- Hawkesworth CJ, Norry MJ, Roddick JC and Baker PE (1979) $^{143}\text{Nd}/^{144}\text{Nd}$, $^{87}\text{Sr}/^{86}\text{Sr}$ and incompatible element variations in calc-alkaline andesites and plateau lavas from South America. *Earth Planetary Science Letters* **42**: 45-57.
- Hawkesworth CJ, Kempton PD, Rogers NW, Ellam R and Van Calsteren P, 1990. Continental mantle lithosphere and shallow level enrichment processes in the Earth's mantle. *Earth and Planetary Science Letters* **96**: 256-268.
- Hegner E, Roddick J, Fortier SM and Hulbert L, 1995. Nd, Sr, Pb, Ar, and O Isotopic Systematics of Sturgeon Lake Kimberlite Saskatchewan, Canada: constraints on emplacement age alteration and source composition. *Contribution Mineralogy Petrology* **120**: 212-222.

- Hegner E and Kröner A, 2001. Review of Nd isotopic data and xenocrystic and detrital zircon ages from pre-Variscan basement in the eastern Bohemian Massif: speculations on palinspastic reconstructions. *In: Franke W, Haal V, Oncken O and Tanner D (Eds.) Orogenic processes: Qualification and Modelling in the Variscan Belt. Geol Soc London Spec Publ* **179**: 113-129.
- Henk A, Von Blanckenburg F, Finger F, Schaltegger U and Zulauf G, 2000. Syn-convergent high-temperature metamorphism and magmatism in the Variscides: a discussion of potential heat sources. *Geological Society of London Special Publications* **179**: 387-399.
- Hoffman AW, 1988. Chemical differentiation of the Earth: The relationship between mantle, continental crust, and the oceanic crust. *Earth and Planetary Science Letters* **90**: 297-314.
- Hofmann A and Köhler H (1973) Whole-rock Rb-Sr ages of anatectic gneisses from the Schwarzwald, SW Germany. *Neues Jahrb Mineral* **119**:163-187.
- Hoskin PWO, 2000. Patterns of chaos: Fractal statistics and the oscillatory chemistry of zircon. *Geochimica Cosmochimica Acta* **64**: 1905-1923.
- Hoskin PWO and Black LP, 2000. Metamorphic zircon formation by solid-state recrystallization of protolith igneous zircon. *Journal of Metamorphic Geology* **18**: 423-439.
- Hoskin PWO and Schaltegger U, 2003. The Composition of Zircon and Igneous and Metamorphic Petrogenesis. *In: Hanchar JM and Hoskin PWO (Eds.), ZIRCON. Reviews in mineralogy and geochemistry* **53**: 27-55.
- Hoskin PWO, Kinny PD, Wyborn D and Chappell BW. 2000. Identifying accessory mineral saturation during differentiation in granitoid magmas: an integrated approach. *Journal of Petrology* **41**: 1365-1395.
- Irvine TN and Baragar WRA, 1971. A guide to the chemical classification of common volcanic rocks. *Canadian Journal of Earth Sciences* **8**: 523-548.
- Kalvoda J, 2003. Carboniferous foraminiferal paleobiogeography in Turkey and its implication for plate tectonic reconstructions. *Rivista Italiana Paleontologia Stratigrafia* **109**: 255-266.
- Kalvoda J, Leichmann J, Babek O and Melichar R 2003. Brunovistulian Terrane (Central Europe) and Istanbul Zone (NW Turkey): Late Proterozoic and Palaeozoic tectonostratigraphic development and paleogeography. *Geologica Carpathica* **54**: 139-152.
- Kapenda D, Kampunzu AB, Cabanis B, Namegabe M, Tshimanga K, 1998. Petrology and geochemistry of post-kinematic mafic rocks from the Palaeoproterozoic Ubendian belt, NE Katanga (Democratic Republic of Congo). *Geologisches Rundschau* **87**: 345-362.
- Kay SM, Ramos VA and Marquez M, 1993. Evidence in Cerro Pampa volcanics for slab melting prior to ridge-trench collision in Southern South America. *Journal of Geology* **101**:

703-714.

Kelemen BP, 1995. Genesis of high Mg andesites and the continental crust. *Contribution to Mineralogy and Petrology* **120**: 1-19.

Kempe U, Gruner T, Nasdala L and Wolf D, 2000. Relevance of cathodoluminescence for the interpretation of U-Pb zircon ages, with example of an application to a study of zircons from the Saxonian Granulite Complex, Norway. In: *Cathodoluminescence in Geosciences*. Pagel M, Barbin V, Blanc P, Ohnenstetter D (Eds.), Springer Berlin, pp.415-455.

Kepezhinskas PK, Defant MJ and Drummond MS, 1996. Progressive enrichment of island arc mantle by melt-peridotite interaction inferred from Kamchatka xenoliths. *Geochimica et Cosmochimica Acta* **60**: 1217-1229.

Kepler H, 1996. Constraints from partitioning experiments on the composition of subduction -zone fluids. *Nature* **380**: 237-239.

Ketin I, 1966. Tectonic units of Anatholian Asia Minor. *MTA Bulletin* **66**: 20-34.

Khain VE, 1975. structure and main stages in the tecton-magmatic development of the Caucasus: An attempt at geodynamic interpretation. *American journal of Science* **275-A**: 131-156.

Kober B, 1986. Whole-grain evaporation for $^{207}\text{Pb}/^{206}\text{Pb}$ -age investigations on single zircons using a double-filament ion source. *Contribution to Mineralogy and Petrology* **93**: 482-490.

Kober B, 1987. Single-zircon evaporation combined with Pb^+ emitter-bedding for $^{207}\text{Pb}/^{206}\text{Pb}$ -age investigations using thermal ion mass spectrometry, and implications to zirconology. *Contribution to Mineralogy and Petrology* **96**: 63-71.

Koçyiğit A, 1991 An example of an accretionary fore-arc basin from northern central Anatolia and its implications for the history of subduction of Neo-Tethys in Turkey. *Bull Geological Society of America* **103**: 22-36.

Koschek G, 1993. Origin and significance of the SEM cathodoluminescence for zircon. *Journal of Micros* **171**:223-232.

Krogh TE, 1973. A low contamination method for hydrothermal decomposition of zircon and extraction of U-Pb for isotopic age determination. *Geochimica et Cosmochimica Acta* **37**: 637-649.

Krogh TE, 1982. Improved accuracy of U-Pb zircon ages by the creation of more concordant samples using air abrasion technique. *Geochimica et Cosmochimica Acta* **46**: 637-649.

Krogh TE, 1993. High precision U-Pb ages for granulite metamorphism and deformation in the Archean Kapuskasigm structural zone, Ontario: implication for structure and development of the lower crust. *Earth and Planetary Science Letters* **119**: 1-18.

- Kröner A, Wendt I, Liew TC, Compton W, Todt W, Fiala J, Vankova V and Vanek J, 1988. U-Pb zircon and Sm-Nd model ages of high-grade Moldanubian metasediments, Bohemian Massif, Czechoslovakia. *Contrib Mineral Petrol* **132**: 1-20.
- Kröner A, Jaeckel P and Williams IS, 1994. Pb-loss patterns in zircons from a high-grade metamorphic terrain as revealed by different dating methods: U-Pb and Pb-Pb ages for igneous and metamorphic zircons from northern Sri Lanka. *Precambrian Research* **66**: 151-181.
- Kröner A, Willner AP, Hegner E, Frischbutter A Hofmann J and Bergner R, 1995. Latest Precambrian (Cadomian) zircon ages, Nd isotopic systematics and P-T evolution of granulite orthogneisses of the Erzgebirge, Saxony and Czech Republic. *Geol Rundsch* **84**: 437-456.
- Kröner A, Jaeckel P, Reischmann T and Kroner U, 1998. Further evidence for an Early Carboniferous (~340Ma) age of high-grade metamorphism in the Saxonian Granulite Complex. *Geologisches Rundschau* **86**:751-766.
- Langer C, Hegner E, Altherr R; Satir M and Henjes-Kunst F, 1995. Carboniferous granulites from the Odenwald, the Schwarzwald and the Vosges: constraints on mantle and crustal sources. *Terra Nostra* **95**: 114.
- Larsen LH and Poldervaart A, 1957. Measurement and distribution of zircon in some granitic rocks of magmatic origin. *Mineralogical Magazine* **31**: 544-564.
- Latouche L, Fabriès J and Guiraud M, 1992. Retrograde evolution in the Central Vosges mountain (northeastern France: implications for metamorphic history of high-grade rocks during the Variscan orogeny. *Tectonophysics* **205**: 387-407.
- Lee JKW, Williams IS and Ellis DJ, 1997. Pb, U and Th diffusion in natural zircon. *Nature* **390**: 159-161.
- Le Maitre, R., 1989. *A Classification of igneous Rocks and Glossary of Terms*, Blackwell, Oxford 193 pp.
- Liew TC and Hofmann AW, 1988. Precambrian crustal components, plutonic associations, plate environment of the Hercynian Fold Belt of Central Europe: indication from a Nd and Sr isotopic study. *Contributions Mineralogy and Petrology* **98**: 129-138.
- Liew TC, Finger F and Höck V, 1989. The Moldanubian plutons of Austria: Chemical and isotopic studies bearing on their environmental setting. *Chemical Geology* **76**: 41-55.
- Linnemann U, Gehmlich M, Tichomirowa M, Buschmann B, Nasdala L, Jonas P, Lützner H and Bombach K, 2000. From Cadomian subduction to Early Palaeozoic rifting: the evolution of Saxo-Thuringia at the margin of Gondwana in light of single zircon geochronology and basin development (Central European Variscides, Germany). *In*: Franke W, Haak V, Oncken

- O and Tanner D. (Eds.) Orogenic processes: Quantification and modelling in the Variscan Belt. Geological Society of London Special Publication **179**: 131-153.
- Longerich HP, Jenner GA, Jackson SE and Fryer BJ, 1990. ICP-MS- a powerful new tool for high precision trace element analysis in earth sciences: evidence from analysis of selected USGS standards. *Chemical Geology* **83**: 133-148.
- Ludwig KR, 1994. A plotting and regression program for radiogenic-isotope data. A revision of the Open File Report, USGS, 91-445: 1-45.
- Ludwig KR, 2000. Users manual for Isoplot/ex rev. 2.49: a geochronological toolkit for Microsoft Excel. Berkeley Geochronology Center Special Publication **1a**: 1-56.
- Machado A, Chemale F Jr., Conceição RV, Kawaskita K, Morata D, Otezia O and Schmus WRV, 2005. Modelling of subduction component in the genesis of the Meso-Cenozoic igneous rocks from the South Shetland Arc, Antarctica. *Lithos* **82**: 435-453.
- Maniar PD and Piccolli PM, 1989. Tectonic discrimination of granitoids. *Bulletin of the American Geological Society* **101**: 133-148.
- Martin H, 1999. Adakitic magmas: modern analogues of Achaean granitoids. *Lithos* **46**: 411-429.
- Martin H, Smithies RH, Rapp R, Moyen J-F and Champion D, 2005. An overview of adakite, tonalite-trondhjemite-granodiorite (TTG) and sanukitoid: relationships and some implications for crustal evolution. *Lithos* **79**: 1-24.
- Matte P, 1986. Tectonics and plate model for the Variscan belt of Europe. *Tectonophysics* **126**: 329-374.
- Matte P, 1991. Accretionary history and crustal evolution of the Variscan belt in western Europe *Tectonophysics* **196**: 309-339.
- Matte P, 1998. Continental subduction and exhumation of HP rocks in Palaeozoic belts: Uralides and Variscides: Special Issue Tectonics and General History of Phanerozoic orogens. *Geol Soc Sweden* **120**: 209-222.
- Matte P, 2001. The Variscan collage and orogeny (480-290 Ma) and the tectonic definition of the American Microplate: a review. *Terra Nova* **13**: 122-128.
- Mattinson JM, Graubard CM, Parkinson DL and McClelland WC, 1996. U-Pb reverse discordance in zircons: the role of fine-scale oscillatory zoning and sub-micron transport of Pb. *American Geophysics Union Monograph* **95**: 355-370.
- Maurel O, Monié P, Respaut JP, Leyreloup AF and Maluski H, 2002. U-Pb ages in HP metagranitoids from the Hercynian belt (France) *Chem. Geol* **189**: 57-67.
- McKenzie D and Bickle MJ, 1988. The volume and composition of melt generated by Extension of the lithosphere. *Journal of Petrology* **29**: 625-679.

- McDonough WF and Sun SS, 1995. The composition of the Earth. *Chemical Geology* **120**: 223-253.
- McKenzie D and Bickle MJ, 1988. The volume and composition of melt generated by extension of the lithosphere. *Journal of Petrology* **29**: 625-679.
- McKenzie D and O'Nions RK, 1983. Mantle reservoirs and oceanic island basalts, *Nature*, **301**: 229-231.
- Meen JK and Eggler DH (1987) Petrology and geochemistry of the Cretaceous Independence volcanic suite, Absaroka Mountains, Montana: clues to the composition of the Archean sub-Montanian mantle. *Geological Society of America Bulletin* **98**: 238-247
- Mezger K and Krogstad EJ, 1997. Interpretation of discordant U-Pb zircon ages: an evaluation. *Journal of Metamorphic Geology* **15**: 127-140.
- Nance RD and Murphy JB, 1996. Basement isotopic signature and Neoproterozoic Palaeogeography of Avalonia-Cadomian and related terranes in the circum-Northern Atlantic. *Geol Soc Am Spec Paper* **304**: 333-346.
- Nance RD, Murphy JB, Strahan RA, D'Lemos RS and Taylor GK, 1991. Late Proterozoic tectonostratigraphic evolution of the Avalonia and Cadomian terranes. *Precambrian Res* **53**: 41-78.
- Nasdala L, Pidgeon RT and Wolf D, 1996. Heterogeneous metamictization of zircon on a microscale. *Geochimica et Cosmochimica Acta* **60**: 1091-1097.
- Nzegge OM, Satir M, Siebel W and Terzioğlu N, 2002. Are all the plutons of the Kastamonu Granitoid Belt, Central Pontides-NW Turkey of Middle Jurassic age? Genesis and geochronology of the Sivrikaya Complex. *European Journal of Mineralogy Abstracts* **14/1**: 120.
- Nzegge OM, Satir M, Siebel W and Boztuğ D, 2006. Late Palaeozoic-Mesozoic magmatism in the Kastamonu granitoid belt, Central Pontides-NW Turkey and regional geological implications. *Geophysical Research Abstracts* **8**: EGU2006-A-07523.
- Nzegge OM, Satir M, Siebel W and Taubald H, 2006. Geochemical and isotopic constraints on the genesis of the Late Palaeozoic Deliktaş and Sivrikaya granites from the Kastamonu granitoid belt (Central Pontides, Turkey). *Neues Jahrbuch für Mineralogie* **183**: 27-40.
- Nzegge OM, Satir M, Boztuğ D and Taubald H, 2007. Zircon ages, geochemistry and isotope systematics of the extension-related Devrekani intrusion, Kastamonu granitoid belt (Central Pontides, Turkey), and geodynamic interpretation. *Geophysical Research Abstracts* **9**: EGU2007-A-08507.

- Nzegge OM and Satir M, 2007. Geochemistry and geochronology of the Eurasian-derived basement of the Central Pontides, Turkey. *Geophysical Research Abstracts* **9**: EGU2007-A-08626.
- Nzegge OM, Boztuğ D and Satir M (accepted). Late Variscan Sivrikaya and Deliktaş plutons from the Kastamonu granitoid belt generated in a Palaeotethyan convergence system (Central Pontides, Turkey). *International Journal of Earth Sciences*.
- Nzegge OM, Boztuğ D and Satir M (accepted). Zircon ages, geochemistry and isotope systematics of Devrekani granitoid from the Kastamonu granitoid belt (Central Pontides, Turkey), and geodynamic interpretation. *Journal of Asian Earth Sciences*.
- Okay AI, 1989. Tectonic units and sutures in the Pontides, Northern Turkey. In: Şengör AMC (Ed) *Tectonic evolution of the Tethyan Region*. NATO Advance Science Institute (ASI) series **C259**: 109-113, Dordrecht-Kluwer.
- Okay AI, 2000. Was the Late Triassic orogeny in Turkey caused by the collision of an oceanic plateau? In: Bozkurt B, Winchester JA and Piper JDA (Eds.), *Tectonics and Magmatism in Turkey and the Surrounding Area*. Special Publication of the Geological Society of London **173**: 25-42.
- Okay AI and Leven EJa, 1996. Stratigraphy and palaeontology of the Upper Palaeozoic sequence in the Pulur (Bayburt) region, Eastern Pontides. *Turkish Journal of Earth Sciences* **5**: 145-155.
- Okay AI and Şahintürk HS (1997) *Geology of the Eastern Pontides*. In: Robertson A (Ed) *Regional and Petroleum Geology of the Black Sea and Surrounding Region*. AAPG Memoir **68**: 291-311.
- Okay AI and Tüysüz O, 1999. Tethyan sutures of northern Turkey. In: Duran B, Jolivet L, Hortháth F and Séranne M. (Eds) *The Mediterranean basins: tertiary extension within the Alpine orogen*. Geological Society of London, Special Publication **156**: 475-515.
- Okay AI and Şengör AMC, Görür N, 1994. Kinematic history of the opening of the Black Sea and its effects on the surrounding regions. *Geology* **22**: 267-270.
- Okay AI, Siyako M and Burkan KA, 1991. Geology and Tectonic Evolution of the Biga Peninsula, northwest Turkey. Special Issue on Tectonics, *Bulletin of the Technical University of Istanbul* **44**: 191-256.
- Okay AI, Satir M, Maluski H, Siyako M, Monie P, Metzger R and Akyu ZS, 1996. Palaeo- and Neo-Tethyan events in northwestern Turkey: geologic and geochronologic constraints. In: Yin A and Harrison M. (Eds) *Tectonics of Asia*. Cambridge University Press 420-441.
- Okay AI and Göncüoğlu MC, 2004. Karakaya Complex: a review of data and concepts. *Turkish Journal of Earth Sciences* **13**: 77-95.

- Okay AI, Satir M, Tüysüz O, Akyüz S and Chen F, 2001. The tectonics of the Strandja Massif: Variscan and mid-Mesozoic deformation and metamorphism in the northern Aegean. *International Journal of Earth Sciences* **90**: 217-233.
- Okay AI, Monod O and Monie P, 2002. Triassic blueschists and eclogites from northwest Turkey: vestiges of the Paleotethyan subduction. *Lithos* **64**: 155-178
- Okay AI, Satir M and Siebel W. 2007, Pre-Alpides Palaeozoic and Mesozoic events in the Eastern Mediterranean region. *European Lithosphere Dynamics*. (Eds) Gee DG and Stephenson, R. Geological Society of London Memoir.
- Okay AI, Tüysüz O, Satir M, Özkan-Altıner S, Altıner D, Sherlock S and Eren R, 2006. Cretaceous and Triassic subduction-accretion of HP-LT metamorphism, and continental growth in the Central Pontides, Turkey. *Bulletin of the Geological Society of America*. **25938**: 1-23.
- Ono A, 1976. Chemistry and zoning of zircon from some Japanese granitic rocks. *Journal of Japanese Association of Mineralogy, Petrology and Economic Geology* **71**:6-17.
- Paquette JL, Peucat JJ, Bernard-Griffiths J and Marchand J, 1985. Evidence for Precambrian relics shown by U-Pb zircon dating of eclogites and associates rocks in the Hercynian belt of south Brittany, France. *Chemical Geology* **52**: 203-216.
- Parrish RR, 1987. An improved microcapsule for zircon dissolution in U-Pb geochronology. *Chemical Geology* **66**: 99-102.
- Patiño Douce AE, 1996. Effects of Pressure and H₂O contents on the composition of primary crustal melts. *Transactions of the Royal Society of Edinburgh, Earth Sciences* **87**: 11-21.
- Patiño Douce AE, 1995. Experimental generation of hybrid silicic melts by reaction of high-Al basalt with metamorphic rocks. *Journal of Geophysical Research* **100**: 15623-15639.
- Patiño Douce AE, 1999. What do experiments tell us about the relative contributions of crust and mantle to the origin of granitic magmas? *In*: Castro A, Fernandez, C. and Vigneresse JL (Eds). *Understanding granites: integrating new and classical techniques*. Geological Society of London, Special Publication **168**: 55-57.
- Patiño Douce AE and Beard JS, 1995. Dehydration melting of biotite gneiss and quartz amphibolite from 3 to 5 kbar. *Journal of Petrology* **36**: 707-738.
- Patiño Douce AE and Johnston AD , (1991): Phase equilibria and melt productivity in the pelitic system: implications for the origin of peraluminous granitoids and aluminous granulites. *Contribution to Mineralogy and Petrology* **107**: 202-218.
- Pearce JA, Harris NB and Tindle AG, 1984. Trace element discrimination diagrams for the tectonic interpretation of granitic rocks. *Journal of Petrology* **25**: 956-983.
- Pearce JA, Bender JF, De Long SE, Kidd WSF, Low PJ, Güner Y, Şaroğlu F, Yılmaz Y,

- Moorbath S and Mitchell JG, 1990. Genesis of collision volcanism in eastern Anatolia, Turkey. *Journal of Volcanology and Geothermal Research* **44**: 189-229.
- Pearce JA and Parkinson IJ, 1993. Trace elements models for mantle melting: application to volcanic arc petrogenesis. In: Prichard HM, Alabaster T, Harris NB and Neary CR. (Eds) *Magmatic Processes and Plate Tectonics*. Geological Society of London, Special Publication **76**: 373-403.
- Peccerillo A and Taylor SR, 1976. Geochemistry of Eocene calc-alkaline volcanic rocks from the Kastamonu area, northern Turkey. *Contribution to Mineralogy and Petrology* **58**: 63-81.
- Pharaoh TC, 1999. Palaeozoic terranes and their lithospheric boundaries within the trans-European Suture Zone (TESZ): a review. *Tectonophysics* **314**: 17-41.
- Pitcher WS, 1982. Granite types and tectonic environment. In Hsü k.J: *Mountain building processes*. Academic Press, 19-40.
- Pitcher WS, Atherton MP, Cobbing EJ and Beckinsale RD, 1985. *Magmatism at a plate edge-the Peruvian Andes*: Glasgow, UK, Blackie and son 329pp.
- Poldervaart A, 1955. Zircon in rocks. 1. Sedimentary rocks. *American Journal of Science* **253**: 433-461.
- Pickett EA and Robertson AHF, 1996. Formation of the Late Palaeozoic-Early Mesozoic Karakaya Complex and related ophiolites in NW Turkey by Palaeotethyan subduction-accretion. *Journal of Geological Society of London* **153**: 995-1009.
- Pidgeon RT, 1992. Recrystallization of oscillatory zoned zircon: some geochronological and petrological implications. *Contribution to Mineralogy and Petrology* **110**:463-472.
- Pidgeon RT, Nemchin AA and Hitchen GJ, 1998. Internal structures of zircons from Archean granites from the Darling Range batholith: implications for zircon stability and interpretation of zircon U-Pb ages. *Contribution to Mineralogy and Petrology* **132**: 288-299.
- Piper JDA, Gürsoy H, Tatar O, İşseven T and Kocyiğit A, 2002. Palaeomagnetic evidence for the Gondwanan origin of the Taurides and rotation of the Isparta Angle, southern Turkey. *Geological Journal* **37**:317-336.
- Plank T and Langmuir CH, 1993. Tracing trace elements from sediments input to volcanic output at subduction zones. *Nature* **362**: 739-743.
- Platt JP and England PC, 1993. Convection removal of lithosphere beneath mountain belts: thermal and mechanical consequences. *American Journal of Science* **293**: 307-336.
- Poitrasson F, Hanchar JM, Poitrasson F and Schaltegger U, 2002. The current state and future of accessory mineral research. *Chemical Geology* **191**: 3-24.

- Poller U, Liebetrau V and Todt W, 1997. U-Pb single-zircon dating under cathodoluminescence control (CLC-method: application to polymetamorphic orthogneisses. *Chemical Geology* **139**: 287-297.
- Poldervaart A, 1956. Zircon in rocks, 2. Igneous rocks. *American Journal of Science* **254**: 521-551.
- Prouteau G, Scaillet B, Pichavant M and Maury R, 2001. Evidence for mantle metasomatism by hydrous silicic melts derived from subducted oceanic crust. *Nature* **410**: 197-200.
- Pupin JP, 1980. Zircon and granite petrology. *Contribution to Mineralogy and Petrology* **73**:207-220.
- Rapp PP and Watson EB, 1995. Dehydration of metabasalt at 8-32 kbar: implication for continental growth and crust-mantle recycling. *Journal of Petrology* **36**: 891-931.
- Rapp PP, Shimizu N, Norman MD and Applegate GS, 1999. Reaction between slab-derived melts and peridotite in the mantle wedge: experimental constraints at 3.8 Gpa. *Chemical Geology* **160**: 335-356.
- Robertson AHF and Dixon JE, 1984. Introduction: aspects of the geological evolution of the Eastern Mediterranean. *In: Dixon, J.E. and Robertson A.H.F. (eds) The Geological Evolution of the Eastern Mediterranean. Geological Society of London Special Publication* **17**: 1-74.
- Robertson AHF, Pickett E, Brown S, Collins A, Morris A, Sharp I. and Ustaömer T, 1996. Alternative tectonic models for the Late Palaeozoic-Early Tertiary development of Tethys in the Eastern Mediterranean region. *In: Morris A and Tarling DH. (Eds) Palaeomagnetism and Tectonics of the Mediterranean Region. Geological Society of London Special Publication* **05**: 239-263.
- Robertson AHF and Pickett EA, 2000. Palaeozoic-Early Tertiary Tethyan evolution of melanges, rift and passive margin units in the Karaburun Peninsula (western Turkey) and Chios island (Greece). *In: Bozkurt E, Winchester JA and Piper JDA. (Eds).*
- Robertson AHF, Ustaömer T, Pickett E, Collins A, Andrew T and Dixon JE, 2004. Testing models of Late Palaeozoic-Early Mesozoic orogeny in Western Turkey: support for an evolving open-Tethys model. *Journal of the Geological Society of London* **161**: 501-511.
- Roberts MP and Clemens JD, 1993. Origin of high-potassium, calc-alkaline, I-type granitoids. *Geology* **21**: 825-828.
- Roberts MP and Finger F, 1997. Do U-Pb zircon ages from granulites reflect peak metamorphic conditions? *Geology* **25**: 319-322.
- Robinson AG, Banks CJ, Rutherford MM and Hirst JP, 1995. Stratigraphic and structural development of the Eastern Pontides, Turkey. *Journal of the Geological Society of London* **152**: 861-872.

- Rogers MP and Hawkesworth CJ, 1989. A geochemical transverse across the North Chilean Andes: evidence for crust generation from the mantle wedge. *Earth and Planetary Science Letters* **91**: 271-285.
- Romick JD, Kay SM and Kay RW, 1992. The influence of amphibole fractionation on the evolution of calc-alkaline andesite and dacite tephra from the central Aleutians, Alaska. *Contribution in Mineralogy and Petrology* **112**: 101-118.
- Rubatto D, 2002. Zircon trace element geochemistry: partitioning with garnet and the link between U-Pb ages and metamorphism. *Chemical Geology* 184:23-138.
- Rubatto D and Gebauer D, 2000. Use of cathodoluminescence for U-Pb zircon dating by ion Microprobe: some examples from the western Alps. In: *Cathodoluminescence in Geosciences*. Pagel M, Barbin V, Blanc P, Ohnenstetter D (Eds.) Springer, Berlin, pp. 373-400.
- Rubatto D, Gebauer D and Compagnoni, 1999. Dating of eclogite-facies zircons: the age of Alpine metamorphism in the Sesia-Lanzo zone (Western Alps) *Earth and Planetary Science Letters* 167:141-158.
- Rubatto D, Williams IS and Buick IS, 2001. Zircon and monazite response to prograde metamorphism in the Reynolds Range, central Australia. *Contribution to Mineralogy and Petrology* 140:458-468.
- Rudnick RL and Fountain DM, 1995. Nature and composition of the continental crust: a lower crustal perspective. *Reviews in Geophysics* **33**: 267-309.
- Sajona FG, Maury RC, Bellon H, Cotton J and Defant M, 1996. High field strength elements of Pliocene-Pleistocene island-arc basalts Zamboanga Peninsula, Western Mindanao (Philippines). *Journal of Petrology* **37**: 693-727.
- Sajona FG, Maury RC, Pubellier M, Leterrier J, Bellon H and Cotton J, 2000. Magmatic source enrichment by slab-derived melts in a young post-collision setting, Central Mindanao-Philippines. *Lithos* **54**: 173-206.
- Saunders AD, Tarney J and Weaver SD, 1980. Transverse geochemical variations across the Antarctic Peninsula: Implications for the genesis of calc-alkaline magmas. *Earth and Planetary Science Letters* **46**: 344-360.
- Schiano P, Clocchiatti R, Shimizu N, Maury RC, Jochum KP and Hofmann AW, 1995. Hydrous, silica-rich melts in sub-arc mantle and their relationship with erupted arc lavas. *Nature* **377**: 595-600.
- Schaltegger U and Fernando C, 1992. The age and source of late Hercynian magmatism in The central Alps: evidence from precise U-Pb ages and initial Hf isotopes. *Contribution to Mineralogy and Petrology* **111**: 329-344.

- Schaltegger U, Schneider JL, Maurin JC and Corfu F, 1996. Precise chronometry of 345-340 Ma old magmatism related to syn-convergence extension in the southern Vosges (central Variscan belt). *Earth and Planetary Science Letters* **144**: 403-419.
- Schaltegger U, Fanning CM, Günther D, Maurin JC, Schulmann K and Gebauer D, 1999. Growth, annealing and recrystallization of zircon and preservation of monzonite in high-grade metamorphism: conventional and in-situ U-Pb isotope, Cathodoluminescence and microchemical evidence. *Contribution to Mineralogy and Petrology* **134**: 186-201.
- Schaltegger U, Audétat A, Pettke T, Heinrich CA, 2001. Dating of magmatic and hydrothermal stages in a Sn-W granite. *Journal of Conference Abstr* 6:681.
- Şengör AMC, 1980. Mid-Mesozoic closure of Permo-Triassic Tethys and its implications. *Nature* **279**: 590-593
- Şengör, A.M.C., 1984. The Cimmeride Orogenic system and the tectonics of Eurasia. Geological Society of America, Special Publication 19/81: **195** pp.
- Şengör AMC, 1987. Tectonics of the Tethyside: orogenic collage development in a collisional setting. *Annual Review in Earth and Planetary Sciences* **15**: 213-244.
- Şengör AMC and Yılmaz Y, 1981. Tethyan evolution of Turkey: A plate tectonic approach. *Tectonophysics* **75**, pp. 181-241.
- Şengör AMC, Yılmaz Y and Ketin I, 1980. Remnants of a pre-late Jurassic ocean in Northern Turkey: fragments of Permian- Triassic Palaeo-Tethys? *Bulletin of the Geological Society of America* **91**: 599-609.
- Şengör AMC, Yılmaz Y and Sungurlu O, 1984. Tectonics of the Mediterranean Cimmerides: Nature and evolution of the western termination of Palaeo-Tethys. In: Dixon JE and Robertson AHF (Eds) *The Geological Evolution of the Eastern Mediterranean*. Geological Society of London, Special Publication **17**: 77-112.
- Şengör AMC, Altiner D, Cin A, Ustaömer T and Hsü KJ, 1988 Origin and assembly of the Tethyside orogenic collage at the expense of Gondwana Land. In: Audrey-Charles MG and Hallam (Eds) *Gondwana and Tethys*. Geological Society of London, Special Publication **37**: 119-181.
- Şengör AMC, Cin A, Rowley DB and Shangyou N, 1991. Magmatic evolution of the Tethysides: a guide to reconstruction of collage history: Palaeogeography, Palaeoclimatology and Palaeoecology **87**:411-440.
- Şengör AMC, Cin A, Rowley DB and Nie S-Y, 1993. Space-Time patterns of magmatism along the Tethysides: A preliminary study. *Journal of Geology* **101**: 51-84.
- Shand SJ, 1927. *Eruptive Rocks*, D. Van Nostrand Company, New York, 360 pp.
- Silver LT and Deutsch S, 1963. Uranium-lead isotopic variations in zircons: a case study.

Journal of Geology **71**: 721-758.

Smithies RH, 2000. The Archean tonalite-trondjemite-granodiorite (TTG) series is not an analogue of Cenozoic adakite. *Earth and Planetary Science Letters* **182**: 115-125.

Söllner F, Nelson DR and Miller H, 1997. Provenance, deposition and age of gneiss units from the KTB drill hole (Germany): evidence from SHRIMP and conventional U-Pb zircon age determinations. *Geologisches Rundsch* **86**: S235-S250.

Stacey JS and Krammers JD, 1975. Approximation of terrestrial lead isotope evolution by a two-stage model. *Earth and Planetary Science Letters* **26**: 207-221.

Steiger RH and Jäger E, 1977. Subcommittee on geochronology: Convention on the use of decay constants in geo- and cosmochronology. *Earth and Planetary Science Letters* **36**: 359-362.

Steiger RH, Bär MT and Büsch W, 1973. The zircon age of an anatectic rock in the central Schwarzwald. *Fortschr Mineral* **50**: 131-132.

Stalder R, Foley SF, Brey GP and Horn I, 1998. Mineral-aqueous fluid partitioning of trace elements at 900-1200°C and 3.0-5.7 GPa: new experimental data for garnet clinopyroxene and rutile and implications for mantle metasomatism. *Geochimica et Cosmochimica Acta* **62**: 1781-1801.

Stampfli GM, 2000. Tethyan Oceans. In: Bozkurt E, Winchester JA and Piper JDA. (Eds) *Tectonics and Magmatism in Turkey and its Surrounding Regions*. Geological Society of London, Special Publications **173**: 1-23.

Stampfli GM, Von Raumer JF and Borel GD, 2002. Paleozoic evolution of pre-Variscan terranes: From Gondwana to the Variscan collision. *Geological Society of America, Special Papers*, 263-380.

Stampfli GM, Vavassis I, De Bono A, Rosselet F, Matti B and Bellini M (2003) Remnants of the Palaeotethys oceanic suture-zone in the western Tethyan area. *Bulletin of the Geological Society of Italy Special Publication* **2**.

Stern RJ, 1994. Arc assembly and continental collision in the Neoproterozoic East African Orogen. *Annual Reviews of the Earth and Planetary Sciences* **22**: 319-351.

Stern CR and Kilian R, 1996. Role of the subducted slab, mantle wedge and continental crust in the generation of adakites from the Andean Austral Volcanic Zone. *Contribution to Mineralogy and Petrology* **132**: 263-281.

Stocklin J, 1974. Possible ancient continental margins in Iran. In: Burk CA and Drake CL. (Eds). *The geology of continental margins*: Berlin Springer-Verlag 873-887.

Sun SS, 1982. Chemical composition and origin of the Earth's primitive mantle. *Geochimica et Cosmochimica Acta* **40**: 1229-1240.

- Stolper E and Newman S, 1994. The role of water in the petrogenesis of Mariana trough magmas. *Earth and Planetary Science Letters* **121**: 293-325.
- Sun SS and McDonough WF, 1989. Chemical and isotopic systematics of oceanic basalts: Implication for mantle composition of the Earth and Mantle evolution. In: Saunders AD and Norry MJ. (Eds) *Magmatism in Oceanic Basins*. Geological Society of London Special Publications 42: 313-345.
- Tait JA, Bachtadse V, Franke W and Soffel H, 1997. Geodynamic evolution of the European Variscan fold belt: palaeomagnetic and geological constraints. *Geol Rundsch* **86**: 585-598.
- Tait JA, Bachtadse V, Franke W and Soffel H, 2000. Palaeomagnetism and Palaeozoic palaeogeography of Gondwana and European terranes. *In*: Franke W, Haak V, Oncken O and Tanner D. (Eds.) *Orogenic processes: Quantification and modelling in the Variscan Belt*. Geol Society of London Special Publication **179**: 21-32.
- Tatsumi Y and Kogiso T, 1997. Trace element transport during dehydration processes in the subducted oceanic crust: 2. Origin of chemical and physical characteristics. *Earth and Planetary Science Letters* **148**: 207-221.
- Tatsumi Y, Hamilton DL and Nesbitt RW, 1986. Chemical characteristics of fluid phase released from a subducted lithosphere and origin of arc magmas: evidence from high-pressure experiments and natural rocks. *Journal of Volcanology and Geothermal Research* **29**: 293-309.
- Taylor HP, 1968. Oxygen isotope geochemistry of igneous rocks. *Contribution to Mineralogy and Petrology* **19**: 1-71.
- Taylor HP, 1974. The application of oxygen and hydrogen isotope studies to problems of hydrothermal alteration and ore deposits. *Economic Geology* **69**: 843-883.
- Taylor HP, 1978. Oxygen and hydrogen isotope studies of plutonic granitic rocks. *Earth and Planetary Science Letters* **38**: 177-210.
- Taylor SR and McLennan, 1985. *The continental crust: its composition and evolution*. Blackwell, Oxford 312pp.
- Teipel U, 2003. Obervendischer und unterordovizischer Magmatismus im Bayerischen Wald-Geochronologische (SHRIMP), geochemische und isotopengeochemische Untersuchungen an Metamagmatiten aus dem Westteil des Böhemischen Massivs. *Münchner Geol Hefte* **A33**: 1-98.
- Tepper, JH, Nelson BK, Bergantz GW and Irving AJ, 1993. Petrology of the Chilliwack batholith, North Cascades, Washington: generation of calc-alkaline granitoids by melting of mafic lower crust with variable water fugacity. *Contribution to Mineralogy and Petrology* **113**: 333-351.

- Todt WA and Büsch W (1981) U-Pb investigations on zircons from pre-Variscan gneisses-I. A study from the Schwarzwald, West Germany. *Geochim Cosmochim Acta* **45**: 1789-1801.
- Topuz G, Altherr R, Schwarz WH and Schaltegger U, 2007. Variscan high-grade metamorphism and anatexis in the Pular complex (Eastern Pontides, Turkey): implications for Palaeo-plate reconstructions. (*International Journal of Earth Sciences*)
- Tribuzio R, Messiga B, Vannucci R and Bottazzi P, 1996. Rare earth element redistribution during high-pressure-low-temperature metamorphism in ophiolitic Fe-gabbros (Liguria, northwestern Italy): implications for light REE mobility in subduction zones. *Geology* **24**: 711-714.
- Tuttle OF and Bowen NL, 1958. Origin of granite in the light of experimental studies in the system $\text{NaAlSi}_3\text{O}_8\text{-KAlSi}_3\text{O}_8\text{-SiO}_2\text{-H}_2\text{O}$. pp. 54-78.
- Tüysüz O, 1990. Tectonic evolution of a part of the Tethyside Orogenic Collage: The Kargi Massif, Northern Turkey. *Tectonics* **9**: 141-160.
- Tüysüz O, 1999. Geology of the Cretaceous sedimentary basins of the Western Pontides. *Geological Journal* **34**: 75-93.
- Tüysüz O and Yiğitbaş E, 1994. The Karakaya basin: A Palaeotethyan marginal basin and its age of opening. *Acta Geochimica Hungarica* **37**: 327-350.
- Tüysüz O, Yiğitbaş E and Serdar H, 1993. An approach to the early Mesozoic evolution of the Central Pontides, the Palaeotethys-Karakaya marginal basin problem. 8th Petroleum Congress of the Turkish Association of Petroleum Geologists 351-362.
- Tüysüz O, Dellaloğlu AA and Terzioğlu N, 1995. A magmatic belt within the Neotethyan suture zone and its role in the tectonic evolution of northern Turkey. *Tectonophysics* **243**: 173-191.
- Ustaömer T and Robertson AFH, 1992. Pre-Late Jurassic Tectonic evolution of the Central Pontides: summary and implication for "Palaeotethyan" evolution. *Bulletin of the Geological Society of Greece*.
- Ustaömer T and Robertson AHF, 1993. Late Palaeozoic-Early Mesozoic marginal basins Along the active southern continental margin of Eurasia: evidence from the Central Pontides (Turkey) and adjacent regions. *Journal of Geology* **28**: 219-238.
- Ustaömer T and Robertson AHF, 1994. Late Palaeozoic marginal basin and subduction-accretion: evidence from the Palaeotethyan Küre Complex, Central Pontides, N Turkey. *Journal of the Geological Society of London* **151**: 291-306.
- Ustaömer T and Robertson AHF, 1995. Palaeotethyan tectonic evolution of the north Tethyan margin in the Central Pontides, N Turkey. In: Erler A, Ercan T, Bingöl E, Orcen S. (eds) *Geology of the Black Sea Region, Proceedings of the International Symposium on the*

Geology of the Black Sea Region. Mineral Research and Exploration Institute of Turkey (MTA) Publications, 24-32.

Ustaömer T and Robertson AHF, 1997. Tectonic-sedimentary evolution of the north Tethyan margin in the Central Pontides of northern Turkey. In: Robinson, A.G. (ed) Regional and Petroleum Geology of the Black Sea and Surrounding Regions: American Society of Petroleum Geology Memoir **68**: 255-290.

Ustaömer T and Robertson AHF, 1999. Geochemical evidence used to test alternative plate tectonic models for pre-Upper Jurassic (Palaeotethyan) units in the Central Pontides, N Turkey. Geological Journal **34**: 25-53.

Ustaömer T and Robertson AFH (1999) The Bolu Massif: remnant of a pre-Early Ordovician active margin in the west Pontides, northern Turkey. Geological Magazine **136**: 576-592.

Uysal IT and Golding SD, 2003. Rare earth element fractionation in authigenic illite-smectite from Late Permian clastic rocks, Bowen Basin, Australia: implications for physico-chemical environments of fluids during illitization. Chemical Geology **171**: 195-211.

Vavassis I, De Bono A, Stampfli GM, Giogis D, Valloton A and Amelin Y (2000) U-Pb and Ar-Ar geochronological data from the Pelagonian basement in Evia (Greece): geodynamic implications for the evolution of Palaeotethys. Schweizerische Mineralogische und Petrologische Mitteilungen **80**: 21-43.

Vavra G, 1990. On the kinetics of zircon growth and its petrogenetic significance: a cathodoluminescence study. Contribution to Mineralogy and Petrology **106**: 90-99.

Vavra G, 1994. Systematics of zircon internal morphology in major Variscan granitoid types. Contribution to Mineralogy and Petrology **117**: 331-344.

Vavra G, Gebauer RD, Schmidt R, and Compton W, 1996. Multiple zircon growth and recrystallization during polyphase Late Carboniferous to Triassic metamorphism in granulite of the Ivrea Zone (Southern Alps): an ion microprobe (SHRIMP) study. Contribution to Mineralogy and Petrology **122**: 337-358.

Vielzeuf D and Holloway JR, 1988. Experimental determination of fluid-absent melting relations in the pelitic system. Contribution to Mineralogy and Petrology **98**: 357-376.

Von Blanckenburg F and Davies JH, 1995. Slab breakoff: a model for syncollisional magmatism and tectonics in the Alps. Tectonics **14**: 120-131.

von Quadt A, 1977. U-Pb zircon and Sr-Nd-Pb whole-rock investigations from the continental deep drilling (KTB). Geol Rundsch **86** (suppl): S258-S271.

Von Raumer JF, Stampfli GM, Borel GD and Bussy F, 2002. Organization of pre-Variscan basement areas at the north-Gondwanan margin. International Journal of Earth Sciences **91**: 35-52.

- Von Raumer JF, Stampfli GM and Bussy F, 2003. Gondwana-derived microcontinents- the constituents of the Variscan and Alpine collisional orogens. *Tectonophysics* **365**: 7-22.
- Warr LN, 2002. The Variscan orogeny: the welding of Pangea. In: Woodcock N and Strachan R (Eds) *Geological history of Britain and Ireland*. pp 271-294. Blackwell Publications Oxford.
- Watson EB, Cherniak DJ, Hanchar JM, Harrison TM and Wark DA, 1997. The incorporation of Pb into zircon. *Chemical Geology* **141**:19-31.
- Watson EB and Harrison TM, 1983. Zircon zonation revisited: temperature and composition effects in a variety of crustal magma types. *Earth and Planetary Science Letters* **64**:295-304.
- Watson EB and Liang Y, 1995. A simple method for sector zoning in slow growth crystals: implications for growth rate and lattice diffusion with emphasis on accessory minerals in crustal rocks. *American Mineralogist* **80**:1179-1187.
- Watson EB, Vicenti EP and Rapp RP, 1989. Inclusion/host relations involving accessory minerals in high-grade metamorphic and anatectic rocks. *Contribution to Mineralogy and Petrology* **101**:220-231.
- Weaver BL, 1990. Geochemistry of highly-undersaturated ocean island basalt suites from the South Atlantic Ocean: Fernando de Noronha and Trinidad Islands. *Contribution to Mineralogy and Petrology* **105**: 502-515.
- Wendt I, 1986. *Radiometrische Methoden in der Geochronologie*. Clausthaler Tektonische Hefte 23, Pilger Verlag Berlin.
- Wendt I, Kröner A, Fiala J and Todt W, 1993. Evidence from zircon dating for existence of approximately 2.1 Ga. old crystalline basement in the Southern Bohemia, Czech Republic. *Geol Rundsch* **82**: 42-50.
- White AJR and Chappell BW, 1983. Granitoid types and their distribution in the Lachlan Fold Belt, south-eastern Australia. *Geological Society of America Memoir* **159**:21-34.
- White AJR and Chappell BW, 1988. Some supracrustal (S-type) granites of the Lachlan Fold Belt. *Transactions of the Royal Society of Edinburgh, Earth Sciences*. **79**: 169-181.
- Whalen JB, Currie KL and Chappell BW, 1987. A-type granites: Geochemical characteristics and discrimination. *Contribution in Mineralogy and Petrology* **95**: 420-436.
- Wiedenbeck M, Allé P, Corfu F, Griffin WL, Meier M, Oberli J, Von Quadt A, Roddick JC and Spiegel W, 1995. Three natural zircon standards for U-Pb-Th, Lu-Hf, trace element and REE analyses. *Geostand Newsletters* **19**: 1-13.
- Winchester JA and The PACE TMR Network Team, 2002. Palaeozoic amalgamation of Central Europe: new results from recent geological and geophysical investigations. *Tectonophysics* **360**: 5-21
- Wolf MB and Wyllie JP, 1994. Dehydration melting of amphibolite at 10 Kbar: The effects of

- temperature and time. *Contribution to Mineralogy and Petrology* **115**: 369-383.
- Woodcock NH and Strachan R, 2002. The Caledonian orogeny: a multiple plate collision. *In*: Woodcock N and Strachan R (Eds.), *Geological History of Britain and Ireland*. pp. 187-206, Blackwell Publishing Oxford.
- Wyllie JP, 1984. Constraints imposed by experimental petrology on possible and impossible magma sources and products. *Philosophical Transactions of the Royal Society of London*, **A310**: 439-456.
- Yiğitbaş E, Elmas A and Yılmaz Y, 1999. Pre-Cenozoic tectono-stratigraphic components of the Western Pontides and their geological evolution. *Geological Journal* **34**: 55-74.
- Yılmaz O and Boztuğ D, 1986.) Kastamonu Granitoid belt of Turkey: First arc plutonism product related to the subduction of the Palaeo-Tethys. *Geology* **14**: 179-183.
- Yılmaz Y, 1980. Tectonics and Lithostratigraphic units of northeastern part of the Daday-Devrekani Massif. *Yerbilimleri* **5-6**: 101-135.
- Yılmaz O and Bonhomme MG, 1991. K-Ar isotopic age evidence from a lower to Middle Jurassic low-pressure and a Lower Cretaceous high-pressure metamorphic events in north-central Turkey. *Terra Abs.* **3**: 501.
- Yılmaz Y and Sengör AMC, 1985 Palaeotethyan ophiolites in northern Turkey: Petrology and Tectonic setting. *Ofioliti*. **10-2/3**: 485-504.
- Yılmaz Y, Tüysüz O, Yiğitbaş E, Can Genç S and Sengör AMC, 1997. Geology and tectonic evolution of the Pontides. *In*: Robinson A (Ed). *Regional and petroleum geology of the Black Sea and surrounding region*. AAPG Memoir **68**: 183-226.
- Yılmaz O, 1980. Tectonics and the Lithostratigraphic units of the northeastern part of the Daday-Devrekani Massif. *Yerbilimleri* **5/6**: 101-135.
- Yılmaz, O., 1983. Mineralogical-petrological study of the Çangal metamorphite and its metamorphic conditions. *Yerbilimleri* **10**, pp. 45-58.
- Yılmaz O and Boztuğ D, 1986. Kastamonu granitoid belt of northern Turkey: First arc plutonism related to the subduction of the Palaeo-Tethys. *Geology* **14**: 179-83.
- Yılmaz Y and Şengör AMC, 1985. Palaeo-Tethyan ophiolites in northern Turkey: Petrology and tectonic setting. *Ofioliti* **10**: 485-504.
- Yılmaz Y, Tüysüz O, Yiğitbaş E, Genç SC and Şengör AMC, 1997. Geology and tectonic evolution of the Pontides. *In*: Robinson AG (ed.) *Regional and Petroleum Geology of the Black Sea and Surrounding Region*. American Association of Petroleum Geologists, Memoir **68**: 183-226.

Yogodzinski GM, Kay RW, Volynets ON, Koloskov AV and Kay SM, 1995. Magnesian andesite in the western Aleutian Komandorsky region: implications for slab melting and processes in the mantle wedge. *Geological Society of America Bulletin* **107**: 505-519.

You CF, Castillo PR, Gieskes, JM, Chan LH and Spivak AJ, 1996. Trace element behaviour in hydrothermal experiments: implications for fluid processes at shallow depths in subduction zones. *Earth and Planetary Science Letters* **140**: 41-52.

Zhang HF, Sun M, Zhou XH and Ying JF, 2005. Geochemical constraints on the origin of Mesozoic alkaline intrusive complexes from the North China Craton and tectonic implications. *Lithos* **81**: 297-317.

Ziegler PA and Stampfli GM, 2001. Late Palaeozoic-Early Mesozoic plate boundary reorganization: collapse of the Variscan orogen and opening of Neotethys. *Natura Bresciana* **25**: 17-34.

Zindler A and Hart S, 1986. Chemical Geodynamics. *Annual Review of Earth and Planetary Science Letters* **14**: 493-571.

APPENDIX

Table 3.5- Rb-Sr ages for selected samples from Sivrikaya and Deliktaş granitoids
The mineral ages were calculated using the method of Wendt (1986) m , measured ratio:

Samples		$\frac{[^{87}\text{Rb}]}{[^{86}\text{Sr}]m}$	Erorr %	$\frac{[^{87}\text{Sr}]}{[^{86}\text{Sr}]m}$	Erorr %	Age at 2 σ Ma	
Sivrikaya granitoid							
SG-116	Whole-rock	0.557	0.06	0.71043	0.07		
	Muscovite	177.8	17.8	1.44870	0.20	283.2 \pm 2.8	
	Biotite	398.8	35.9	2.24570	0.42	271.0 \pm 2.6	
	K-feldspar	1.276	0.13	0.71110	0.07		
	Biotite	398.8	35.9	2.24570	0.42	271.3 \pm 2.6	
	Muscovite	177.8	17.8	1.44870	0.20	293.0 \pm 2.9	
	Hornblende	0.190	0.02	0.70480	0.07		
	Muscovite	177.8	17.8	1.44870	0.20	294.0 \pm 2.9	
	SG-132	Whole-rock	0.342	0.034	0.70899	0.07	
		Biotite (300-180 μm)	158.79	15.9	1.33150	0.30	276.5 \pm 2.8
Biotite (>300 μm)		148.74	14.9	1.28370	0.17	272.6 \pm 2.7	
K-feldspar		4.118	0.41	0.71844	0.07		
SG-132 (Bt 300-180 μm)		158.79	15.9	1.33150	0.30	279.0 \pm 2.8	
SG-132 (Bt>300 μm)		148.74	14.9	1.28370	0.17	275.0 \pm 4.1	
SG-186a	Whole-rock	5.884	0.58	0.73246	0.07		
	Muscovite (>300 μm)	971.62	97.1	4.60007	2.3	281.7 \pm 2.8	
Deliktaş granitoid							
DLG-4	Whole-rock	5.889	0.59	0.73540	0.07		
	Muscovite	215.8	21.58	1.58138	0.30	283.2 \pm 2.8	
DLG-82	Whole-rock	5.720	0.57	0.73461	0.09		
	Muscovite	139.2	13.92	1.29110	0.30	292.2 \pm 2.9	
DLG-83	Whole-rock	5.779	0.58	0.73479	0.08		
	Muscovite	159.0	15.9	1.36617	0.30	289.8 \pm 2.9	
	K-feldspar	21.3	2.13	0.79330	0.08	273.8 \pm 2.8	
	K-feldspar	21.3	2.13	0.79330	0.08		
	Muscovite	159.0	15.9	1.36617	0.30	292.5 \pm 2.8	
DLG-84	Whole-rock	7.563	0.76	0.74231	0.07		
	Muscovite	836.7	83.6	4.23018	1.70	295.2 \pm 2.9	

Table 5.1a- Major, trace and rare earth elements analyses of the Deliktaş (MN) and Sivrikaya (BÜ, ÖS) basements

Sample	MN-1	MN-3	MN-5	MN-11	MN-12	MN-72	BÜ-20	BÜ-22	BÜ-26
SiO ₂	63.5	72.7	59.7	79.8	65.6	75.1	59.9	53.4	53.7
TiO ₂	0.79	0.11	0.62	0.05	0.64	0.60	0.94	1.22	1.71
Al ₂ O ₃	17.0	16.0	15.9	14.1	16.7	15.2	16.9	15.5	15.4
Fe ₂ O ₃	6.8	0.9	6.4	0.7	5.6	0.2	6.1	13.2	13.3
MnO	0.06	0.01	0.11	0.04	0.10	<0.1	0.11	0.20	0.21
MgO	2.6	0.3	6.3	0.2	2.4	0.1	2.9	4.4	4.8
CaO	1.6	1.4	5.2	0.6	1.3	0.1	5.3	6.8	7.1
Na ₂ O	2.2	5.2	2.8	2.7	2.8	1.5	4.4	3.2	3.2
K ₂ O	2.7	1.6	1.4	2.5	2.3	4.9	0.8	0.3	0.3
P ₂ O ₅	0.161	0.055	0.143	0.056	0.086	0.027	0.228	0.095	0.201
Ba	639	266	562	306	670	351	462	119	233
Cr	108	7	392	6.4	98	33	106	30	113
Nb	15	2	8	9.3	10	8	9	1.0	12
Ni	62	6	109	<0.1	45	8	42	1.0	8
Rb	92	61	75	83.6	91	216	17	5	8
Sr	278	579	588	78.0	255	80	585	255	214
V	124	16	126	6	97	39	96	436	394
Y	35	10	19	19.0	22	28	29	21	30
Zn	81	13	83	<0.1	79	5	74	87	91
Zr	201	63	130	98.0	125	262	277	59	117
LOI	2.75	1.34	1.82	1.64	2.27	1.58	2.23	2.3	2.04
Sum	100.3	99.8	100.6	102.4	99.8	99.3	99.9	99.8	99.2
ASI	1.8	1.1	1.0	1.7	1.5	1.8	0.9	0.8	0.8
Mg#	62.6	66.1	81.4	60.2	65.5	77.8	67.3	59.5	59.3
Li	—	—	116.0	—	47.7	—	22.9	—	26.7
Mo	—	—	0.5	—	0.8	—	0.4	—	0.9
Cs	—	—	18.8	—	7.0	—	2.5	—	1.1
La	—	—	24	—	28	—	26	—	19
Ce	—	—	50	—	58	—	60	—	45
Pr	—	—	5.6	—	6.7	—	7.4	—	6.0
Nd	—	—	22	—	26	—	31	—	28
Sm	—	—	4.4	—	5.0	—	6.4	—	6.7
Eu	—	—	1.1	—	1.4	—	1.7	—	2.0
Gd	—	—	3.7	—	3.8	—	5.8	—	7.0
Tb	—	—	0.5	—	0.5	—	0.9	—	1.1
Dy	—	—	3.2	—	2.7	—	5.2	—	6.7
Ho	—	—	0.6	—	0.5	—	1.0	—	1.4
Er	—	—	1.8	—	1.2	—	2.9	—	3.9
Tm	—	—	0.3	—	0.2	—	0.4	—	0.5
Yb	—	—	1.6	—	1.1	—	2.5	—	3.5
Lu	—	—	0.2	—	0.2	—	0.4	—	0.5
Hf	—	—	2.5	—	0.8	—	0.8	—	0.4
Ta	—	—	0.5	—	0.7	—	0.5	—	0.6
Tl	—	—	0.7	—	0.7	—	0.0	—	0.0
Pb	—	—	38	—	25	—	6	—	2
Bi	—	—	0.1	—	0.1	—	0.0	—	0.0
Th	—	—	9	—	10	—	5	—	3
U	—	—	2.5	—	3.2	—	0.7	—	0.8
Eu/Eu*	—	—	0.87	—	0.96	—	0.86	—	0.91
K ₂ O/Na ₂ O	1.24	0.28	0.46	0.93	0.67	2.76	0.19	0.07	0.07

- = not determined; ASI= aluminium saturation index= [molar Al₂O₃/(CaO+K₂O+Na₂O)];
Mg# = 100 x molar [MgO/(MgO+0.9xFe₂O₃)]; (Eu/Eu* = √[Sm_{cn} x Gd_{cn}])

Table 5.1a, continued

Sample	ÖS-70	ÖS-75b	ÖS-77a	ÖS-77b	ÖS-78	ÖS-80	ÖS-88a	ÖS-131	ÖS-185a
SiO ₂	60.7	60.3	57.4	62.1	52.4	65.0	58.8	52.2	56.0
TiO ₂	0.75	0.73	0.89	0.69	1.03	0.40	0.43	1.34	0.95
Al ₂ O ₃	18.0	15.5	17.1	16.3	17.3	18.0	15.57	16.19	16.62
Fe ₂ O ₃	7.0	5.7	7.0	5.3	8.3	3.1	4.01	8.90	7.59
MnO	0.39	0.11	0.15	0.11	0.16	0.06	0.12	0.17	0.18
MgO	3.1	4.1	4.1	2.9	4.9	1.3	3.14	5.68	4.27
CaO	3.5	4.3	5.7	4.1	7.1	3.8	6.50	8.33	5.87
Na ₂ O	1.2	3.2	2.6	2.6	2.6	3.7	2.60	2.46	2.49
K ₂ O	3.1	2.9	2.2	2.5	2.0	2.1	2.19	0.87	1.97
P ₂ O ₅	0.13	0.261	0.215	0.108	0.282	0.186	0.106	0.19	0.243
Ba	403	1173	580	330	529	596	448	272	582
Cr	127	148	53	109	260	71	183	270	62
Nb	16	6.0	6.0	7.0	5.0	8.5	19	10	15
Ni	92	58	23	46	10	17	58	79	39
Rb	120	104	81	69	85	69	63	23	64
Sr	160	500	421	143	417	490	141	226	489
V	141	115	155	86	175	43	79	197	149
Y	30	26	18	20	25	10	15	24	31
Zn	110	82	64	58	71	34	60	70	75
Zr	162	178	111	128	140	128	88	124	133
LOI	2.02	1.71	2.35	2.41	2.59	1.57	5.77	2.64	2.73
Sum	100.1	99.1	99.9	99.2	98.8	99.4	99.3	99.1	99.1
ASI	1.5	0.9	0.9	1.0	0.8	1.1	0.8	0.8	0.9
Mg#	66.1	76.0	71.5	70.1	71.6	65.7	76.9	73.3	70.9
Li	-	32.3	-	-	-	-	5.34	-	50.23
Mo	-	0.5	-	-	-	-	0.074	-	2.316
Cs	-	4.7	-	-	-	-	2.88	-	5.68
La	-	32	-	-	-	-	6.2	-	22.5
Ce	-	64	-	-	-	-	13	-	50
Pr	-	7.9	-	-	-	-	1.4	-	7.0
Nd	-	32	-	-	-	-	5.3	-	30
Sm	-	6.5	-	-	-	-	1.3	-	6.8
Eu	-	1.6	-	-	-	-	0.31	-	1.7
Gd	-	5.5	-	-	-	-	1.14	-	6.5
Tb	-	0.7	-	-	-	-	0.22	-	0.9
Dy	-	4.1	-	-	-	-	1.38	-	5.7
Ho	-	0.8	-	-	-	-	0.26	-	1.1
Er	-	2.1	-	-	-	-	0.79	-	3.2
Tm	-	0.3	-	-	-	-	0.13	-	0.5
Yb	-	1.8	-	-	-	-	0.98	-	2.8
Lu	-	0.3	-	-	-	-	0.15	-	0.4
Hf	-	2.0	-	-	-	-	1.7	-	0.8
Ta	-	0.6	-	-	-	-	4.9	-	1.0
Tl	-	0.7	-	-	-	-	0.6	-	0.5
Pb	-	19	-	-	-	-	44	-	16
Bi	-	0.3	-	-	-	-	0.98	-	0.18
Th	-	12	-	-	-	-	4.63	-	7.43
U	-	4.9	-	-	-	-	15.2	-	1.6
Eu/Eu*	-	0.84	-	-	-	-	0.76	-	0.79
K ₂ O/Na ₂ O	2.49	0.78	0.71	0.82	0.64	0.47	0.28	0.62	0.70

- = not determined; ASI= aluminium saturation index= [molar Al₂O₃/(CaO+K₂O+Na₂O)];
Mg# = 100 x molar [MgO/(MgO+0.9xFe₂O₃)]; (Eu/Eu* = √[Sm_{cn} x Gd_{cn}])

Table 5.1b- Major, trace and rare earth elements analyses Devrekani basements (Devrekani metamorphics) and Bekirli metamorphics (BM) for comparison

DG-4a	DM-5	MN-30	MN-32	MN-33	DM-16	DM-17	DM-18	DM-21	DM-23	DM-25	DM-26	DM-27	DM-28	DM-29
70.1	67.2	67.3	74.0	74.9	56.7	48.9	47.7	75.2	49.8	66.3	67.0	55.7	73.1	68.2
0.38	0.75	0.80	0.89	0.53	0.86	1.53	1.24	0.14	1.53	0.50	0.74	1.06	0.14	0.31
15.2	14.9	18.2	12.0	13.9	18.1	14.5	19.5	12.3	18.8	16.8	15.1	18.1	14.1	17.0
2.1	5.24	6.96	5.03	3.66	6.78	10.64	9.12	1.19	10.17	4.05	4.13	7.41	1.24	2.56
0.03	0.12	0.38	0.17	0.10	0.14	0.18	0.12	0.04	0.17	0.11	0.08	0.12	0.04	0.09
1.19	2.30	2.16	1.88	1.31	4.18	7.25	6.67	0.58	4.81	1.60	1.52	4.22	0.48	0.86
2.0	1.7	2.0	0.8	2.1	4.8	9.9	10.4	3.3	7.1	2.2	2.6	5.9	1.0	1.8
4.1	2.7	4.8	1.6	3.1	3.3	2.4	3.1	3.6	3.5	3.9	3.3	2.9	3.8	5.4
3.8	2.5	3.2	2.4	4.7	2.9	1.7	0.8	1.4	1.7	3.0	3.5	2.4	5.1	2.9
0.147	0.16	0.21	0.08	0.11	0.19	0.14	0.11	0.02	0.21	0.24	0.20	0.28	0.25	0.40
0.87	1.48	1.86	1.13	1.15	2.55	1.91	1.37	1.53	1.09	0.77	0.49	1.00	0.56	0.83
100.9	99.1	99.9	100.0	99.9	100.6	99.2	100.2	99.4	99.1	99.5	98.7	99.2	99.8	100.5
1.0	1.4	1.2	1.8	1.0	1.0	0.6	0.8	0.9	0.9	1.2	1.1	1.0	1.0	1.1
89	91	93	92	93	88	87	86	90	90	92	92	89	92	93
36.2	72	165	86	92.5	58	282	50	19	28	57	84	38	40	32
1.2	54	66	39	34.3	25	65	20	18	7	20	28	28	25	26
34	97	127	91	72	140	281	278	12	253	37	49	146	8	22
494	750	632	386	335.7	452	179	214	210	364	533	558	517	474	549
104	93	177	78	164	130	72	24	61	84	187	130	105	168	150
204	377	225	143	138	302	152	419	123	414	248	158	410	91	190
10	13	11	12	11.4	6	3	5	7	9	21	4	8	13	30
160	222	191	245	237	144	101	89	115	133	242	229	163	94	161
32	66	104	64	54	122	83	46	19	89	75	60	84	34	65
18	25	28	22	18	25	35	27	8	30	28	26	26	21	19
29.7	35.1	38.6	-	31.7	-	-	-	-	-	34.6	-	-	-	-
47.0	74.2	60.5	-	42.1	-	-	-	-	-	69.0	-	-	-	-
24.7	33.0	28.7	-	15.8	-	-	-	-	-	29.0	-	-	-	-
4.0	6.2	4.7	-	4.1	-	-	-	-	-	5.3	-	-	-	-
0.7	1.5	0.6	-	0.3	-	-	-	-	-	1.1	-	-	-	-
25.2	22.7	17.0	-	34.3	-	-	-	-	-	21.3	-	-	-	-
2.0	3.7	1.7	-	0.0	-	-	-	-	-	8.8	-	-	-	-
16.6	13.2	16.7	-	18.4	-	-	-	-	-	13.1	-	-	-	-
1.3	0.85	-	-	-	-	-	-	-	-	1.01	-	-	-	-
2.13	3.82	-	-	-	-	-	-	-	-	5.14	-	-	-	-
15	33	-	-	-	-	-	-	-	-	32	-	-	-	-
0.91	0.80	-	-	-	-	-	-	-	-	2.83	-	-	-	-
1.82	0.90	-	-	-	-	-	-	-	-	1.08	-	-	-	-
0.69	0.31	-	-	-	-	-	-	-	-	1.28	-	-	-	-
0.10	0.18	-	-	-	-	-	-	-	-	0.23	-	-	-	-
0.48	0.48	-	-	-	-	-	-	-	-	1.14	-	-	-	-
5.14	8.37	-	-	-	-	-	-	-	-	7.69	-	-	-	-
3.25	4.40	-	-	-	-	-	-	-	-	4.18	-	-	-	-
0.46	0.55	-	-	-	-	-	-	-	-	0.57	-	-	-	-
2.50	2.64	-	-	-	-	-	-	-	-	3.04	-	-	-	-
0.46	0.44	-	-	-	-	-	-	-	-	0.51	-	-	-	-
1.21	1.03	-	-	-	-	-	-	-	-	1.26	-	-	-	-
0.17	0.15	-	-	-	-	-	-	-	-	0.17	-	-	-	-
0.14	0.12	-	-	-	-	-	-	-	-	0.14	-	-	-	-
14.1	27.5	16.1	-	14.1	-	-	-	-	-	22.9	-	-	-	-
0.62	0.87	-	-	-	-	-	-	-	-	0.70	-	-	-	-
0.93	0.92	0.67	1.51	1.53	0.86	0.70	0.26	0.37	0.49	0.78	1.05	0.81	1.31	0.53

- = not determined; ASI= aluminium saturation index= [molar Al₂O₃/(CaO+K₂O+Na₂O)];

Mg#= 100 x molar [MgO/(MgO+0.9xFe₂O₃)]; (Eu/Eu*= √[Sm_{cn} x Gd_{cn}])

Table 5.1b, continued.

Sample	DM-30	DM-32	DM-33	DM-01-1	DM-01-2	DM-01-4	DM-01-5	DM-01-6	BM-6	BM-7	BM-8	BM-9
SiO ₂	66.7	53.9	74.0	72.3	71.6	68.6	67.2	66.6	57.0	52.8	55.2	50.9
TiO ₂	0.47	1.19	0.15	0.20	0.19	0.40	0.38	0.42	0.17	0.20	0.19	1.06
Al ₂ O ₃	16.6	16.6	14.3	14.2	14.0	15.7	15.8	16.4	12.5	12.8	12.8	16.3
Fe ₂ O ₃	3.76	8.62	1.21	1.52	1.46	3.08	2.97	3.38	6.90	7.99	7.40	8.82
MnO	0.10	0.18	0.03	0.05	0.04	0.06	0.08	0.07	0.07	0.11	0.08	0.15
MgO	1.46	5.76	0.36	0.65	0.60	1.37	1.35	1.32	8.63	11.15	8.97	7.75
CaO	2.0	5.6	0.63	0.86	0.78	2.20	2.33	2.20	9.52	8.40	9.74	9.18
Na ₂ O	4.0	2.2	3.96	4.33	4.12	4.54	4.80	5.74	3.27	3.13	2.97	4.92
K ₂ O	3.0	3.5	5.14	4.23	4.34	3.23	2.85	2.12	0.21	0.53	0.35	0.17
P ₂ O ₅	0.22	0.30	0.12	0.10	0.12	0.13	0.14	0.23	0.04	0.19	0.19	0.26
LOI	0.79	1.47	0.49	0.78	0.57	0.48	0.72	0.42	1.74	2.77	2.01	0.58
Sum	99.3	99.5	99.7	99.3	97.8	99.8	98.7	99.0	100.3	100.2	100.0	100.1
ASI	1.2	0.9	1.1	1.1	1.1	1.0	1.0	1.0	0.5	0.6	0.6	0.6
Mg#	92	87	94	91	92	91	91	92	78	76	78	83
Cr	12	183	13	13	14	15	15	17	589	664	640	223
Ni	8	30	12	<0.1	<0.1	<0.1	<0.1	<0.1	244	311	280	114
V	34	185	7	13	14	51	45	33	220	200	212	210
Ba	515	536	529	593	609	522	655	353	14	55	56	106
Rb	186	280	169	143.7	153.8	135.5	109.6	147.8	4	8	7	6
Sr	170	148	114	121	119	182	255	224	132	140	151	192
Nb	16	10	10	8.1	10.3	0.0	9.9	21.6	2	5	4	5
Zr	231	144	115	140	133	128	144	193	30	34	32	80
Zn	84	108	34	22	26	48	43	74	14	34	20	58
Y	23	31	20	24	20	12	16	20	8	8	6	21
La	—	21.4	28.0	30.5	28.8	31.7	27.3	45.4	—	—	—	—
Ce	—	46.7	41.2	52.8	40.5	42.6	32.2	70.5	—	—	—	—
Nd	—	23.8	16.1	24.8	32.2	19.0	16.5	31.6	—	—	—	—
Sm	—	5.2	2.4	4.3	3.6	3.0	3.1	4.9	—	—	—	—
Eu	—	1.5	0.3	0.5	0.1	0.6	0.8	0.8	—	—	—	—
Pb	—	9.1	43.6	32.4	32.5	9.5	19.0	18.6	—	—	—	—
U	—	1.9	0.0	0.0	0.0	1.7	>0.1	>0.1	—	—	—	—
Th	—	3.8	14.4	17.6	16.7	3.6	4.6	15.5	—	—	—	—
Yb	—	2.22	—	—	—	—	—	—	—	—	—	—
Cs	—	7.08	—	—	—	—	—	—	—	—	—	—
Li	—	43	—	—	—	—	—	—	—	—	—	—
Ta	—	1.07	—	—	—	—	—	—	—	—	—	—
Hf	—	1.40	—	—	—	—	—	—	—	—	—	—
Mo	—	1.29	—	—	—	—	—	—	—	—	—	—
Bi	—	0.69	—	—	—	—	—	—	—	—	—	—
Tl	—	1.84	—	—	—	—	—	—	—	—	—	—
Pr	—	5.64	—	—	—	—	—	—	—	—	—	—
Gd	—	5.15	—	—	—	—	—	—	—	—	—	—
Tb	—	0.80	—	—	—	—	—	—	—	—	—	—
Dy	—	4.78	—	—	—	—	—	—	—	—	—	—
Ho	—	0.94	—	—	—	—	—	—	—	—	—	—
Er	—	2.58	—	—	—	—	—	—	—	—	—	—
Tm	—	0.36	—	—	—	—	—	—	—	—	—	—
Lu	—	0.31	—	—	—	—	—	—	—	—	—	—
[La/Yb] _N	—	6.5	—	—	—	—	—	—	—	—	—	—
Eu/Eu*	—	0.8	—	—	—	—	—	—	—	—	—	—
K ₂ O/Na ₂ O	0.75	1.61	1.30	0.98	1.05	0.71	0.59	0.37	0.06	0.17	0.12	0.04

- = not determined; ASI= aluminium saturation index= [molar Al₂O₃/(CaO+K₂O+Na₂O)];
Mg#= 100 x molar [MgO/(MgO+0.9xFe₂O₃)]; (Eu/Eu*= √[Sm_{cn} x Gd_{cn}])

Table 5.2a- Rb-Sr, Sm-Nd and O isotopic data of the Deliktas (MN) and Sivrikaya (BÜ, ÖS) basement.

Sample	Rb (ppm)	Sr (ppm)	$[\frac{87}{86}\text{Rb}]{\text{Sr}}_i$	$[\frac{87}{86}\text{Sr}]{\text{Sr}}_m$	$[\frac{87}{86}\text{Sr}]{\text{Sr}}_i$	Sm (ppm)	Nd (ppm)	$[\frac{147}{144}\text{Sm}]{\text{Nd}}_i$	$[\frac{143}{144}\text{Nd}]{\text{Nd}}_m$	$[\frac{143}{144}\text{Nd}]{\text{Nd}}_i$	$\epsilon\text{Nd}_{(t)}$	T_{DM} (Ga)	$\delta^{18}\text{O}_{(\text{SMOW})}$ (‰)
MN-1	92.0	278.0	0.958	0.71590 ± 10	0.71256	9.0	51.6	0.1056	0.512118 ± 9	0.511911	-6.60	1.3	9.9
MN-3	60.0	544.0	0.347	0.71332 ± 10	0.71232	9.6	56.6	0.1029	0.512184 ± 8	0.511982	-5.20	1.2	11.3
MN-5	75.0	588.0	—	—	—	5.0	22.0	0.1233	0.512283 ± 10	0.512041	-4.10	1.3	10.5
MN-11	83.6	78.0	3.168	0.72045 ± 10	0.70620	15.0	75.6	0.1203	0.512250 ± 9	0.512014	-4.60	1.2	10.9
MN-12	91.2	254.6	1.386	0.71251 ± 10	0.70990	5.6	31.3	0.1090	0.512287 ± 9	0.512073	-3.40	1.1	10.3
BÜ-20	16.9	587.9	0.088	0.70420 ± 10	0.70360	9.4	45.1	0.1260	0.512632 ± 10	0.512218	2.6	0.7	9.4
BÜ-22	5.4	268.7	0.053	0.70391 ± 10	0.70352	3.2	9.8	0.1971	0.512983 ± 10	0.512335	6.8	0.6	8.4
BÜ-26	7.8	265.4	0.129	0.70567 ± 14	0.70445	—	—	—	—	—	—	0.8	8.2
ÖS-75b	109.2	500.0	0.654	0.70912 ± 10	0.70684	6.4	32.6	0.1198	0.512346 ± 11	0.512110	-2.7	1.1	9.5
ÖS-77a	100.7	492.3	0.599	0.70864 ± 12	0.70655	5.4	30.9	0.1207	0.512374 ± 9	0.512136	-2.2	1.1	9.0
ÖS-78	107.4	512.9	0.606	0.70866 ± 9	0.70606	6.9	32.3	0.1294	0.512424 ± 9	0.512169	-1.5	1.1	8.7
ÖS-80	69.1	507.4	0.409	0.70843 ± 10	0.70668	3.6	27.5	0.1237	0.512315 ± 10	0.512071	-3.5	1.2	10.3
ÖS-185a	116.9	533.3	0.509	0.70883 ± 10	0.70660	6.6	34.3	0.1158	0.512403 ± 9	0.512176	-1.4	1.0	8.8

m = measured isotopic ratios; i = calculated initial isotopic ratios; $\epsilon\text{Nd}_{(t)}$ values were calculated using present day ($^{143}\text{Nd}/^{144}\text{Nd}$)_{CHUR} = 0.512638 and ($^{147}\text{Sm}/^{144}\text{Nd}$)_{CHUR} = 0.1967, (CHUR = Chondritic Uniform Reservoir; $\lambda = 6.54 \cdot 10^{-12} \text{ a}^{-1}$). The age data was used for the $\epsilon\text{Nd}_{(t)}$ and $\text{Sr}_{(t)}$ calculations [$\text{Sr}_{(t)} = (\frac{87}{86}\text{Sr}/\text{Sr})_i (\frac{87}{86}\text{Sr}/\text{Sr})_m - \text{Rb}/^{86}\text{Sr}(e^{\lambda t} - 1)$, where $\lambda = 1.42 \cdot 10^{-11} \text{ a}^{-1}$]. — . Not determined

Table 5.2b - Rb-Sr, Sm-Nd and O isotope data of the Devrekani basement and Devrekani (DM) and Bekirli (BM) metamorphics for comparison

Sample	Rb (ppm)	Sr (ppm)	$[\frac{87}{86}\text{Rb}]m$	$[\frac{87}{86}\text{Sr}]m$	$[\frac{87}{86}\text{Sr}]i$	Sm (ppm)	Nd (ppm)	$[\frac{147}{144}\text{Sm}]m$	$[\frac{147}{144}\text{Sm}]m$	$[\frac{143}{144}\text{Nd}]m$	$[\frac{143}{144}\text{Nd}]i$	$\epsilon\text{Nd}_{(t)}$	T_{DM} (Ga)	$\delta^{18}\text{O}_{(\text{VSMOW})}$ (‰)
DG-4a	104.0	204.0	1.435	0.71126±10	0.706770	4.54	21.5	0.1278	0.512333±22	0.512149	-5.40	1.25	10.1	
DM-5	101.0	306.4	0.954	0.70989±10	0.705818	6.17	33.0	0.1241	0.512310±8.5	0.512043	-3.60	1.69	11.4	
MN-30	119.0	216.0	1.595	0.71641±10	0.709601	5.67	33.6	0.1020	0.512305±9.2	0.512085	-2.90	1.30	-	
MN-32	79.0	146.0	1.567	0.71116±10	0.705470	6.71	37.0	0.1096	0.512436±10	0.512200	-0.60	1.23	8.8	
MN-33	54.0	139.0	1.125	0.71401±9	0.709207	7.19	38.9	0.1118	0.512276±8	0.512035	-3.80	1.50	10.7	
DM-17	73.9	162.5	1.316	0.70962±9	0.703998	3.74	11.1	0.2041	0.512945±8	0.512544	-1.83	0.63	-	
DM-21	61.0	123.0	1.409	0.71511±9	0.709093	1.40	7.6	0.1108	0.512439±10	0.512221	-0.60	0.90	-	
DM-23	84.4	414.0	0.606	0.70827±10	0.705761	5.39	23.3	0.1399	0.512439±8	0.512164	-1.70	1.24	-	
DM-25	190.6	239.2	2.307	0.71561±10	0.705761	6.42	38.1	0.1126	0.512378±12	0.512157	-1.90	1.00	-	
DM-27	108.0	405.8	0.770	0.70898±10	0.705693	4.81	20.1	0.1445	0.512438±10	0.512154	-1.90	1.32	-	
DM-30	192.0	171.6	3.241	0.71991±11	0.705954	6.11	37.6	0.0981	0.512317±8	0.512124	-2.50	0.96	10	
DM-32	270.5	148.3	4.085	0.72314±10	0.705703	5.27	25.5	0.1249	0.512507±8.4	0.512262	0.20	0.92	8.5	
DM-33	172.3	117.5	5.250	0.72783±12	0.705417	10.54	60.3	0.1057	0.512333±10	0.512125	-2.50	1.00	10.3	
BM-6	1.6	142.2	0.033	0.70539±10	0.705250	0.48	1.9	0.1518	0.512613±10	0.512315	1.20	1.05	-	
BM-7	0.5	136.6	0.010	0.70546±10	0.705419	0.54	2.1	0.1530	0.512596±14	0.512296	0.80	1.11	-	
BM-8	2.1	149.2	0.040	0.705231±9	0.705060	0.49	2.0	0.1529	0.512608±9.4	0.512308	1.10	1.08	-	

m= measured isotopic ratios; i=calculated initial isotopic ratios; $\epsilon\text{Nd}_{(t)}$ values were calculated using present day ($^{143}\text{Nd}/^{144}\text{Nd}$)_{CHUR}=0.512638 and ($^{147}\text{Sm}/^{144}\text{Nd}$)_{CHUR}=0.1967, (CHUR =Chondritic Uniform Reservoir; $\lambda=6.54 \cdot 10^{-12} \text{ a}^{-1}$). The age 300 Ma is used for the $\epsilon\text{Nd}_{(t)}$ and $\text{Sr}_{(t)}$ calculations [$\text{Sr}_{(t)} = (^{87}\text{Sr}/^{86}\text{Sr})_i (e^{\lambda t} - 1)$], where $\lambda = 1.42 \cdot 10^{-11} \text{ a}^{-1}$].

Table 5.3a- U-Pb zircon isotopic dilution analytical results of Sivrikaya-Deliktaş basement

Fraction	Zircon description	Weight ¹ U ¹ (mg)	Pb ¹ (ppm)	Isotopic ratios			Apparent ages (Ma)			Rho		
				$\frac{^{206}\text{Pb}}{^{238}\text{U}}$	$\frac{^{207}\text{Pb}}{^{235}\text{U}}$	$\frac{^{207}\text{Pb}}{^{206}\text{Pb}}$	$\frac{^{206}\text{Pb}}{^{238}\text{U}}$	$\frac{^{207}\text{Pb}}{^{235}\text{U}}$	$\frac{^{207}\text{Pb}}{^{206}\text{Pb}}$			
BU-20 Homogeneous zircon population, the difference is the grain-size.												
1	s, cls, euh, spr, cl, rtp, ~70µm	0.0412	707	66	402	0.080544±86	0.642185±75	0.057826±28	499.4	503.7	523.2	0.9144
2	s, cls, euh, spr, cl, rtp, ~63µm	0.0413	382	55	671	0.131282±486	1.039997±541	0.057454±232	795.2	723.9	508.9	0.9035
3	m, lpk, euh, spr, cl, rtp, ~90µm	0.0582	446	60	176	0.095349±101	0.80258±93	0.061048±29	587.1	598.3	640.9	0.9148
4	b, thk, cls, lpr, euh, trl, ~125µm	0.0406	558	49	633	0.080916±94	0.642395±146	0.057580±107	501.6	503.8	513.8	0.9285
5	lg, thk, ly, lpr, euh, trl, >125µm	0.0465	533	45	816	0.080224±87	0.637658±75	0.057648±26	497.5	500.9	516.4	0.9267
6	m, thk, ly, lpr, euh, trl, ~100µm	0.0210	2507	194	682	0.069622±88	0.547745±71	0.057060±14	433.9	443.5	493.9	0.9828
7	lg, thk, cls, lpr, euh, tr, >125µm	0.0315	1325	115	944	0.080301±83	0.641407±67	0.057931±10	497.9	503.2	527.2	0.9852
8	st, thk, cls, pr, euh, tr, ~100µm	0.0255	834	88	207	0.080559±80	0.641238±104	0.057730±68	499.5	503.1	519.5	0.6800
9	s, st, ly, spr, euh, cl, ~63µm	0.0242	991	86	303	0.079812±79	0.630459±102	0.057291±68	495.0	496.4	502.8	0.6826
10	m, st, cls, lpr, euh, trl, ~100µm	0.0205	126	24	582	0.080178±59	0.638747±104	0.057779±84	497.2	501.5	521.3	0.5973
OS-80 Generally zircon grains are euhedral and have dark brown tips.												
1	l, ndl, ly, lpr, euh, cl, ~63µm	0.0351	1230	60	2885	0.047285±25	0.341443±19	0.052371±06	297.8	298.3	301.7	0.9765
2	m, ndl, ly, lpr, euh, cl, ~80µm	0.0400	872	44	1375	0.047513±49	0.343609±46	0.052418±05	299.4	299.9	303.7	0.9576
3	s, cls, euh, lpr, cl, ~70µm	0.0367	891	42	2101	0.046657±35	0.338106±36	0.052558±10	294.0	295.7	309.7	0.9594
4	thk, tr, lpk, spr, euh, cl, ~100µm	0.0378	634	30	4533	0.04700±35	0.340852±36	0.052376±08	294.6	295.4	301.9	0.9620
5	l, th, lbr, lpr, euh, tr, ~90µm	0.0212	1700	87	2777	0.048639±43	0.353498±43	0.052711±06	306.2	307.3	316.3	0.9904
6	l, ndl, lpk, tr, spr, euh, cl, ~63µm	0.0366	860	41	2463	0.047397±53	0.345339±53	0.052844±07	298.5	301.2	322.0	0.9915
7	m, ndl, ly, tr, spr, euh, cl, ~80µm	0.0323	993	47	2071	0.047194±47	0.341827±47	0.052532±08	297.3	298.6	308.6	0.9852
8	m, thk, lpk, m-fac, euh, cl, ~80µm	0.0370	358	18	1014	0.049011±33	0.363703±36	0.053821±15	308.4	315.0	363.5	0.9035
9	b, ly, lpr, euh, cl, ~80µm	0.0434	609	30	6837	0.050281±51	0.375103±53	0.054106±17	316.2	323.4	375.4	0.9469
10	thk, l, tr, lpk, spr, euh, cl, ~125µm	0.0394	696	37	8115	0.048347±35	0.350622±34	0.052598±05	304.4	305.2	311.5	0.9895
11	3twins, m-fac, lbr, spr, euh, cl, ~90µm	0.0265	913	45	4966	0.048624±39	0.353298±44	0.052698±22	306.1	307.2	315.8	0.8669
12	m, th, cls, lpr, tr, euh, cl, ~100µm	0.0206	785	39	3237	0.048509±40	0.351598±41	0.052568±09	305.4	305.9	310.2	0.9741
OS-185a Homogeneous zircon population, the differences are colour and grain-size.												
1	l, ndl, cls, lpr, euh, cl, ~63µm	0.0255	740	37	1341	0.046303±198	0.335491±199	0.052550±19	291.8	293.7	309.4	0.9952
2	m, lbr, m-fac, euh, cl, ~80µm	0.0382	514	27	1899	0.050709±37	0.367036±37	0.052496±09	318.9	317.5	307.0	0.9678
3	l, m-frg, ly, s-euh, tr, ~100µm	0.0436	545	27	1438	0.047794±62	0.347019±63	0.052660±14	301.0	302.5	314.1	0.9763
4	s, st, lbr, euh, spr, tr, ~70µm	0.0365	525	27	1746	0.050659±53	0.367255±54	0.053264±11	315.5	318.4	340.0	0.9808
5	m, ndl-frg, lbr, lpr, euh, cl, ~90µm	0.0499	532	26	1997	0.047817±48	0.346786±49	0.052599±10	301.1	302.3	311.5	0.9771
6	s-frg, lbr, s-euh, tr, ~63µm	0.0466	523	28	925	0.047535±47	0.344669±49	0.052589±15	299.4	300.7	311.0	0.9545
7	l, thk, br, m-fac, tr, spr, ab, >125µm	0.0948	440	26	1170	0.051212±53	0.370417±53	0.052525±05	321.2	319.7	308.3	0.9989
8	m, br, m-fac, tr, spr, ab, ~90µm	0.0268	452	25	2405	0.051789±45	0.374994±45	0.052624±11	324.8	323.3	312.6	0.9926
9	thk, br, m-fac, tr, spr, ab, ~100µm	0.0316	495	25	1059	0.047723±33	0.346441±34	0.052639±09	300.6	302.0	313.2	0.9613
10	l, thk, lbr, m-fac, tr, spr, ab, ~100µm	0.0425	566	28	5086	0.044101±51	0.318661±51	0.052487±09	277.7	280.8	306.6	0.9954

¹, Weight and concentration error better than 20%; ², measured ratio corrected for mass discrimination and spike contribution; ³, Corrected for blank Pb, U and initial common Pb based on the Stacey and Kramers (1975) model. Errors are 2 σ_{meas} . *Rho*, correlation coefficient. *l*, long; *lg*, large; *m*, medium; *s*, small; *st*, short; *sr*, stout; *th*, thin; *thk*, thick; *euh*, euhedral; *lpr*, long prism; *frg*, fragment; *spr*, short prism; *tr*, transparent; *ntl*, needle; *y*, yellow; *ly*, light yellow; *cl*, clear; *cls*, colourless; *m-fac*, multi-facet; *br*, brown; *lbr*, light brown; *unab*, unabraded; *ab*, abraded; *s-euh*, sub-euhedral; *r*, rounded; *ntp*, rounded tip

Table 5.3b- U-Pb zircon isotopic dilution analytical results for selected Devrekani metamorphic samples

Fraction	Zircon description	Weight ¹ U ¹ (mg)	Pb ¹ 206Pb ² 204Pb (ppm)	Isotopic ratios			Apparent ages (Ma)			Rho		
				$\frac{206\text{Pb}^3}{238\text{U}}$	$\frac{207\text{Pb}^3}{235\text{U}}$	$\frac{207\text{Pb}^3}{206\text{Pb}}$	$\frac{206\text{Pb}}{238\text{U}}$	$\frac{207\text{Pb}}{235\text{U}}$	$\frac{207\text{Pb}}{206\text{Pb}}$			
DG-4a Generally zircon grains are euhedral and have dark brown tips.												
1	l, m, y, euh, lpr, cl, tr, ~90µm	0.0139	213	6	673	0.029694±170	0.204731±174	0.050689±32	186.1	189.1	226.6	0.9826
2	s, st, lbr, pr, euh, tr, ~63µm	0.0139	579	24	209	0.034702±102	0.245592±203	0.051372±162	219.9	223.0	255.5	0.6125
3	m, st, ly, pr, euh, tr, ~100µm	0.0131	321	11	640	0.034743±58	0.243834±82	0.051494±57	217.7	212.6	263.0	0.7251
4	lg, st, lbr, pr, euh, tr, ~200µm	0.0580	369	11	1028	0.030262±37	0.212198±42	0.050856±19	192.2	195.4	234.3	0.8900
5	thk, cls, pr, euh, tr, ~125µm	0.0110	407	42	646	0.10004±405	1.50984±406	0.109123±13	616.5	934.6	1784.8	0.9995
6	m, st, y, pr, euh, tr, ~100µm	0.0139	466	17	323	0.032792±75	0.236138±133	0.052226±100	208.0	215.3	295.3	0.6641
7	l, thk, m-fac, y, lpr, cl, ~80µm	0.0406	588	19	539	0.030768±41	0.213032±51	0.050379±30	195.4	195.8	199.6	0.8040
8	l, thk, m-fac, br, spr, tr, ~110µm	0.0139	292	9	2206	0.030597±52	0.212025±8±53	0.049558±35	198.8	196.9	233.3	0.9752
DM-5 All have characteristic brown tips and irregular prisms												
1	m, st, cls, lpr, euh, tr, rtp, ~90µm	0.0080	1107	75	1263	0.063516±72	0.483373±60	0.055195±08	397.0	400.4	420.1	0.9004
2	l, thk, ly, euh, lpr, tr, ~125µm	0.0266	330	20	1393	0.056862±93	0.421931±08	0.053817±11	356.5	357.4	363.4	0.6465
3	m, sh, cls, lpr, euh, tr, rtp, 100µm	0.0205	310	23	788	0.068443±84	0.532357±79	0.056412±48	426.8	433.4	468.6	0.8239
4	lg, thk, ly, euh, lpr, tr, m-fac, >125µm	0.0345	157	12	451	0.063755±122	0.476253±146	0.054178±128	398.4	395.5	378.5	0.6300
5	s, euh, m-fac spr, cl, ~63µm	0.0305	150	11	713	0.063677±67	0.605365±73	0.068949±38	398.0	480.6	897.2	0.8853
6	m, st, lbr, lpr, euh, tr, ~70µm	0.0463	440	27	3880	0.059456±433	0.462279±433	0.056391±08	372.3	385.8	467.7	0.9999
7	s, cls-ly, lpr, euh, tr, ~60µm	0.0323	795	40	3031	0.051841±116	0.384833±117	0.053839±10	325.8	330.6	364.3	0.9962
8	s, euh, cls, pr, cl, tr, <63µm	0.0198	716	38	1674	0.051760±174	0.401212±174	0.056218±09	325.3	342.5	461.0	0.9988
9	s, m-fac, cls, spr, euh, tr, ~70µm	0.0422	414	20	872	0.046442±144	0.337702±145	0.052737±20	292.6	295.4	317.5	0.9902
DM-23 All have characteristic dark brown tips.												
1	lnd, cls, euh, lpr, cl, ~63µm	0.0122	1440	80	1624	0.047563±51	0.343935±52	0.052445±11	299.5	300.1	304.8	0.9786
2	thk-frg, lbr, euh, cl, ab, ~125µm	0.0421	1294	66	5254	0.044312±50	0.319095±50	0.052227±06	279.5	281.2	295.3	0.9938
3	l, m, lbr, spr, euh, tr, ab, ~100µm	0.0408	957	45	7105	0.046440±43	0.335487±42	0.052394±05	292.6	293.7	302.6	0.9922
4	lg, m, ly euh, lpr, cls, ~125µm	0.0330	755	38	2078	0.045662±41	0.327955±43	0.052090±16	287.7	288.0	289.3	0.9320
5	thk-frg, cls, euh, tr, ab, >125µm	0.0240	917	41	1656	0.045802±52	0.330863±52	0.052392±09	288.7	290.2	302.5	0.9850
6	s, ly euh, lpr, cls, ab, ~80µm	0.0361	902	44	2774	0.046867±64	0.337965±69	0.052301±26	295.3	295.6	298.5	0.9270
7	ndl, ly, lpr, euh, cl, unab, ~100µm	0.0353	984	45	3559	0.046288±41	0.333918±41	0.052320±11	291.7	292.6	299.4	0.9651
8	th-frg, cls, euh, cl, unab, ~70µm	0.0422	582	26	2579	0.043256±37	0.311309±38	0.052197±13	273.0	275.2	294.0	0.9424
9	m-frg, euh, ly, tr, unab, ~90µm	0.0434	460	21	1845	0.046754±39	0.335934±42	0.052112±16	294.6	294.1	290.3	0.9251
10	ndl, y, lpr, euh, tr, ab, ~80µm	0.0243	4171	200	622	0.04715±135	0.34279±139	0.052729±27	297.0	299.3	317.1	0.9809
11	s, l, cls, lpr, euh, tr, ab, ~63µm	0.0167	840	80	1745	0.047419±66	0.343791±67	0.052557±06	299.3	300.6	303.5	0.9880
12	b, br, euh, lpr, tr, unab, ~125µm	0.0449	798	32	2053	0.047468±42	0.345253±43	0.052752±09	299.0	301.1	318.1	0.9766
DM-33 All have characteristic brown tips and regular prisms (short and long)												
1	m, thk, lpk, spr, euh, cls, cl, ~125µm	0.0180	1810	90	1638	0.057707±37	0.439125±38	0.055190±12	361.7	369.6	419.9	0.9510
2	m, lbr, lpr, m-fac-euh, tr, ~90µm	0.0224	2074	107	332	0.051572±37	0.40940±104	0.057575±94	324.2	348.4	513.6	0.4495
3	thk, lg, lbr, spr, euh, fr, tr, ~80µm	0.0185	1816	86	905	0.053932±44	0.444920±44	0.059832±09	338.6	373.7	597.4	0.9785
4	m, thk, lbr, spr, euh, tr, ~100µm	0.0275	948	46	229	0.045234±34	0.331677±47	0.053180±34	285.2	290.8	336.5	0.6951
5	thk, l, lbr, spr, euh, tr, ~125µm	0.0235	2216	122	447	0.057557±33	0.561520±35	0.070757±15	360.7	452.5	950.3	0.9028
6	m, th, br, euh, lpr, tr, >63µm	0.0223	2063	100	609	0.046017±41	0.339458±43	0.053501±15	290.0	296.8	350.1	0.9381
7	s, br, euh, lpr, cl, tr, ~63µm	0.0284	603	28	888	0.047017±32	0.338340±49	0.052810±17	292.8	295.9	320.4	0.9841
8	thk, m-fac, lpk, euh, tr, ~100µm	0.0228	995	52	2534	0.048216±55	0.353722±55	0.053208±08	303.6	307.5	337.6	0.9904
9	s, lbr, spr, s-euh, tr, rtp, ~70µm	0.0376	324	20	346	0.057763±49	0.440836±56	0.055351±29	362.0	370.8	426.4	0.8601

¹ Weight and concentration error better than 20%; ² measured ratio corrected for mass discrimination and spike contribution; ³ Corrected for blank Pb, U and initial common Pb based on the Stacey and Kramers (1975) model. Errors are 2σ_{meas}. Rho, correlation coefficient. l, long; lg, large; m, medium; s, small; sh, short; st, stout; th, thin; thk, thick; euh, euhedral; lpr, long prism; frg, fragment; spr, short prism; tr, transparent; trl, translucent; ndl, needle; y, yellow; ly, light yellow; cl, clear; cls, colourless; m-fac, multi-facet; br, brown; lbr, light brown; unab, unabraded; ab, abraded; s-euh, sub-euhedral; r, rounded; rrp, rounded tip.

Publications

- Nzegge OM, Satir M, Siebel W, Chen F and Reiter E (2001) Geochemistry and geochronology of the Sivrikaya and Devrekani granitoids, and basement of the Middle-Jurassic Kastamonu granitoid belt: further evidence for the tectonic evolution of the Central Pontides, NW Turkey *Terra Nostra* Extended Abstracts **5/01**: 54-56.
- Nzegge OM, Satir M, Siebel W and Terzioğlu N (2002) Are all the plutons of the Kastamonu Granitoid Belt, Central Pontides-NW Turkey of Middle Jurassic age? Genesis and geochronology of the Sivrikaya Complex. *European Journal of Mineralogy Absts* **14/1**: 120.
- Nzegge OM, Satir M, Siebel W and Boztuğ D (2006) Late Palaeozoic-Mesozoic magmatism in the Kastamonu granitoid belt, Central Pontides-NW Turkey and regional geological implications. *Geophysical Research Abstracts* **8**: EGU2006-A-07523.
- Nzegge OM, Satir M, Siebel W and Taubald H (2006)** Geochemical and isotopic constraints on the genesis of the Late Palaeozoic Deliktaş and Sivrikaya granites from the Kastamonu granitoid belt (Central Pontides, Turkey). *Neues Jahrbuch für Mineralogie* **183**: 27-40.
- Nzegge OM, Satir M, Boztuğ D and Taubald H (2007) Zircon ages, geochemistry and isotope systematics of the extension-related Devrekani intrusion, Kastamonu granitoid belt (Central Pontides, Turkey), and geodynamic interpretation. *Geophysical Research Abstracts* **9**: EGU2007-A-08507.
- Nzegge OM and Satir M (2007) Geochemistry and geochronology of the Eurasian-derived basement of the Central Pontides, Turkey. *Geophysical Research Abstracts* **9**: EGU2007-A-08626.
- Nzegge OM, Boztuğ D, Siebel W and Satir M.** (accepted). Late Variscan Sivrikaya and Deliktaş plutons from the Kastamonu granitoid belt generated in a Palaeotethyan convergence system (Central Pontides, Turkey). *International Journal of Earth Sciences*.
- Nzegge OM, Boztuğ D, Siebel W and Satir M** (accepted). Zircon ages, geochemistry and isotope systematics of Devrekani granitoid from the Kastamonu granitoid belt (Central Pontides, Turkey), and geodynamic interpretation. *Journal of Asian Earth Sciences*.
- Nzegge OM** (*Submitted*: Special Issue for session TS10/EGU-2007) Geochronology and isotopes systematics of the Eurasian-derived basement of the Central Pontides: evidence for pre-Variscan basement.

Geochemical and isotopic constraints on the genesis of the Late Palaeozoic Deliktaş and Sivrikaya granites from the Kastamonu granitoid belt (Central Pontides, Turkey)

Nzegge, O. M. ^{a,b,*}, Satir, M. ^a, Siebel, W. ^a & Taubald, H ^a

^a Institute of Geosciences, University of Tübingen, Wilhelmstr. 56, D-72074, Tübingen-Germany

^b Institut des Recherches Géologiques et Minières, B. P. 4100, Nlongkak-Yaounde, Cameroun

* Corresponding author, E-mail: odinzeggs@yahoo.com

Abstract

The Late Palaeozoic Sivrikaya and Deliktaş granitoids of the Kastamonu granitoid belt (KGB) are of sub-alkaline affinity, belong to the high-K calc-alkaline series and display features of transitional to S-type granites. Sivrikaya granitoid is host to biotite-hornblende granodiorite-tonalite and minor two-mica granites. The rocks are 303-300 Ma old, have low initial $^{87}\text{Sr}/^{86}\text{Sr}$ ratios (0.7041 - 0.708), moderately low $\epsilon\text{Nd}_{(t)}$ values (-1 to -3.8) and young T_{DM} model ages (0.75 to 1.08 Ga). All these characteristics, combined with low $\text{Al}_2\text{O}_3/(\text{FeO}+\text{MgO}+\text{TiO}_2)$ and $(\text{Na}_2\text{O}+\text{K}_2\text{O})/(\text{FeO}+\text{MgO}+\text{TiO}_2)$ and $\delta^{18}\text{O}$ values of 10-11.6 ‰ point to dehydration melting of heterogeneous protoliths dominated by amphibolite and greywackes-type sources with mantle contribution. Chondrite-normalized REE patterns of the Sivrikaya rocks are characterized by concave-upward patterns suggesting that amphibole played a more significant role than garnet during magma segregation. The main portion of the Deliktaş granitoid consists of peraluminous muscovite-rich monzogranite. Compared to Sivrikaya, rocks from this pluton have higher initial Sr ratios (0.7109 - 0.7185), older Nd model ages (1.2 to 2.2 Ga) and similar $\epsilon\text{Nd}_{(t)}$ values (-2.0 to -4.7). U-Pb zircon analyses give an age range of 295-275 Ma. The nearly constant $\delta^{18}\text{O}$ values (~11.5 to 11.7 ‰) in conjunction with the chemical characteristics indicate a predominantly pelitic source similar to the basement, which consists of felsic high-grade granulite-facies metasedimentary rocks, of continental origin.

Key words: NW Turkey; Central Pontides; Kastamonu granitoid belt; Palaeotethys; Hercynian magmatism; Genesis; VAG, volcanic-arc granitoids; Sr-, Nd-, O- isotopes.

(In review *Journal of Asian Earth Sciences*)

Zircon ages, geochemistry and isotope systematics of the Devrekani intrusion, Kastamonu granitoid belt, Central Pontides (Turkey)

Nzegge, O. M. ^{a, b, *}, Boztuğ, D. ^c, W Siebel ^a & Satir, M. ^a

^a Institute of Geosciences, University of Tübingen, Wilhelmstr. 56, D-72074, Tübingen-Germany

^b Institut des Recherches Géologiques et Minières, B. P. 4100, Nlongkak-Yaounde, Cameroun

^c Cumhuriyet University, Dept. of Geological Engineering, 58140 Sivas, Turkey

* Corresponding author, E-mail: odinezggs@yahoo.com, ✉: Philosophenweg 67/29, D-72076 Tübingen-Germany

Abstract

The Middle Jurassic Devrekani pluton (DG) belong to the Kastamonu granitoid belt (KGB), and intrudes the Late Palaeozoic-Mesozoic imbricated basement units. The DG includes low-K tholeiitic and medium-K, calc-alkaline, metaluminous I-type (ASI= 0.73-0.94) hornblende-biotite diorites, quartz diorites and tonalites. Rocks have moderate initial $\epsilon\text{Nd}_{(t)}$ values (-0.8 to -2.2) and relatively low initial $^{87}\text{Sr}/^{86}\text{Sr}$ ratios (0.7052-0.7063). These features combined with high Mg# suggest an origin through partial melting of mafic lower crustal source rocks with additional input of mantle-derived material. In addition, samples have almost flat chondrite-normalized (cn) REE patterns ($[\text{La}/\text{Yb}]_{\text{cn}} = 2.6-14.0$) and positive Eu anomalies ($\text{Eu}/\text{Eu}^* = 1.04-2.22$) indicating plagioclase played an important role in the magma petrogenesis. Overall, geochemical and isotopic data indicate the existence of two magma sources for the rocks: a depleted source with low initial $\text{Sr}_{(t)}$ and $\epsilon\text{Nd}_{(t)}$ ratios, and low $\delta^{18}\text{O}$ values (7.2-8.2 ‰) for the diorites, and an enriched source with intermediate compositions for quartz diorites and tonalites. U-Pb and Pb-Pb zircon ages range from 185-160 Ma with a cluster at 165 Ma. The Latest Palaeozoic-Earliest Mesozoic saw the opening of the Küre back-arc marginal basin and brief southward underthrusting beneath the recently imbricated Palaeozoic-Mesozoic arc massif.

Keywords: NW Turkey. Central Pontides. Kastamonu granitoid belt. Palaeotethyan collision. Devrekani granitoid. Sr-Nd-O isotopes. Zircon ages.

Late Variscan Sivrikaya and Deliktaş plutons from the Kastamonu granitoid belt generated in a Palaeotethyan convergence system (Central Pontides, Turkey)

Odilia Nzegge ^{a, b, *}, Durmuş Boztuğ ^c, Wolfgang Siebel ^a, Muharrem Satir ^a

^a Institut für Geowissenschaften, Universität Tübingen, Wilhelmstr. 56, 72074 Tübingen, Germany

^b Institute for Geological and Mining Research. B. P. 4100, Nlongkak-Yaounde, Cameroon

^c Dept. of Geological Engineering, Cumhuriyet University, 58140 Sivas, Turkey

* Corresponding author, E-mail: odinzeggs@yahoo.com, ✉: Philosophenweg 67/29, D-72076 Tübingen-Germany

Abstract

The Late Palaeozoic Sivrikaya (SG) and Deliktaş (DLG) plutons of the Kastamonu granitoid belt (KGB) pierced the Late Palaeozoic-Mesozoic imbricated basement units that formed during the collision of the western and the Eastern Pontides. SG consists of biotite-hornblende granodiorite-tonalite and minor two-mica granites, with low initial $^{87}\text{Sr}/^{86}\text{Sr}$ ratios and $\epsilon\text{Nd}_{(t)}$ values. In conjunction with moderate $\delta^{18}\text{O}$ values, these features indicate crystallization from heterogeneous protoliths dominated by amphibolite and greywackes-type sources with mantle contribution. Chondrite-normalized (cn) REE patterns characterized by concave-upward shapes of HREE and lack of significant Eu anomalies suggest that amphibole played a significant role during magma segregation. The Deliktaş pluton includes primary muscovite-rich monzogranite, with high initial Sr ratios, constant $\delta^{18}\text{O}$ values but similar $\epsilon\text{Nd}_{(t)}$ values. The isotopic signatures, mineralogy and geochemistry of the Deliktaş monzogranites suggest formation from meta-igneous crustal protoliths (metapelites).

Here, we present the first U-Pb and Pb-Pb zircon emplacement time of ~295-270 Ma and ~303 Ma respectively for Deliktaş and Sivrikaya plutons. Zircon xenocryst ages as old as 2.6 Ga bear the memory of an ancient basement, that suggests an association of the Central Pontides with Laurasia and Gondwana. Many analyzed zircon fractions show records of Variscan metamorphism, indicating the Sivrikaya and Deliktaş plutons, and the basement were components of the Variscan orogenic belt.

Key words: Variscan plutonism; Palaeotethyan convergence system; Kastamonu granitoid belt; Sr-Nd-O isotopes and zircon ages; Central Pontides-Turkey

(In preparation)

Geochemistry and geochronology of the Eurasian-derived basement of the Central Pontides (NW Turkey): evidence for pre-Variscan basement relic.

Nzegge O. M.

Institute for Geosciences, University of Tübingen, Germany

Institute for Geological and Mining Research. B. P. 4100, Nlongkak-Yaounde, Cameroon

* Corresponding author, e-mail: odinzeggs@yahoo.com, ✉: Philosophenweg 67/29, D-72076

Tübingen-Germany

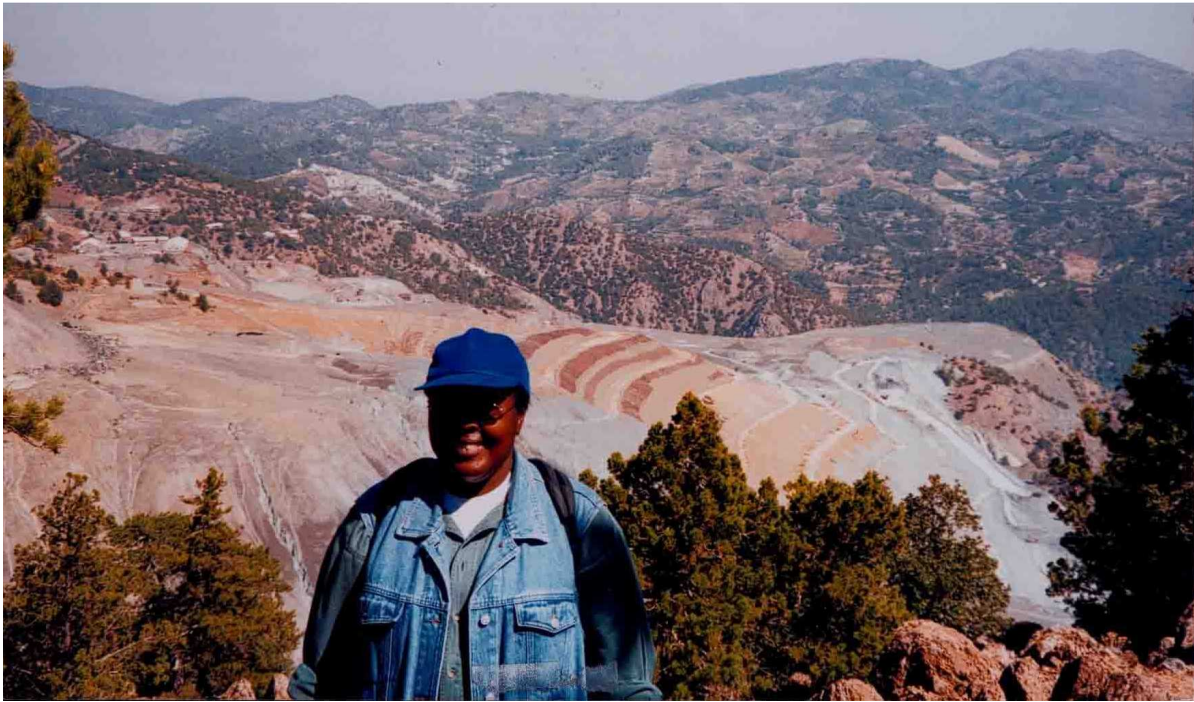
Abstract

The Central Pontides orogenic belt documents the Early Cretaceous juxtaposition of the Western and Eastern Pontides. This belt includes two remnant Palaeotethyan oceanic basins, separated by a continental fragment (Devrekani metamorphic unit) and an oceanic arc. The basement (Devrekani metamorphic unit) is a fault-bound tectonic window between the Küre accretion complex and the Çangaldağ arc complex. During Palaeozoic-Mesozoic, these units were soaked with mafic to felsic magmas, the Kastamonu granitoids. The Devrekani unit comprising amphibolite-granulite facies gneisses and amphibolites, is inferred to have rifted from the south Eurasian margin, to form a sliver within the Palaeotethys.

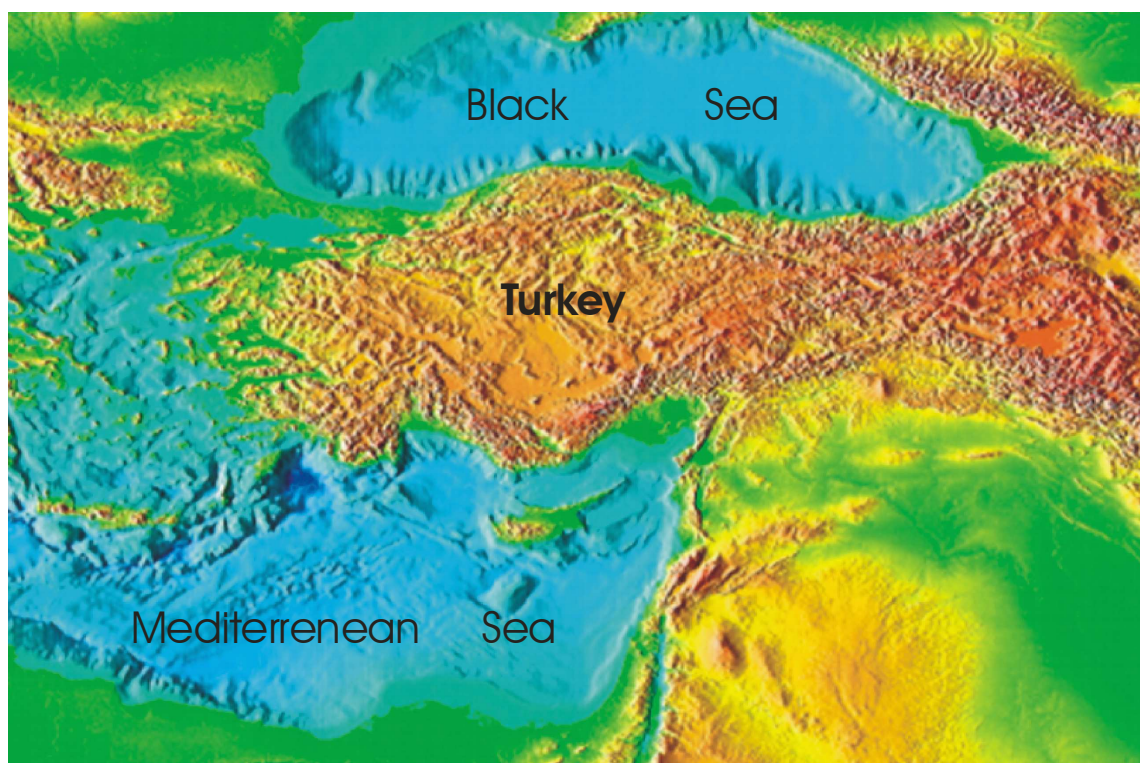
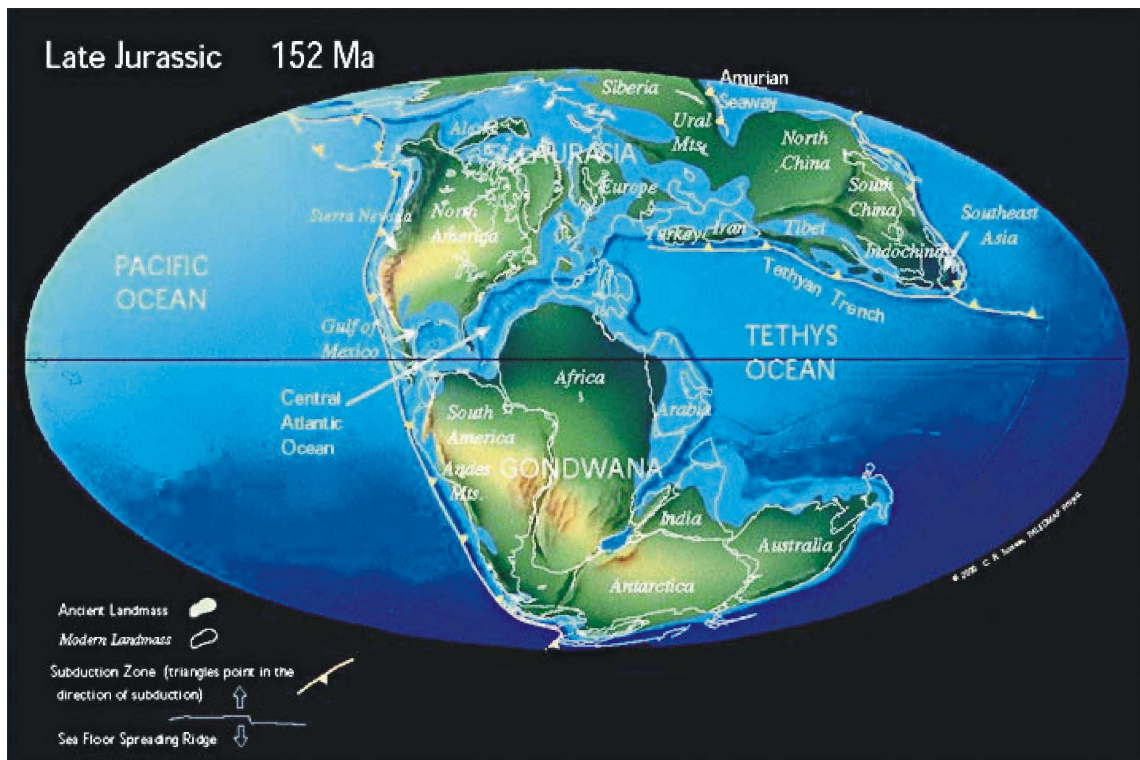
Pioneer U-Pb and Pb-Pb zircon ages and Sr-Nd-O data for the Devrekani metamorphic unit are presented. Geochemistry (ASI= 0.58-2.20) and isotopic data; Sr_i (0.704 to 0.712), $\epsilon Nd_{(t)}$ (-1.4 to 6.8) and $\delta^{18}O_{\text{whole-rock}}$ values (8-12 ‰), indicate a continental arc setting and material contribution from mantle and crustal sources. Fractionated Chondrite-normalized (cn) REE patterns ($[La/Yb]_{cn} = 6.4-27.6$), negative Eu anomalies ($Eu^*/Eu = 0.62-0.96$) and troughs in Ba, Nb and Ti, are consistent with arc-related milieus. U-Pb and Pb-Pb zircon ages indicate rocks formation during Variscan 540-300 Ma magmatic events. Late Variscan and Mesozoic ages (and/or Pb loss episodes) obtained from zircon analyses reflect regional metamorphism and magmatic growth of zircon during the Palaeozoic-Mesozoic time. Xenocryst ages in the range of 1.2 - 2.1 Ga indicate Proterozoic-material presence, confirming the basement of the Central Pontides was a component of the south Eurasian margin.

Key words: Central Pontides orogenic belt; Turkey; Continental sliver; Devrekani metamorphic unit; Çangaldağ arc complex; Zircon ages; Sr-Nd-O data; Variscan belt

*Magmas reflect differences in source and process in
response to changing geological environment!*



Field photo: Sivrikaya Anticline and Asbestos mine

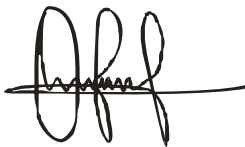


Eidesstattliche Erklärung

Hiermit versichere ich, dass

- Die vorliegende Arbeit mit dem Titel **“Petrogenesis and geochronology of the Deliktaş, Sivrikaya and Devrekani granitoids and basement, Kastamonu belt-Central Pontides (NW Turkey): evidence for Late Palaeozoic-Mesozoic plutonism, and Geodynamic Interpretation“** selbständig und ohne Benutzung anderer als der von mir angegebenen Hilfsmittel verfasst habe.
- Alle Stellen, die wortgetreu oder sinngemäß aus anderen Veröffentlichungen entnommen sind, wurden als solche kenntlich gemacht.
- Die Arbeit hat noch keine anderen Stellen zum Zwecke der Erlangung eines Doktorgrades vorgelegt.

Tübingen, 2008



Nzegge Odilia Mbonguh

